

**EVALUATION OF GEOPHYSICAL TECHNIQUES
FOR SITE CHARACTERIZATION
HIGHWAY 407E EXTENSION**

Report to

**Ministry of Transportation
Ontario, Canada**

Thurber Engineering Ltd.
2010 Winston Park Drive, Suite 103
Oakville, Ontario
L6H 5R7
Phone: (905) 829 8666
Fax: (905) 829 1166

September 5, 2013
File: 19-2805-11

H:\19\2805\11 Hwy407 East Ext - Geophysics\Reports and
Memos\MTO Comments\Geophysical Report Thurber.doc

TABLE OF CONTENTS

1	INTRODUCTION.....	1
2	RATIONALE FOR GEOPHYSICAL TRIAL.....	1
3	SCOPE OF WORK.....	2
4	SITE SELECTION AND LOCATION.....	3
5	INVESTIGATION METHODS.....	3
5.1	Geophysical Methods.....	4
5.2	Boreholes.....	5
5.3	Cone Penetration Tests (CPT).....	5
5.4	Laboratory Tests.....	6
6	RESULTS AND DISCUSSIONS.....	6
6.1	Electrical Resistivity (ER).....	6
6.2	Seismic Refraction (SR).....	8
6.3	Multi-channel Analysis of Surface Waves (MASW).....	9
7	CONCLUSIONS.....	11
8	GENERAL GUIDELINES.....	12
9	RECOMMENDATIONS.....	13
10	CLOSURE.....	14
11	REFERENCES.....	15

Appendices

Appendix 1	University of Waterloo Report Part 1 Geophysical Field Test Results
Appendix 2	University of Waterloo Report Part 2 Geophysical Lab Test Results
Appendix 3	Borehole Logs

**EVALUATION OF GEOPHYSICAL TECHNIQUES
FOR SITE CHARACTERIZATION
HIGHWAY 407E EXTENSION**

1 INTRODUCTION

This report presents an executive summary of the results of trial geophysical investigations performed at the wetland along the proposed alignment of the Highway 407E Extension east section near 1881 Nash Road, Oshawa, Ontario. It refers to the following three appended reports prepared by the University of Waterloo and Thurber Engineering Ltd. that provide the technical background for this report:

APPENDIX 1	University of Waterloo Report Part 1 Geophysical Field Test Results
APPENDIX 2	University of Waterloo Report Part 2 Geophysical Lab Test Results
APPENDIX 3	Borehole Logs

The purpose of these investigations was to evaluate the applicability of non-invasive geophysical methods for the characterization of subsurface stratigraphy at MTO sites in general and specifically to characterize the subsurface conditions at this site. The investigations generally consisted of carrying out trials of three geophysical methods and verifying interpreted subsurface conditions against conventional drilled boreholes and laboratory tests.

The geophysical trials were conducted by the University of Waterloo and the borehole drilling and CPT tests were conducted by Thurber Engineering Ltd. under the Ministry of Transportation Ontario (MTO) Purchase Order No. 2007-E-0041. During the course of the investigation and in the preparation of this report, extensive consultation occurred between Thurber, the University of Waterloo, and MTO. Thurber retained the expertise of Dr. Giovanni Cascante of University of Waterloo to carry out the geophysical investigations. Dr. Cascante was supported by members of the NDT group and Earth Sciences Department of the University of Waterloo. Dave Dundas, P.Eng. and Zahid Khan of MTO provided the terms of reference for the project and with the participation of Minkyung Kwak, P.Eng. provided comments on the report.

2 RATIONALE FOR GEOPHYSICAL TRIAL

Design of foundations and construction contracts require information about the vertical and horizontal extents of the subsurface stratigraphy and geotechnical properties of the foundation

soils. An important aspect of foundation investigation is the identification of a competent founding layer and its depth. Conventional site characterization techniques typically involve the drilling of boreholes at discrete locations to generate a stratigraphic profile. The number of boreholes that can be drilled is constrained by many factors such as budget, access limitations for drilling equipment to swamps and wetlands, stricter environmental regulations and permissions to enter private property. On a typical MTO project, a combination of these constraints can result in non-optimal ground characterization, which in turn can lead to the following issues:

- conservative and thus more expensive designs to compensate for uncertainties in subsurface conditions
- erroneous estimates of material quantities for subexcavation or fill
- designs that are not cost-effective
- delays in completion of construction leading to potential claims.

In light of these challenges, MTO has been considering innovative techniques such as geophysical methods to aid in the site characterization and geotechnical investigations.

Geophysical methods could be used to assist in planning, design, construction, and maintenance projects. They are non-intrusive, relatively inexpensive, fast, and environmentally-friendly techniques that can provide subsurface profiles by measuring the changes in properties of different soil layers and can often be conducted from the ground surface. The accuracy and resolution of these techniques have improved significantly in recent years due to advances in equipment, analytical methods, data processing and computer speeds.

Geophysical techniques, if planned wisely and executed properly, provide detailed profiles of subsurface stratigraphy particularly where the difference in the properties of soil layers is large. Improved knowledge of variable subsurface conditions reduces project risk by improving the design and reducing construction costs associated with construction claims arising from differing site conditions - especially in swamps and wetlands.

3 SCOPE OF WORK

Generally the scope of the geophysical investigation consisted of the selection, application, and evaluation of suitable geophysical techniques for future use on MTO projects. As per the terms of reference, the main components of the scope are listed below:

- Review available geophysical methods and select three methods judged to be capable of characterizing soils in general and identifying competent founding layers in particular.
- Select a representative test site and conduct geophysical tests using each of the selected methods on two 180 m long lines.

- Drill six sampled boreholes across the site for verification of geophysical results and collection of disturbed and undisturbed soil specimens.
- Perform routine and specialized laboratory testing on undisturbed samples of soil layers and conduct Cone Penetration Tests for independent verification of soil properties.
- Prepare reports presenting the results of the work and including recommendations for the implementation of geophysical investigation on future MTO projects including swamps and wetlands.

4 SITE SELECTION AND LOCATION

The geophysical test area was located on the south side of 1881 Nash Road in Oshawa, Ontario (See Figure 1 in Appendix 1). The selection of the test site was based on the following considerations:

- Available studies for the area suggested the presence of very soft to firm compressible clay deposit underlain by very dense glacial till. The stratigraphical setting of the site was expected to resemble a typical swamp.
- It is located within an area that is close to environmentally sensitive areas of Oak ridges moraine, Black Creek Wetland and the Harmony-Farewell Iroquois Beach Wetlands.
- The geophysical test area is an MTO property with easy access off Nash Road.
- This site is part of Highway 407 east extension. As highlighted in the workshop of stakeholders (February 25, 2008), geophysical methods could assist in delineating wetlands and soft soils amid concerns of budget, environment, and permissions to enter.

The generally flat topography of the test site is considered favorable for an initial geophysical test. The test area is surrounded by trees and bushes. The land is generally vacant and undeveloped. A presence of creek and a pond located within the site was not expected to influence the test results.

5 INVESTIGATION METHODS

The investigation of the selected site was completed by carrying out geophysical tests supported by conventional investigation methods including boreholes, Cone Penetration Tests (CPT) and specialized laboratory testing. The geophysical investigations were carried out from May 2008 to July 2008. The NDT group from the University of Waterloo, led by Dr. Giovanni Cascante, completed the geophysical and specialized laboratory tests. The drilling of boreholes and routine testing of soil samples were performed by Thurber Engineering Ltd. Brief descriptions of the investigation methods and their relevance are presented in the following sections.

5.1 Geophysical Methods

There are a variety of geophysical methods available for subsurface investigation. Each method has specific advantages and disadvantages depending on the intended use. The geophysical methods for this project were selected on the basis of an assessment of their potential to successfully define the stratigraphical profile at the site and for future applications at swamps and wetlands, which are characterized by weak soil layer(s) overlying very dense glacial till deposits or bedrock. The selected methods were;

- electrical resistivity (ER) imaging
- seismic refraction (SR)
- multiple-channel analysis of surface waves (MASW)

A summary of these methods is provided below. More details of these methods and typical results are provided in the Appendices.

The selected methods essentially represent two broad categories of geophysical methods. The electrical resistivity method is based on the electrical properties of the soils, whereas the seismic refraction and multiple-channel analysis of surface waves methods are based on propagation of seismic waves.

Although the more widely known ground penetrating radar (GPR) method has been used in near-surface geophysical surveys, it was not selected for consideration because of its limitations. The depth of penetration is limited where high conductivity materials such as clays, rock with high metal content, or soils saturated with conductive pore water are present (Kong et al. 1994).

Electrical resistivity imaging (ERI) measures the resistivity (units of Ohm-metre, Ω -m) or its reciprocal (electrical conductivity, units of Siemens/meter, S/m) of the tested medium. Electrical resistivity methods delineate the subsurface stratigraphy of a site based on the electrical resistivity contrasts between different soil layers. However, the presence of high conductivity pore water in dense overburden can bias the results (Zonge et al. 2006). This limitation could be beneficial in geophysical investigations of swamp and wetland areas because of the typical very dense underlying layer of glacial till or bedrock, which will create a sharp electrical contrast with overlying weak soils.

The seismic refraction method (SR) utilizes the refraction of seismic waves in different soil layers in order to characterize the subsurface stratigraphy. This information is then interpreted to determine the thickness of soil layers. The method provides reliable results where the stiffness of the ground increases with depth (ASTM D5777-00). Soils in general and in swamps and wetland settings in particular present a stratigraphy in which the stiffness of the soil deposit increases with depth. As a result, this method has the

potential to provide reasonably accurate prediction of subsurface stratigraphy where there is sufficient contrast between stiffness of layers.

The multiple-channel analysis of surface wave method has been successfully used for geophysical site characterization (Gucunski et al. 1996, 1998; Phillips et al. 2000; Strobbia and Fotti 2006; Nasser et al. 2007). However, its limitation is that a variety of interpretations of stratigraphy can be predicted for the same site. This limitation has recently been managed with the use of advanced computer analysis techniques. This technique is increasingly being used due to its ability to identify stratigraphy even where stronger layers overlie weaker layers.

5.2 Boreholes

The evaluation of geophysical techniques involved the drilling of boreholes at several locations along the geophysical test lines (See Figure 1, Appendix 1) to calibrate the geophysical methods. Six sampled boreholes were advanced in accordance with MTO standards following the completion of the geophysical tests and their interpretation. Details of sub surface soils, physical properties of soils, ground water conditions and other relevant information are presented on the borehole log sheets in Appendix 3.

The objectives of advancing boreholes for this project are listed below:

- generation of subsurface soil profiles for comparison with geophysical findings
- collection of undisturbed samples for specialized testing
- calibration of geophysical techniques
- measurement of groundwater levels, resistivity, and Total Dissolved Solids (TDS).

5.3 Cone Penetration Tests (CPT)

Cone Penetration Tests (CPT) were advanced at four (4) locations along the geophysical test lines as an independent measure of the shear wave velocity and the penetration resistance of different soil layers. Shear wave velocity profiles for subsurface soils are obtained by using seismic sensors embedded into the cone penetrometer.

Cone Penetration tests provide many other important physical properties of soils such as penetration resistance for foundation design, pore water pressure measurement for liquefaction assessment, and ground water levels. Appendix 2 presents a summary of the CPT testing. Shear wave velocity results from the CPT's and comparison with measurements from geophysical methods are also included in Appendix 2.

5.4 Laboratory Tests

Geophysical methods differentiate between the layers of soils on the basis of differences between the physical properties of the layers such as the electrical resistivity and shear wave velocity. Laboratory tests on representative soil specimens were performed to measure the electrical resistivities and shear wave velocities of selected soil samples to compare with the results obtained from the in-situ geophysical tests.

Soil samples were collected from strategically-selected boreholes and depths representative of stratigraphy at the site. The laboratory testing was performed at the NDT laboratory of University of Waterloo. Shear wave velocities were measured by a modified Stokoe type Resonant Column device, which is an ASTM standard test (ASTM D4015-92). Details of specialized laboratory tests are presented in Appendix 2.

6 RESULTS AND DISCUSSIONS

This section focuses on the results of depth estimates of different soil layers and in particular the depth to the competent layer (glacial till) generated from interpretations of the three geophysical methods carried out along the two test lines at the site. The estimated subsurface profiles from geophysical testing were compared to the subsurface profiles interpreted from the boreholes. Tables 1 to 4 present the comparison of depths to very dense glacial till from geophysical tests and from the borehole data.

The depths and properties of the soil layers overlying the glacial till at the borehole locations were identified by geophysical methods with varying degree of accuracy depending on the degree of contrast between soil layers. In general, the results for tests along Line 2 are more reliable than those along Line 1 because the soil layers along Line 2 exhibit a clearer contrast in the properties used for interpretation. The overlying soils at Line 1 are not as soft as those at Line 2 as indicated by the SPT tests performed during the drilling of boreholes.

The following sections present a summary of the geophysical findings.

6.1 Electrical Resistivity (ER)

The spacing of the electrodes that measure the electrical resistance of the ground governs the effective depth of penetration of the test. Therefore, measurements using different spacings of electrodes provide information that can be used to generate depth estimates of soil layers based on measured resistivities or conductivities. The maximum depth of exploration of the ER test was 20 meters. Since the presence of the groundwater table would strongly influence the resolution of soil layers by the ER test, only significant differences in the density (porosity) of the ground could be used to delineate deposits using ER tests as would be the case for a typical swamp.

The interpreted stratigraphy based on the resistivity results and their comparison with the borehole data are presented in Figures 3 and 4 in Appendix 1 and in Table 1. The cross-sections generated for lines 1 and 2 generally show two soil layers - a high conductivity (up to 13.2 mS/m) layer overlying a lower conductivity (as low as 2 mS/m) layer.

The interpreted stratigraphy for line 1 (Figure 3, Appendix 1), shows an upper clay-rich layer and a lower layer containing densely packed materials of sands, silts and gravels. The top layer shows higher conductivity values (between 12.5 and 13.2 mS/m) likely because of the interaction of groundwater and the clay content in the soil structure of the top layer. The underlying layer showing lower conductivity values (between 2 and 4 mS/m) has been interpreted to represent the glacial till layer.

Figure 3 in Appendix 1 indicates that the depth to the very dense till layer varies from 4.8 m to 5.7 m, which corresponds to the combined thickness of the three overlying layers identified from the borehole data (total thickness from 4.6 m to 6.1 m). Hence, the depth of the competent layer (glacial till) estimated from the ER results compares favourably with the depth obtained from boreholes. The apparent discrepancy in the stratigraphy in the areas between the boreholes is due to the linear interpolation of borehole findings.

The glacial till layer identified in Figure 3, Appendix 1 shows a feature that seems to be an old buried channel (7.0 m deep, 12 m wide) located approximately 88 m from the start of the line. This feature is also in good agreement with the data obtained from BH 08-5. However, full delineation of this channel would require additional boreholes.

The interpreted stratigraphy for line 2 (Figure 4, Appendix 1) shows three main soil layers. The thickness of the top layer varies from 2.0 to 3.4m, which corresponds to the thickness of the upper two layers identified from the borehole data (total thickness from 3.0 m to 3.6 m). There was insufficient resolution in the resistivity tests carried out along this line to determine the location of first layer. However, the depth of the interface between the sand and the clay layers as well as the depth of the underlying glacial till layer are in good agreement with the depths noted in the boreholes, except at the location of BH08-1 where the elevation of the top of the glacial till layer interpreted from the ER tests is approximately 2.5 m higher than actual.

Table 1: Depth to Dense Till from Boreholes and ER tests (Lines 1 and 2)

BH No.	Depth to Dense Till* [m]		Error
	From BH	From ER	
08-1	9.0	6.5	28 %
08-3	6.1	6.3	3 %
08-4	11.3	12.0	6 %
08-5	6.1	5.7	7 %

08-6	4.6	4.8	4 %
08-7	10.1	9.9	2 %

* Interpreted as having a conductivity between 2 to 4 mS/m

Table 1 presents the comparison of interpreted depths to the glacial till layer obtained from boreholes and ER tests at the BH locations. Except at BH 08-1, the ER-interpreted depths are within 10 % of the actual, which is considered to be good correlation in view of the uncertainties inherent to subsurface profiling, even using conventional boreholes.

The electrical conductivity of different soil specimens from laboratory testing generally agree well with the values obtained in the field (Appendix 2, Table 3).

6.2 Seismic Refraction (SR)

This method measures the velocity of waves as they are refracted from the interfaces of different layers. The waves arrive at different times from layers due to differences in the corresponding transmission velocities. As noted before, one of the limitations of seismic refraction is its inability to detect inverse layering (shear wave velocity decreasing with depth or hard layer over softer layer scenarios). Thus, if there is a softer layer below the stiffer crust, which is the case for this site, the velocity measurements are inverted and the thickness of underlying softer layer and the overlying crust are not accurately depicted.

The analysis of the recorded test data was performed first by the reciprocal method and then by the tomographic inversion method (described in Appendix 1, Section 6.2) to determine more accurate wave velocities and depth estimate of each layer.

The reciprocal method revealed two main refracting boundaries (three layers) throughout the site. The depth to the underlying dense layer (glacial till) cannot be obtained accurately using seismic refraction because of smaller contrast between the overlying clay and the underlying glacial till. Due to this limitation, the prediction by SR of depth to the underlying glacial till layer in line 1 has a maximum error of 2 m higher than actual. For comparison purposes, the predicted depths of the dense layer were shifted to match the depth of the till layer according to the data from only one of the boreholes.

To improve the analysis, the tomographic inversion (Ray Tracing Method, Menke 1999) was then completed for both line 1 and line 2 by inputting the velocities and approximate depths obtained from the reciprocal analysis using the software Seisimager/2D. The results from three-layer tomography models for lines 1 and 2 using tomographic inversion are shown in Figures 8 to 12 in Appendix 1. For line 1 (Figure 8 and 9), the depth of the overlying soil layer and the depth to the underlying glacial till layer are consistently underestimated by approximately 1 m. As expected, the thickness of the second layer could not be identified from the SR data because of the limitation of the method as

described above. Consequently, the estimate of depth to the underlying dense glacial till layer also has inaccuracies.

For line 2 (Figures 10 to 12 in Appendix 1), the depth of the glacial till layer is generally in good agreement with the borehole data. However, the thickness of the first layer is underestimated. As noted above, Line 2 consisted of soils with significant contrast in soil properties, which make the identification of layers easier.

Table 2 presents a comparison of depth estimates to the dense glacial till layer from Borehole data and the corrected SR tests at the borehole locations. The table indicates that the estimate of depth to dense glacial till is in good agreement with the borehole data with an average error of 10 % which is considered to be good in spite of the greater inaccuracies that were encountered at Line 1 due to the more complex soil layering at that location.

Table 2: Depth to Dense Till from Boreholes and SR tests (Lines 1 and 2 combined)

BH No.	Depth to Hard Till* [m]		Error
	From BH	From SR	
08-1	9.0	8.0	11 %
08-3	6.1	-	-
08-4	11.3	10.1	11 %
08-5	6.1	5.2	15 %
08-6	4.6	5.0	9 %
08-7	10.1	9.8	3 %

The overburden layers and the underlying dense glacial till layer are characterized by average shear wave velocities of 350 m/s and 700 m/s respectively (Appendix 1). These velocities are in agreement with the measurements taken during CPT testing (Appendix 2, Table 2).

6.3 Multi-channel Analysis of Surface Waves (MASW)

The depth of penetration of surface waves into the ground is a function of their wavelength, with longer wavelengths penetrating deeper into the ground. Therefore, to characterize deeper layers, lower frequencies (longer wavelengths) have to be generated. A 170 lb weight was used to generate low frequency waves in this study by impact at the surface.

The interpreted soil profile is shown in Figures 15 to 21 in Appendix 1 with dashed lines. These figures show that the depth to the till layer is consistently underestimated by an

average of 22 % for line 1 and by an average of 22.5 % for line 2. Consequently the depth to the glacial till layer is underestimated by approximately 0.5 to 2.7 m. The interface of the glacial till layer (dashed line) is based on interpolation between the 2 profiles carried out using an array of 48 sensors at each subsurface profile.

The MASW was able to show an additional soil layer of lesser velocity underlying the upper layer of higher velocity material (Figures 15 and 16 in Appendix 1). This layer was not identified in the seismic refraction data because of the limitation of the refraction method. On the other hand, the presence of a velocity inversion makes the analysis of MASW more complex.

One of the limitations of the MASW method is the lower resolution in the delineation of deeper layers if the generation of frequencies below 15 Hz is limited by equipment. The drop-weight source used in this project generated low frequencies but they were not strong enough to provide a better resolution of the deeper layers. For future MASW tests, the drop-weight source should be modified to enhance the generation of low frequencies. Possible modifications to provide this improvement in test performance include the use of a heavier wave generation weight (>170 pounds or 80+Kg) against a larger area of impact.

Tables 3 and 4 compare the thickness of each soil layer obtained from MASW tests and from boreholes. The combined average error in MASW results versus borehole results as the control is -22 %. As noted earlier, a large portion of this error is associated with the inability of generating low frequency waves and the fact that in Line 1 there is a transition between the stiffness of till and overlying layers instead of an abrupt change. Moreover, the location of geological boundaries from borehole data depends on the sampling interval.

Table 3: Thickness of layers over Till from Boreholes and MASW tests (Line 1)

Layer	Line 1-1		Line 1-2	
	MASW (m)	From BH (m)	MASW (m)	From BH (m)
1	1.4	1.3	1.4	1.4
2	1.1	1.0	1.1	1.3
3	1.6	3.8	1.6	1.9
4	Till	Till	Till	Till
Error	(33 %)		(11 %)	

Table 4: Thickness of layers over Till from Boreholes and MASW tests (Line 2)

Layer	Line 2-1		Line 2-2	
	MASW (m)	From BH (m)	MASW (m)	From BH (m)
1	0.7	1.2	0.6	0.5
2	1.5	1.7	1.4	3.2
3	5.2	6.1	5.4	6.4
4	Till	Till	Till	Till
Error	(-18 %)		(-27 %)	

7 CONCLUSIONS

MTO has been considering innovative techniques to compliment conventional geotechnical investigation methods such as sampled boreholes. The purpose of these innovative methods is to generate efficient and cost-effective detailed subsurface stratigraphic models for sites with a variety of constraints such as access (especially swamps), environmental concerns at wetlands, and significant costs associated with drilling an adequate number of boreholes. Geophysical methods were tested to evaluate their potential in estimating the thickness of soft soils and depth to competent ground. The main conclusions of the geophysical trial carried out at this site are:

- This site presented challenges for geophysical tests because the soft clay layer was overlain by a relatively denser layer of silty sand.
- In spite of the complexity of the site stratigraphy, the tested geophysical methods provided good estimate of the depth to the underlying competent glacial till layer.
- The depth predicted by the geophysical tests consistently underestimated the actual depth of the soil strata to varying degrees, depending on the test method.
- The Electrical Resistivity method provided the depth estimate to the underlying dense glacial till with an average error of about 5 %, which represents an error of 0.5 m for a depth of 9 m. This method is expected to clearly identify the profile of hard bottom in a typical swamp.
- The Seismic refraction method, once corrected for the effect of inverse layering, provided the depth estimate to the underlying dense glacial till with an average error of -10 % (that is it underestimates depth). This corresponds to an error of 0.9 m for a depth of 9 m. The depth estimates of the overlying layers were not accurate due to the limitation of this method in detecting soft soil layers underlying hard soil layers. This method would provide reasonably accurate estimate of hard bottom in a typical swamp where there is no inversion of soil layering (that is, the sequence of layers varies from soft to hard or dense with depth).

- The MASW method indicated the depth of dense till with an average error of -22 %. This corresponds to an error of 2.0 m for a depth of 9 m. However, this method provided the advantage of clearly showing the presence of all layers on the site although the thicknesses of layers and depth to dense till were underestimated. The results of the MASW technique can be significantly improved by changing the source for generating waves of larger wavelength and the MASW method shows potential for characterization of the properties of individual layers.
- Independent verification of the properties of soils from cone penetration tests and laboratory tests generally agreed well with the findings from geophysical methods. This confirmation is a good indicator of the reliability of depth estimates from geophysical tests.

8 GENERAL GUIDELINES

The methods evaluated in this study are found suitable for the purpose of characterizing sites; especially for identifying the thickness of soft deposits overlying bedrock or hard/dense glacial till. The accuracy and success of geophysical methods depends on the availability of existing information. Following are general guidelines for the application of geophysical techniques at MTO sites:

- Where access to the site is limited, limited number of conventional boreholes should be advanced as close as possible to the test site for selection, planning, and interpretation/calibration of the selected geophysical method.
- A conservative factor should be applied to depth predictions based on geophysical testing in order to compensate for the apparently consistent underestimation of the depth predicted by geophysical methods.
- Where drill rigs cannot access a site to provide calibration information, a combination of geophysical methods should be used. This would involve preliminary testing with electrical resistivity and limited MASW for the planning of detailed geophysical survey.
- ER, SR and MASW methods show potential for delineation of depth to firm bottom, especially at swamps and wetlands where the soil profile consists of soft soils overlying competent firm bottom.
- In wet areas, waterproofing of the geophysical equipment would be required to prevent damage. Moreover, the source for generation of waves would also have to be modified to ensure that the required frequencies are generated.
- Deep cuts and high fill areas in a typical MTO project usually require a large number of boreholes. The number of boreholes in such areas could be reduced by employing geophysical techniques.

- Geophysical tests such as Seismic refraction (SR) and MASW could also be used to measure the low strain elastic moduli of soils. Elastic moduli are required for foundation modelling, settlement analysis, and earthquake design. Since SR and MASW use similar equipment, both tests should be performed at the same time for comparison of the results.
- MASW tests can be effectively used to characterize the asphalt pavement and the underlying fill and native soils. High frequency waves would be required to characterize thin layers.

9 RECOMMENDATIONS

Success of geophysical techniques requires knowledge of specific limitations, testing methodology, recent developments, and equipment specifications. For inclusion of geophysical test methods into standard MTO terms of reference, the following are recommended:

- A test standard for each geophysical method based on most recent advances should be developed. Such a test standard will present detailed guidelines on different aspects of testing including applications, planning, equipment selection, calibration, test layouts, limitations, specifications, data analysis, field data forms, and reporting.
- The site selected for this trial was neither a swamp nor strictly a wetland. Geophysical testing on a typical swamp site is recommended as it will require modifications to the equipment and test setup. Results of this testing will significantly improve the test standards.
- The test standards shall be reviewed every three years for updates on recent advances in equipment specifications, testing methodologies, and data analysis techniques.

10 CLOSURE

Funding for this program was provided by the Ministry of Transportation Ontario. The guidance and review comments provided by Mr. Dave Dundas, P.Eng., and Ms. Minkyung Kwak, P.Eng., of the Foundations office during the execution of the work and preparation of the report were invaluable.

The geophysical testing and laboratory testing were conducted by the NDT Group from the University of Waterloo, led by Dr. Giovanni Cascante, P.Eng., Professor, Civil Engineering Department. Significant contribution to this program by Dr. Cascante is gratefully acknowledged.

The drilling and sampling equipment was provided by DBW Drilling. Ltd. The field work was supervised on a full time basis by Stephane Loranger of Thurber Engineering.

Dr. P.K. Chatterji, P.Eng., a Designated Principal Contact for MTO Foundations, reviewed the report.



THURBER ENGINEERING LIMITED

P.K. Chatterji, Ph.D., P.Eng.

Review Principal, Designated MTO Contact

11 REFERENCES

- Annual book of ASTM standards, 2002. Standard Guide for Using the Seismic Refraction Method for Subsurface Investigations, ASTM D 5777-00, 04(02), pp. 309-312.
- ASTM D4015-92, 2000, "Standard Test Methods for Modulus and Damping of Soils by the Resonant-Column Method," American Society for Testing and Materials, Annual Book of Standards.
- Gucunski, N., Ganji, V., and Maher, M.H., 1996. Effects of obstacles on Rayleigh wave dispersion obtained from the SASW test. *Soil Dynamics and Earthquake Engineering*, Volume 15: 223-231.
- Khan, Z., Cascante, G., and El-Naggar, H., Lai, C.G., 2008. Measurement of Frequency Dependent Dynamic Properties of Soils Using the Resonant Column Device. *Journal of Geotechnical and Geoenvironmental Engineering*, ASCE.
- Kong, F.N., H. Westerdahl, and By, T.L., 1994. Borehole Radar Tunnel Detection at Gjovik, Norway. Norwegian Geotechnical Institute, Publication 194, pp. 1-10.
- Menke W., 1999, *Geophysical Data Analysis: Discrete Inverse theory*, International Geophysics Series. San Diego: Academic Press. 289 pp.
- Nasseri, A., Phillips, Cascante, G., C. and Hutchinson, J., 2007. Effects of Underground Cavities on Rayleigh Waves – Numerical and Experimental Study. *Soil Dynamics and Earthquake Engineering*. 27(4): 300-313.
- Nazarian, S. and Stokoe, K. H., 1984, In-situ shear wave velocities from spectral analysis of surface waves: in *Proc. of the Eighth World Conf. on Earthquake Engineering*, San Francisco, California, Vol. III, 31–38.
- Palmer, D., 1980, The Generalized Reciprocal Method of Seismic Refraction Interpretation, in Burke, K.B.S. (Ed.), *Society of Exploration Geophysicists*.
- Perk C.B., Miller R.D., Xia J., 1999, Multichannel analysis of surface waves, *Geophysics*, 64(3), 800-808.
- Phillips, C., Cascante, G., and Hutchinson, D.J. 2000. Seismic surface waves to detect underground voids. *Proceedings of the Symposium on the Application of Geophysics to Engineering and Environmental Problems*, Arlington, Virginia: 29-37.
- Strobbia C. and Foti S., 2006, Multi Offset Phase Analysis (MOPA), *Journal of Applied Geophysics*, 56:300-313.
- Strobbia, C., 2002. Surface wave methods: acquisition, processing and inversion. PhD Diss. Politecnico di Torino. Italy.

Zonge, K., Wynn, J., and Urquhart, S. 2006. Resistivity, Induced Polarization, and Complex Resistivity. In Near-Surface Geophysics, Ed. D. Butler, SEG. Tulsa, OK. pp. 357-438

Appendix 1

Geophysical Tests for Subsurface Investigations Highway 407 East Extension

Part 1: Geophysical Test Results

Geophysical Tests for Subsurface Investigations Highway 407 East Extension

Part I: Geophysical test results

Prepared for

Thurber Engineering Ltd.

November 15, 2008

Prepared by:

Giovanni Cascante Ph.D., P.Eng.
Paul Groves,
Fernando Tallavo, M.Sc.,
Yanjun Yang, M.Sc.,
Scott Piggott, M.Sc., and
Claudio Strobbia, Ph.D.

Department of Civil and Environmental Engineering
University of Waterloo Canada, N2L 3G1
E-mail: gcascant@uwaterloo.ca
Tel: (519) 888-4567 ext. 32098
Fax: (519) 888-4349

November 15, 2008

P.K. Chatterji, P.Eng., Ph.D.
President, Chairman of the Board
Thurber Engineering Ltd.
Suite 103, 2010 Winston Park Drive
Oakville, ON L6H 5R7

**Subject: Technical report on geophysical tests for subsurface investigations - Highway 407
East Extension**

Dear Dr. Chatterji,

Thank you for considering our expertise at the University of Waterloo for this project. Please find enclosed the report for the geophysical tests performed on two 180-meter survey lines at the site located at 1881 Nash Road, Oshawa, Ontario. Resistivity, seismic refraction, and multiple-channel analysis of surface waves tests were performed between the dates of April 25, and May 7 to May 9 of 2008. In addition, resonant column tests were performed on six samples from boreholes; conductivity and total dissolved solids measurements were taken in water samples from three boreholes; and cone penetration tests were performed at four locations on the week of August 4.

The initial two sections of the report: introduction and the scope of the investigation were adapted from documentation provided by your office. I trust that this report fulfills your requirements. Please contact me if you have any questions regarding the results presented in this report.

Respectfully submitted,



Giovanni Cascante, Ph.D., P.Eng.
Associate Professor, University of Waterloo
(Phone: (519) 888-4567 ext.32098)
(email: gcascant@civmail.uwaterloo.ca)

Attachments: Technical Report and Appendices A to I

1- Introduction

The purpose of this investigation is to conduct an evaluation of geophysical methods that could be used for the delineation of wetland deposits and deposits of soft clays along the Highway 407 East Extension corridor. This report summarizes the results of geophysical tests performed at the 1881 Nash Road site in Oshawa that is located along the East link row of proposed Highway 407 East Extension. These geophysical methods would eventually be equally applicable to other projects in the MTO regions. The geophysical investigation assessed the applicability of combining three geophysical methods consisting of electrical resistivity imaging, seismic refraction surveying, and multiple multiple-channel analysis of surface waves (MASW). Sections of the Hwy 407 East Extension alignment crosses the wetland complexes associated with the south slope of the Oak Ridges moraine. This is particularly the case of the East Durham link that crosses the Black Creek wetland and the Harmony-Farewell Iroquois Beach Wetland Complexes. This link also potentially crosses some deposits of compressible clay soils, particularly towards the south end as it approaches Hwy 401.

The soil conditions in these areas present a number of highway design and costing issues; which include the depth of organic soils, the depth of compressible soils, the engineering properties of the soils, and the variation of stratigraphy along the alignment. At the Highway 407 project, the wetlands investigation was constrained by the following factors: permission to enter - refusals or delays in permission to enter or constraints regarding the cutting of trees or use of drill rigs; accessibility across some wetland areas without causing environmental damage; and significant costs associated with drilling a sufficient number of conventional, sampled boreholes to adequately delineate the extent of the wetland deposits. In light of the above restrictions, geophysical techniques have been investigated to assess if the combination of information from geophysical test and a limited number of boreholes is suitable for delineating the stratigraphy in a wetland area. The site located at 1881 Nash Road was chosen for the geophysical trial. This site lies in the East link Row on the south side of Nash Road. Preliminary investigation showed that the site is underlain by sand, silt, soft to firm clay and a very dense till deposit at depths in the order of 11 m. This stratigraphy was considered suitable for the evaluation of the geophysical techniques (electrical resistivity, seismic refraction, and surface waves). This site was accessible because it is MTO property.

2- Scope of investigation

The scope of this investigation consisted of the following:

- Review of the available geophysical methods and selecting at least three methods judged to be most suitable for MTO projects.
- Conduct a field program consisting of a series of geophysical tests at the test site, using each of the selected methods along two 180 m long survey lines at the test site.
- Conduct a geotechnical investigation based on six sampled boreholes across the site to be used for ground truthing and to obtain soil samples for routine and specialized testing consisting of shear wave velocity at low strain levels using the resonant column device on undisturbed samples of various layers of subsurface soils.
- Analyze the geophysical data, comparing the data to ground truthing data and preparing a report evaluating the applicability of each method to current and future MTO projects
- Provide input to the preparation of specifications and guidelines for the implementation of geophysical investigation on future MTO projects

3- Geophysical investigation

Three geophysical methods were chosen from the literature for the investigation of the site based on their potential success to assess stratigraphy and shear wave velocity profile. The selected methods are electrical resistivity imaging, seismic refraction, and surface wave inversion. The geophysical tests were performed along two 180-meter lines at the site located at 188 1 Nash Road, Oshawa, Ontario. An aerial picture of the site is shown in Figure 1; the approximate location of the boreholes is also shown.

This report presents the results of three geophysical surveys: electrical resistivity, seismic refraction, surface waves, the results from field water sampling on three boreholes, as well as the results from resonant column testing on six specimens from the site. The geophysical surveys on the two 180-meter lines were performed during three days from May 7 to May 9 of 2008. A preliminary MASW test was also performed on a short line (24-metre long) on April 25, 2008 to select the seismic source capable of generating the required frequencies in the site. A brief section on the selection of the methods is presented first, followed by the results from the geophysical tests. After this section, the comparison of and discussion of the results is presented. Next, the results from resonant column tests and water sampling are summarized. Finally, the results from the geophysical test are compared with the results

from the laboratory tests. A detailed description of the geophysical methods is presented in the appendices as well as additional results not included in the main body of the report.

4- Selection of geophysical methods

Different geophysical methods are available for subsurface investigations; however, each method has specific advantages and disadvantages depending on the characteristics of the site. The three methods selected for this project were considered the most promising methods for the characterization of sites with complex geotechnical conditions including sand and clay layers in a soft-hard-soft arrangement. Ground penetrating radar has been quite successfully used in near-surface geophysics; however, it has penetration problems when high conductivity materials are involved, such as clays, rocks with high metal content, or soils saturated with conductive pore water (Kong et al. 1994). Electrical resistivity methods (Appendix A) can detect the stratigraphy of a site based on the electrical resistivity contrasts between different soil layers; nevertheless, the presence of highly resistive or fractured materials overlying a bedrock or bottom layer, and the presence of high conductivity pore water can bias the results (Zonge et al. 2006). The electrical resistivity survey is fast to perform because the installation of the electrodes on the ground is simple. The effort required to perform a 48-electrode resistivity test in the field is approximately three hours with a crew of two technicians in a flat and clean terrain with a clay layer at the top. The seismic refraction method (Appendix C) is one of the oldest near-surface seismic methods; it can be used to locate soil interfaces in the specific case where the stiffness of a horizontally layered media increases with depth (ASTM D5777-00). The multiple-channel analysis of surface waves (MASW, Appendix E) method have been successfully used for geophysical site characterization (Gucunski et al. 1996, 1998; Phillips et al. 2000; Strobbia and Fotti 2006; Nasser et al. 2007), however it has been mostly used for shallow applications due to the physical difficulty of generating long wavelengths (low frequencies) with high signal-to-noise ratios. This limitation has recently been overcome with the use of ambient vibrations or microtremors in the REMI method (e.g. Strobbia 2002). The MASW and the seismic refraction require the proper installation of geophones vertically, the effort required performing a 48-geophone MASW or refraction survey in the field is approximately 4 hours with a crew of three technicians and five different source locations and an average of three shots per location.

5- Site description and experimental setup

The geophysical tests were performed on two 180-meter lines at the site located at 1881 Nash Road, Oshawa, Ontario (Figure 1). The electrical resistivity was performed on the entire lengths of lines 1 and

2. A higher resolution resistivity line (94-m long) was also performed on line 2. Given the required resolution for the seismic tests (refraction and surface waves); the seismic surveys were performed on shorter lines (48-m long) beside the resistivity lines. Line 1 was subdivided into lines 1-1 and 1-2, whereas line 2 was split into lines 2-1, 2-2, and 2-3. The gap between the seismic lines 1-1 and 1-2 is generated by the presence of a creek. The seismic lines did not cover the full extension of lines 1 and 2 because of the additional 20 m required at each side of the seismic lines to locate the seismic source. For all geophysical methods, the horizontal distance is stated in metres along the survey line, where 0 m represents the location of the first receiver and 47 m or 188 m represent the location of the last receiver (Figure 1). The topography over the geophysical survey lines was measured at 4-metre intervals using a total station and is presented with the geophysical results. Glaciofluvial deposits, consisting of sand, silt, and clay overlie a hard till in the area to a depth of approximately 9 m to 12 m according to geotechnical boreholes drilled by Thurber Engineering near the area. The surveyed lines for the resistivity and seismic tests were almost the same (Figure 1). Additional information from boreholes will be used as ground truthing to evaluate the success of each geophysical method.

6- Geophysical tests results

6.1- Electrical resistivity imaging

The electrical resistivity imaging (ERI) or electrical resistivity ground imaging (ERGI) measures the change in resistivity (units of Ohm-metre, Ω -m) or its reciprocal (electrical conductivity, units of Siemens/metre, S/m) of the tested medium between a pair of potential electrodes when a current is generated between two separate current electrodes (Figure 2). It is common practice to plot the conductivity of the medium instead of the resistivity because it is better correlated with the stratigraphy of the medium. The resistivity method maps the pattern of subsurface flow of a current introduced at the surface between a pair of electrodes. The measured voltage is related to the energy required for the current to pass through the material, thus it is an indirect measurement of the resistivity of the tested material. The spacing of the electrodes is changed to generate a resistivity profile. The increase of electrode spacing increases the effective depth of penetration. The resistivity test involves many individual measurements of resistivity. Each measurement involves two electrodes that introduce current flow into the ground and two different electrodes, located in different locations that simultaneously measure the electrical potential (voltage) in the ground due to the current flow. Inversion software (Geotomo Software 2006, Res2dinv ver. 3.55) is used in this project to generate a two-dimensional electrical resistivity structure of the ground below the survey line. The conductivity of sands and clays varies approximately from 0.5 mS/m to 20 mS/m depending on the groundwater conditions. Typical

conductivities for deionized water, fresh water, and seawater are 10^{-3} mS/m, 1 mS/m, and 4000 mS/m respectively; whereas most soil forming minerals have much smaller conductivities between 10^{-12} and 10^{-4} mS/m.

With the exception of electrically conductive minerals such as magnetite, specular hematite, carbon, graphite, pyrite and pyrrhotite, soil and rock minerals generally do not conduct electricity. In the majority of sites in southern Ontario, the electrical conductivity of rocks and soils is controlled by the water in the pore spaces. The conductivity is then determined by the following factors: porosity, degree of saturation, the concentration of dissolved electrolytes in the pore water, the temperature and phase state of the water in the pore spaces, and the amount of clay minerals and colloidal material (McNeill 1980). The conductivity of soils and rocks is larger when the water content of the material is larger. The water content can vary above and below the water table and can vary within the saturated zone according to the porosity. The conductivity is higher where the concentration of dissolved solids is higher. The electrical conductivity decreases when the temperature decreases and electrolytic conduction is suppressed when soil and rock is frozen. There is also an important effect of clays and colloids. Most mineral surfaces are negatively charged because of mineral imperfections; therefore, cations in solution become easily adsorbed (loosely bound) to the mineral surface. Because clays and colloids have a very high surface area compared to their size, their capacity to adsorb cations from solution is large. Such cations are loosely bound to the surface; they are exchangeable with ions from the solution, and are able to conduct currents along mineral surfaces. A small amount of clay content in wet conditions can increase the electrical conductivity significantly.

The resistivity survey can give some indication of lithology, especially when used in conjunction with other information such as borehole soil samples. On its own, it is difficult to determine lithology from resistivity surveys because the electrical resistivity/conductivity is affected by several different factors at the same time (e.g. porosity, degree of saturation, concentration of dissolved electrolytes in the pore water, temperature and phase state of the water in the pore spaces, and the amount of clay minerals and colloidal material). The basic theory of the resistivity tests is given in Appendix A.

Equipment and testing procedure. A 48-electrode system was used for the resistivity measurements (Syscal Junior Switch). The electrodes are driven into the ground in a straight line at 4 m (Lines 1 and 2, Figure 1) or 2 m spacing for higher resolution. The resistivity meter was positioned at the centre of the line and the electrodes connected to two cables of 24 independent connectors each. The two lines were surveyed using the Wenner electrode array (equal spacing between electrodes). Each line was 188 m long (47 x 4 m) long (Figure 1). Line 1 ran from almost south to north, passing west of the pond ending near the road; whereas line 2 ran from southwest to northeast near the southeast side of the pond (Figure

1). In addition to the two main lines, a higher resolution survey with a 2-metre electrode spacing was performed from between 48 m and 142 m from the start of the line (Figure 1). This shorter survey (94 m long) gives a shallower and more detailed indication of the resistivity structure over the middle part of line 2. The system automatically performs a series of electrical resistivity measurements using different electrode locations and different electrode spacings. Changing of electrode locations corresponds to changing the lateral location of the measurement. After all the required measurements are made along the line, the data can be processed (inverted).

Test results. The maximum depth of penetration of the resistivity test was 20 meters; which is proportional to the length of the line. The data was inverted and corrected for topography. The interpreted resistivity results and their comparison with the borehole data are presented in Figures 3 to 5 and in Table 1. This table shows a maximum error of -19% in the estimation of the depth of the hard layer (till). The corresponding resistivity pseudosections are given in Appendix B. Both cross-sections for lines 1 and 2 generally show two obvious layers, a high conductivity (up to 13.2 mS/m) layer overlying a lower conductivity layer (as low as 2 mS/m).

The interpreted resistivity pseudosection over line 1 (Figure 3) shows two main layers. In a homogeneous material with a shallow water table, two layer conductivity structure can be expected, with a low conductivity unsaturated zone overlying a higher conductivity saturated zone. The fact that the sections show the opposite situation (high conductivity overlying low) means that there must be some lithology change at the interface between the two main layers. A sharp change in pore water chemistry at the interface is unlikely. The simplest lithological system that is consistent with these results is an upper clay rich layer and a lower layer containing more sands, silts and gravels. The less conductive material likely represents the hard bottom layer (conductivities between 2 and 4 mS/m). The top layer shows higher conductivity values (between 12.5 and 13.2 mS/m). The thickness of the top layer varies from 2.4 m to 6.5 m (Table 1, Figure 3); which corresponds to the first three layers identified from the borehole data (total thickness from 3.5 m to 7.2 m). There is not enough resolution in the resistivity data to determine the location of the first three layers in line 1; however, the depth of the competent layer (till) matches well the depth obtained from boreholes (less than 17% error).

The conductivity around the creek (Figure 1-B, Appendix B) is lower than the conductivity of the top layer; indicating that the conductivity of the fresh water is smaller than the conductivity of the pore water in of the top layer. The hard or till layer identified in Figure 3 shows a feature that seems to be an old channel (6.2 m deep, 12 m wide) centered at 88 m from the start of the line; this feature is also in good agreement the data from BH 5.

Table 1: Summary of electrical conductivities (σ) and layer thicknesses (H) from electrical resistivity surveys and boreholes (BH) for Lines 1 and 2. Values in parenthesis represent the error in the depth of the hard layer according to borehole information.

Layer	Line 1 (spacing = 4 m)			Line 2 (spacing = 4 m)			Line 2 (spacing = 2 m)		
	σ (mS/m)	H (m)	BH - H (m)	σ (mS/m)	H (m)	BH - H (m)	σ (mS/m)	H (m)	BH - H (m)
1	12.5- 13.2	2.4 - 6.5	0.6 - 1.4	7.6 - 9.7	2.0 - 4.0	0.5 - 1.2	9.0 - 13.2	0.6 - 1.9	0.5
2			1.0 - 1.7			1.5 - 3.2	7.6-9.7	1.9 - 3.2	3.2
3			1.9 - 4.1			3.8 - 8.6	10.4-13.2	3.8 - 4.9	6.4
4	2.0-4.0	4.5	5.4	2.0- 4.0	9.5	9.4	2.0 - 4.0	8.2	10.1
Depth		(-17%)			(+1%)			(-19%)	

The interpreted resistivity pseudosection for line 2 (Figure 4) shows three main layers. The thickness of the top layer varies from 2.0 m to 4.0 m (Table 1); which corresponds to the first two layers identified from the borehole data (total thickness from 2.0 m to 4.4 m). There is not enough resolution in the resistivity data to determine the location of the first layer. The depth of the interface between the sand and the clay layers as well as the depth of the till layer are in good agreement with the depths obtained from boreholes (less than 10% error); as it was the case of Line 1. The depth of the hard layer varies from 5.5 m to 10.0 m for horizontal distances between 40 m and 140 m; thus, the average slope of the bottom layer in this subsection is 4.5%. Figure 5 shows the interpreted higher resolution pseudosection (line 2, from 48 m to 142 m, spacing $\Delta x = 2$). This subsection shows four main layers. The interface of the sand and clay layers is in good agreement with the borehole (BH) information (less than 5% error, Table 1); whereas, the location of the till layer shows a 19% error with respect to BH data. The thickness of the first layer is not identified correctly from the resistivity data likely because of variations in water content and capillary rise created by the shallow depth of the water table (approximately 2 m, BH 1, 3, and 7). The measured elevation of the water surface in the pond was 96.9 m; assuming good hydraulic contact between the pond and the surrounding soil, the saturated zone is higher than this elevation due to capillary action.

There is a discrepancy between the conductivity values obtained for the top layers in lines 1 and 2 (Figures 3 and 4). Line 1 shows an average conductivity for the top layer of 12.8 mS/m (Table 1); whereas line 2 presents average value of 8.6 mS/m (32% smaller). A possible explanation is that parts of line 2 are sheltered with trees and line 1 has no trees. The trees may cause a decrease in soil moisture by the moisture uptake through roots.

6.2 Seismic refraction

This method measures the velocity of seismic body waves (compressional or shear waves) as they are refracted from different layers in the subsurface (Figure 6). A refraction survey requires an array of equally spaced geophones, which measure vertical or horizontal motion, and a seismic source, such as a sledgehammer, weight drop, or explosive charge. Seismic traces (velocity versus time) are collected from the geophone array for several source locations along the line. Seismic refraction surveys analyze the first arrival event to the geophone array. For the geophones located closest to the source, the first arrival event is usually the direct wave from the source. This direct wave propagates entirely in the upper medium and is a measure of the wave velocity of the near surface medium.

For a two-layer medium (low velocity layer over a higher velocity half-space), there is a distance from the source where body waves that are refracted along the interface between the layers arrive faster than the direct wave (Figure 6). The first arrivals at greater distances from the source correspond therefore to the refracted waves. A plot of first arrival times versus distance for the two-layer medium shows two linear events. Relationships, such as the plus-minus method (Hagedoorn 1959) and the generalized reciprocal method (Palmer 1980) have been developed to determine the medium velocities and depths of different layers even if the interfaces are irregular. In addition, the ray tracing modelling technique can be used (Cerveny et al. 1974) to account for horizontal and vertical velocity gradients within the layers. One of the limitations of the seismic refraction is the inability to detect inverse layering (shear wave velocity decreasing with depth), which is the case for this site. Thus if there is a stiff layer after the first layer, the second layer is inverted with an average velocity and the depth of the third layer is not accurately determine. The basic theory of the refraction test is given in Appendix C.

Equipment and testing procedure. The seismic refraction survey was performed using a 48-channel seismograph (Geode seismic recorder) and horizontal 50 Hz-geophones. The geophone spacing was 1 metre for a total spread length of 47 metres. The top soil was removed at the location of the geophones and the seismic source to enhance the coupling of the equipment with the ground. Good coupling is required to increase the signal-to-noise ratio. Seismic refraction surveys were completed for lines 1-1, 1-2, 2-1, 2-2, and 2-3 (Figure 1). The seismic source was a 5-pound sledgehammer; shear waves were

generated by hitting a c-shape steel plate in the direction perpendicular to the geophone line (Figure 7). The edges of the c-plate were partially inserted into the ground to enhance the coupling between the plate and the ground. Seismic traces were collected for source offsets of 0.5 m, 10 m, and 20 m at the left and right hand sides of the geophone array. In addition, the source was located at the centre of the array. The source offsets were selected in the field so that sufficient refraction from the shallow and deep layers was obtained. The farthest offset shots for line 1-2 were placed at 18 m because of the interference of Nash road (Figure 1). For each source location, positive and negative polarity shear waves were generated by hitting the steel plate in opposite directions. The change in wave polarity is used to enhance the interpretation of the first arrival times. Five blows on either side of the plate were recorded and stacked to improve the signal-to-noise ratio.

Test results. The reciprocal method (Appendix C) was used to determine the layer transmission velocities and approximate depths to layer interfaces in each line. The results from the reciprocal method for lines 1 and 2 are summarized in Appendix D (Tables 1-D and 2-D; Figures 1-D to 5-D). This analysis revealed two main refracting boundaries throughout the site. The velocity values are in the range of expected velocities for the site; however, the layers are not correctly identified in this method. The top layer in line 1 seems to represent layers 1 and 2 from the BH data. There is not enough resolution in the reciprocal analysis to determine the location of the first layer in lines 1 and 2.

The depth of the hard layer (till) using seismic refraction cannot be obtained accurately because of the hard layer of sand located at 1.4 m (velocity inversion, Appendix C). For comparison purposes, the predicted depths of the hard layer were shifted in Figures 1-D to 5-D to match the depth of the till layer according to the data from only one of the boreholes. The variation of depth for the till layer in line 1-1 is predicted correctly (less than 10% error). However, the depth variation for this layer is computed reliably only for the first ten meters of line 1-2 using the reciprocal method.

A tomographic inversion (ray tracing method, Menke 1999) was then completed for each line by inputting the velocities and approximate depths obtained from the reciprocal analysis using the software Seisimager/2D. The results from three-layer tomography models for lines 1 and 2 are shown in Figures 8 to 12. The ray tracing method generally shows the same trends as the reciprocal method; however, the interfaces are more regular because the ray tracing inversion uses regularization that forces the interfaces to be smooth. The reciprocal analysis is less accurate than the tomographic inversion because of the difficulties in accurately selecting the change in the travel time slope (Figure 3-C) due to the presence of the second and third layers. The velocity values are in the range of expected velocities for the site; however, there is a significant variation in the computed wave velocities for shallow layers (up to 150%). The average velocities and layer thicknesses are given in Tables 2 and 3 (percentage errors in the

depth of the hard layer given in parenthesis). For line 1 (Table 2), the depth of the first layer and the depth of the till layer are in good agreement with the borehole data. As expected, the thickness of the second layer cannot be identified from refraction data because of the velocity inversion (Appendix C).

Table 2: Summary of shear wave velocities (Vs) and layer thicknesses (H) from refraction surveys (tomographic inversion) and boreholes (BH) for Lines 1-1 and 1-2.

Layer	Line 1-1			Line 1-2		
	Vs (m/s)	H (m)	BH - H (m)	Vs (m/s)	H (m)	BH - H (m)
1	115	1.4-1.6	1.3-1.4	130	0.8-1.2	1.10
2	440	3.7-4.7	1.0-1.3	460	2.8-4.5	N/A
3			1.9-3.8			4.1
4 Depth	760	5.7 (+6%)	5.4	760	4.7 (-10%)	5.2

Table 3: Summary of shear wave velocities (Vs) and layer thicknesses (H) from refraction surveys (tomographic inversion) and boreholes (BH) for Lines 2-1, 2-2, and 2-3.

Layer	Line 2-3			Line 2-1			Line 2-2		
	Vs (m/s)	H (m)	BH - H (m)	Vs (m/s)	H (m)	BH - H (m)	Vs (m/s)	H (m)	BH - H (m)
1	130	1.1-1.4	0.6-1.4	125	1.9-2.1	0.5-1.2	125	1.6-2.1	0.5-0.6
2	380	5.3-3.4	1.3-1.7	410	6.1-7.6	1.7-3.2	430	7.0-7.9	1.5-3.2
3			1.9-6.1			6.1-6.4			6.4-8.6
4 Depth	810	5.6 (-14%)	6.5	805	8.9 (-7%)	9.6	900	9.3 (-11%)	10.4

For line 2 (Table 3), the depth of the first layer is not clearly defined in this line; thus the error with respect to the borehole data varies from 24% to more than 200%. The refraction inversion shows a transition zone between first and the third layer instead of clear interfaces. There is also a transition zone between the clay layer and the till layer. The depth of the till layer is generally in good agreement with the borehole data (between 7% and 14% error). In general, the depth of the till layer differs in +/- 1 m from the borehole data.

6.3- Spectral analysis of surface waves (MASW).

When a seismic pulse is created on the surface on an elastic medium, seismic waves propagate through the medium. Most of the energy is in the form of surface waves, known as Rayleigh waves; which are similar to ripples in a pond. These waves propagate near the surface boundary of the medium. They cause both horizontal and vertical particle displacement. In the presence of different soil layers, the surface wave velocity depends not only on the properties of the medium but also on the frequency content of the excitation (Graff 1991). High frequencies (short wavelengths) propagate at the velocity of the first layer; whereas, low frequencies (large wavelengths) propagate at a velocity determined by the characteristics of different layers. Their depth of penetration into the medium is a function of their wavelength, with longer wavelengths penetrating deeper into the medium. A schematic representation of the test setup is shown in Figure 13. The curves of different colours represent surface waves of different wavelengths thus different penetration depths. The velocity of Rayleigh waves is similar to the shear wave velocity of the medium, with a maximum difference of 5% (Richart et al., 1970, Park et al. 1999). Rayleigh waves can be used to determine the shear profile of a medium. The effective depth of penetration of a surface wave is commonly taken as 1/3 the wavelength. The basic theory of the MASW test is given in Appendix E.

Equipment and testing procedure. The MASW and REMI data was collected at the same locations and using similar equipment as the seismic refraction data. MASW and REMI surveys were completed for lines 1-1, 1-2, 2-1, 2-2, and 2-3 (Figure 1). Three source offsets were chosen (2 m, 6 m, and 20 m) to either side of the lines. The shorter offset is used to study the propagation of high frequencies (shallower layers); whereas the larger offset is used to study the propagation of low frequencies (deeper layers). The surface wave and REMI surveys were performed using a 48-channel seismograph (Geode seismic recorder) and low-frequency vertical 4.5 Hz geophones. The geophone spacing was 1 metre for a total spread length of 47 metres. The top soil was removed from the selected source locations and geophone locations to enhance the coupling between the source, the geophones and the ground (Figure 14a). The seismic source was a 170-pound drop-weight that was selected to generate low frequencies (Figure 14b). Different seismic sources were tested to select the source capable of generating lower frequencies. To

improve the energy transmission in the sledgehammer test, a new plate was designed in the shape of a dumbbell. The new plate has a rubber sheet between the cap and the top plate to generate more energy at low frequencies and to reduce the energy lost during the bouncing of the hammer. Ambient vibrations coming mostly from the roads near the site were used in the REMI method to enhance the resolution at low frequencies (deeper layers).

Test results. MASW and REMI inversion was completed for each line using the computer package SWAN. The resulting four-layer models from the inversion for line 1 are presented in Figures 15 and 16, and the corresponding interpreted soil profile in Figure 17. This figure shows that the first two layers in line 1-1 are identified correctly by the MASW tests; however, the location of the till layer is underestimated by 24%. The results from the shot locations at the left and right hand sides of the array (minus and plus in the plots) generally show good agreement, thus, the layers are mainly horizontal. The N-values from the borehole data (BH-5) in line 1-1 show a linear increase with depth starting at $H = 4$ m; which is the depth of the stiff (till) layer according to the MASW results. The location of the till layer in borehole EL-17-3 (Figure 17) shows a good agreement with the results from the MASW tests but the thicknesses of the first two layers are not predicted correctly. Nevertheless, this borehole is located almost 50 m away from the end of line 1. The average shear wave velocities for the top layers are in agreement with the results from the seismic refraction test but the velocity of the till layer is 55% higher.

The computed and measured dispersion curves for line 1 are given in Appendix F (Figures 2-F to 7-F). The sensitivity of the inverted velocity profile to the thicknesses of the layers was evaluated by taking the final models (Figures 15 and 16) and successively changing the thickness of the first two layers by ± 0.5 m, and the thickness of the third layer by ± 1 m. The results, given in Appendix F, show that the thickness of the first layer has a significant effect on the modeled dispersion curve; because, it affects the depths of all layers in the profile. Conversely, the thickness of the third layer can be increased by one metre without causing a significant change in the dispersion curve; hence, the depth of the till layer could be increased by one metre (Figure 17) without a significant effect on the results.

For line 2, the resulting four-layer models are given in Figures 18 to 20; the corresponding interpreted soil profile is shown in Figure 21. The MASW profiles are in general in good agreement with the borehole information. However, the depth of the till layer is consistently underestimated (up to 30%). The borehole data shows that the increase in N-values generated by the presence of the till layer is observed even before the till layer; this result is in agreement with the MASW results that show consistently a shallower depth for the till layer. The soil profile obtained from the MASW test is governed by changes in the impedance (wave velocity and density) of the layers. The significant reduction in N-values shown in BH 8-04 is not observed in the shear wave velocity profile (Figure 20);

which suggests that the clay layer is a soft-to-stiff soil according to its shear wave velocity (200 m/s; NBCC 2005) and not a soft soil according to the standard penetration resistance ($N < 15$). The computed and measured dispersion curves for line 2 are given in Appendix G (Figures 2-G to 18-G). The sensitivity of the inverted velocity profile to the thicknesses of the layers was evaluated by taking the final models (Figures 18 to 20) and successively changing the thickness of each layer by ± 1 m. The results show (Appendix G,) that the thicknesses of all the layers have a significant effect on the modeled dispersion curve. Contrary to the previous results for line 1, the thickness of the third layer has a significant effect on the modeled dispersion curve; because, the thickness of this layer represents between half and two thirds of the total depth of the soil profile in line 2.

The summary of average velocities and layer thicknesses for lines 1 and 2 are given in Tables 4 and 5, respectively. The results show a velocity inversion between the second and third layer (e.g. decrease in shear wave velocity after the second layer). This layer was not identified in the seismic refraction data because of the limitation of the refraction method mentioned before. On the other hand, the presence of a velocity inversion makes the analysis of surface wave tests also more complex and requires the consideration of higher modes. The results presented in Appendices F and G show that effects of higher modes are more important for line 1. Thus, the MASW results for line 2 are more reliable than the results for line 1. The velocity inversion acts as a low-pass filter reducing the penetration of large wavelengths into the ground. One of the limitations of the MASW method is the lower resolution in the definition of deeper layers if the generation of frequencies below 15 Hz is limited. The drop-weight source used in this project generated low frequencies but they were not strong enough to have a better resolution of the deeper layers. For future MASW tests, the drop-weight source should be modified to enhance the generation of low frequencies. Possible modifications include the use of a heavier weight (>170 pounds) and a larger area of impact. The error in the estimation of the depth of the hard layer was smaller than 24% for line 1; whereas, it reached 30% for line 2. These are average errors relative to the information obtained from boreholes; which obviously represent measured values at single points.

Table 4. Summary of shear wave velocities and layer thicknesses from MASW tests for Line 1. Percentage errors in the depth of the hard layer given in parenthesis.

Layer	Line 1-1			Line 1-2		
	V _s (m/s)	H (m)	BH - H (m)	V _s (m/s)	H (m)	BH - H (m)
1	119	1.42	1.4	115	1.49	1.1
2	433	1.13	1.2	423	1.82	N/A
3	295	1.62	2.9	334	1.87	4.1
4 Depth	1266	4.2 (-24%)	5.4	1160	5.2 (0%)	5.2

Table 5: Summary of velocities and layer thicknesses from MASW test for Line 2. Percentage errors in the depth of the hard layer given in parenthesis.

Layer	Line 2-3			Line 2-1			Line 2-2		
	V _s (m/s)	H (m)	BH - H (m)	V _s (m/s)	H (m)	BH - H (m)	V _s (m/s)	H (m)	BH - H (m)
1	90	0.92	1.1	80	0.71	0.9	62	0.60	0.60
2	423	1.95	1.6	408	1.50	2.5	320	1.36	2.40
3	218	3.14	3.9	212	5.20	6.3	188	5.44	7.50
4 Depth	662	6.0 (-9%)	6.5	736	7.4 (-24%)	9.6	569	7.4 (-30%)	10.4

7- Laboratory testing and CPT tests

Shear wave velocity and electrical conductivity tests were performed in the laboratory and in the field on selected soil specimens to compare laboratory and field results. The testing program included resonant column tests, pore-water conductivity measurements, soil conductivity measurements, and cone penetration tests. Cone penetration tests were performed in-situ to estimate shear wave velocities and electrical conductivities in-situ using a different method. Resonant column tests and electrical conductivity measurements were performed on soil samples extracted from the boreholes: BH08-03, BH08-04, BH08-06, and BH08-07.

7.1- Resonant column tests

The results of resonant column tests tested using Stokoe type resonant column (RC) apparatus according to the standard ASTM D4015-92 are presented next. This device permits testing a specimen under axisymmetric loading in steady state vibration. This device operates at small shear strains between 10^{-6} and 10^{-3} . Two parameters are obtained from resonant column measurements: resonant frequency and damping coefficient. Wave velocity and attenuation are computed from these measurements. The computation of the damping coefficient assumes an equivalent, uniform, linear viscoelastic specimen. The shear strain varies radially throughout the specimen; the representative value most often selected is the volumetric average shear strain.

Specimen preparation and testing methodology. The specimens were extracted from the Shelby tube using a hydraulic sample extractor. After removing the coverings, the weights and dimensions of the specimens were recorded. The specimens were then placed into a rubber membrane using a membrane holder and then placed in resonant column apparatus. The isotropic confinement was increased to achieve effective confinement equal to the effective vertical stress on the specimen.

At the specified effective confinement, each specimen was allowed to consolidate for 2 hours; then, the RC test was performed. Dynamic properties were evaluated using drained conditions. RC tests were performed first at low shear strain levels ($\gamma < 10^{-5}$); then the dynamic properties were evaluated at larger shear strain levels (maximum capacity of the RC device). A summary of the resonant column results and specimen properties is given in Table 6. The degradation curves for the specimens tested are presented in Appendix H. The experimental setup used for resonant column testing is presented in Appendix I. Sand specimens were not tested because the samples were completely disturbed (Appendix I).

Table 6: Summary of resonant column results and specimen characteristics.

Specimen	Confinement [kPa]	Depth [m]	Initial unit weight [kN/m ³]	Water content w [%]	Shear velocity [m/s]	Damping ratio [%]	Resonant frequency [Hz]
08-3 SH #1	76.7	4.88	19.5	19.5	53.5	3.90	17.2
08-4 SH #1	94.6	6.40	20.0	25.1	50.0	3.40	18.0
08-4 CS	215.9	14.33	22.8	20.1	381.2**	0.93	126.0
08-6 SH #2	25.8	1.22	21.2	12.3	84.5	5.28	29.3
08-7 SH #1	19.6	0.91	21.5	11.0	148.7*	9.50	50.1*
08-7 SH #5	109.2	7.93	19.9	26.3	58.9	3.32	19.1

Notes: * Extrapolated value, ** Velocity corrected for the stiffness of the device

The measurement of shear wave velocities and material damping ratios using the resonant column device were performed also using the non-resonant method (Khan et al. 2007), which allows the evaluation of wave velocity and damping as function of frequency. The summary results from the non-resonant, CPT, and geophysical tests is presented in Table 7.

The frequency content of the measured signals in CPT tests is critical for the correct interpretation of results. During CPT tests, the frequency content of the source was measured by placing four vertical and four horizontal geophones around the seismic source. The location of geophones, time traces, and Fourier spectra of the signals recorded at the ground surface are presented in Appendix J. The frequency ranges used in resonant column, CPT, and MASW tests are also summarized in Table 7.

The wave velocities computed from CPTs for deeper layers (depth > 4 m, silty clay) are generally in very good agreement with the values obtained from the MASW tests and the stratigraphy obtained from boreholes. The wave velocities for the shallower layers (depth < 4m, sand and silt) are significantly underestimated or overestimated (-150% to +50%) because the main wavelengths generated in these tests are between 2 m to 3.5 m (main frequencies between 60 Hz and 80 Hz, Appendix J). Thus, the computed wave velocities for shallow layers are affected by near-field effects and the relatively high velocity of the sand layer close to the ground surface.

The resonant column results are in good agreement with MASW test results and the stratigraphy indicated by borehole data only for superficial layers (depth < 1 m). The wave velocities for the silty clay and the till are significantly underestimated up to -250% and -63%, respectively, by the resonant column data measurements. The higher the clay content in the soil the larger is the underestimation of wave velocity in resonant column results. This underestimation is likely due to two main factors: sample disturbance and the generation of excess pore pressure during the extraction of the specimens from the Shelby tube. To evaluate the effect of the later factor, a clay specimen will be tested in the resonant column after allowing the sample to consolidate for a full week.

7.2- Measurements of soil and pore-water electrical conductivity

The results of laboratory measurements of electrical conductivity of five cylindrical soil specimens and of in-situ measurements of pore-water electrical conductivity are presented next. The experimental setup used for these measurements is given in Appendix I. The summary of conductivity tests on water samples from BH 8-03, BH 8-04, and BH 8-05 is also given in Appendix I.

Specimen preparation and testing methodology. The cylindrical soil specimens have an average diameter and length of 6.3 cm and 16.0 cm, respectively. Each measurement was completed by connecting the soil specimen in series with an amp meter and a power supply. An alternating voltage of 10 V peak-to-peak with a frequency of 500 Hz was used. The experimental setup was calibrated against conductivity measurements in de-ionized water with various salt concentrations using a conductivity meter (HACH CO150). The calibration showed good agreement between the two measuring techniques (Appendix I). Stainless steel wire mesh electrodes were used at the two opposing circular faces of the specimens. The ends of the sample were wetted with de-ionized water before applying the electrodes and the electrodes were held in place using elastic bands to improve the contact. The potential drops across various intervals along the length of the sample were also measured using two 1.6 mm diameter stainless steel electrodes. These electrodes were pushed up to the centre of the specimen in four different arrangements. Five-centimetre spacing measurements were taken along the length of the specimen (centre, centre left, and centre right); and, a ten-centimetre spacing measurement was taken at the centre of the specimen. The conductivity of the specimen is computed as the average of these four measurements.

The comparison of electrical conductivity measurements in the field and in the laboratory is given in Table 8. Field and laboratory measurements are in good agreement. The conductivity of the pore-water is larger than the conductivity of the soil as expected (Archie's Law).

Table 7: Comparison of results from resonant column, CPT, and geophysical tests.

	Resonant Column				MASW			Refraction		CPT Test			
	Depth m	Vs m/s	f-range Hz	D-ratio %	Depth m	Vs m/s	f-range Hz	Depth m	Vs m/s	Depth m	Vs m/s	f-range surf. Hz	f-range Hz
BH 08-3					0.46	90	13 - 44	0.75	130				
					1.90	423							
	4.88	62	22 - 50	4.6	4.44	218		3.55	380	3.04	191	25-200	12-200
					6.01	662		5.60	810	5.77	320	25-200	12-200
BH 08-4					0.30	62	9 - 26	0.93	125				
					1.28	320							
	6.40	61	22 - 50	3.8	4.68	188		5.58	430	4.92	242	10-140	10-200
	14.33	348	125 - 137	1.2	7.40	569		9.30	900	8.64	228	10-140	10-200
BH 08-6					0.71	119	16 - 37	0.75	115				
	1.22	90	25 - 45	5.8	1.99	433				2.76	118	25-200	10-150
					3.36	295		3.45	440	4.27	272	25-200	10-150
					4.17	1266		5.70	760				
BH 07-7					0.33	71	10 - 30	0.96	125				
	0.92	149	45 – 55	9.5	1.63	364							
					5.01	200		5.51	420	4.50	307	20-150	10-175
	7.93	57	22 - 50	3.5	7.40	653		9.10	858	8.52	225	20-150	10-175

Notes: Vs: shear wave velocity; f-range: frequency range of the measurement; f-range surf.: frequency range of the signals measured at the surface; D-ratio: material damping ratio.

Table 8: Comparison of electrical conductivity measurements.

	Field Measurements				Lab Measurements		
	Depth m	σ_{soil} mS/m	Dtw m	σ_{water} mS/m	Depth m	σ_{soil} mS/m	w %
BH 08-3	1.2	7.6 - 9.7	1.48				
	4.2	10.4 - 13.2					
	6.1	2.0 - 4.0		53.8	15.6	1.4	9
BH 08-4	1.1	7.6 - 9.7	0.70				
	6.4	10.4 - 13.2					
	10.7	2.0 - 4.0		34.2	7.6	2.6	26
BH 08-5	3.1	12.5 - 13.2	1.18				
	6.1	2.0 - 4.0		49.6			
BH 08-6	2.3	12.5 - 13.2			3.1	18.8	18
	4.6	2.0 - 4.0					
BH 07-7	1.9	7.6 - 9.7			3.8	9.1	19
	6.9	10.4 - 13.2			6.1	31.6	21
	10.1	2.0 - 4.0					

Notes: dtw: depth to water; σ : electrical conductivity.

8- Summary and Conclusions

- The most suitable geophysical methods for MTO projects were found to be electrical resistivity imaging, seismic refraction method, and the multiple-channel analysis of surface waves (MASW) method.
- These three geophysical methods were used at a test site (1881 Nash Road). The resistivity tests were conducted on two 188-m-long survey lines and one higher resolution 94-m-long survey line. The seismic refraction and MASW tests were performed on five 48-m-long survey lines (1-1, 1-2, 2-1, 2-2, and 2-3); which overlapped with the resistivity lines.
- A geotechnical investigation consisting of six boreholes was conducted in the site to be used as ground truthing. The results from each geophysical test were analyzed and compared with the data from the boreholes. The electrical resistivity method gave the best indication of the depth of the till layer (less than 19% error). On the other hand, the MASW tests gave the best indication of the layering in the area. The MASW tests were able to identify the velocity inversion generated by the presence of a hard sand layer. The maximum average error in the evaluation of the depth of the hard layer was 30% with respect to the borehole information.
- The comparison of the shear velocities and average values obtained from the seismic refraction and the MASW tests is given in Tables 9 and 10. The average velocities show the presence of four main units: top soft layer, underlain by a dense layer, followed by a medium dense layer, and the hard layer at bottom (depths between 5 and 10 m). The maximum difference in wave velocities between MASW and refraction tests is observed for the hard (till) layer in line 1 (66%), this difference is likely caused by the effect of high modes in the MASW data. The mean values given in the table for the till layer are computed by giving more weight to the refraction data. The refraction tests were not able to identify the presence of the velocity inversion (stiff layer underlain by softer material); and the expected reliability of the MASW data was reduced by this type of stratigraphy. The reliability and variability of the results from both methods in a typical stratigraphy of increasing stiffness with depth would be better than for the tested site. Especially if soft layers are underlain by a stiff bottom layer, as it could be expected in other MTO projects close to swamps and wetlands. In this case, hydrophones should be used instead of the standard geophones. The resistivity tests would require some modification of the electrodes for the use in swamp areas.
- Tables 11 to 14 summarize the thicknesses of all the layers identified as well as the average depth of the hard (till) layer. The use of complementary information from the three geophysical methods allow the evaluation of the depth of the hard layer with less than 10% error for line 1; whilst, the error was less than 23%. In average, the depth of the till layer is underestimated by the geophysical techniques in comparison with the values from borehole information. It is likely that the transition zone between the silty clay layer and the hard till layer is stiff enough to generate a significant increase in shear wave

velocities so that the seismic methods detect the till layer before the depth indicated by the borehole data.

- For the application of the geophysical tests in other MTO projects located in swamp areas the following testing guidelines are recommended: **a)** Perform electrical resistivity tests using two different electrode spacing for low and high vertical resolution. The maximum penetration of the resistivity tests could be approximately taken as one tenth of the total length of the array. Thus, a 48-electrode array spaced at 4 m could provide layering information up to 20 m depth, and a 2 m spacing could provide information up to 10 m depth. **b)** Perform a preliminary inversion of the resistivity data in the field to guide the selection of the hydrophone spacing to be use in MASW and seismic refraction tests. **c)** Perform MASW tests using vertical hydrophones with two different hydrophone spacings to generate a low and a high vertical resolution soil profiles. The maximum penetration depth of surface waves can be estimated as one-half of the length of the array. A 48-hydrophone array with 1 m spacing would provide information up to 20 m depth; whereas a spacing of 0.5 m would provide information up to 10 m depth. At least five source locations should be used: two at each side of the hydrophone array and one in the middle of the array. At each source location, at least three shots should be performed to compute an average soil profile. The hydrophones should have a resonant frequency no less than 4.5 Hz. The length of the spike of the hydrophones should be selected according to the stiffness of the top layer. Different spike lengths should be tested before the actual site investigation to select the optimum length. A short spike (0.1 m) would not provide a good coupling in swamp areas; whereas a long spike could modify the response of the hydrophone. The seismic weigh-drop source has to be also modified for a swamp area. In desolated areas, a buffalo gun source could be an alternative. Preliminary MASW tests should be performed in a typical swamp are to select the optimum source, hydrophone coupling, and hydrophone spacing. Once that basic characteristics of the swamp area are measured (wave velocities, layer thickness, resistivity), computer simulations of MASW tests can be used as an economic alternative to select the optimum testing configuration. **d)** Perform seismic refraction tests using horizontal hydrophones, as in the case of the MASW tests, two different hydrophone spacing should be used: low resolution for deeper layers (1 m to 2 m hydrophone spacing), and high resolution for superficial layers (0.25 m to 0.50 m hydrophone spacing). High-resolution surveys could be performed using flexible spacers between hydrophones to speed up the field-testing.
- Laboratory and field measurements of wave velocity and electrical conductivity in general showed good agreement. CPT requires a higher frequency seismic source to improve the accuracy for shallow layers. Resonant column tests on clays are significantly affected by the excess pore pressure produced during sample extraction and sample disturbance.

Table 9: Comparison of shear wave velocities (V_s) from refraction and MASW tests. Lines 1-1 and 1-2. The values in parenthesis (MASW test) represent the average velocity for layers 2 and 3.

Layer	Line 1-1			Line 1-2		
	Refraction (m/s)	MASW (m/s)	Mean (m/s)	Refraction (m/s)	MASW (m/s)	Mean (m/s)
1	115	119	117	130	115	120
2	440	433	430	460	423	420
3		295 (364)	295		334 (378)	330
4	760	1266	900	760	1160	900

Table 10: Comparison of shear wave velocities (V_s) from refraction and MASW tests. Lines 2-1, 2-2, and 2-3. The values in parenthesis (MASW test) represent the average velocity for layers 2 and 3.

Layer	Line 2-3			Line 2-1			Line 2-2		
	Refraction, (m/s)	MASW (m/s)	Mean (m/s)	Refraction (m/s)	MASW (m/s)	Mean (m/s)	Refraction, (m/s)	MASW (m/s)	Mean (m/s)
1	130	90	100	125	80	100	125	62	95
2	380	423	400	410	408	410	410	320	365
3		218 (320)	220		212 (310)	215		188 (254)	200
4	810	662	740	805	736	750	900	569	730

Table 11: Comparison of layer thicknesses (H) from resistivity, refraction, and MASW tests. Lines 1-1 and 1-2. The values in parenthesis (MASW test) represent the average thickness for layers 2 and 3.

Layer	Line 1-1			Line 1-2		
	Refraction (m)	MASW (m)	Resistivity (m)	Refraction (m)	MASW (m)	Resistivity (m)
1	1.4 - 1.6	1.4	2.4 - 6.5	0.8 - 1.2	1.5	2.4 - 6.5
2	3.7 - 4.7	1.2		2.8 - 4.5	1.8	
3		1.6 (2.8)			1.9 (3.7)	
Depth	5.7	4.2	6.5	4.7	5.2	6.5

Table 12: Comparison of average layer thicknesses (H) from resistivity, refraction, and MASW tests with borehole data (BH). Lines 1-1 and 1-2. Percentage errors in the depth of the hard layer given in parenthesis.

Layer	Line 1-1		Line 1-2	
	H (m)	BH (m)	H (m)	BH (m)
1	1.5	1.3 - 1.4	1.2	1.1
2	1.3	1.0 - 1.3	1.8	N/A
3	2.0	1.9 - 3.8	2.0	4.1
Depth (Error)	4.8 (-10 %)	5.35	5.0 (-4 %)	5.2

Table 13: Comparison of layer thicknesses (H) from resistivity, refraction, and MASW tests. Lines 2-1, 2-2, and 2-3. The values in parenthesis (MASW and Refraction tests) represent the average thickness for layers 2 and 3.

Layer	Line 2-3		Line 2-1			Line 2-2		
	Refraction (m)	MASW (m)	Refraction (m)	MASW (m)	Resistivity (m)	Refraction (m)	MASW (m)	Resistivity (m)
1	1.1 - 1.4	0.9	1.9 - 2.1	0.7	1.2	1.6 - 2.1	0.6	1.2
2	5.3 - 3.4	2.0	6.1 - 7.6	1.5	2.5	7.0 - 7.9	1.4	2.5
3		3.1 (5.1)		5.2 (6.7)	4.4 (6.9)		5.4 (6.8)	4.4 (6.9)
Depth	5.6	6.0	8.8	7.4	8.1	9.3	7.4	8.1

Table 14: Comparison of average layer thicknesses (H) from resistivity, refraction, and MASW tests with borehole data (BH). Lines 2-1, 2-2, and 2-3. Percentage errors in the depth of the hard layer given in parenthesis.

Layer	Line 2-3		Line 2-1		Line 2-2	
	H (m)	BH (m)	H (m)	BH (m)	H (m)	BH (m)
1	1.1	1.1	1.3	0.9	1.2	0.6
2	2.0	1.6	2.0	2.5	2.0	2.4
3	3.1	3.9	4.8	6.3	4.9	7.5
Depth (Error)	6.2 (-6 %)	6.6	8.1 (-16 %)	9.7	8.1 (-23 %)	10.5

9- References

- Annual book of ASTM standards, 2002. Standard Guide for Using the Seismic Refraction Method for Subsurface Investigations, ASTM D 5777-00, 04(02), pp. 309-312.
- ASTM D4015-92, 2000, "Standard Test Methods for Modulus and Damping of Soils by the Resonant-Column Method," American Society for Testing and Materials, Annual Book of Standards.
- Cerveny, V., Langer, J. and Psencik, I. (1974): Computation of geometrical spreading of seismic body waves in laterally inhomogeneous media with curved interfaces. *Geophys. J. R. astr. Soc.*, 38, 9-19.
- Graff, K. (1991). Wave motion in elastic solids. New York: Dover publications Inc.
- Gucunski, N., Ganji, V., and Maher, M.H., 1996. Effects of obstacles on Rayleigh wave dispersion obtained from the SASW test. *Soil Dynamics and Earthquake Engineering*, Volume 15: 223-231.
- Gucunski, N., Krstic, V., and Maher, M.H., 1998. Experimental procedures for detection of underground objects by the SASW test. In *Geotechnical Site Characterization*. Edited by Robertson and Mayne, Balkeme, Rotterdam: 469-472.
- Hagedoorn J.G. 1959, The Plus-Minus Method of Interpreting Seismic Refraction Sections, *Geophysical Prospecting* 7, 158–182
- Khan, Z., Cascante, G., and El-Naggar, H., Lai, C.G., 2008. Measurement of Frequency Dependent Dynamic Properties of Soils Using the Resonant Column Device. *Journal of Geotechnical and Geoenvironmental Engineering*, ASCE. In print.
- Kong, F.N., H. Westerdahl, and By, T.L., 1994. Borehole Radar Tunnel Detection at Gjovik, Norway. Norwegian Geotechnical Institute, Publication 194, pp. 1-10.
- McNeill, J. D., 1980. Electrical conductivity of soils and rocks, Geonics Technical Note TN-5, Geonics Limited, Mississauga.
- Menke W., 1989, *Geophysical Data Analysis: Discrete Inverse theory*, International Geophysics Series. San Diego: Academic Press. 289 pp.
- Nasseri, A., Phillips, Cascante, G., C. and Hutchinson, J., 2007. Effects of Underground Cavities on Rayleigh Waves – Numerical and Experimental Study. *Soil Dynamics and Earthquake Engineering*. 27(4): 300-313.
- NBCC 2005. National Building Code of Canada (NBCC) Volumes 1 and 2. 12th edition, National Research Council, Ottawa, Canada.
- Palmer, D., 1980, The Generalized Reciprocal Method of Seismic Refraction Intepretation, in Burke, K.B.S. (Ed.), *Society of Exploration Geophysicists*.
- Park C.B., Miller R.D., Xia J., 1999, Multichannel analysis of surface waves, *Geophysics*, 64(3), 800-808.
- Phillips, C., Cascante, G., and Hutchinson, D.J. 2000. Seismic surface waves to detect underground voids. *Proceedings of the Symposium on the Application of Geophysics to Engineering and Environmental Problems*, Arlington, Virginia: 29-37.
- Richart Jr., F.E.; Hall, J.R. and Woods, R.D., 1970. *Vibration of Soils and Foundations*. Prentice Hall, Inc., Englewood Cliffs, New Jersey.

- Strobbia C., Foti S., 2006, Multi Offset Phase Analysis (MOPA), *Journal of Applied Geophysics*, 56:300-313.
- Strobbia, C., 2002. Surface wave methods: acquisition, processing and inversion. PhD Diss. Politecnico di Torino. Italy.
- Zonge, K., Wynn, J., and Urquhart, S. 2006. Resistivity, Induced Polarization, and Complex Resistivity. In *Near-Surface Geophysics*, Ed. D. Butler, SEG. Tulsa, OK. pp. 357-438

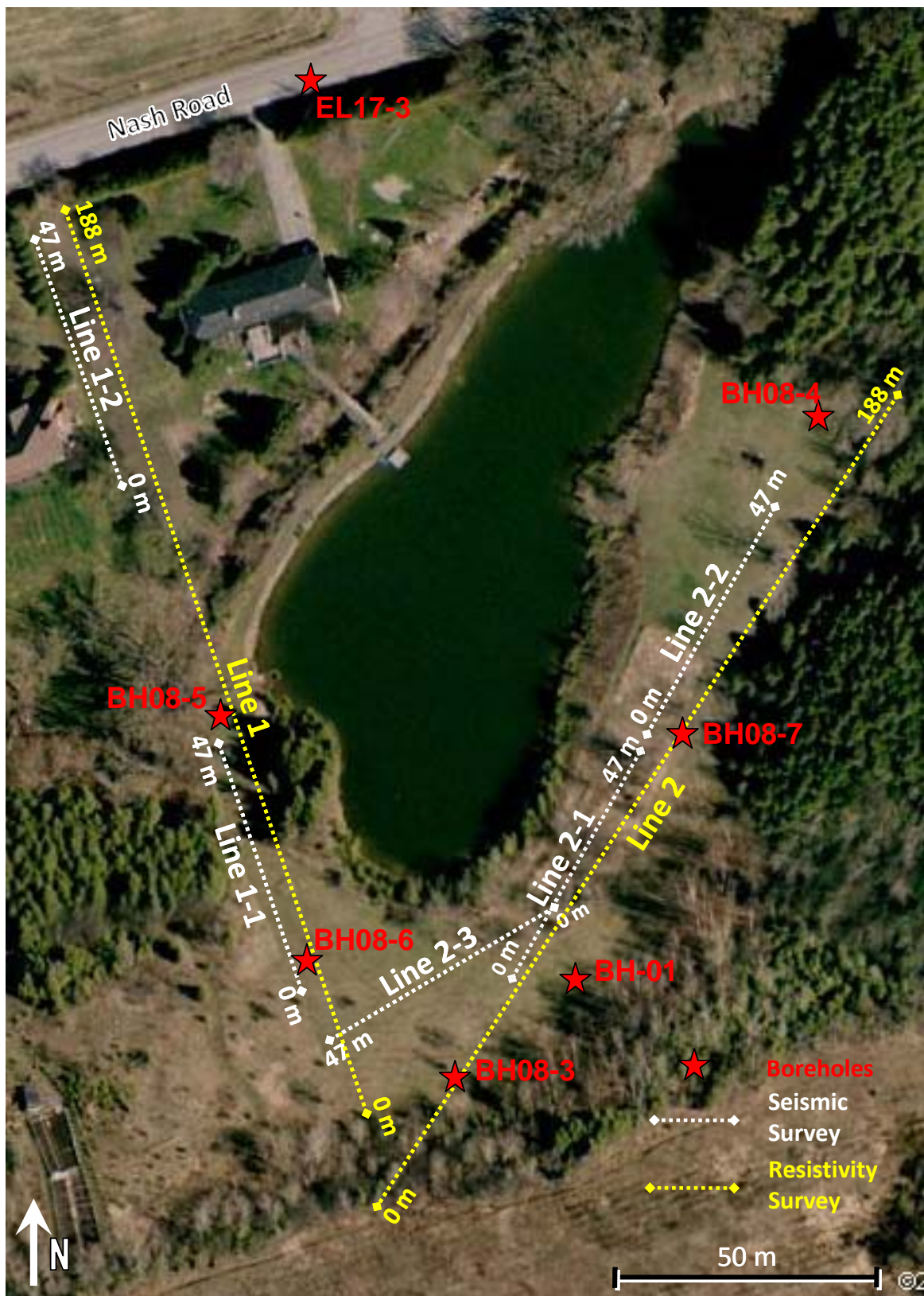


Figure 1: Location of survey lines and boreholes

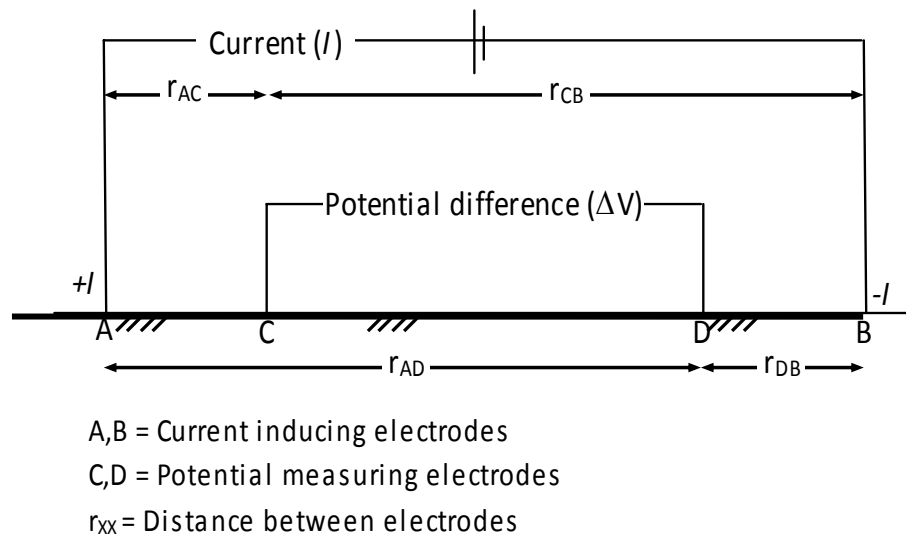


Figure 2: General electrode configuration for an electrical resistivity survey

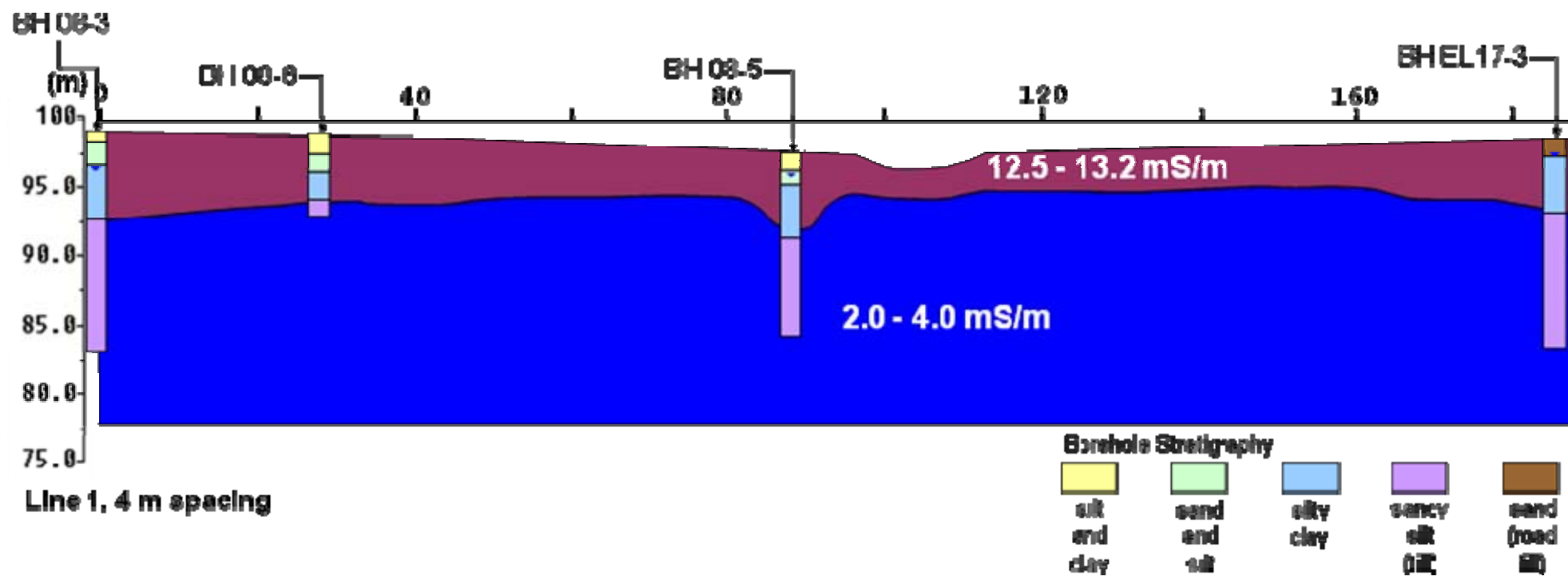


Figure 3. Interpreted conductivity pseudosection and boreholes for Line 1 (4 m electrode spacing, Appendix B)

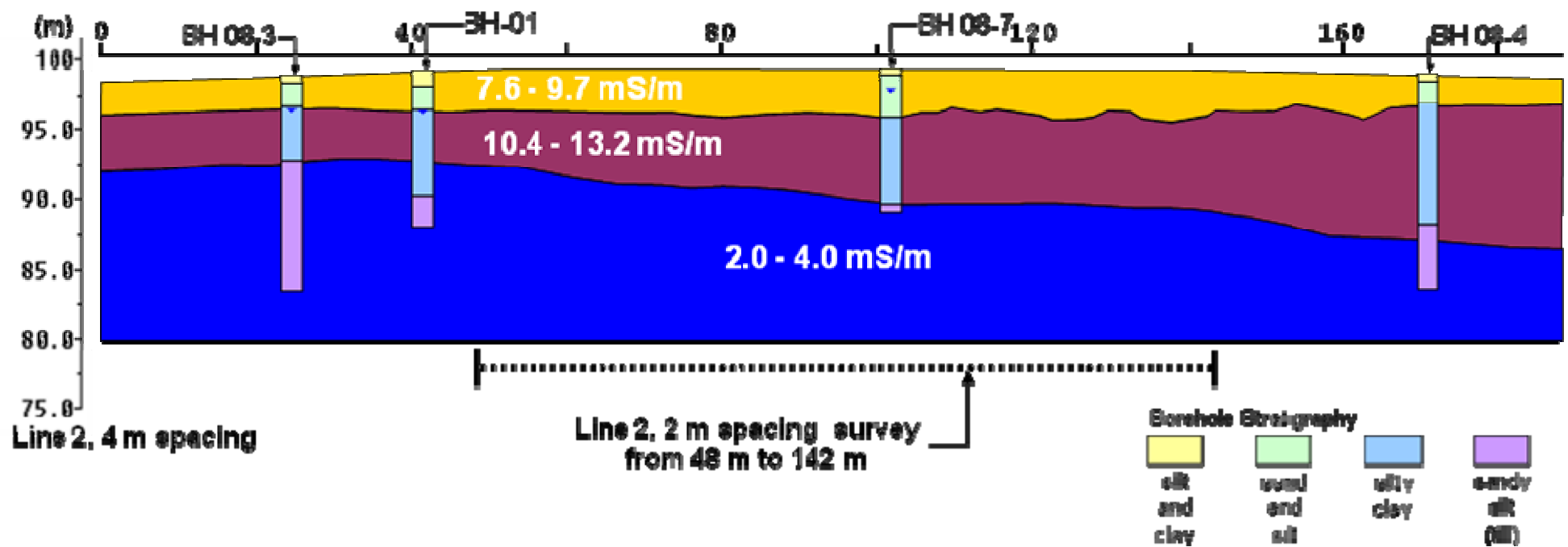


Figure 4. Interpreted conductivity pseudosection and boreholes for Line 2 (4 m electrode spacing, Appendix B)

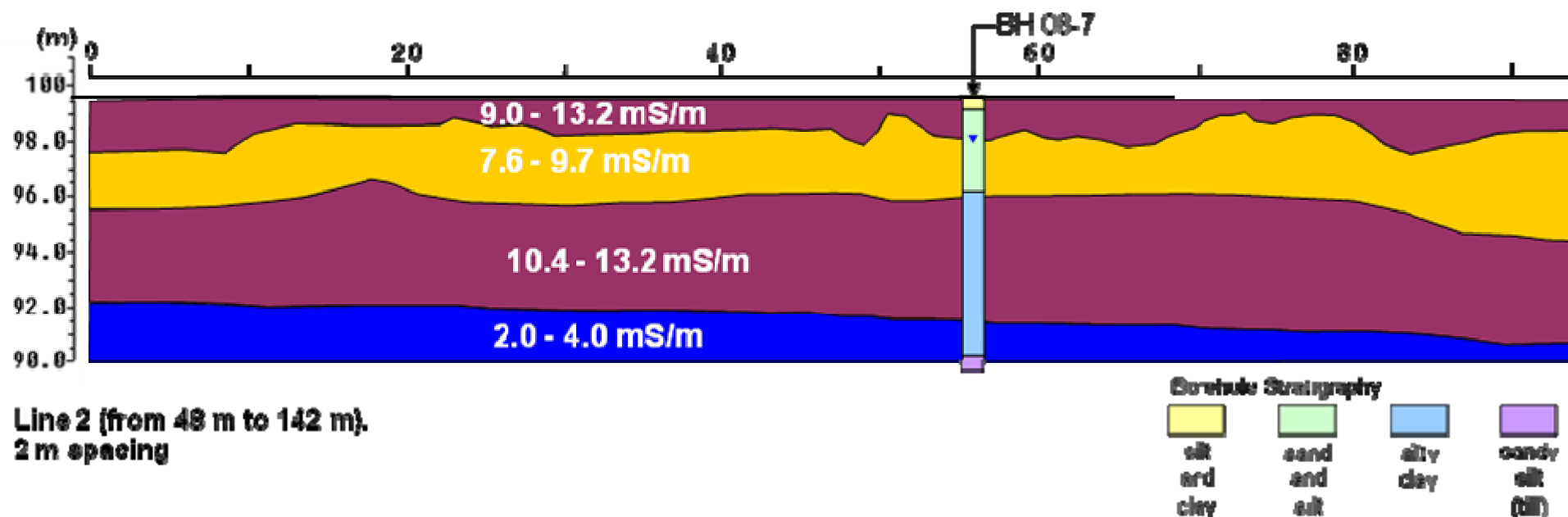


Figure 5. Interpreted conductivity pseudosection and boreholes for subsection of Line 2 (2 m electrode spacing, 48 m to 142 m, Appendix B)

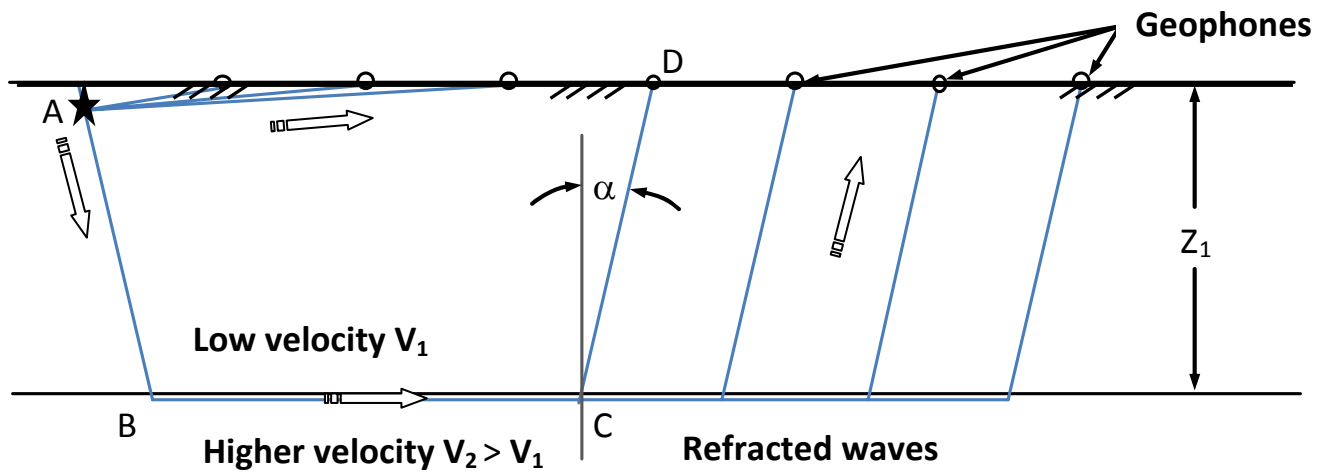


Figure 6 : Simple seismic refraction survey raypaths



Figure 7: Shear wave source for seismic refraction tests

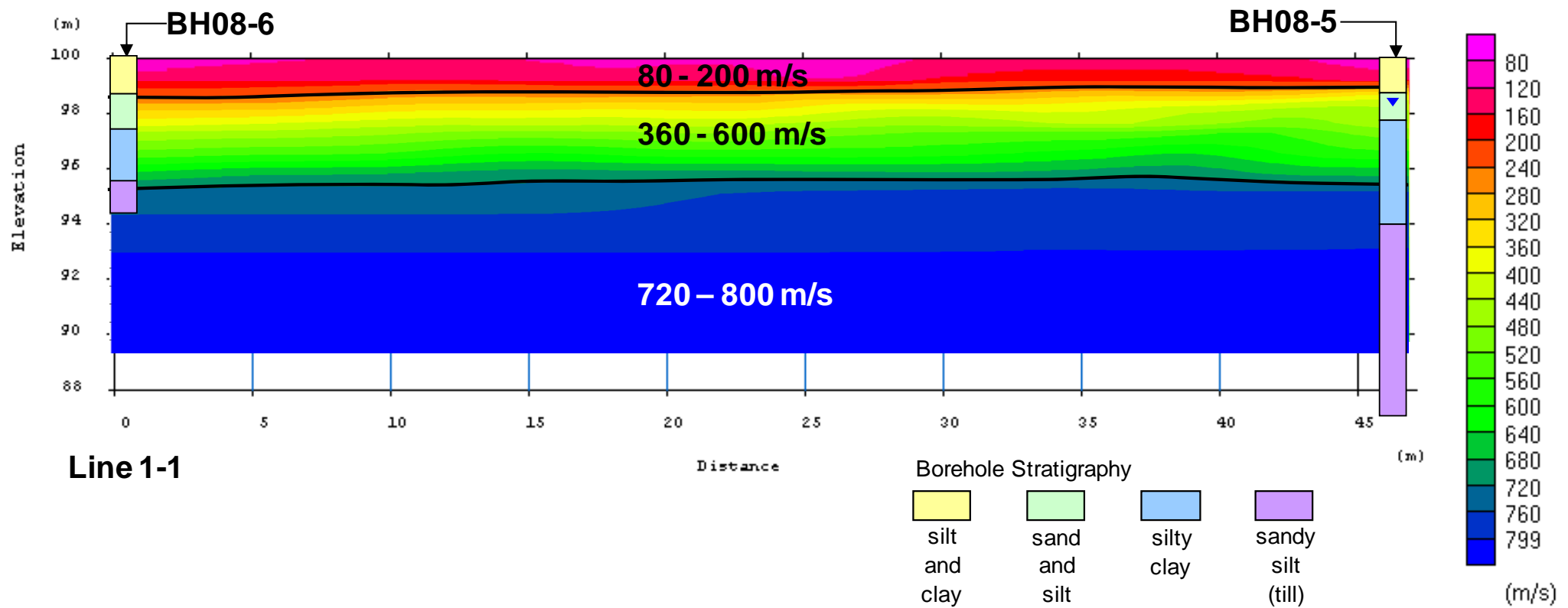


Figure 8. Seismic refraction results (tomography inversion) and BH information for Line 1-1

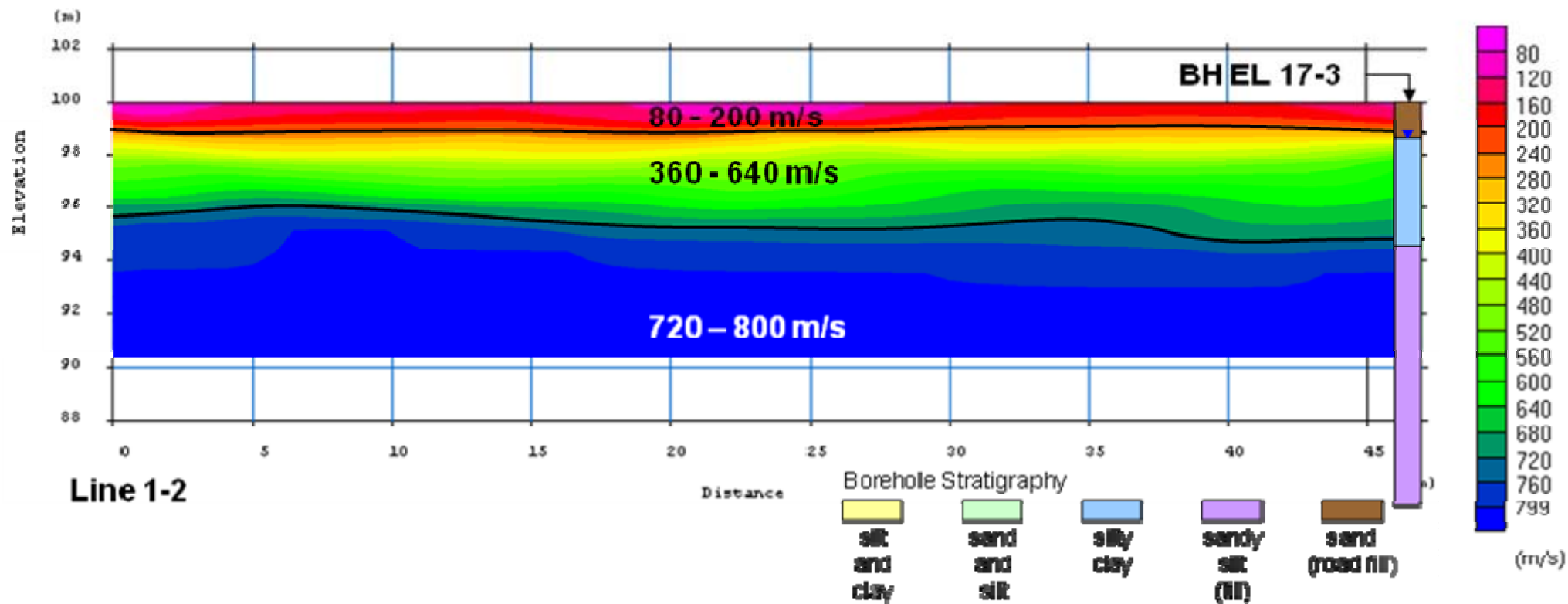


Figure 9. Seismic refraction results (tomography inversion) and BH information for Line 1-2

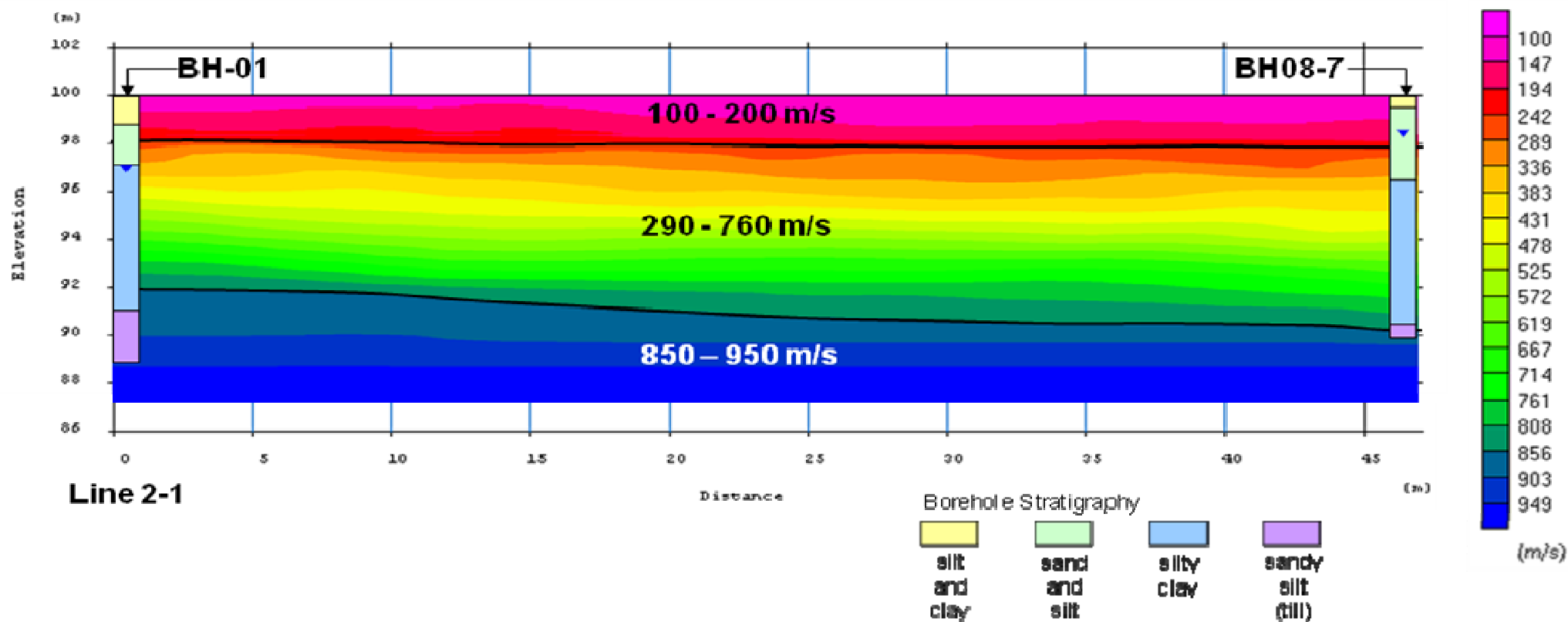


Figure 10. Seismic refraction results (tomography inversion) and BH information for Line 2-1

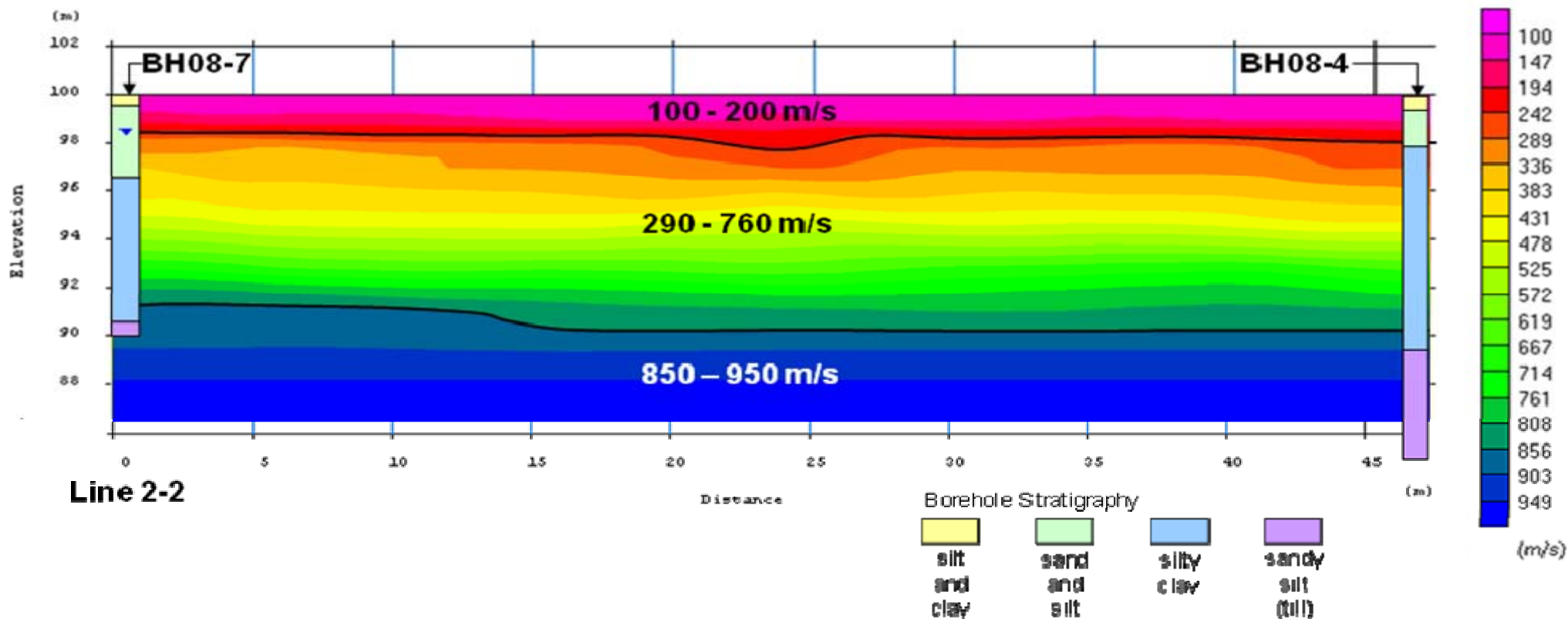


Figure 11. Seismic refraction results (tomography inversion) and BH information for Line 2-2

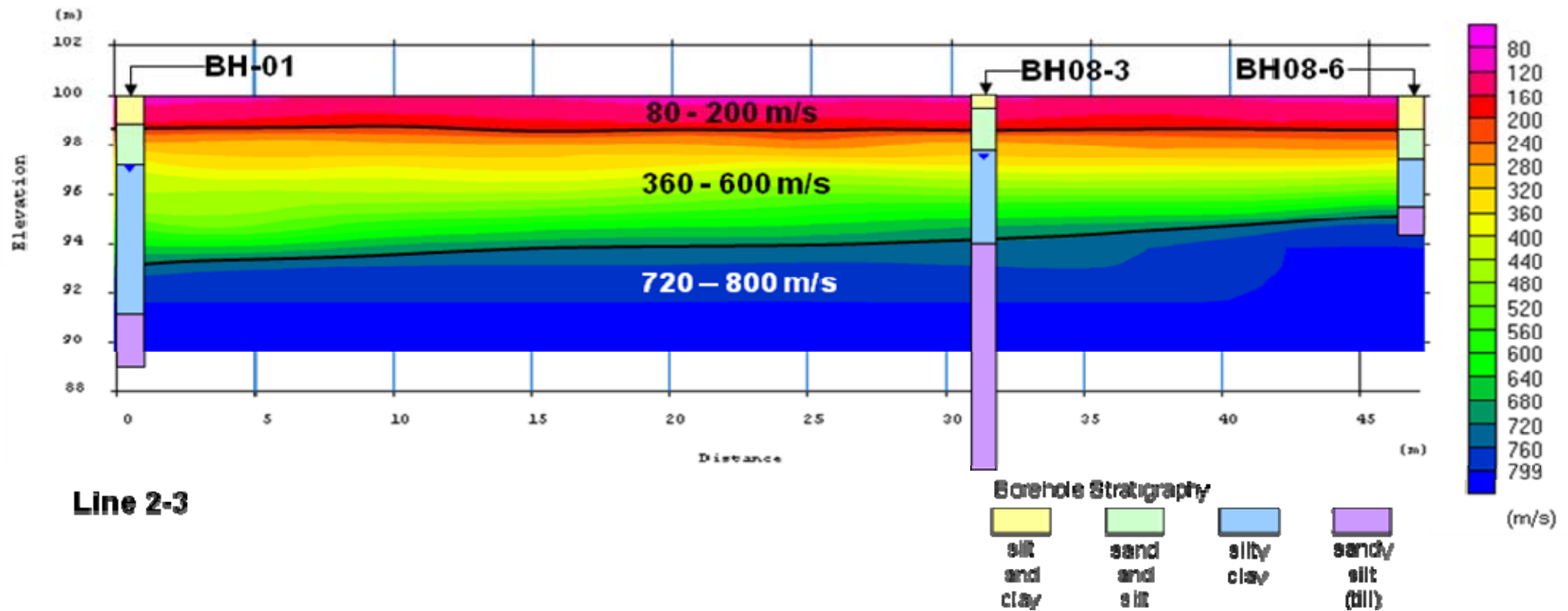


Figure 12. Seismic refraction results (tomography inversion) and BH information for Line 2-3

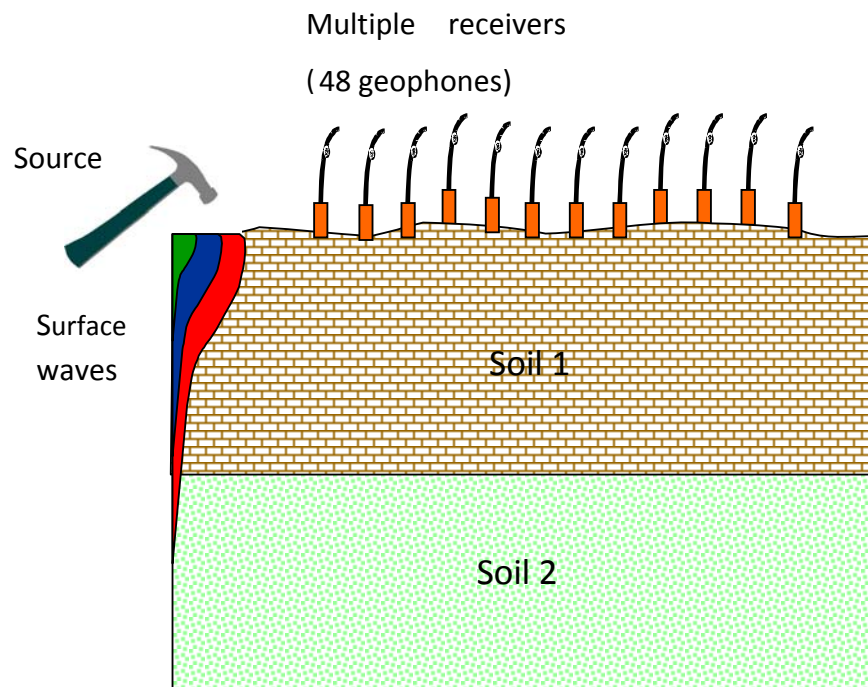


Figure 13: Typical MASW test configuration (two-layer soil profile)



Figure 14: (a) Planting of geophones (Line 2-2). (b) Surface wave 170-lb seismic source

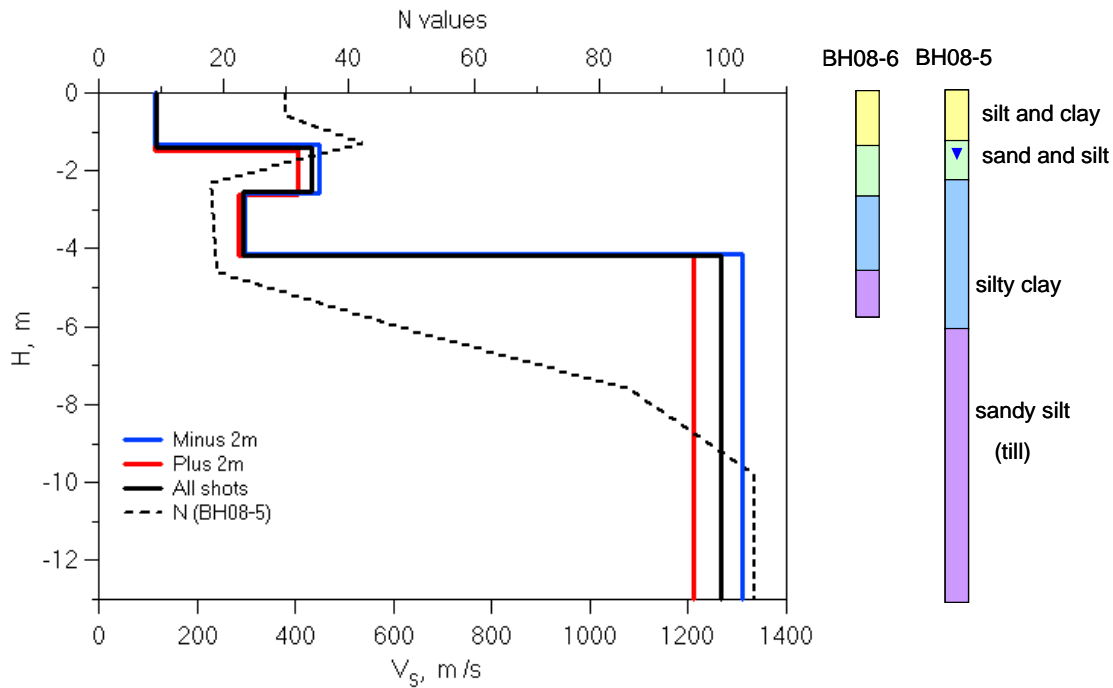


Figure 15: Shear wave velocity profile and borehole information. Line 1-1

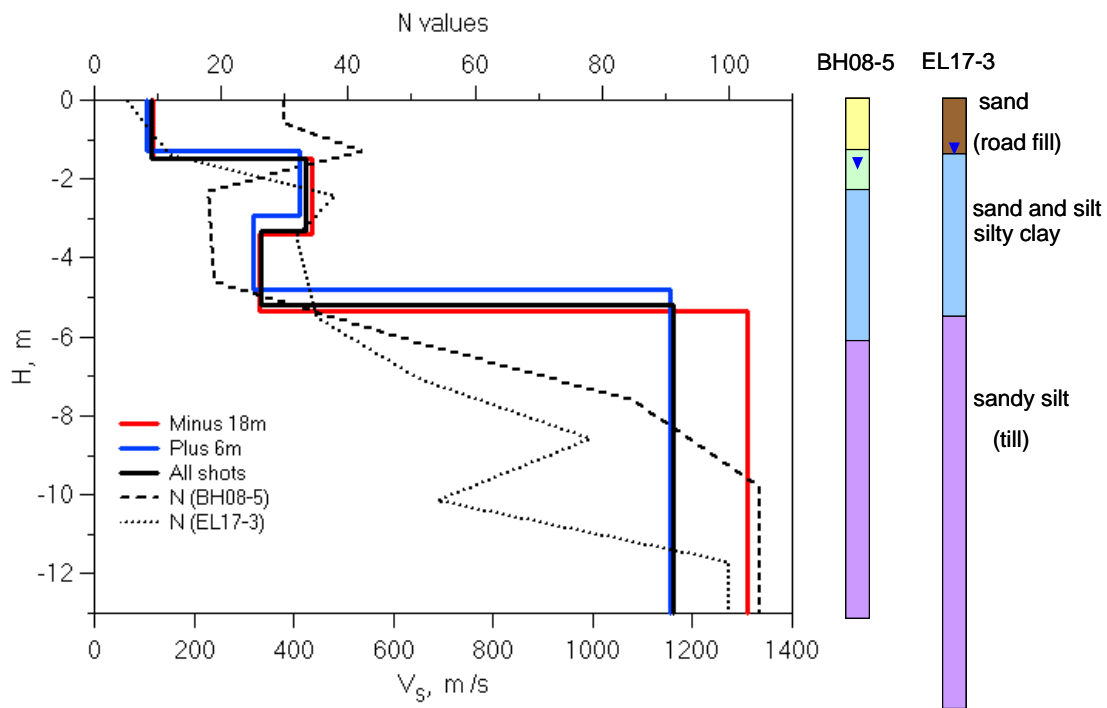


Figure 16: Shear wave velocity profile and borehole information. Line 1-2

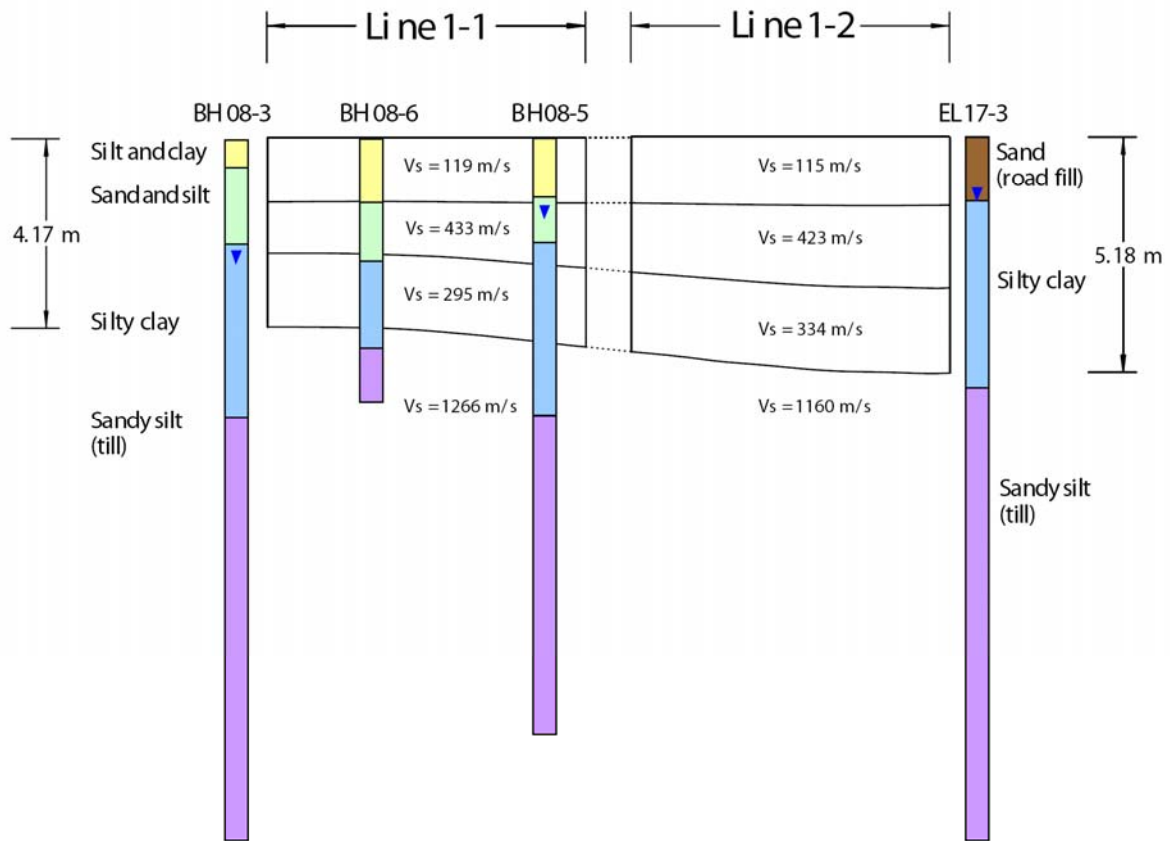


Figure 17 Interpreted soil profile for Line 1 from MASW and borehole data

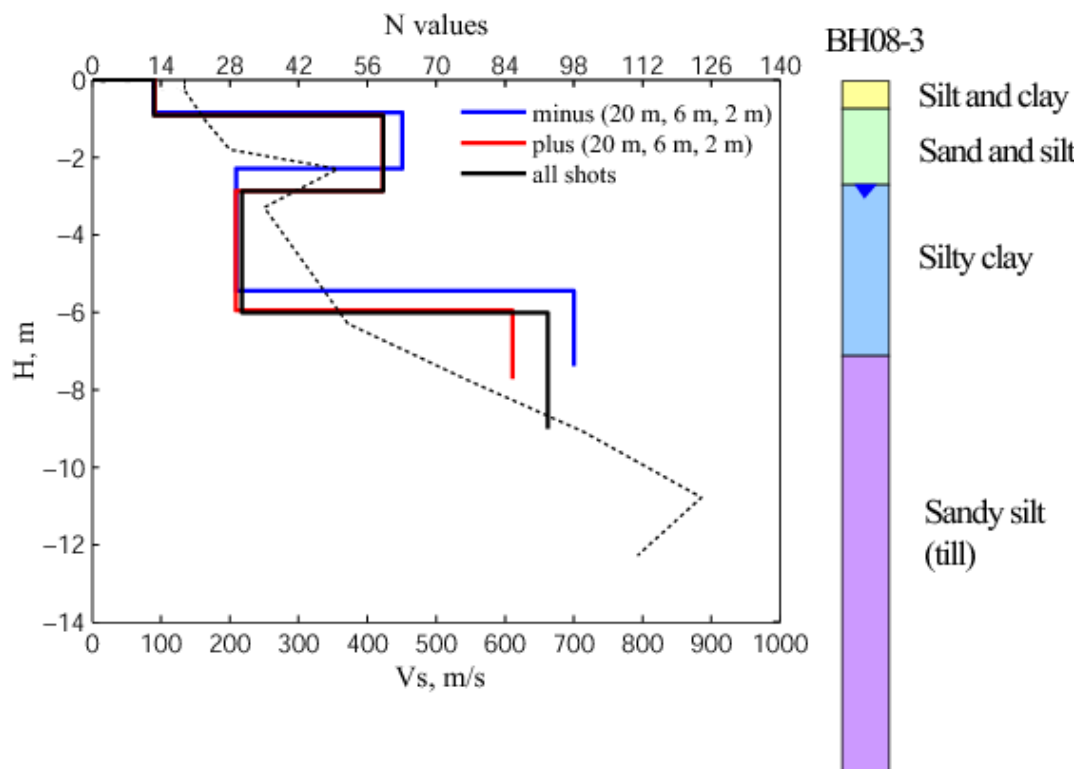


Figure 18: Shear wave velocity profile and borehole information. Line 2-3

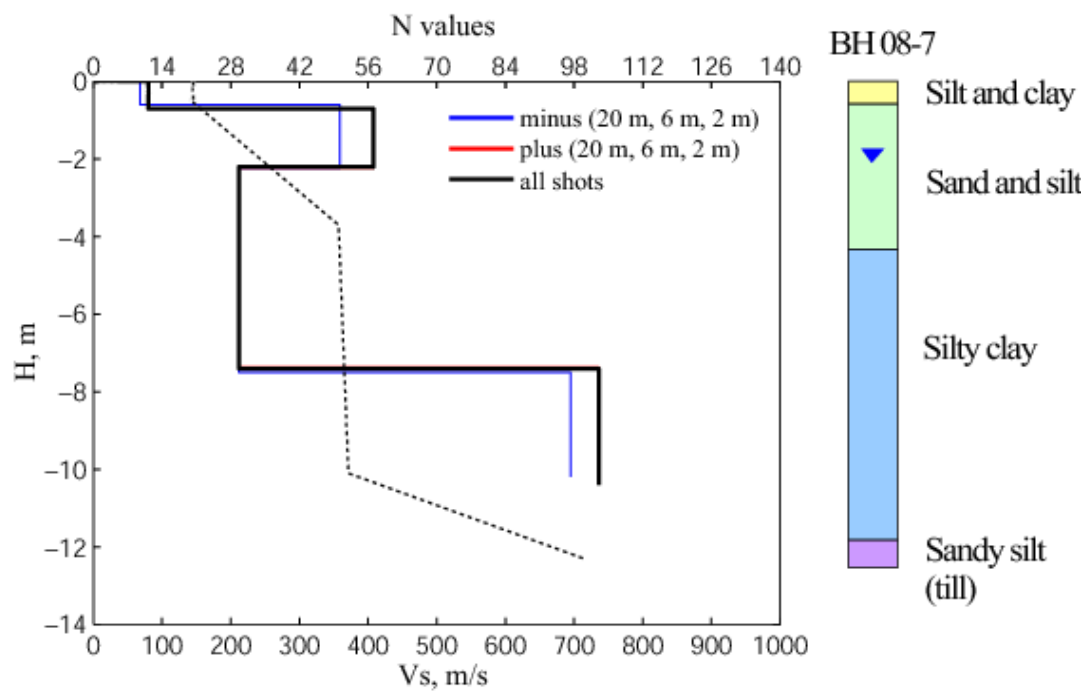


Figure 19: Shear wave velocity profile and borehole information. Line 2-1

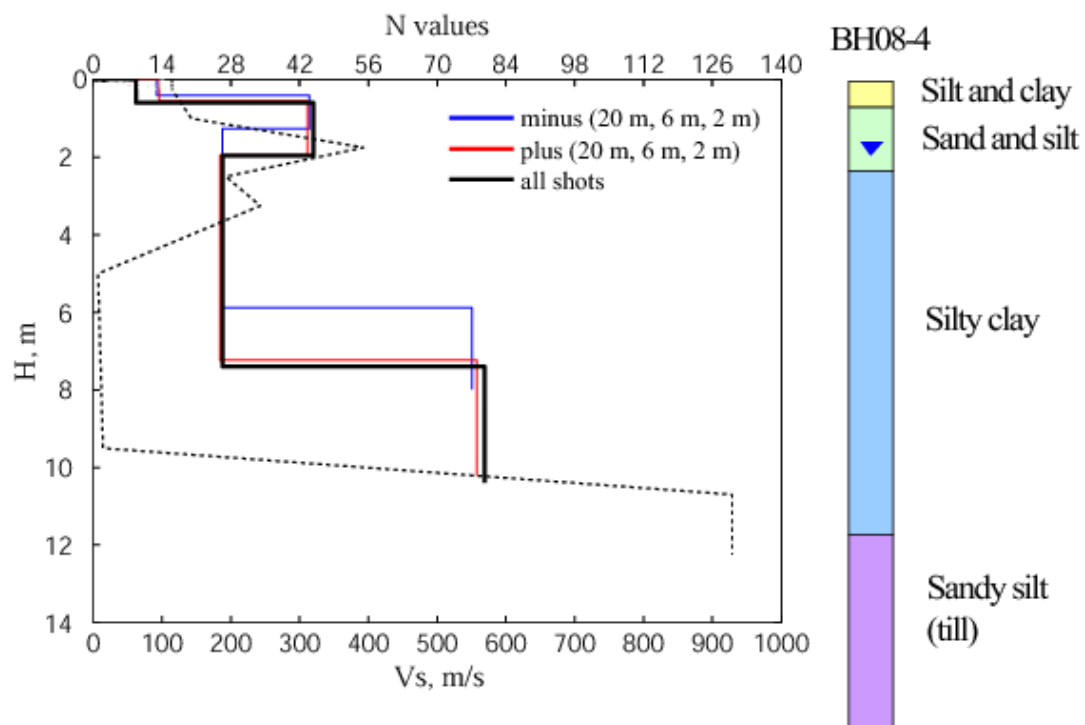


Figure 20: Shear wave velocity profile and borehole information. Line 2-2

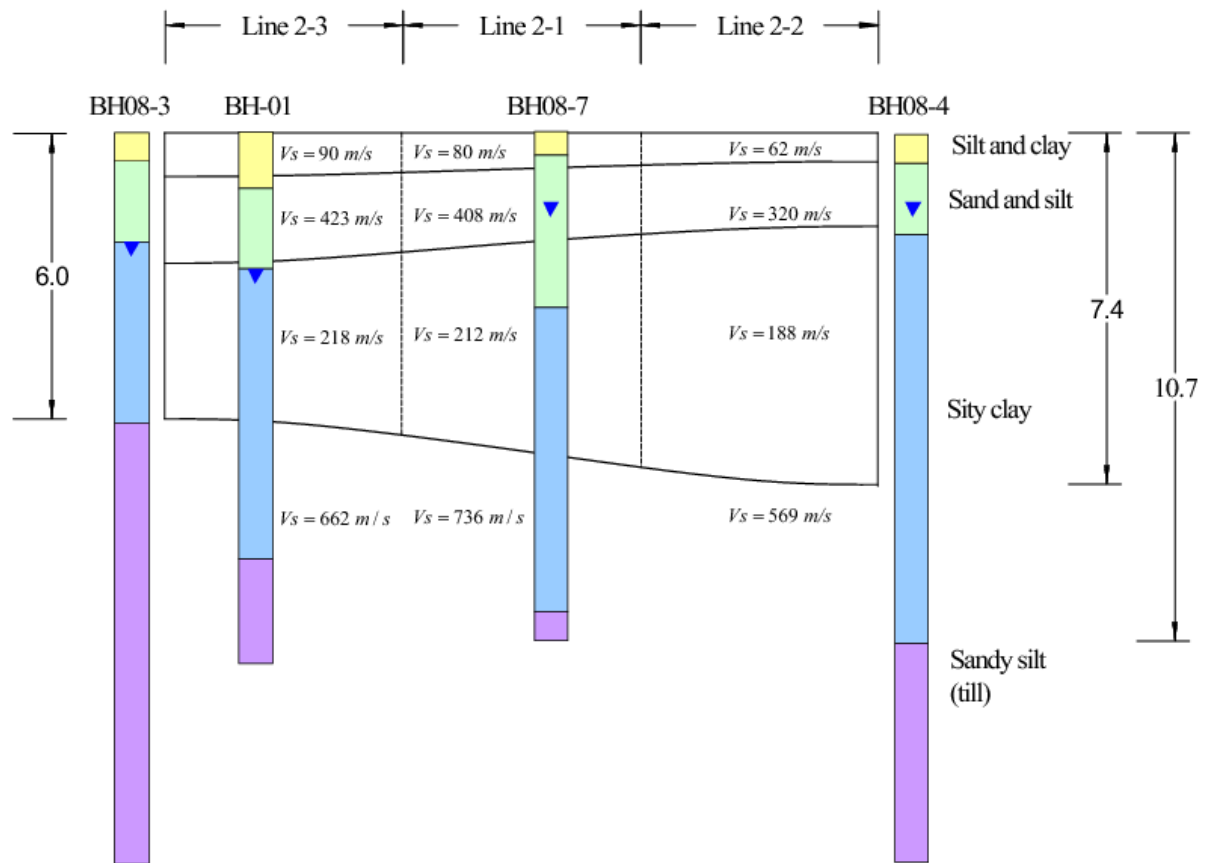


Figure 21: Interpreted soil profile for Line 2 from MASW and borehole data

Appendix A

Basics of the electrical resistivity test

ELECTRICAL RESISTIVITY IMAGING

Introduction

Electrical resistivity imaging is used to infer subsurface structure based on the different electrical resistivities of different geological materials. The test is accomplished by generating a current through the ground and measuring the resulting potential differences at the surface. Measured deviations from normal potentials are used as an indication of subsurface variations in electrical conductivity resulting from changes in lithology or the presence of water. The following summary was prepared with reference to Keary et al. (2002).

Fundamentals of electrical resistivity imaging

The fundamentals of electric current flow through the ground are illustrated by considering a homogeneous cylinder of length δL , resistance δR , and with a cross-sectional area δA (Figure A-1). The potential drop $-\delta V$ across the cylinder created by an induced current I is given by Ohm's law

$$-\delta V = \delta R I \quad (\text{A-1})$$

The resistivity (ρ) of a material is defined as its resistance per unit length to electric current as

$$\rho = \frac{\delta R \delta A}{\delta L} \quad (\text{A-2})$$

substituting for δR into equation A-1 gives

$$\frac{\delta V}{\delta L} = -\frac{\rho I}{\delta A} \quad (\text{A-3})$$

For a single electrode on the surface inducing a current (Figure A-2), the current flows radially away from the electrode. As the current reaches a distance, r , from the source, it is evenly distributed over a hemispherical surface-area of $2\pi r^2$. Substituting for δA in equation A-3, the potential gradient with respect to r is given by

$$\frac{\delta V}{\delta r} = -\frac{\rho I}{2\pi r^2} \quad (\text{A-4})$$

Integrating equation A-4 gives a formula that can be used to calculate the potential, V_r , at any distance r from the electrode:

$$V_r = \int \partial V = - \int \frac{\rho I \delta r}{2\pi r^2} = \frac{\rho I}{2\pi r} \quad (\text{A-5})$$

Finally, for the case where the circuit is completed with a current source electrode at point A and a sink electrode at point B (Figure A-3); the potential V_C at point C is given by adding the potential contributions from the source and sink electrodes (V_A and V_B respectively):

$$V_C = V_A + V_B \quad (\text{A-6})$$

From equation A-5

$$V_C = \frac{\rho I}{2\pi} \left(\frac{1}{r_{AC}} - \frac{1}{r_{BC}} \right) \text{ and } V_D = \frac{\rho I}{2\pi} \left(\frac{1}{r_{AD}} - \frac{1}{r_{BD}} \right) \quad (\text{A-7})$$

The potential difference ΔV between C and D is given by

$$\Delta V = V_C - V_D = \frac{\rho I}{2\pi} \left\{ \left(\frac{1}{r_{AC}} - \frac{1}{r_{BC}} \right) - \left(\frac{1}{r_{AD}} - \frac{1}{r_{BD}} \right) \right\} \quad (\text{A-8})$$

Therefore

$$\rho = \frac{2\pi \Delta V}{I \left\{ \left(\frac{1}{r_{AC}} - \frac{1}{r_{BC}} \right) - \left(\frac{1}{r_{AD}} - \frac{1}{r_{BD}} \right) \right\}} \quad (\text{A-9})$$

In summary, the resistivity of a material can be obtained by measuring the potential difference across two electrodes placed between an additional two electrodes that are generating a current through the material.

The depth of current penetration in a resistivity survey increases as the spacing between the electrodes increases. In a homogeneous subsurface, the calculated resistivity should be constant throughout and independent of surface location and electrode spacing. When inhomogeneities are present, the resistivity depends on the relative positions and spacing of the electrodes. Any calculated value for resistivity is called the apparent resistivity (ρ_a) and depends on the geometry and size of the inhomogeneity.

Electrical conductivity of rocks and soil

With the exception of electrically conductive minerals such as magnetite, specular hematite, carbon, graphite, pyrite and pyrrhotite, soil and rock minerals generally do not conduct electricity because they are highly resistive. In the majority of sites in southern Ontario, the electrical conductivity (inverse of resistivity) of rocks and soils is controlled by the water in the pore spaces. The conductivity is then affected by the following factors: porosity, degree of saturation, the concentration of dissolved electrolytes in the pore water, the temperature and phase state of the water in the pore spaces, and the amount of clay minerals and colloidal material (McNeill, 1980). The conductivity of soils and rocks is larger when the water content is higher. The water content varies above and below the water table and within the saturated zone according to the porosity. The conductivity is higher where the concentration of dissolved solids is higher. The electrical conductivity decreases when the temperature decreases and electrolytic conduction is suppressed when soil and rock is frozen.

There is also an important effect of clays and colloids (microscopic grains of material). Most mineral surfaces are negatively charged because of mineral imperfections so much so that cations in solution become easily and adsorbed (loosely bound) to the mineral surface. Because clays and colloids have a very high surface area compared to their size, their capacity to adsorb cations from solution is large. Such cations are loosely bound to the surface, are exchangeable with ions from the solution, and are able to conduct electricity along mineral surfaces. Even a small amount of clay, in wet conditions, can increase the electrical conductivity significantly. So the resistivity survey can give some indication of lithology especially when used in conjunction with other geotechnical information from soil samples. On its own, it is difficult to determine lithology from resistivity surveys because the electrical resistivity/conductivity is affected different factors mentioned before.

The Wenner electrode array

Different electrode configurations have been designed for electrical resistivity surveys; one of the most commonly used is the Wenner configuration. In this configuration, the spacing 'a' between the current and potential electrodes is the same (Figure A-4). Substituting 'a' into the equation A-9 gives

$$\rho = \frac{2\pi a \Delta V}{I} \quad (\text{A-10})$$

In a standard survey, the array of electrodes is sequentially moved down the desired line with a fixed value of 'a'.

Interpretation of electrical resistivity imaging

Inversion software (e.g. Geotomo Res2dinv) is commonly used to interpret resistivity data and generate a two-dimensional electrical resistivity structure of the ground below the survey line.

Problems and limitations

The results of a resistivity data inversion can be ambiguous because multiple models can generate the same electric potentials as measured in the field. Thus, this geophysical method is commonly completed in tandem with exploration boreholes. Furthermore, interpretations are limited to simple subsurface conditions (e.g. gradual changes in thickness and depth of layers). Finally, topography and near-surface resistivity variations can interfere with detection of effects resulting from deeper variations.

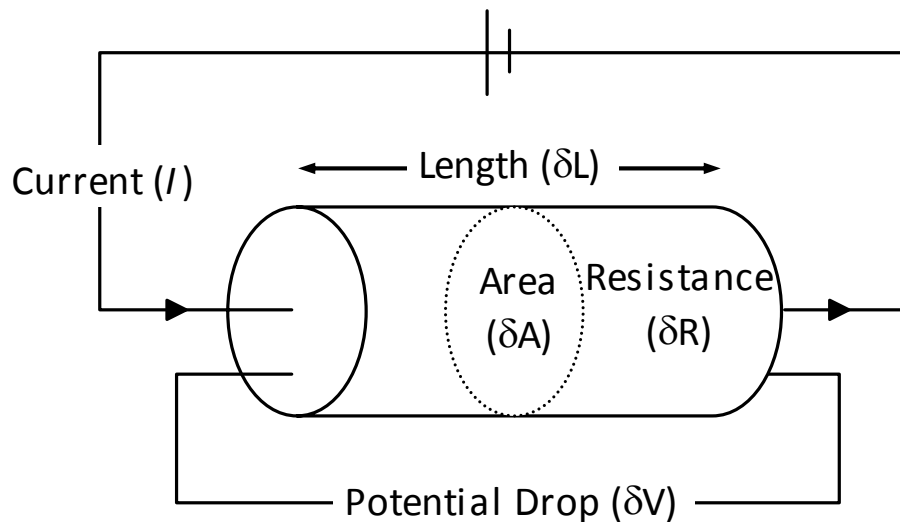


Figure A-1: Variables required for computation of resistivity

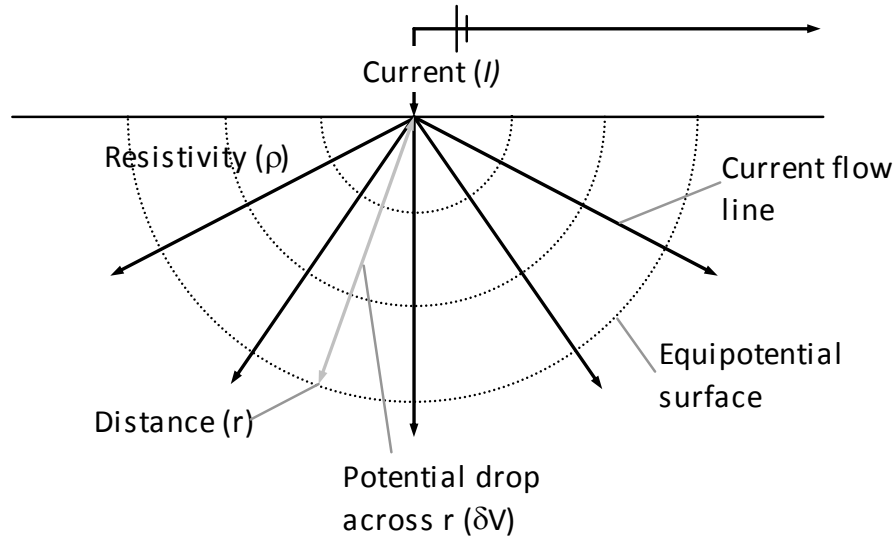
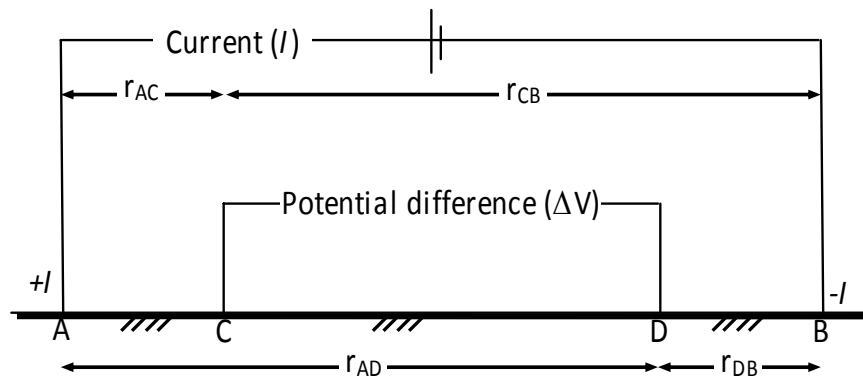


Figure A-2: Current induced by single electrode at the surface



A,B = Current inducing electrodes
 C,D = Potential measuring electrodes
 r_{xx} = Distance between electrodes

Figure A-3: General electrode configuration

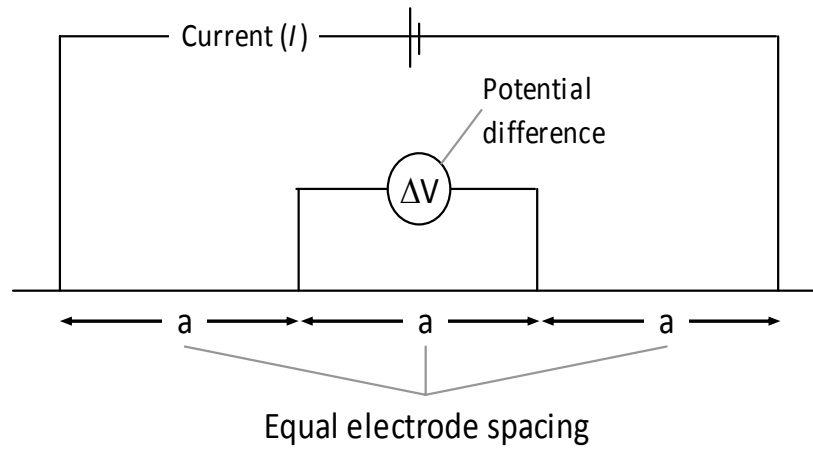


Figure A-4: Wenner electrode array

References

Keary, P., Brooks, M., and Hill, I., 2002, *An Introduction to Geophysical Exploration: Third Edition*, Blackwell Science Ltd., Malden Massachusetts.

McNeill, J. D., 1980, *Electrical conductivity of soils and rocks*. Geonics Technical Note TN-5, Geonics Limited, Mississauga.

Appendix B

Electrical resistivity tests

Pseudosections for Lines 1 and 2

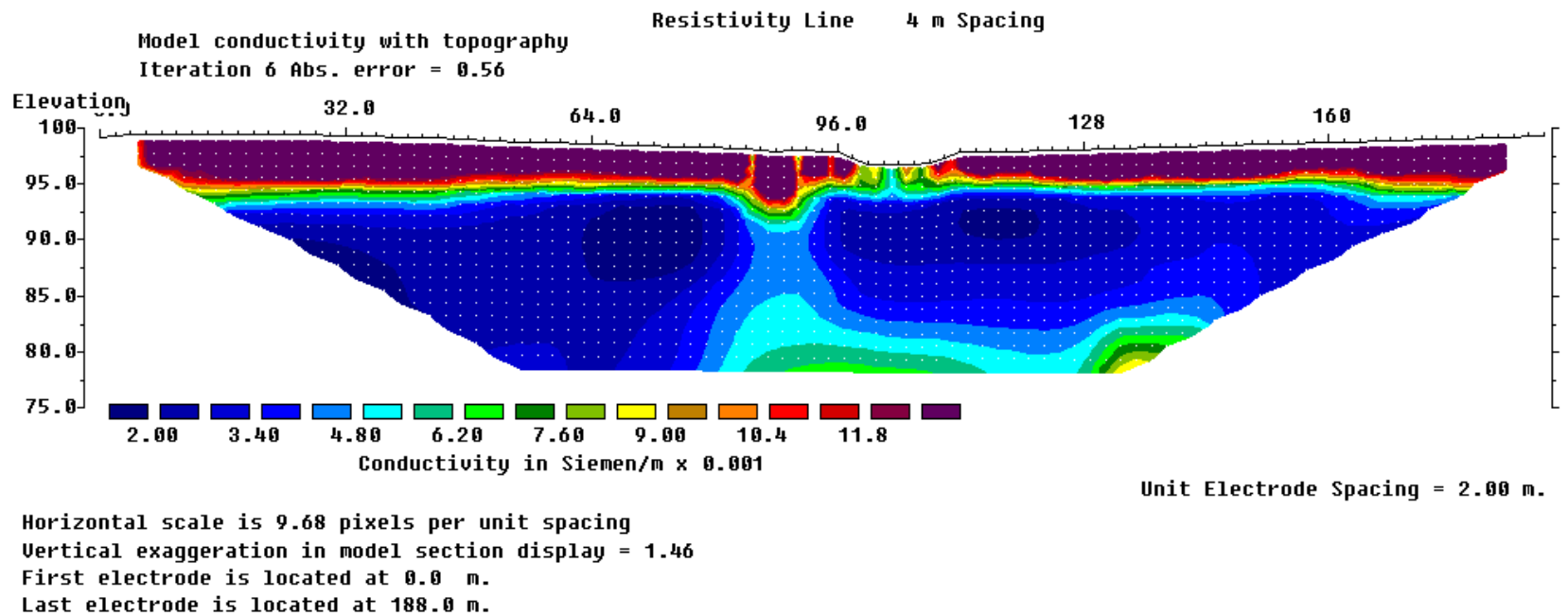


Figure 1-A. Conductivity Pseudosection for Line 1, 4 m electrode spacing, Wenner array

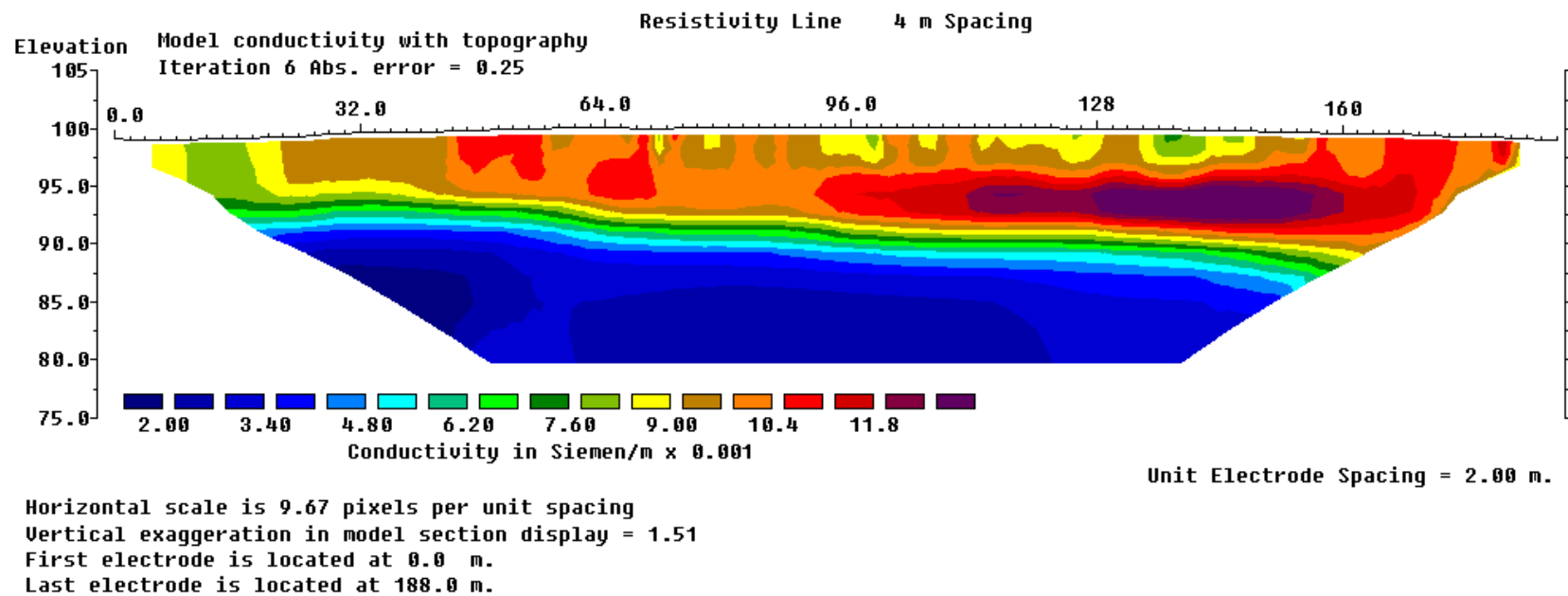
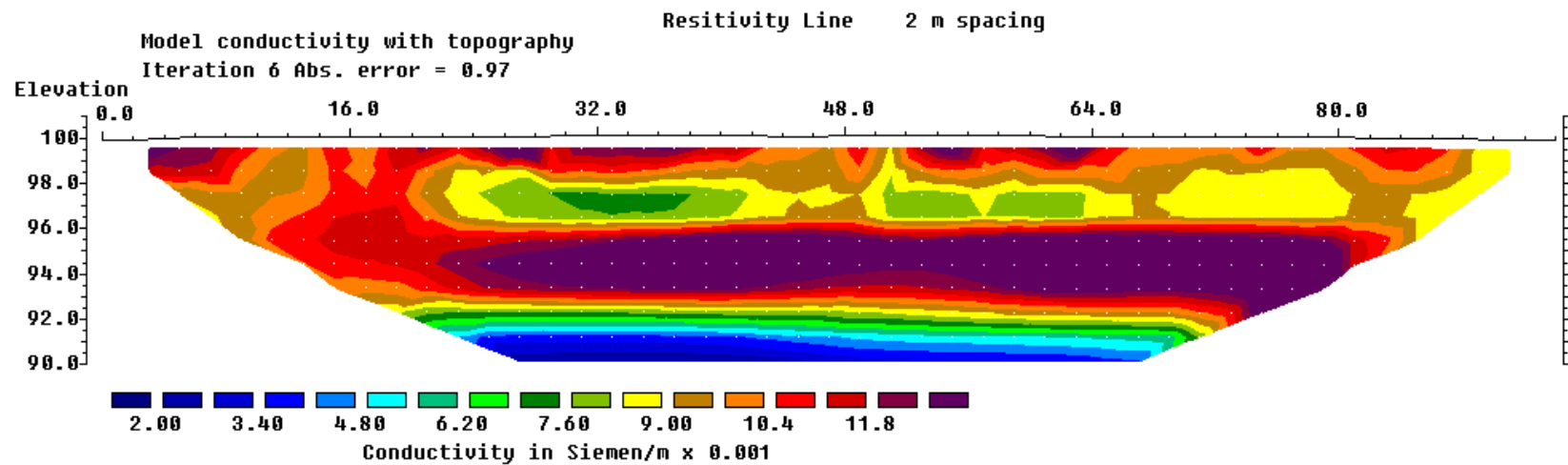


Figure 2-A. Conductivity Pseudosection for Line 2, 4 m electrode spacing, Wenner array



Horizontal scale is 19.36 pixels per unit spacing
Vertical exaggeration in model section display = 1.46
First electrode is located at 0.0 m.
Last electrode is located at 94.0 m.

Figure 3-A. Conductivity Pseudosection for Line 2, 2 m electrode spacing, span from 48 m to 142 m, Wenner array

Appendix C

Basics of the seismic refraction test

SEISMIC REFRACTION SURVEYING

Introduction

Seismic investigations make use of the fact that seismic waves travel through different media at different velocities. By generating seismic waves and recording their arrival times at numerous points on the ground surface, subsurface interfaces between different geological materials can be located using the reflected or refracted waves (Sharma 1997). Seismic refraction surveying specifically was the first major geophysical method to be used in oil exploration. This method has become increasingly popular for use in site investigations for civil engineering applications. It is most useful for shallow subsurface studies, in particular when used in combination with borehole drilling.

The seismic refraction survey method involves the artificial generation of seismic waves which and the measurement of the travel times of the refracted waves at different points along the ground surface. The resulting data consists of travel times and distances. A representation of the subsurface is obtained through interpretation of these data based on laws of energy propagation. The following summary is mostly based on Redpath (1973).

Fundamentals of seismic refraction surveying

The propagation of seismic energy through a layered medium is governed by two main principles: Snell's law and the critical angle of incidence (Figure 1-C). Snell's law describes the relationship between the angular deviation or refraction of a wave front and the ratio of the seismic velocities of the two materials, when a seismic pulse crosses an interface between the two materials. This law only applies when the velocity of the second medium is greater than that of the first. In most cases, this condition is met in the field as transmission velocities increase with successively deeper more compacted materials. Critical incidence is the specific case where the refracted pulse is parallel to the layer interface ($\beta = 90^\circ$, Figure 1-C). This phenomenon occurs at a critical angle of incidence, when the sine of this incident angle equals the ratio of the first and second layer transmission velocities ($\sin \alpha = V_1/V_2$).

Figure 2-C illustrates a general seismic survey setup and raypaths in a simple two-layer case. When a seismic pulse reaches the interface between layers at the critical angle of incidence (point B), the wave propagates along the boundary (BC) at the higher velocity of the lower layer. As the refracted pulse follows the interface, it generates waves that depart at the critical incident angle (point C) into the upper layer at the lower velocity. At relatively short distances from the source (less than AD), the first waves to arrive at the surface are those travelling directly from the source to the surface through the upper layer. At

a certain distance from the source (point D), the arrival of these shallow waves is overtaken at by waves refracted at the interface. The refracted energy follows a longer ray path (ABCD) but travels at a higher velocity along the layer boundary; and it is able to overcome the movement of the slower waves in the upper layer given enough distance. In a scenario with multiple layer interfaces, the arrival of waves refracted from one boundary will eventually be overtaken by pulses refracted by any subsequently deeper interface with a layer of higher velocity.

Interpretation techniques

There are a variety of methods used to interpret seismic refraction data. Each has its own benefits and drawbacks depending on specific site conditions. A brief overview of some commonly used interpretation techniques is given below. Explanations that are more detailed can be found in a number of geophysical references (e.g. Keary et al. 2002).

Time-Intercept Method. The time-intercept method is the simplest method used for analyzing seismic refraction data. First, a time distance-plot is generated by plotting the first arrival times against the corresponding distance-from-source at each detector as shown in Figure 3-C for the simple two layer case. The initial arrivals are those from direct pulses through the first layer. The slope of the line through these early data points ($\Delta T/\Delta X$) is the reciprocal of the transmission velocity of the first layer ($1/V_1$). Where the direct arrivals are overtaken by the refracted wave arrivals, a decrease in the slope through the data points is observed. This location of the break in slope is known as the critical distance (X_c). The decreased slope through the points beyond the critical distance represents the reciprocal of the velocity of the second layer ($1/V_2$). Projecting a line through the refracted points back to the time axis gives the intercept time (T_i).

The depth of the interface between the layers (Z_1) is given by

$$Z_1 = \frac{T_i V_1}{2 \cos \left(\sin^{-1} V_1/V_2 \right)} \quad (C-1)$$

This formula is derived by solving for the travel time of the refracted wave using the geometry of the raypath and rearranging to solve for Z_1 (Redpath 1973). The time-intercept method can be modified for cases with multiple layers and dipping layers. However, one significant disadvantage of this method is that it is only applicable to planar and parallel layer interfaces; which is not the case for many geological boundaries that are irregular and dipping. In addition, the depth computed using this method is actually a

depth projected back to the location of the seismic source. If the survey consists of only one shot, only one depth to the refracting surface can be obtained.

Reciprocal Method. This method gives greater detail than the time-intercept method. It uses the concept of delay times to calculate refractor depths below individual detector or geophone in the survey line. The delay time is the difference between the time spent by the seismic wave travelling up or down through the upper layer, and the time it would have spent travelling along the layer interface at the refractor velocity (Figure 4-C). The depth to the refractor below the detector (Z_D) according to the delay time at that specific detector (ΔT_D) is given by

$$Z_D = \frac{\Delta T_D V_1}{\cos(\sin^{-1} V_1/V_2)} \quad (C-2)$$

Delay times can be determined from a seismic refraction survey by capturing shots from both ends of the line. The total travel time (T_t : arrival time recorded at the detector furthest from the source for the reversed shots) and the arrival times at a detector from the forward and reverse shots (T_{D1} and T_{D2} respectively) can be used to calculate ΔT_D :

$$\Delta T_D = \frac{1}{2}(T_{D1} + T_{D2} - T_t) \quad (C-3)$$

The delay time at a specific geophone can only be calculated when the arrivals from the forward and reverse shots are from the same refracting surface. Shots can be fired beyond the ends of the survey line to increase the overlap in reversed arrival times. The reciprocal method can also be expanded for a multiple layer case. This technique allows detection of dipping and irregular layer interfaces as depths below each individual geophone in the survey line can be determined. However, multiple shots are required to provide sufficient overlap in the arrival times; and the data interpretation is more involved than in the simple time intercept-interpretation.

Tomographic Inversion. Tomographic inversion generally requires specialized software packages such as SeisImager/2D. This method begins with an initial velocity model of multiple layers with a range of velocities specified by the user. The time-intercept or the reciprocal methods can be used to determine an applicable velocity range for the initial model. This initial model consists of many individual constant velocity cells. The size of cells can be adjusted by the user.

A tomographic inversion involves iteratively tracing rays through different source and receiver combinations in the model. The velocities in each cell are adjusted following each iteration to minimize the difference between the calculated and measured arrival times. The mathematical procedures to

minimize the error are involved, but the raypath through each cell is governed by the fundamental principles of seismic wave propagation discussed above. The result is a model showing contours of cells with the same refraction velocity as an alternative to continuous constant velocity layers. Although tomographic inversion requires software packages, it can model gradual changes in refraction velocity and localized anomalies.

Problems and limitations

A significant problem that can limit the success of a seismic refraction survey is a velocity reversal. A velocity reversal occurs when a low-velocity layer underlies a higher-velocity layer. In this case the seismic wave is actually refracted downwards, away from the layer interface as show in Figure 5-C. Refractions from this low-velocity layer are not detected at the surface. Therefore, the effect on the analysis is the computation of depths greater than actual values because arrival times are larger than they would be if the waves did not pass through the low-velocity layer. In addition, gradual variations in velocity in both vertical and lateral directions can dramatically affect the success of time-intercept and delay time methods. Both of these methods assume layers of constant velocity. However, a tomographic inversion can successfully identify such gradual variations.

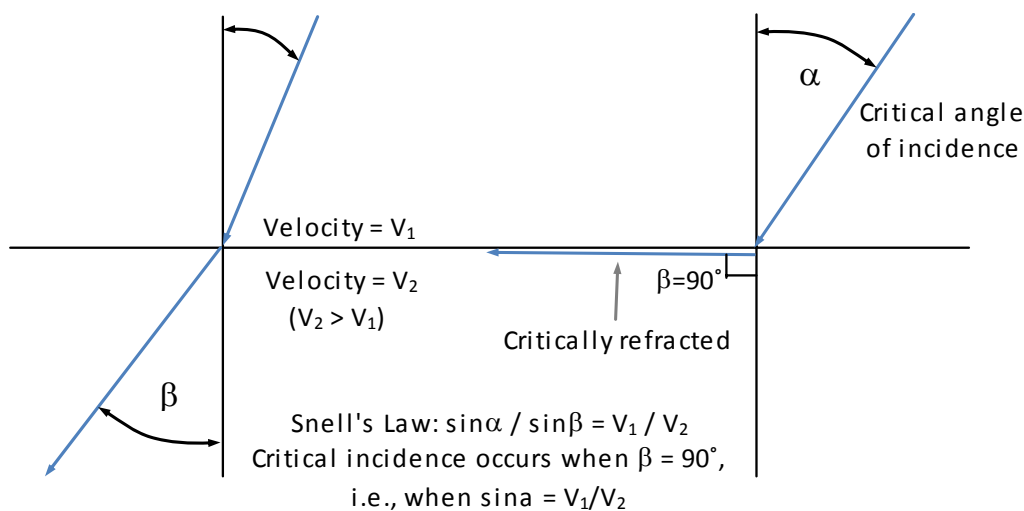


Figure 1-C: Snell's Law and critical incidence

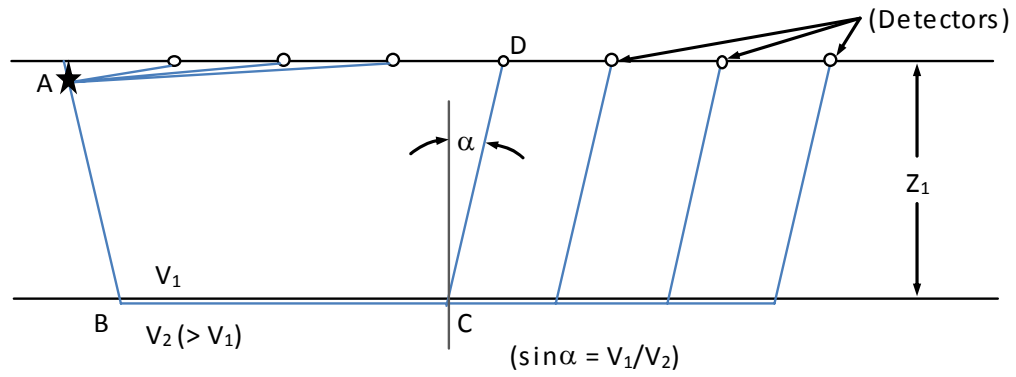


Figure 2-C: Simple seismic refraction survey raypaths

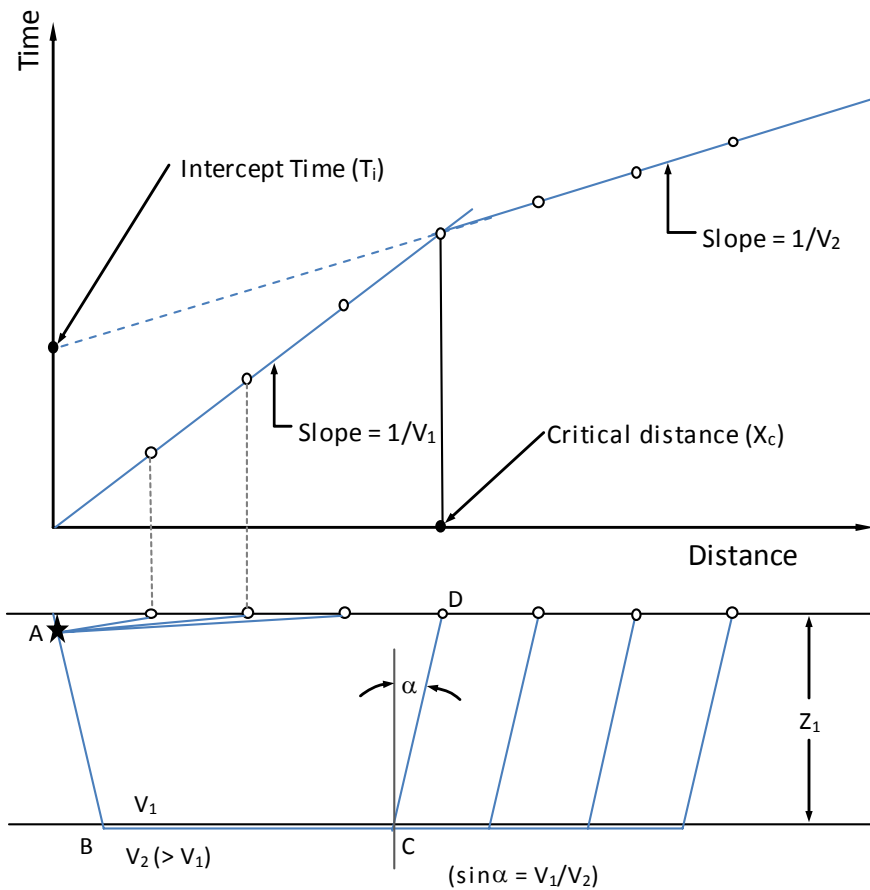


Figure 3-C: Time-distance curve from simple two-layer case

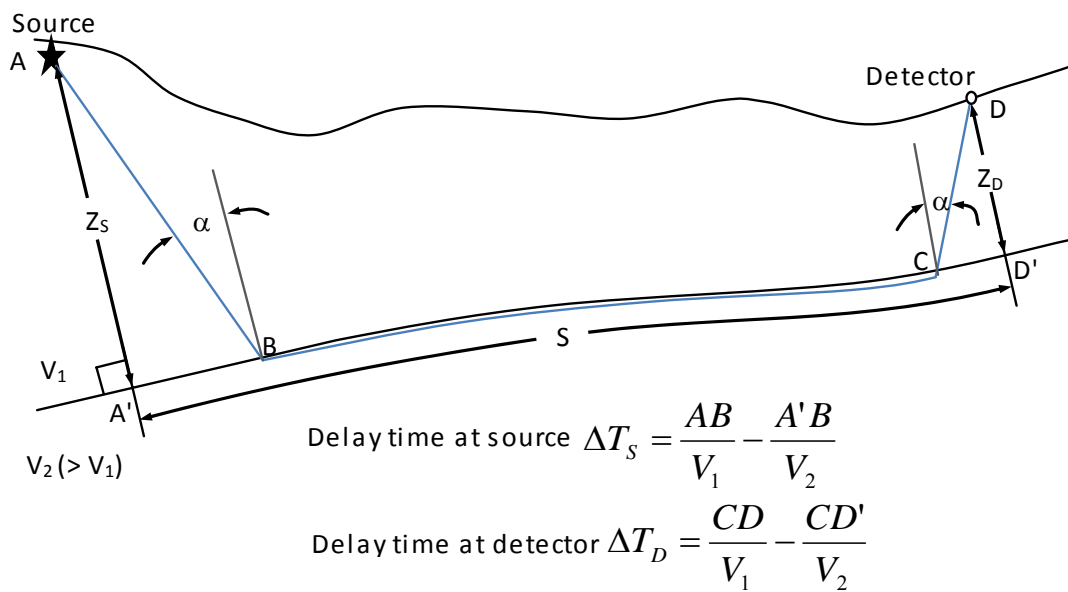


Figure 4-C: Definition of delay time (after Redpath 1973)

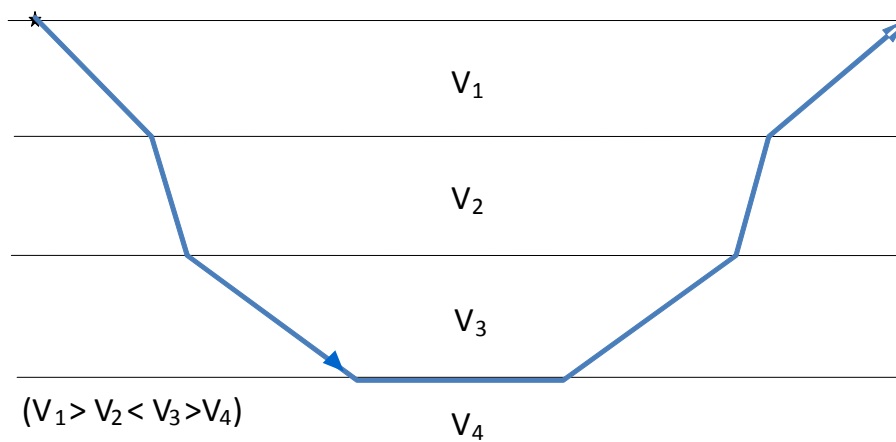


Figure 5-C: Refraction caused by velocity reversal

References

Keary, P., Brooks, M., and Hill, I., 2002, An Introduction to Geophysical Exploration: Third Edition, Blackwell Science Ltd., Malden Massachusetts.

Sharma, P., 1997, Environmental and Engineering Geophysics, Cambridge University Press, New York, New York.

Redpath, B., 1973, Seismic Refraction Exploration for Engineering Site Investigations, Explosive Excavation Research Laboratory, Livermore, California.

Appendix D

Seismic Refraction

Reciprocal method results and BH data

Table 1-D: Summary of shear wave velocities (Vs) and layer thicknesses (H) from refraction surveys (reciprocal method) and boreholes (BH) for Lines 1-1 and 1-2.

Layer	Line 1-1			Line 1-2		
	Vs (m/s)	H (m)	BH - H (m)	Vs (m/s)	H (m)	BH - H (m)
1	133	2.2	1.4	103	1.5	N/A
2	420	3.8	1.2	500	4.9	N/A
3			2.9			4.1
4	742	N/A	N/A	742	N/A	N/A

Table 2-D: Summary of shear wave velocities (Vs) and layer thicknesses (H) from refraction surveys (reciprocal method) and boreholes (BH) for Lines 2-1, 2-2, and 2-3.

Layer	Line 2-3			Line 2-1			Line 2-2		
	Vs (m/s)	H (m)	BH - H (m)	Vs (m/s)	H (m)	BH - H (m)	Vs (m/s)	H (m)	BH - H (m)
1	161	2.2	1.1	109	1.4	0.9	111	1.9	0.6
2	290	4.3	1.6	301	9.1	2.5	309	9.3	2.4
3			3.9			6.3			7.5
4	779	N/A	N/A	723	N/A	N/A	908	N/A	N/A

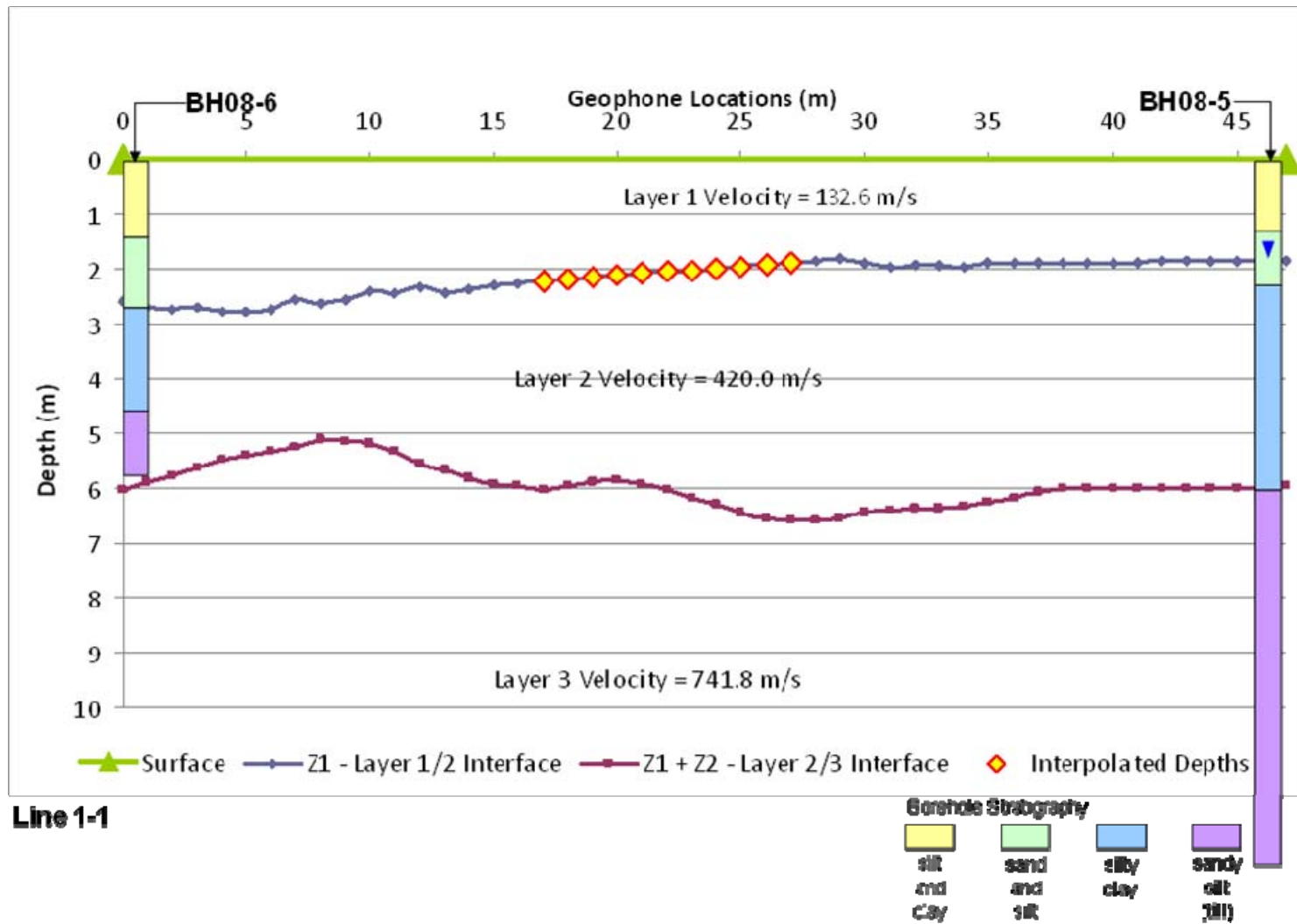


Figure 1-D. Seismic refraction results (reciprocal method) and BH information for Line 1-1

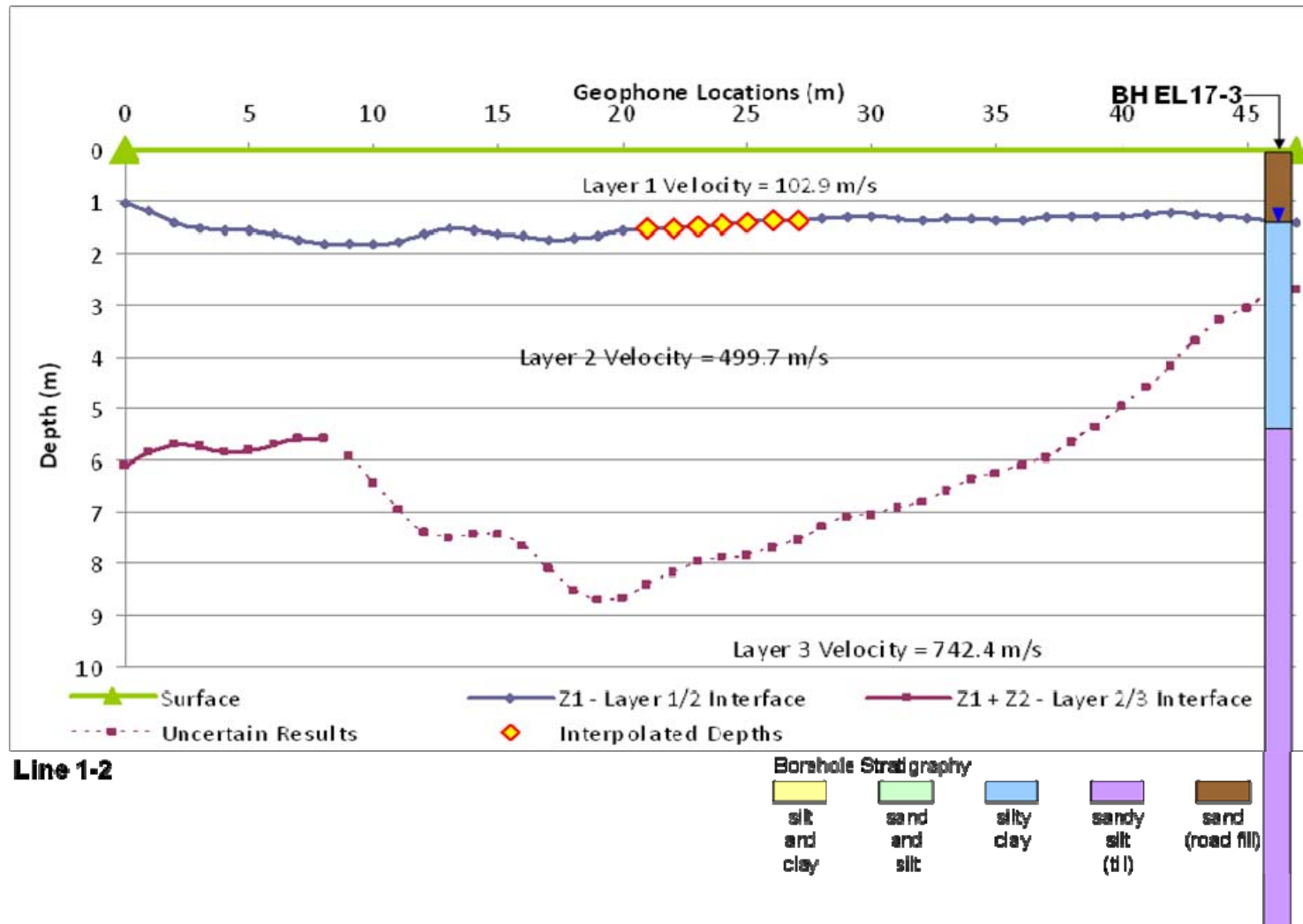


Figure 2-D. Seismic refraction results (reciprocal method) and BH information for Line 1-2

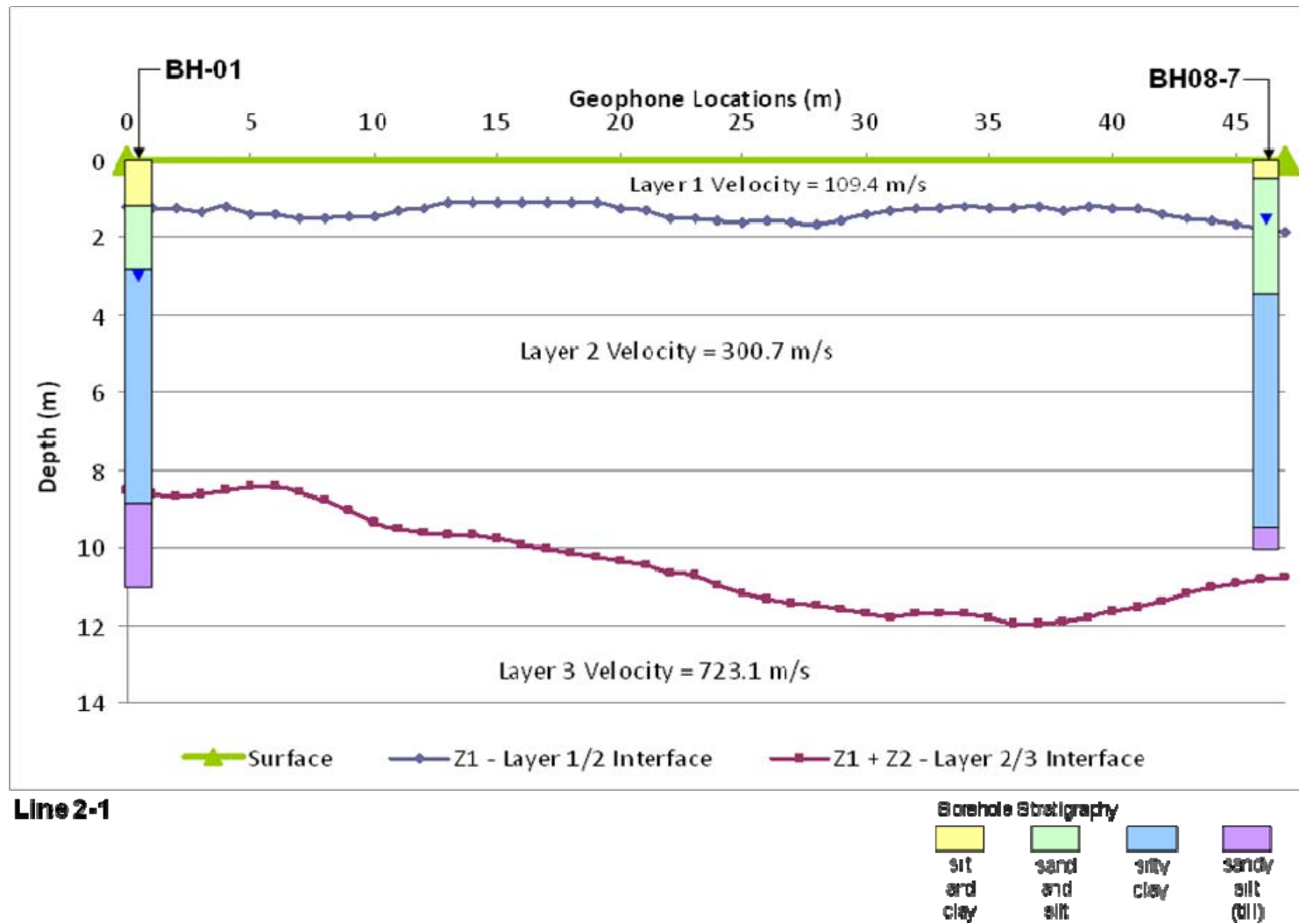


Figure 3-D. Seismic refraction results (reciprocal method) and BH information for Line 2-1

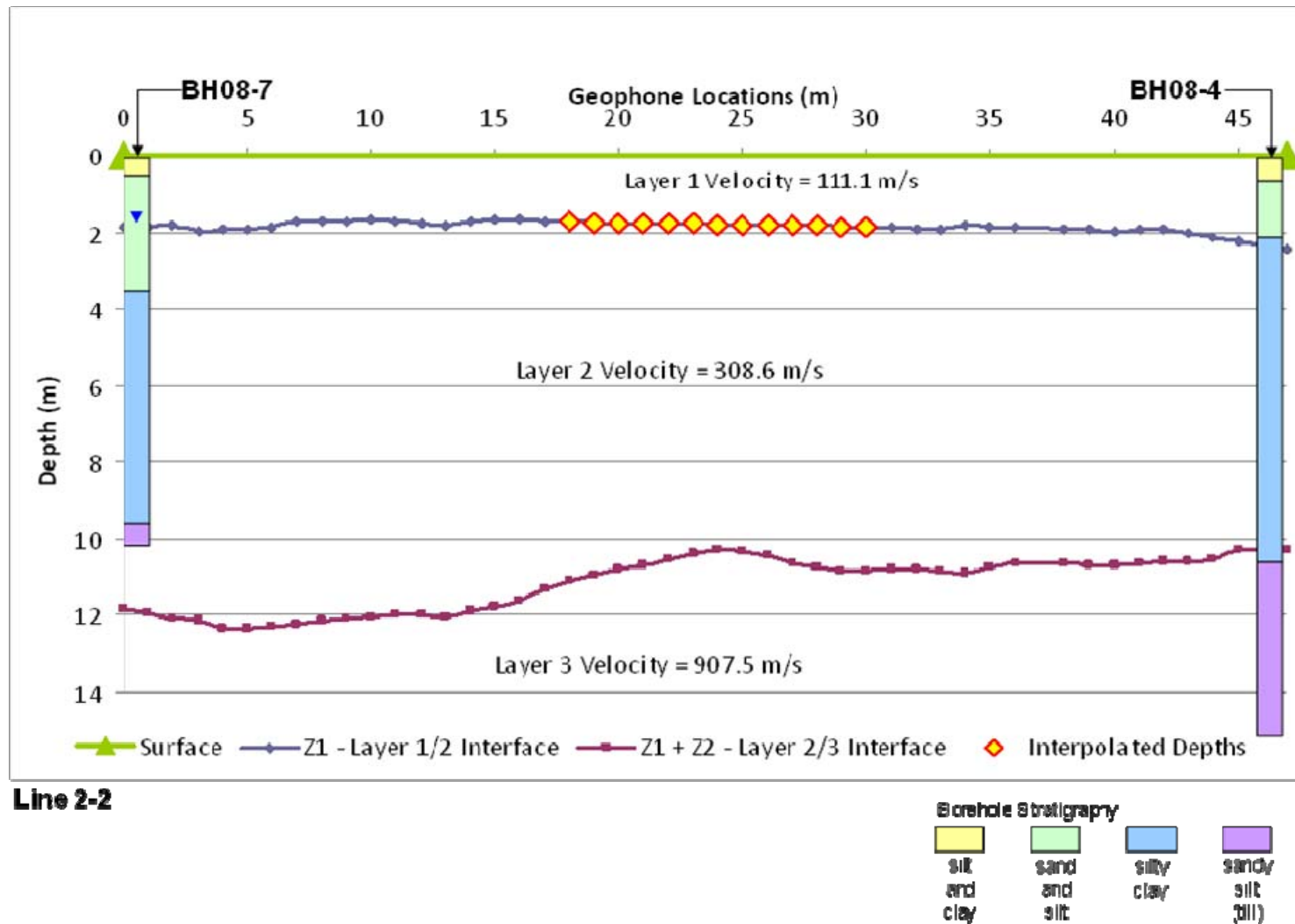
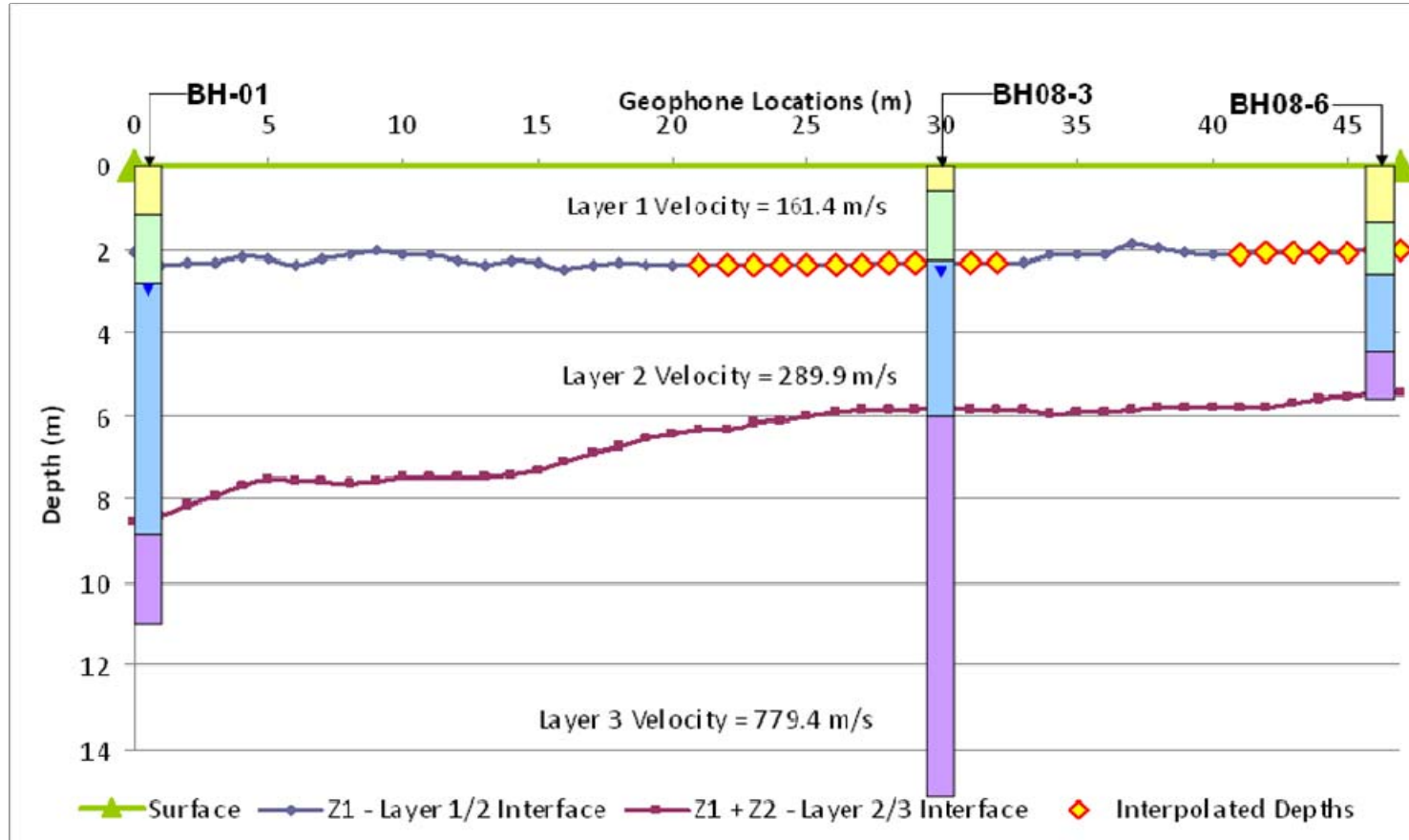


Figure 4-D. Seismic refraction results (reciprocal method) and BH information for Line 2-2



Line 2-3

Borehole Stratigraphy



Figure 5-D. Seismic refraction results (reciprocal method) and BH information for Line 2-3

Appendix E

Basics of the multiple channel analysis of surface waves method (MASW)

SURFACE WAVE SURVEYING

Introduction

The MASW test layout is the same as the seismic refraction method, however only off-end sources are recorded. In addition, the MASW method typically requires a larger seismic source to generate long wavelengths with sufficient energy (Figure 1-E). A MASW test consists of a seismic source located at different distances from an array of geophones. (Park et al. 1999, Nazarian and Stokoe, 1984). The area between the source and the receivers is not studied as in the case of the seismic refraction method, but rather the area between the receivers. The change in phase with frequency for different Rayleigh waves propagating along the seismic array is measured. This variation of wave velocity with frequency or wavelength is known as dispersion curve (Figure 2-E). The processing of surface wave data consists of extracting the dispersion curve from experimental data. The inversion of the dispersion curve is performed by using an iterative algorithm that fits a theoretical dispersion curve to the field data. The shear-wave velocity profile (wave velocity and thickness) that minimizes the error between the theoretical and measured dispersion curves is considered the solution to the inversion problem (Figure 3-E).

Fundamentals of the MASW method

The test geometry used in the MASW method determines the range of wavelengths that can accurately be measured (Stokoe et al. 1988; Al-Hunaidi 1993). Seismic waves must travel a minimum distance from the source before being fully formed (near-field effects). Moreover, low signal-to-noise ratios can be present at large distances from the source, relative to the wavelength (far-field effects). The Rayleigh wavelength (λ) is related to Rayleigh wave velocity (V), and frequency (f) as:

$$\lambda = \frac{V}{f} \quad [1-E]$$

The phase velocity is obtained from the absolute phase difference of each frequency component, $\Delta\phi(f)$, and is defined as

$$V(f) = 2\pi \cdot f \cdot \frac{\Delta x}{\Delta\phi(f)} \quad [2-E]$$

where Δx is the offset between the two receivers. The calculated phase velocity is therefore an average velocity of the medium between the two receivers. Errors in unwrapping of the phase function will result in incorrect phase velocities for all frequencies greater than the frequency at which the phase function was erroneously unwrapped. Rayleigh waves dominate ground motion; however, other seismic waves may

significantly affect the phase function over certain ranges. To determine the range of wavelengths for which the phase is dominated by well formed Rayleigh waves, different empirical relationships for given test geometries have been proposed (Heisey et al. 1982; Gucunski 1991, 1996). The most commonly employed are the criteria proposed by Heisey et al. (1982), where the offset from the source to the first receiver is equal to the receiver spacing, Δx , and is given by

$$\frac{\lambda}{3} \leq \Delta x \leq 2\lambda \quad [2-E]$$

where λ is the Rayleigh wavelength. To collect a wide range of wavelengths, the phase difference from several receiver separations and source offsets must be used to obtain a dispersion curve. Microtremors and ambient noise have been successfully used as seismic sources (Horike 1985; Takimatsu et al. 1992; McMechan and Yedlin 1981, Zywicki and Rix 1999) for exploration of depths greater than 30 metres. Because of the problems associated with the generation of low frequency waves with high signal-to-noise ratios.

In usual active configurations (Park et al., 1999, Socco and Strobbia, 2004), the source is aligned with the array, and hence the apparent velocity is coincident with the real velocity. When the source is not aligned with the array, but is far enough to assume plane wave propagation, the angle between the directions of the propagation and of the array is non-zero, and only an apparent velocity can be observed with the linear array. The refraction microtremors technique (REMI) has recently been proposed to estimate the seismic response of different sites. This technique can be applied using the standard equipment for seismic refraction and with the standard linear geophone array (Strobbia et al. 2008). The record is segmented in overlapping subwindows, which are amplitude normalised. For each subwindow the frequency-wavenumber (f-k) spectrum is computed, normalised (normalised at each frequency) and stacked. The symmetry of the final stacked spectrum is analysed to evaluate the validity of the basic hypothesis of the REMI. The processing then considers all the frequencies one at a time including negative and positive wavenumbers. Each of the two sections of the f-k spectrum is inverted, fitting with the theoretical spectrum computed for the given geometry of the array and a uniform source distribution.

Interpretation techniques

In the MASW method, there are primarily three different techniques to compute the dispersion curve (plot of phase velocity versus wavelength, Figure 1-E): the one-third rule, the phase unwrapping method, and the f-k analysis or 2D Fourier transform. The simplest method is to assign the measured Rayleigh wave velocity to a depth equal to one third of the corresponding wavelength (one-third rule). Since depth of

penetration of surface waves is proportional to the wavelength, longer wavelengths penetrate deeper into the ground (Figure 1-E), and should therefore generally have a faster velocity than shorter wavelengths, assuming seismic velocity increases with depth.

The phase unwrapping method consists of measuring the phase difference of Rayleigh waves as they travel between the geophones (Stokoe and Nazarian 1983). Phase velocity is computed as distance over travelttime (eq. 2-A), where distance, d , is the geophone spacing and travel-time, t , is computed from the phase difference of each wavelength. The most effective technique is to compute the dispersion curve by application of a 2D Fourier transform (Park et al. 1999); which convert the data from the time-offset domain into a frequency-phase velocity or frequency-slowness, or frequency-wavenumber domain (McMechan and Yedlin, 1981). Using a forward-iterative model, the dispersion curve is best fit to a ground profile to obtain a stiffness profile of the tested ground with respect to depth (Thomson 1950; Haskell 1953; Kausel and Roësset 1981; Kennet 1974).

Surface wave inversion. Tomographic inversion requires specialized software packages such as SWAN. This method begins with an initial velocity model of multiple layers with a range of velocities specified by the user. The one-third rule can be used to determine an applicable velocity range for the initial model. This initial model consists of a selected number of constant velocity layers. The thickness of the layers can be adjusted by the user at the end of the inversion to assess the effect of thickness in the predicted dispersion curve. Collecting data in a given frequency range can be accomplished by either using a vibroseis seismic source or by using an impulsive source. Dispersion curves in this case can be calculated not only for the fundamental-mode Rayleigh waves, but also for higher-mode Rayleigh waves. Figures 4-E and 5-E show typical results of the measured and predicted dispersion curves for lines 1-1 and 2-1. Predicted higher modes are also shown in these figures. For line 1-1 (Fig. 4-E), the fundamental and the first high mode are very close at 32 Hz. Therefore, higher modes affect the results and they must be considered in the data interpretation. For line 2-1 (Fig. 5-E), higher modes are farther apart from the fundamental mode; thus the interpretation of the results for this line is easier.

Problems and limitations

The inherent problem of the MASW method is the difficulty of generating low frequencies to reach greater penetration depths with high signal-to-noise ratio. As in the case of seismic refraction, a velocity reversal makes the data interpretation more difficult because the propagation is not governed by the fundamental mode only but also by higher modes (Stokoe et al. 1988). The effect of higher modes on the phase function has been shown to be associated with MASW test geometry (Al-Hunaidi 1993; Stokoe et

al. 1988), and can be minimized by changing the test configuration. The effect of higher modes affects the phase function and the calculation of phase velocity. Since most MASW inversion algorithms account only for the fundamental mode, inversion in these settings can give incorrect results. A gradual variation in velocity in the vertical direction can be detected with the MASW if the frequency content of the source is adequate. However, variations in the lateral direction can dramatically affect the success of this method.

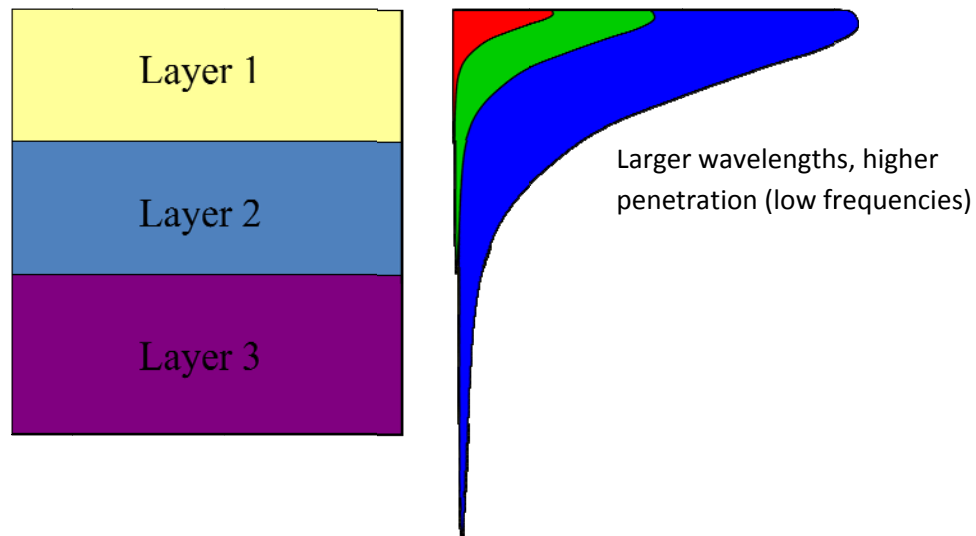


Figure 1-E: Penetration of surface waves for different frequencies (wavelengths)

Figure 2-E: Measured dispersion curve

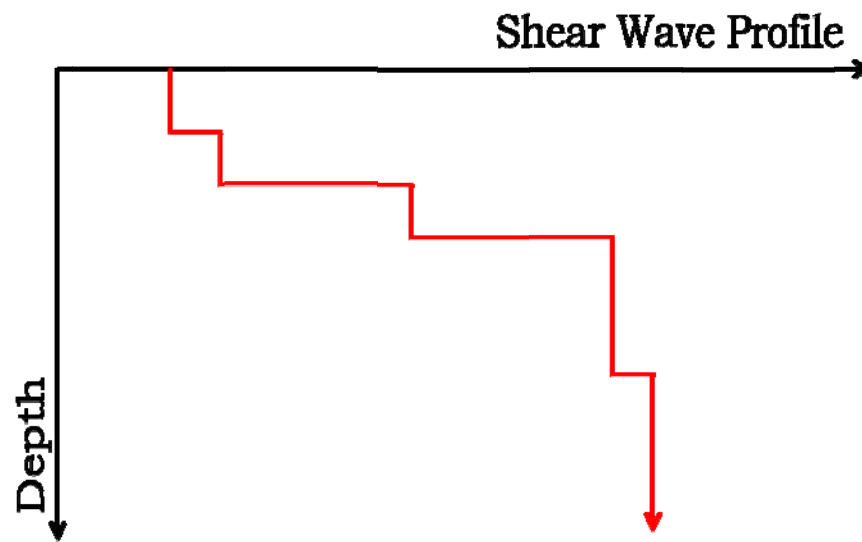


Figure 3-E: Inverted soil profile from measured dispersion curve

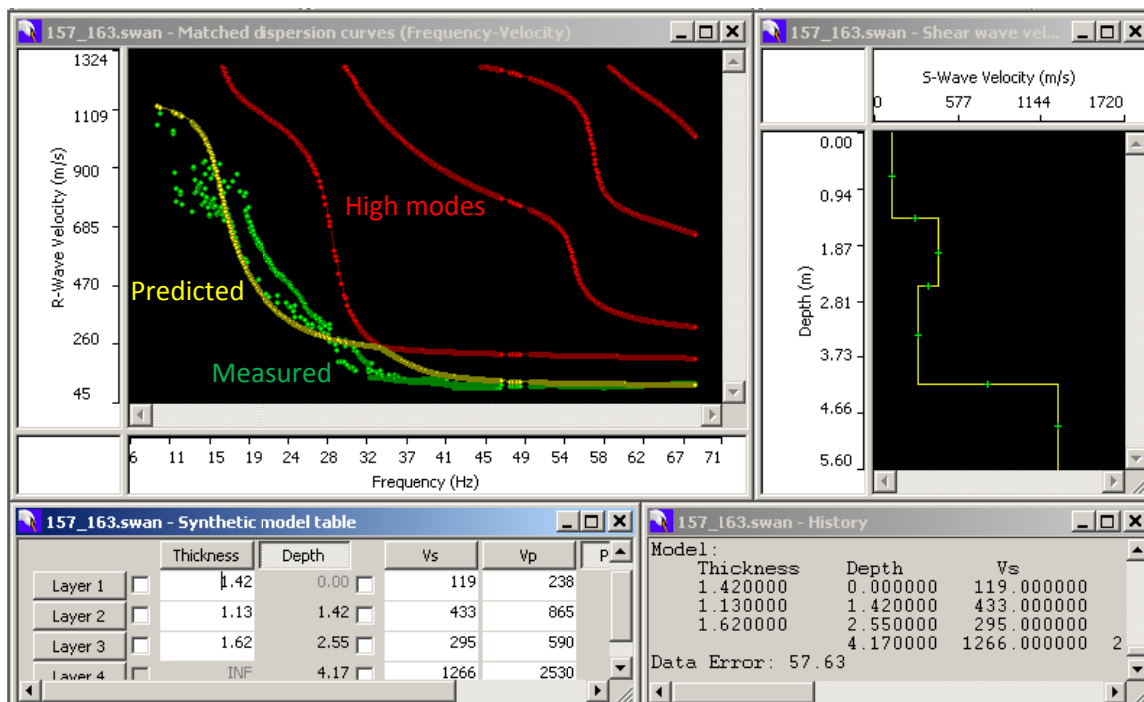


Figure 4-E: Typical dispersion curve and soil profile Line 1-1. Shots at -2 and 2 m.

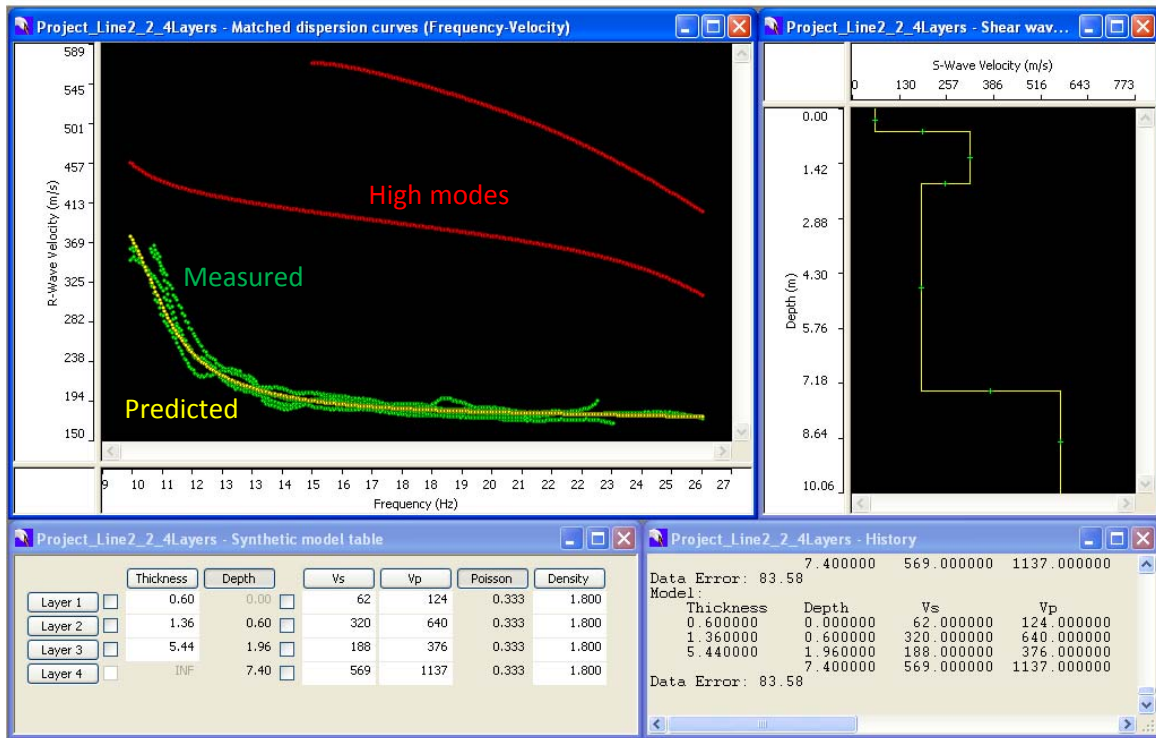


Figure 5-E Typical dispersion curve and soil profile Line 2-2. Shots at 2, 6, and 20 m.

References

- Al-Hunaidi, M.O., 1993, Insights on the SASW nondestructive testing method: *Canadian Journal of Civil Engineering*, 20, 940-950.
- McMechan G.A., Yedlin M.J., 1981, Analysis of dispersive wave by wave field transformation, *Geophysics*, 46, 869-874
- Takimatsu, K., Tamura, S., and Kojima, H., 1992, Effects of multiple modes on Rayleigh wave dispersion characteristics: *Journal of Geotechnical Engineering, ASCE*, 118(10), 1529-1543.
- Gucunski, N., Ganji, V., & Maher M.H., 1996, Effects of obstacles on Rayleigh wave dispersion obtained from the SASW test: *Soil Dynamics and Earthquake Engineering*, 15(4), 223-231
- Gucunski, N., 1991, Generation of low frequency Rayleigh waves for the spectral-analysis-of-surface-waves method: Ph.D. Dissertation, University of Michigan.
- Haskel, N.A., 1953, The dispersion of surface waves on multilayered media: *Bull. Seismol. Soc. Am.*, 54(2), 627-679.
- Heisey, J.S., Stokoe II, K.H., and Meyer, A.H., 1982, Moduli of Pavement Systems from Spectral Analysis of Surface Waves: *Transportation Research Record* 852: 22-31.
- Horike, M., 1985, Inversion of Phase Velocity of Long-Period Microtremors to the S-Wave-Velocity Structure down to the Basement in Urbanized Areas: *Journal of Physics of the Earth*, 33: 59-96.
- Kausel, E., and Roësset, J.M., 1981, Stiffness matrices for layered soils: *Bulletin of the Seismological Society of America*, 71(6): 1743-1761.
- Kennet, B.L.N., 1974, Reflections, rays and reverberations: *Bulletin of the Seismological Society of America*, 64(6): 1685-1696.
- McMechan, G. A., and Yedlin, M. J., 1981, Analysis of dispersive waves by wave field transformation: *Geophysics*, 46, 869-874.
- Nazarian, S., Stokoe, K. H., 1984, In-situ shear wave velocities from spectral analysis of surface waves: in *Proc. of the Eighth World Conf. on Earthquake Engineering*, San Francisco, California, Vol. III, 31–38.
- Park, C.B., Miller, R.D., & Xia, J., 1999, Multichannel analysis of surface waves: *Geophysics*, 64(3), 800-808.
- Socco, V., and Strobbia, C., 2004. Surface-wave method for near-surface characterization: a tutorial. *Near Surface Geophysics*, 2: 165-185.
- Strobbia, C., 2002. Surface wave methods: acquisition, processing and inversion. PhD Diss. Politecnico di Torino. Italy.

Stokoe II, K.H., Nazarian, S., Rix, G.J., Sanchez-Salinero, I., Sheu, J.C., and Mok, Y.J., 1988, In-Situ Seismic Testing of Hard-To-Sample Soils by Surface Wave Method: Earthquake Engineering and soil dynamic II - Recent advances in ground-motion evaluation, Von Thun, J.L (ed), Utah, Geotechnical special publication 20: 264-279.

Stokoe II, K.H., and Nazarian, S., 1983, Effectiveness of Ground Improvement from Spectral Analysis of Surface Waves: Proceedings, The 8th European Conference on Soil Mechanics and Foundation Engineering, Improvement of Ground, Rathmayer, H.G., and Saari, K.H.O. (eds), Helsinki: 91-94.

Thomson, W., 1950, Transmission of elastic waves through a stratified soil medium: J. Appl. Physics, 21(2), 89-93.

Zywicki, D.J., and Rix, G., 1999, Frequency-wavenumber Analysis of Passive Surface Waves: 12th Annual Symposium on the Application of Geophysics to Environmental and Engineering Problems, Oakland, California: 75-84.

Appendix F

Measured and Computed Dispersion Curves for Line 1 (MASW)

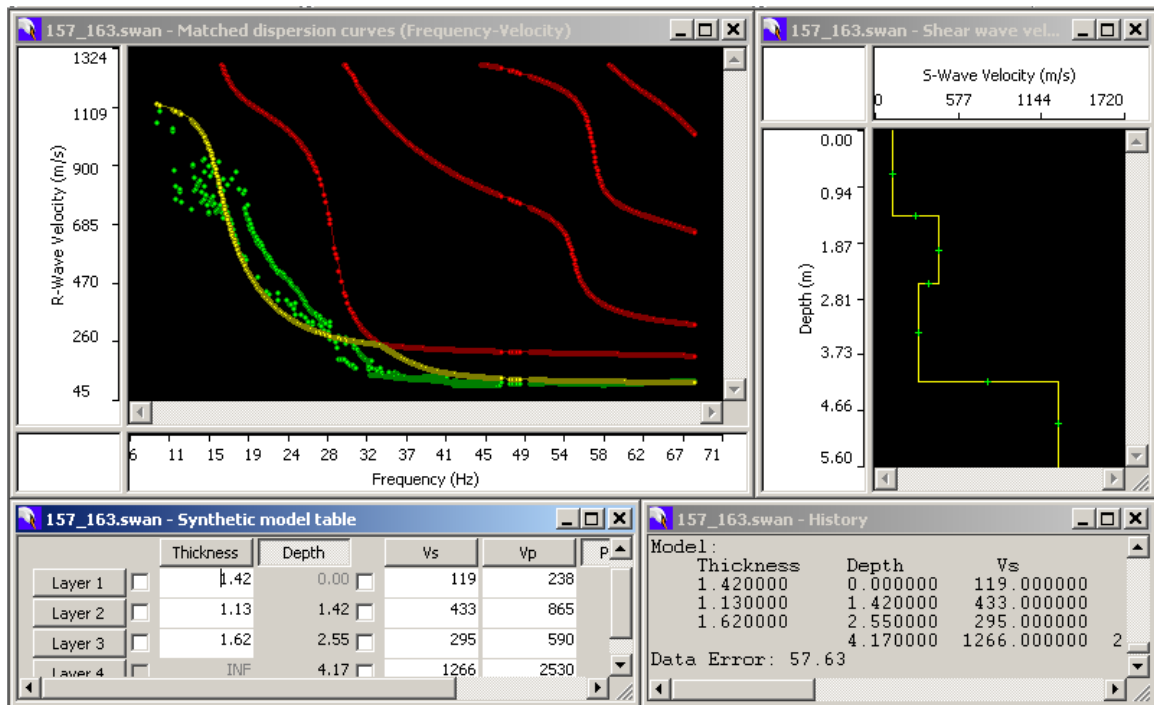


Figure 1-F Dispersion curve and soil profile Line 1-1 with shot at -2m and +2m.

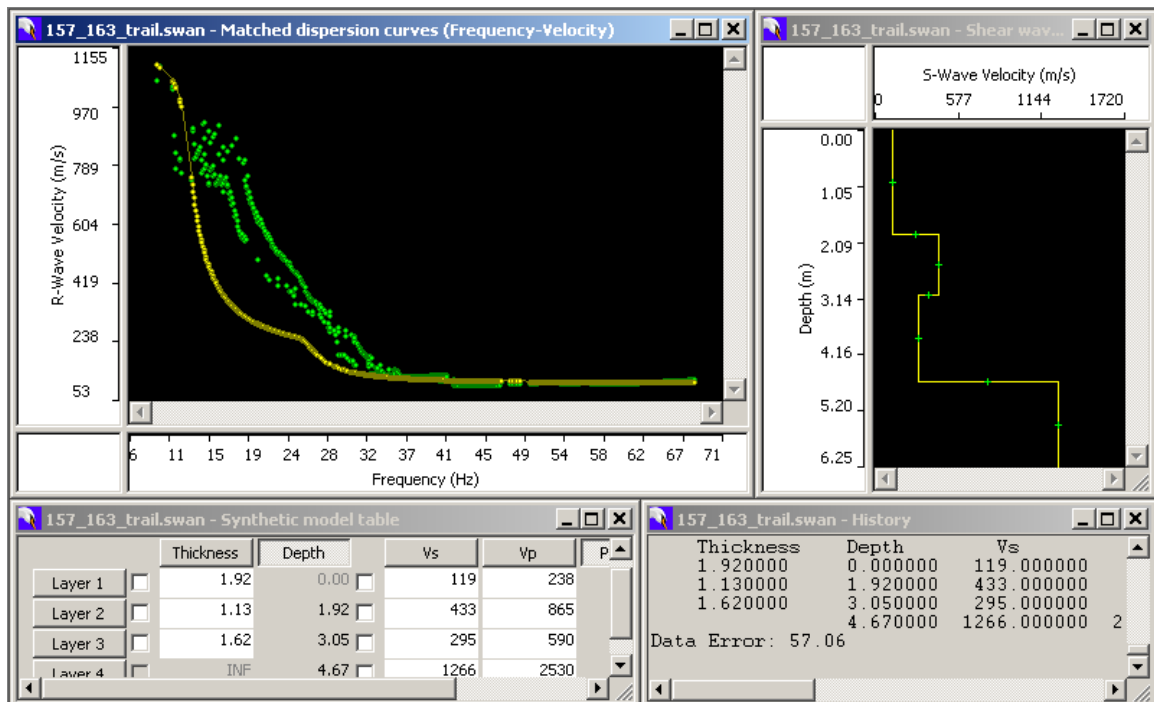


Figure 2-F Dispersion curve and soil profile Line 1-1 with shot at -2m and +2m (first layer increased by 0.5 m).

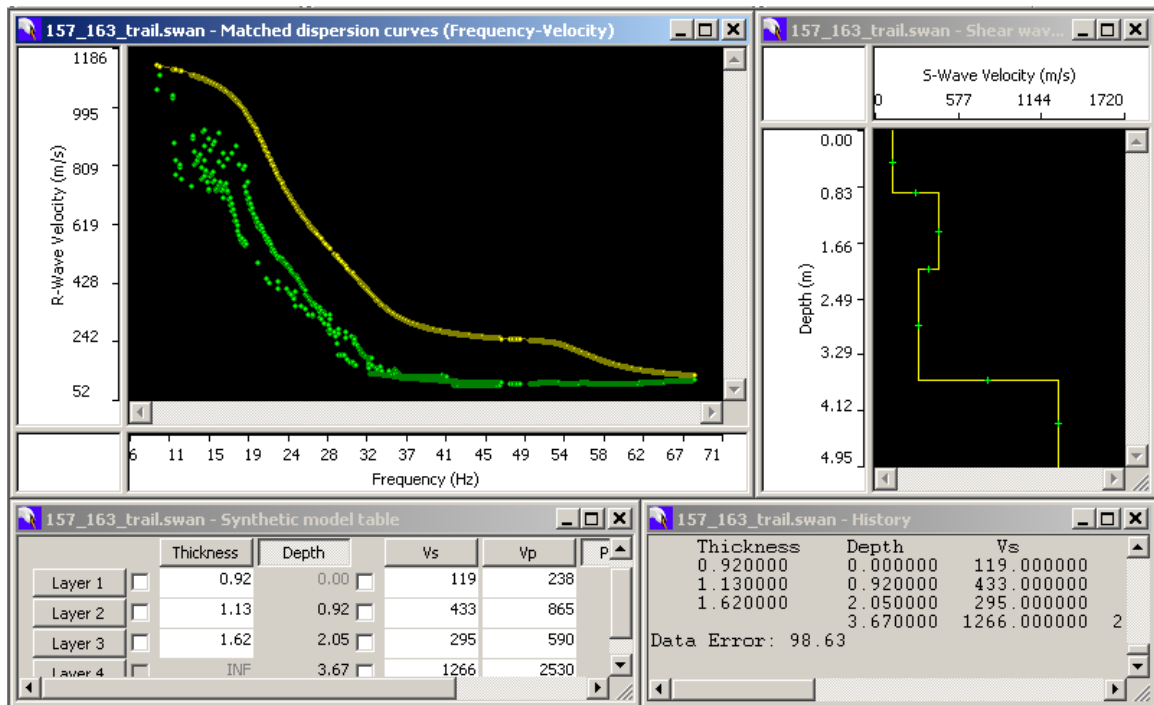


Figure 3-F Dispersion curve and soil profile Line 1-1 with shot at -2m and +2m (first layer decreased by 0.5 m).

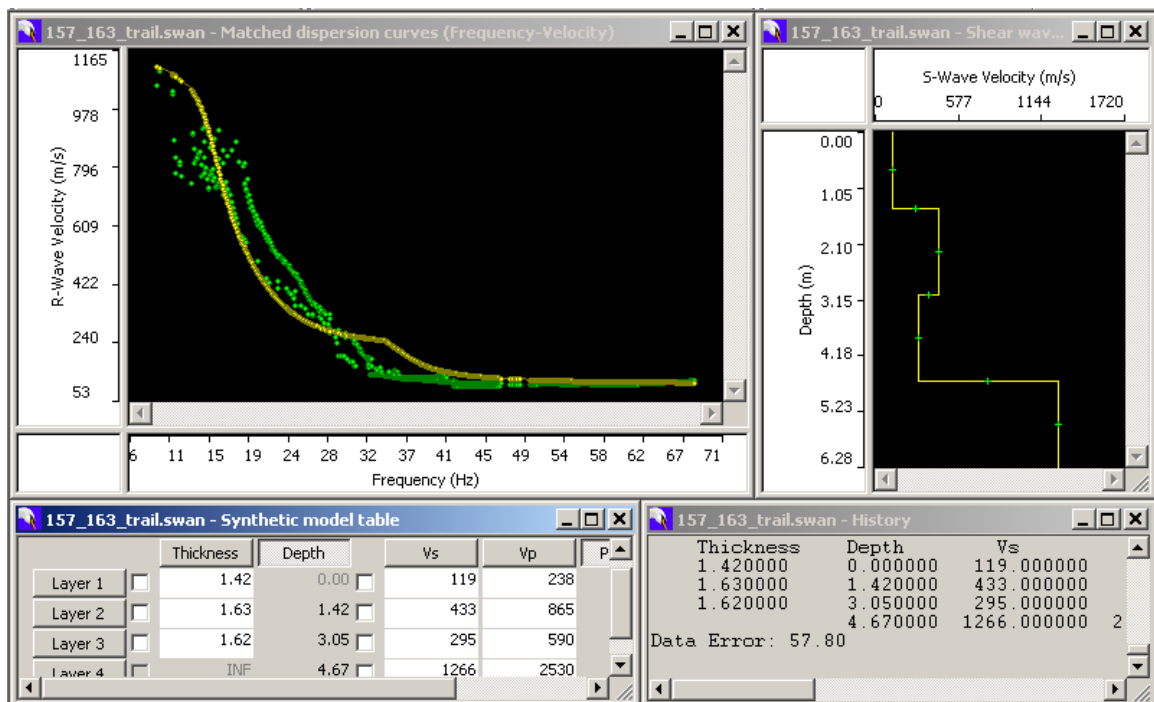


Figure 4-F Dispersion curve and soil profile Line 1-1 with shot at -2m and +2m (second layer increased by 0.5 m).

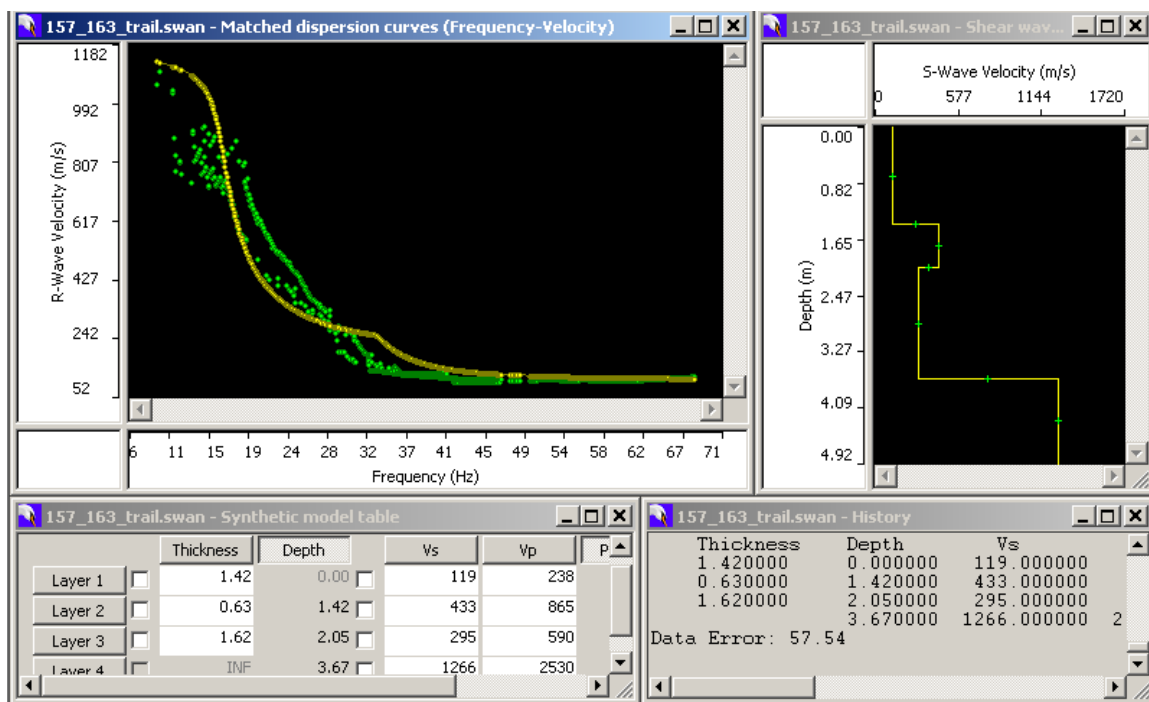


Figure 5-F Dispersion curve and soil profile Line 1-1 with shot at -2m and +2m (second layer decreased by 0.5 m).

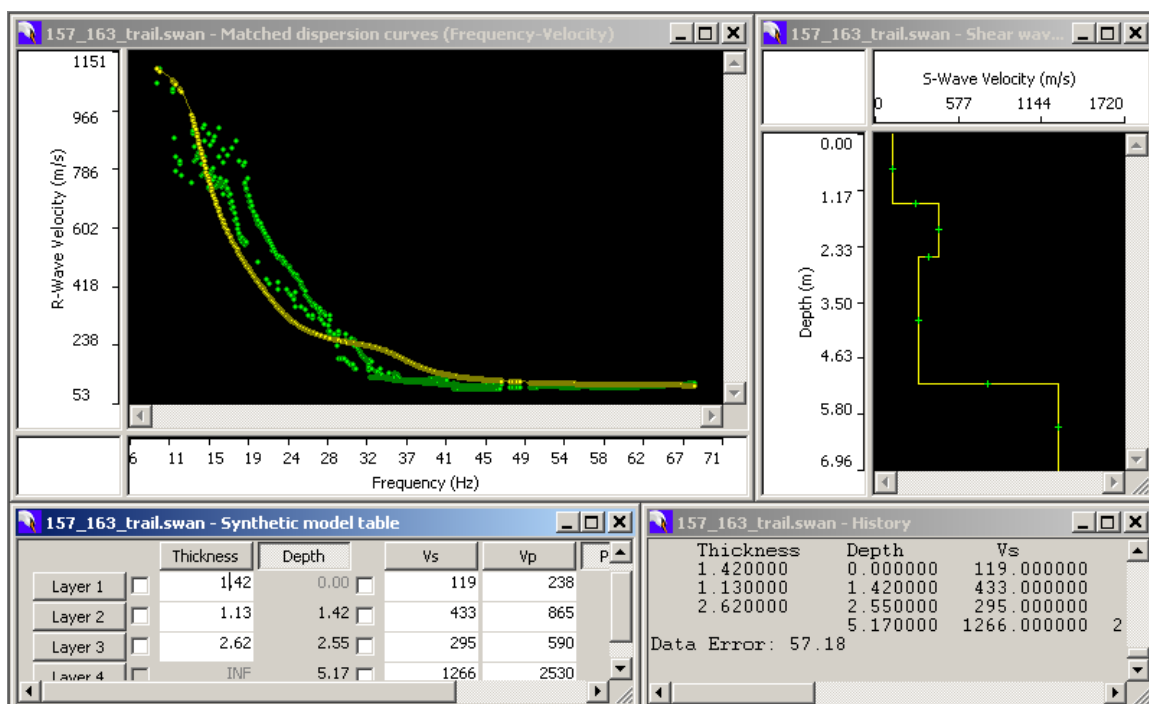


Figure 6-F Dispersion curve and soil profile Line 1-1 with shot at -2m and +2m (third layer increased by 1 m).

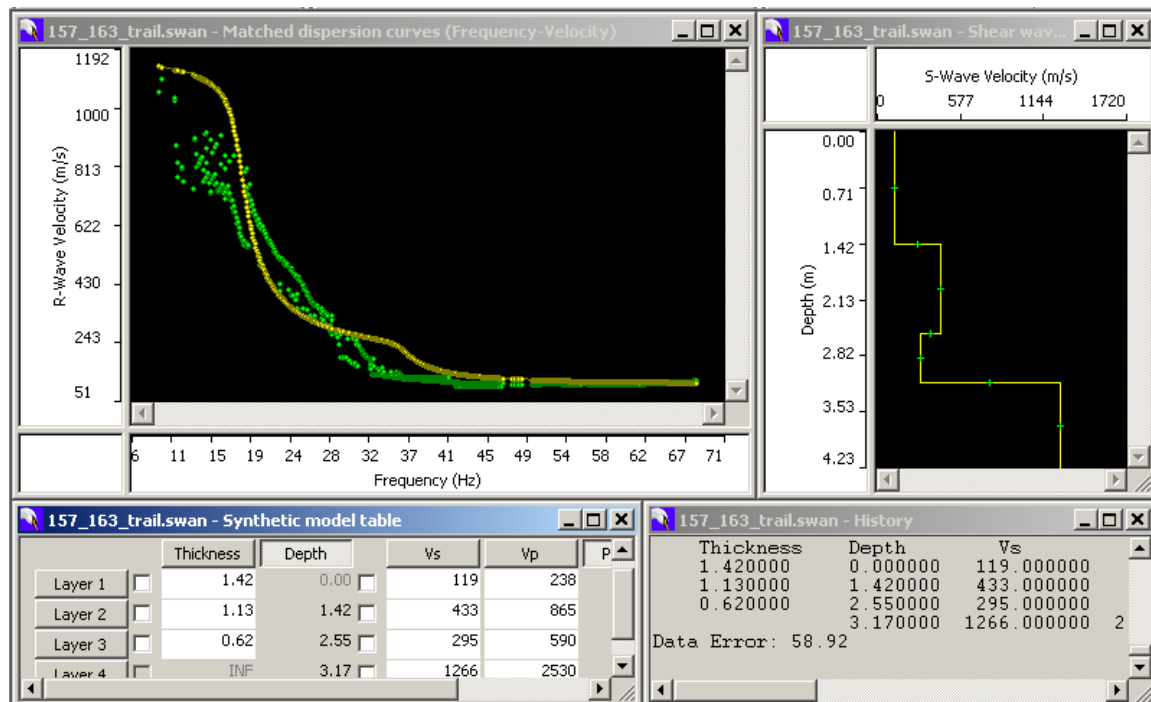


Figure 7-F Dispersion curve and soil profile Line 1-1 with shot at -2m and +2m (third layer decreased by 1 m).

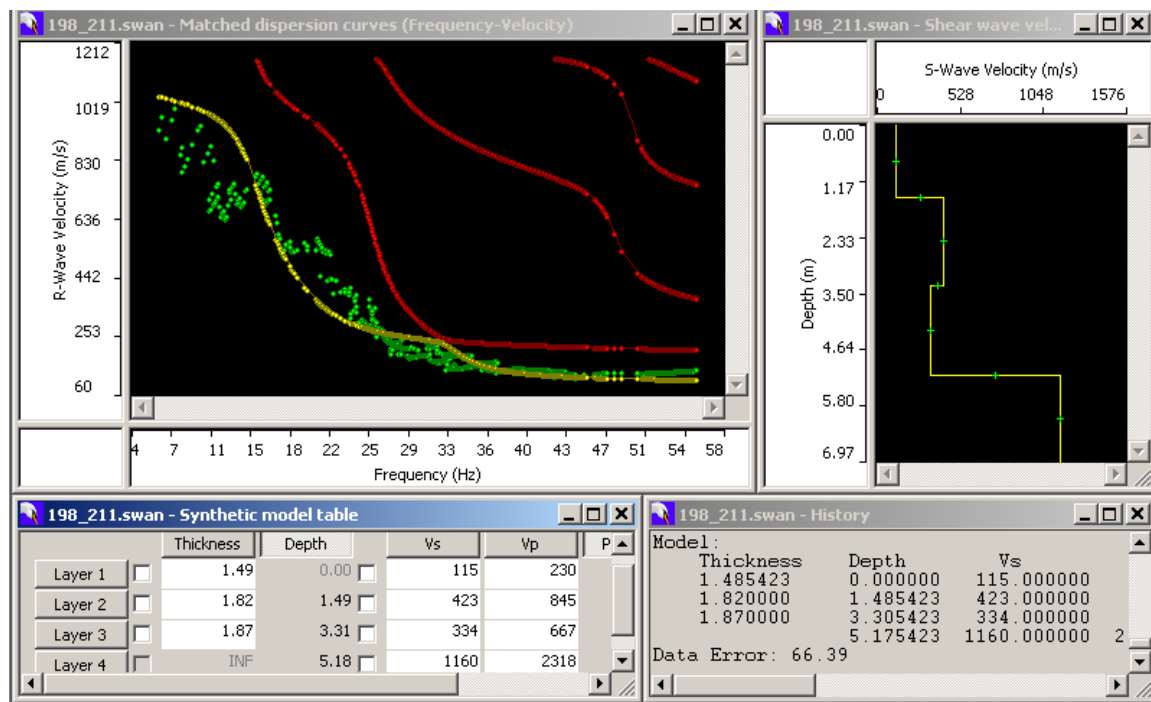


Figure 8-F Dispersion curve and soil profile Line 1-2 with shot at -18m and +6m.

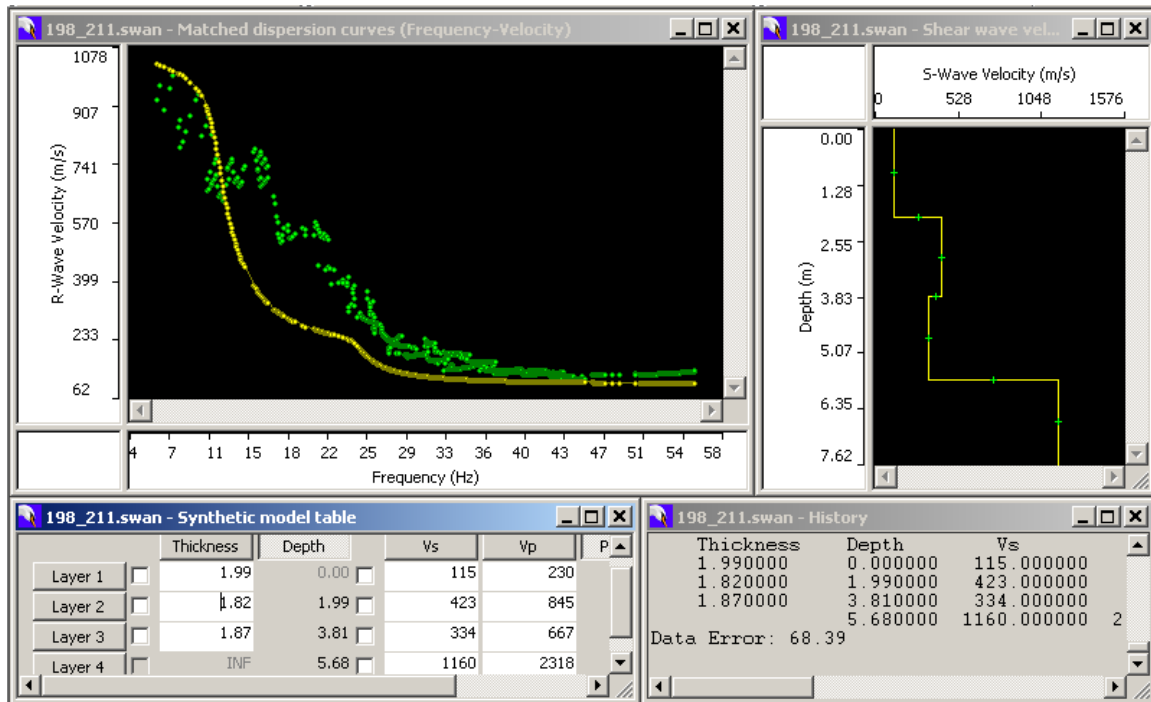


Figure 9-F Dispersion curve and soil profile Line 1-2 with shot at -18m and +6m (first layer increased by 0.5 m).

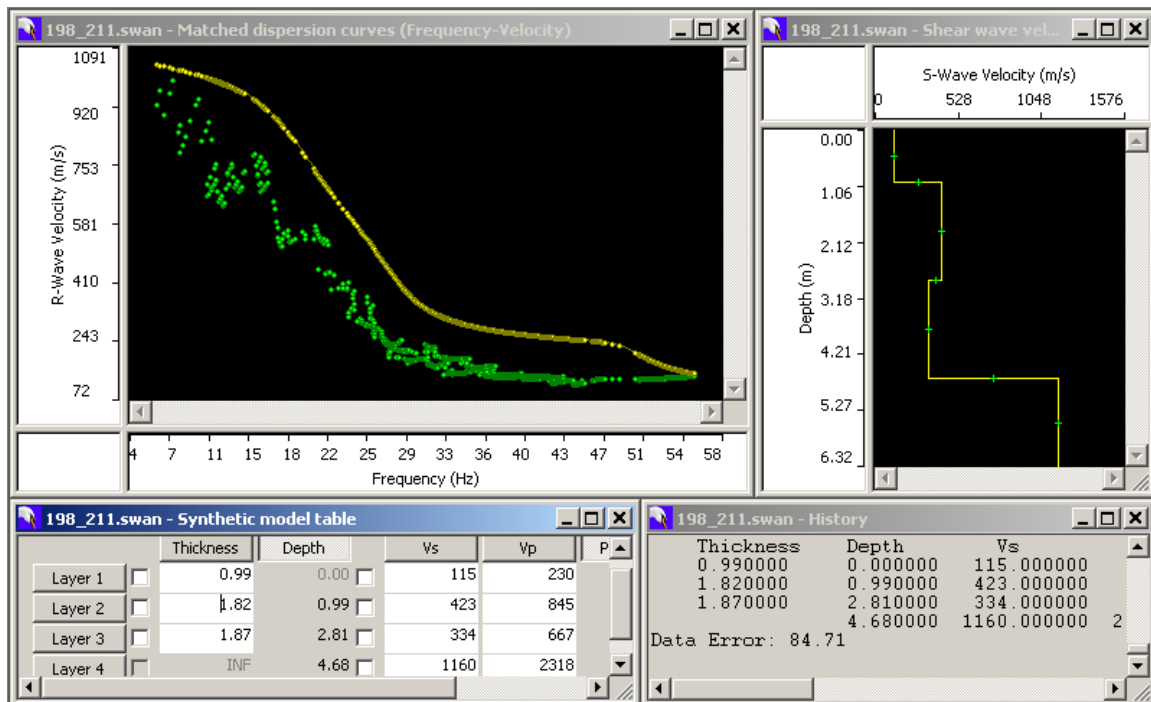


Figure 10-F Dispersion curve and soil profile Line 1-2 with shot at -18m and +6m (first layer decreased by 0.5 m).

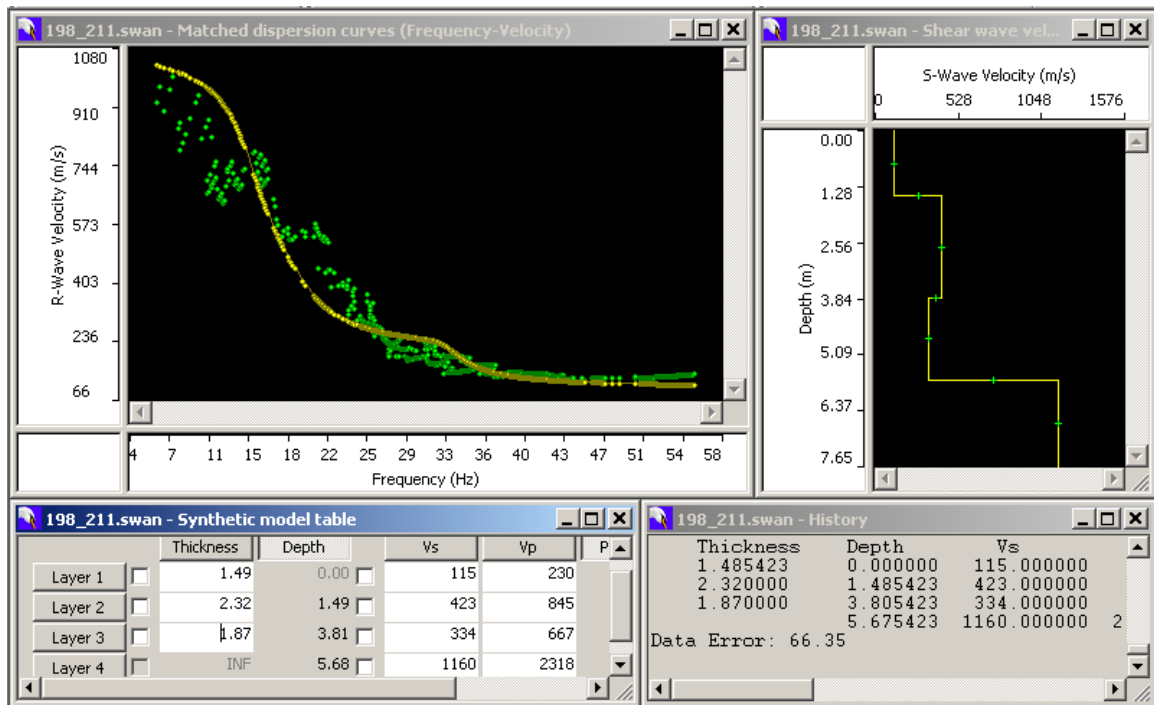


Figure 11-F Dispersion curve and soil profile Line 1-2 with shot at -18m and +6m (second layer increased by 0.5 m).

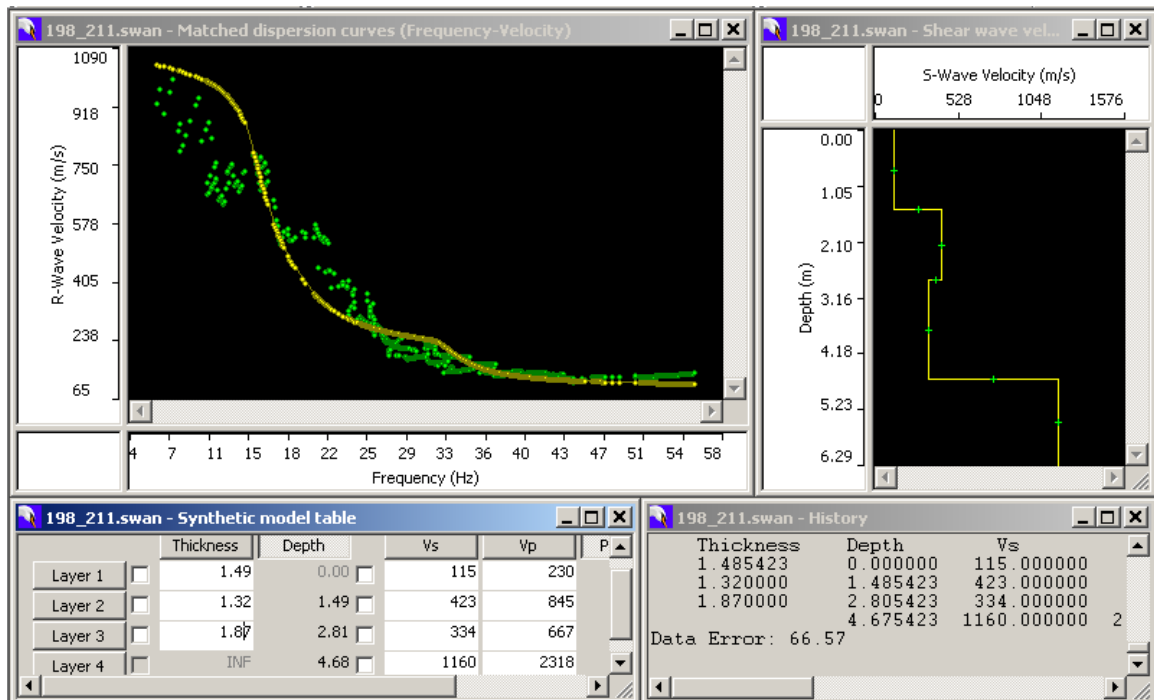


Figure 12-F Dispersion curve and soil profile Line 1-2 with shot at -18m and +6m (second layer decreased by 0.5 m).

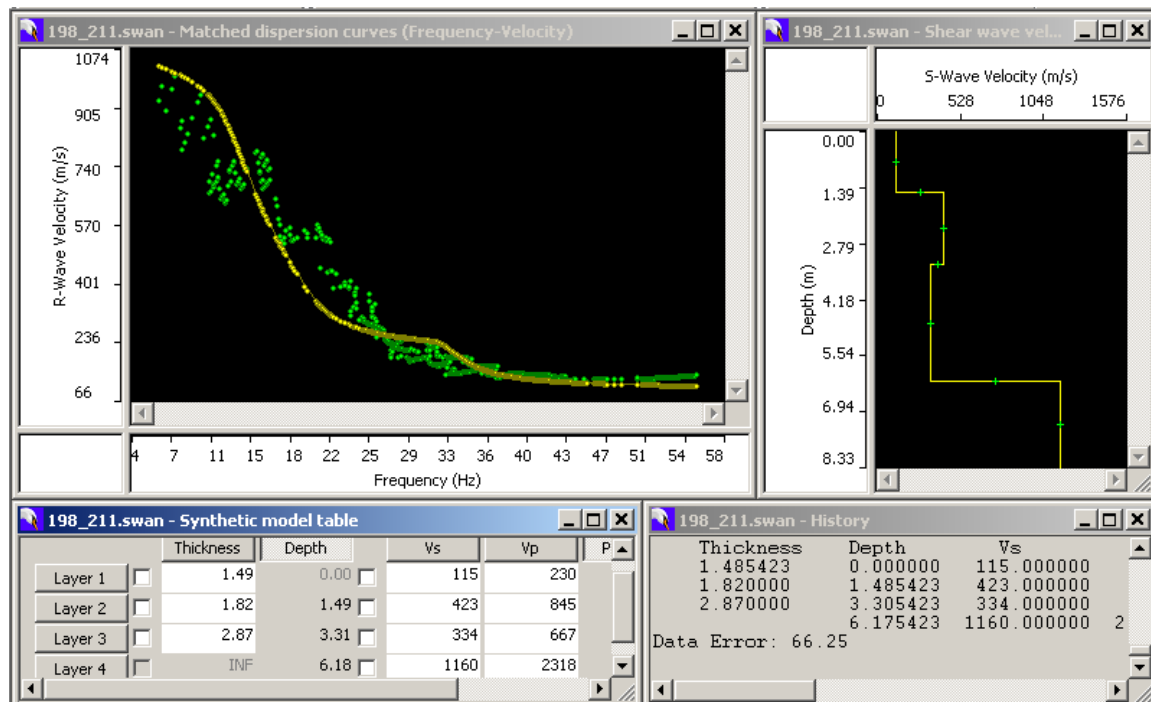


Figure 13-F Dispersion curve and soil profile Line 1-2 with shot at -18m and +6m (third layer increased by 1m).

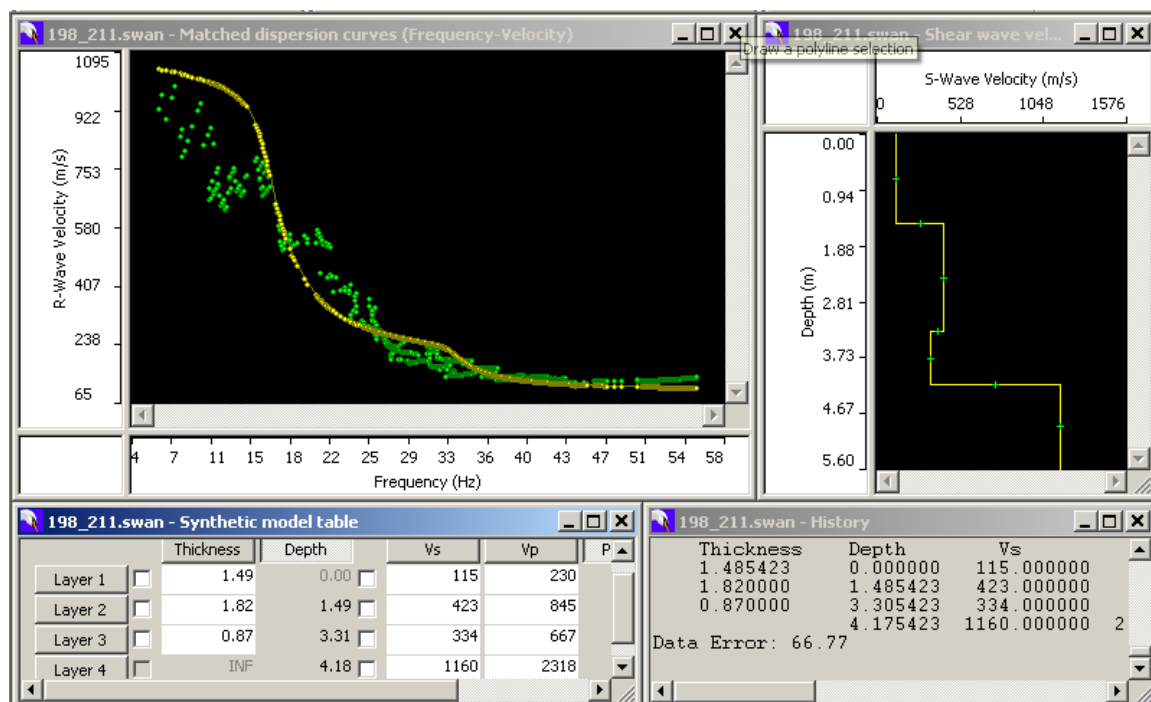


Figure 14-F Dispersion curve and soil profile Line 1-2 with shot at -18m and +6m (third layer decreased by 1 m).

Appendix G

Measured and Computed Dispersion Curves for Line 2 (MASW)

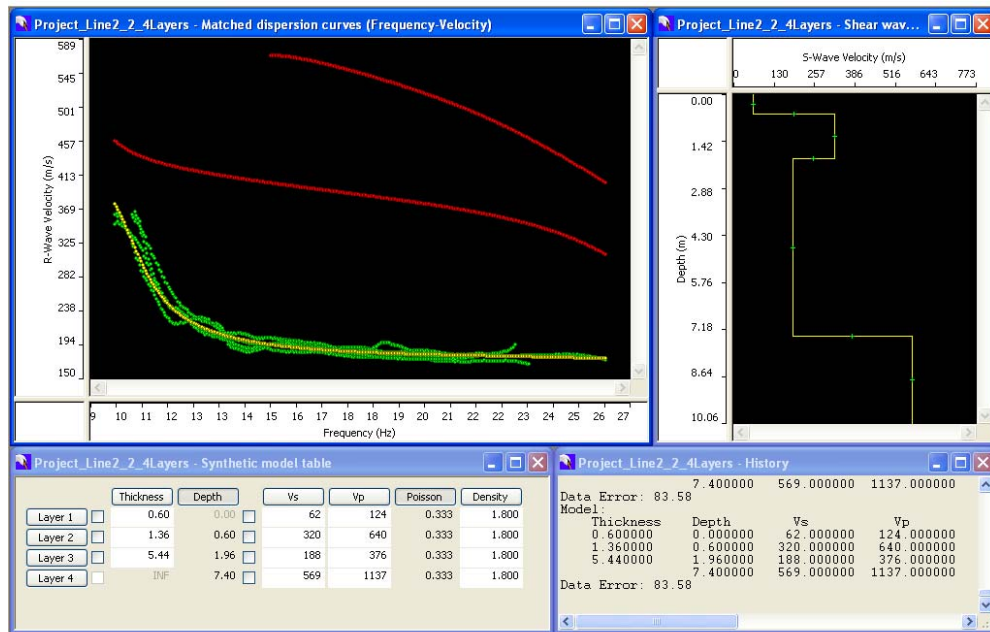


Figure 1-G Dispersion curve and soil profile Line 2-2

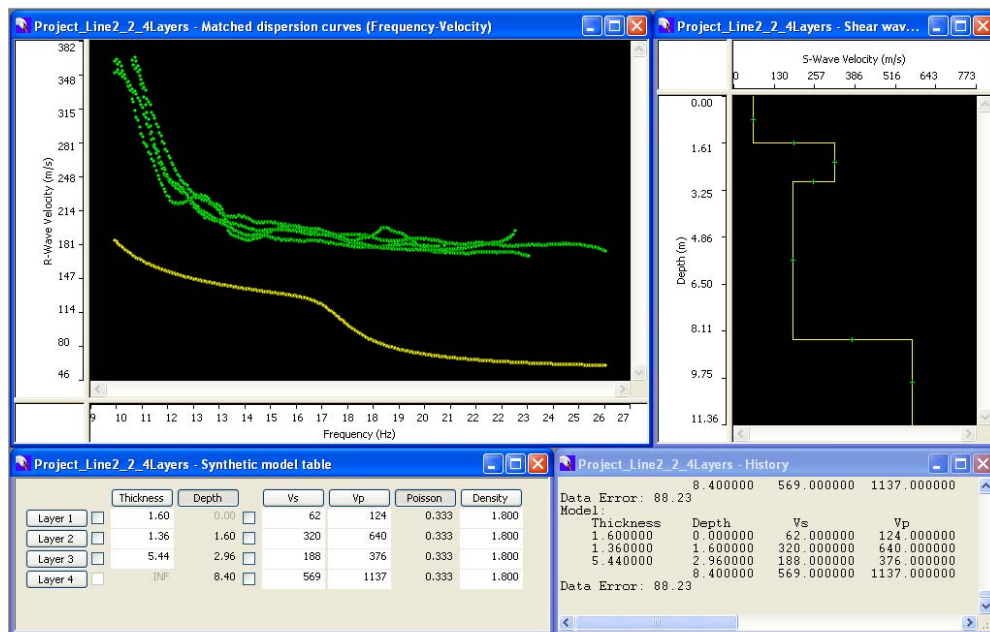


Figure 2-G Dispersion curve and soil profile Line 2-2 (thickness first layer increased in 1 m)

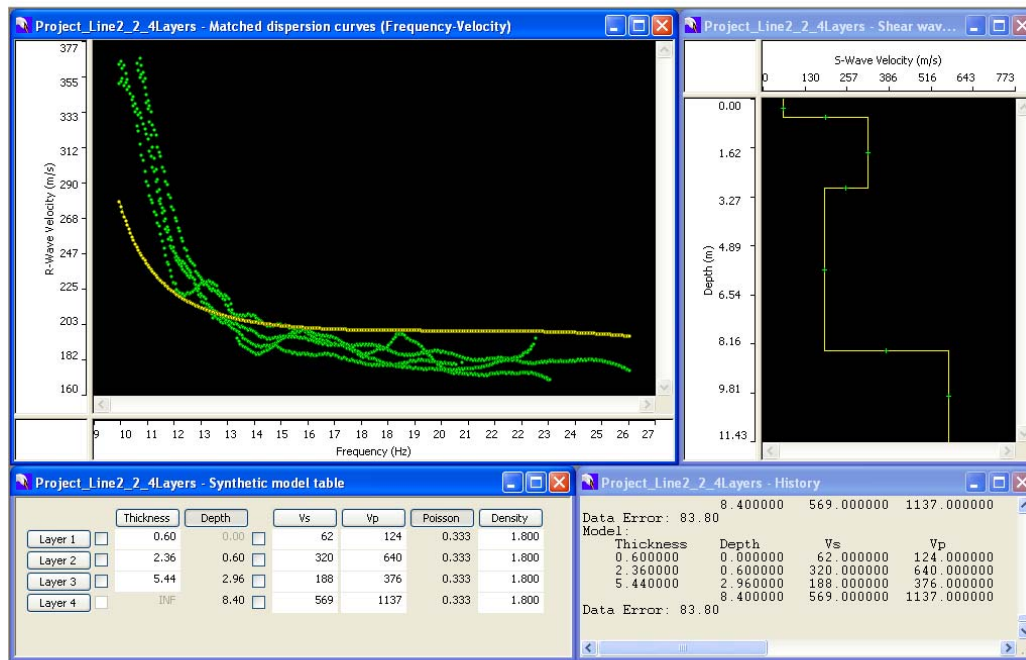


Figure 3-G Dispersion curve and soil profile Line 2-2 (thickness second layer increased in 1 m)

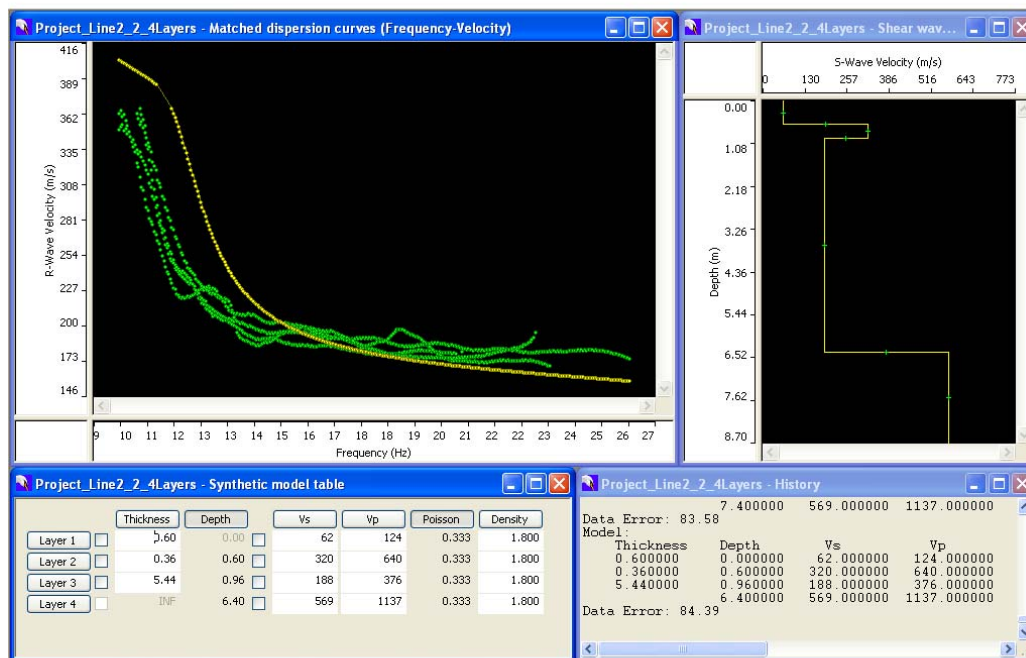


Figure 4-G Dispersion curve and soil profile Line 2-2 (thickness second layer decreased in 1 m)

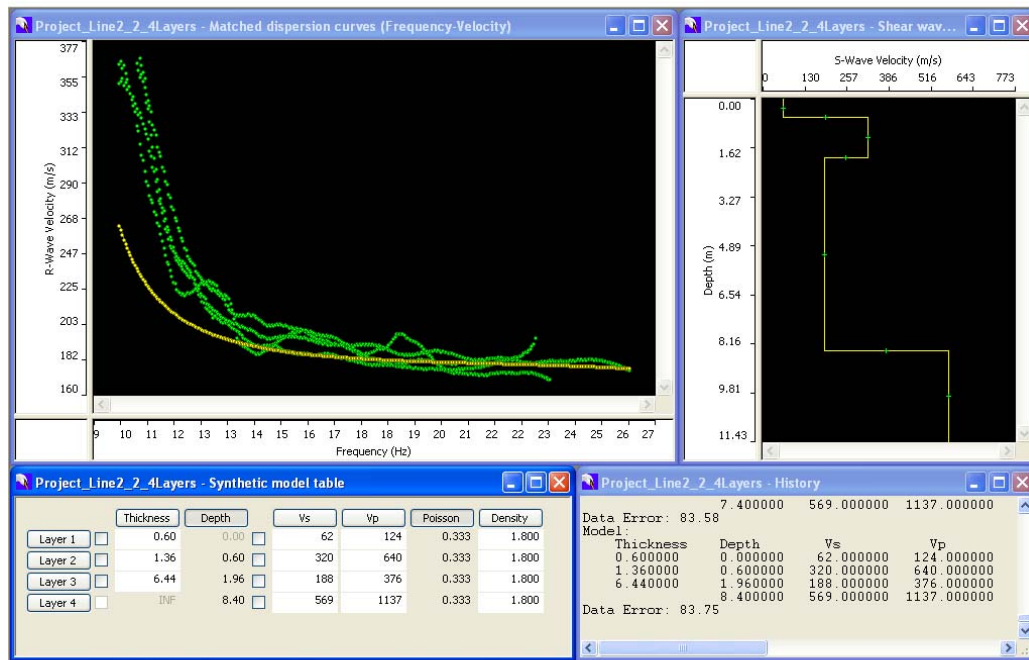


Figure 5-G Dispersion curve and soil profile Line 2-2 (thickness third layer increased in 1 m)

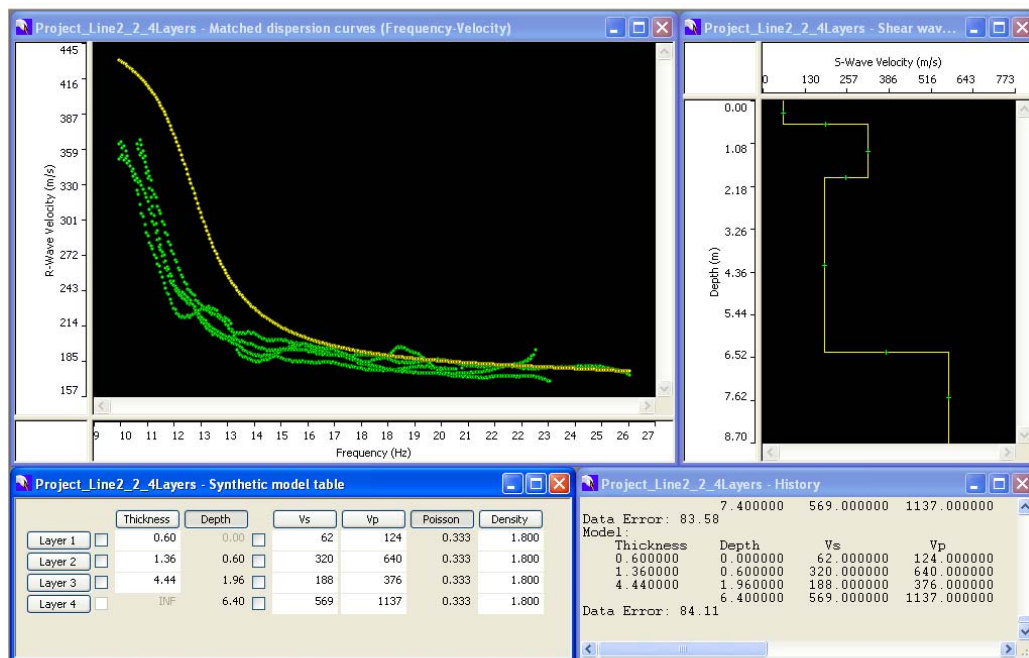


Figure 6-G Dispersion curve and soil profile Line 2-2 (thickness third layer decreased in 1 m)

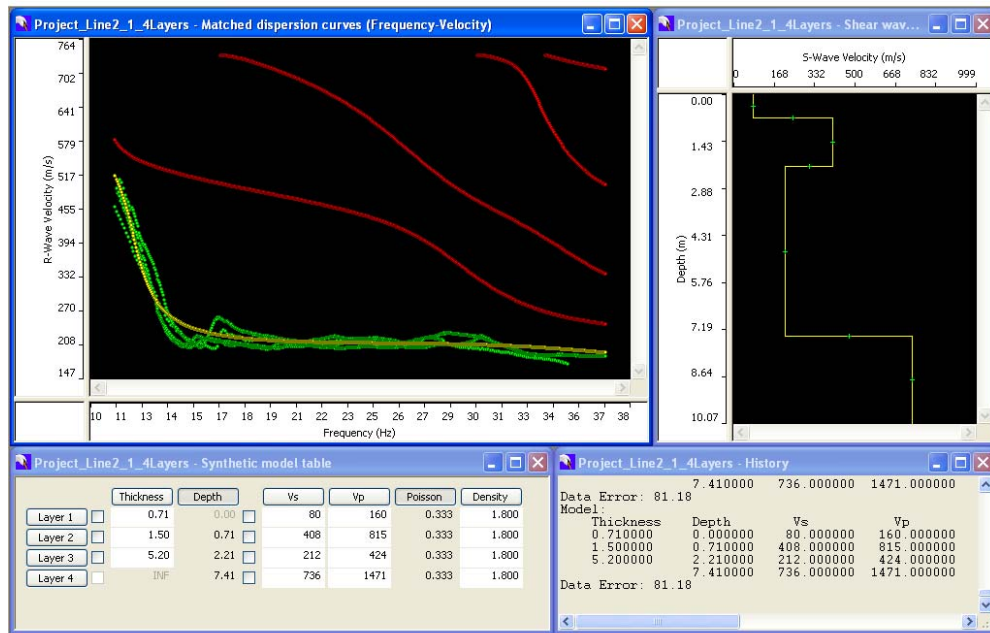


Figure 7-G Dispersion curve and soil profile Line 2-1

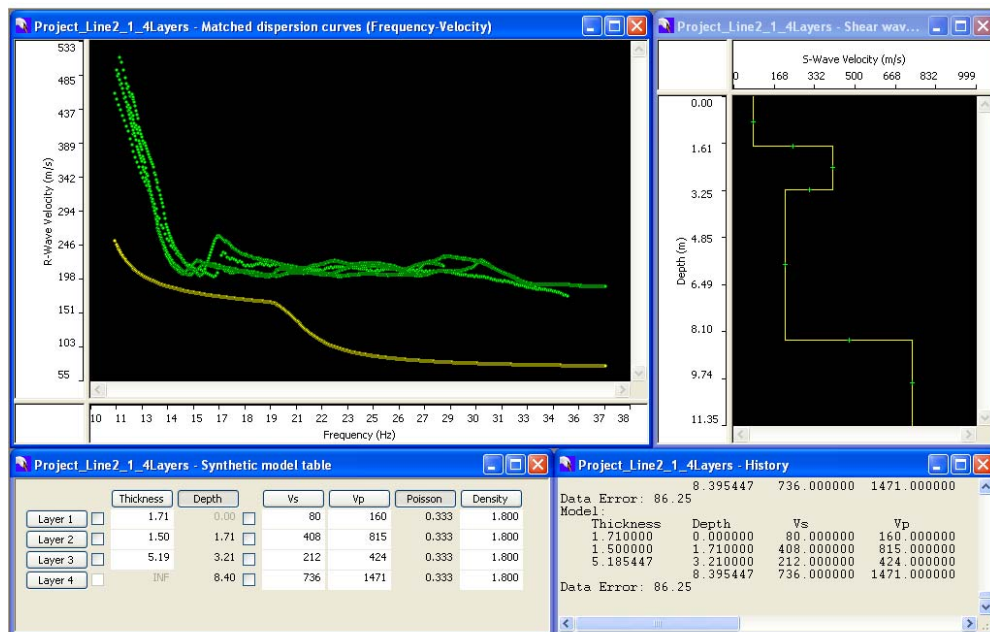


Figure 8-G Dispersion curve and soil profile Line 2-1 (thickness first layer increased in 1 m)

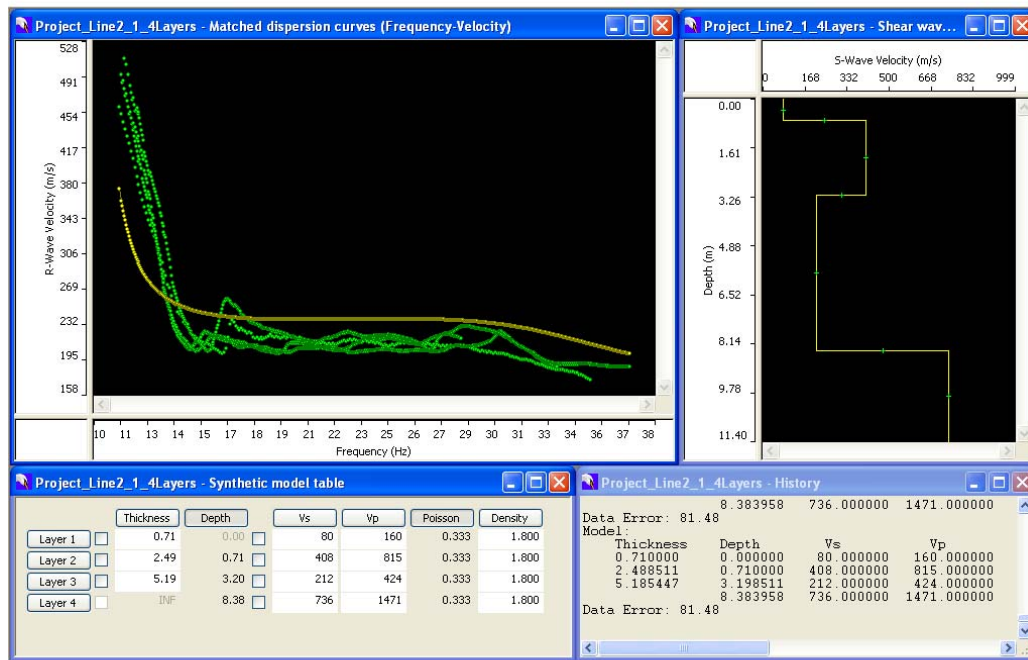


Figure 9-G Dispersion curve and soil profile Line 2-1 (thickness second layer increased in 1 m)

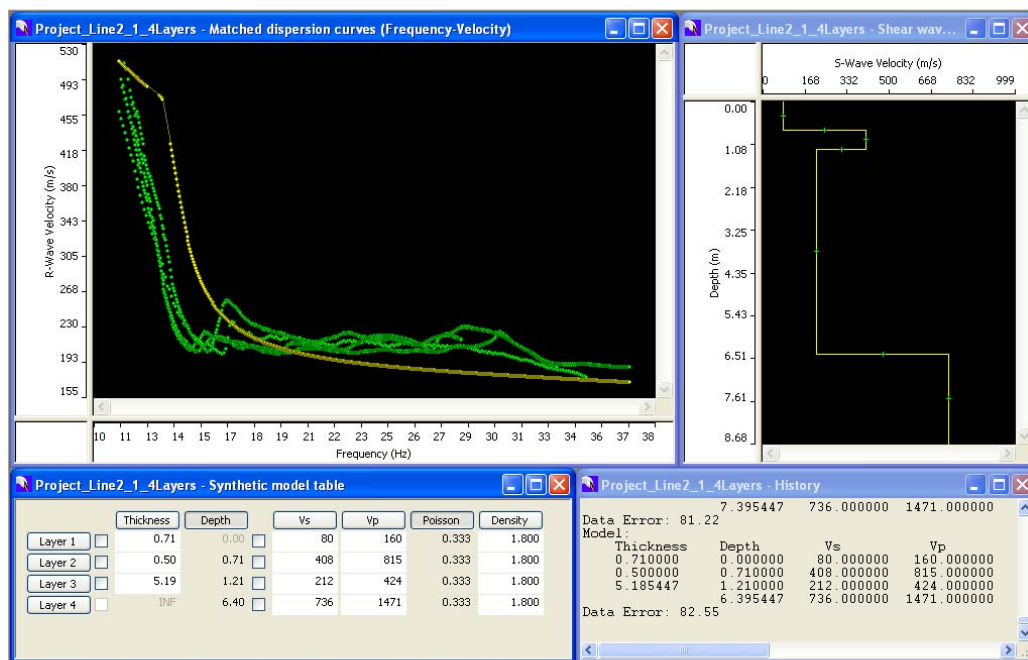


Figure 10-G Dispersion curve and soil profile Line 2-1 (thickness second layer decreased in 1 m)

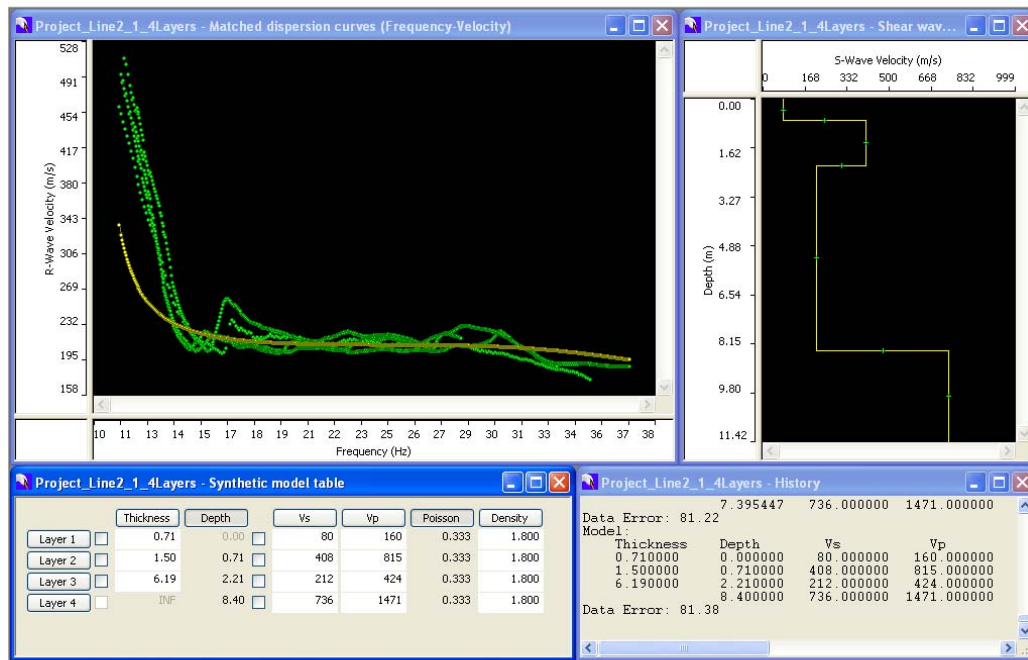


Figure 11-G Dispersion curve and soil profile Line 2-1 (thickness third layer increased in 1 m)

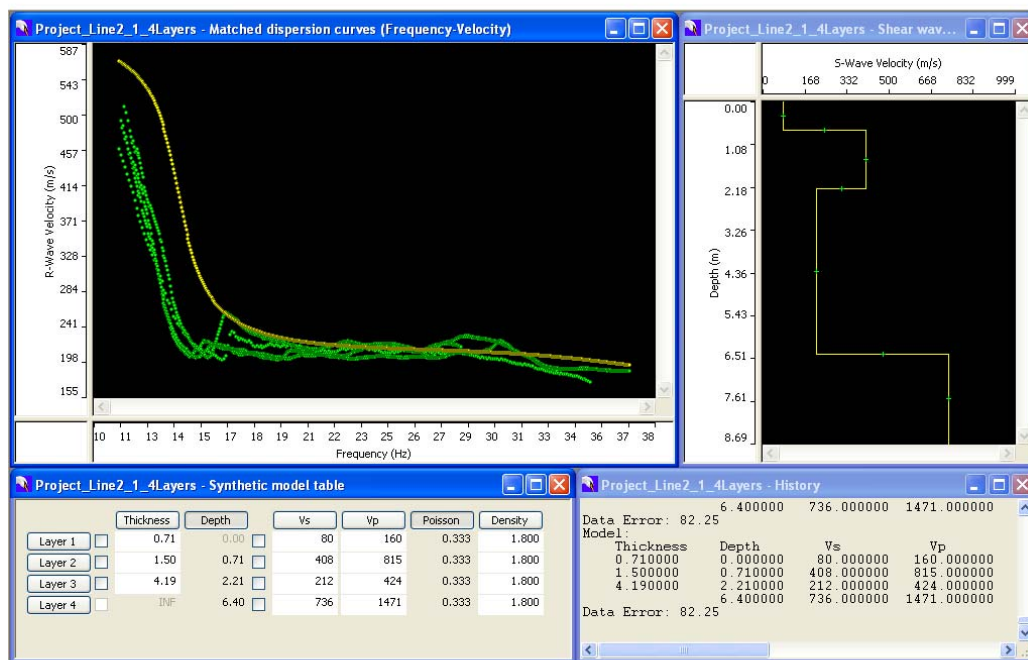


Figure 12-G Dispersion curve and soil profile Line 2-1 (thickness third layer decreased in 1 m)

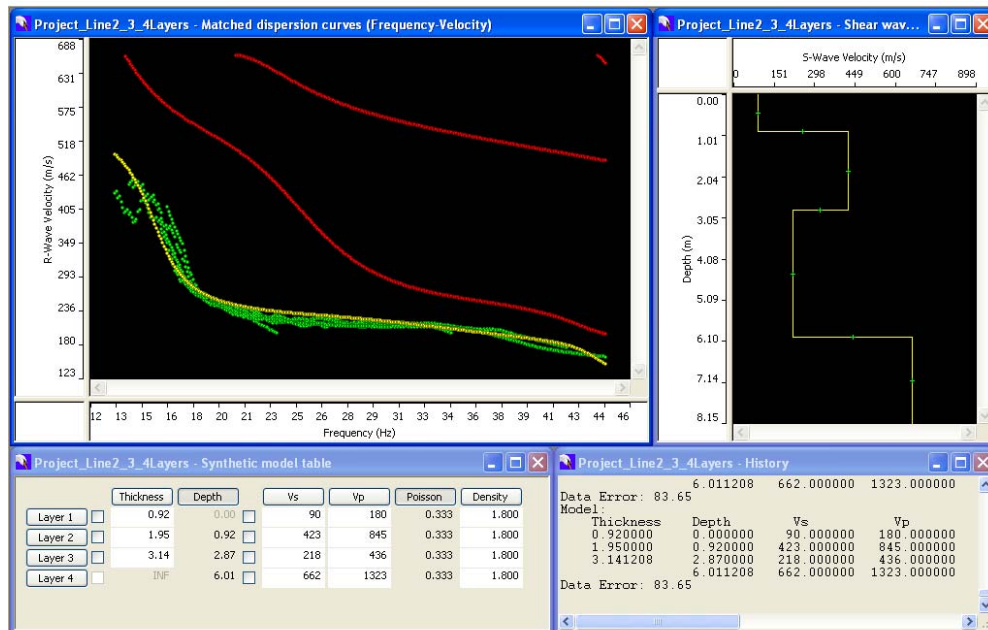


Figure 13-G Dispersion curve and soil profile Line 2-3

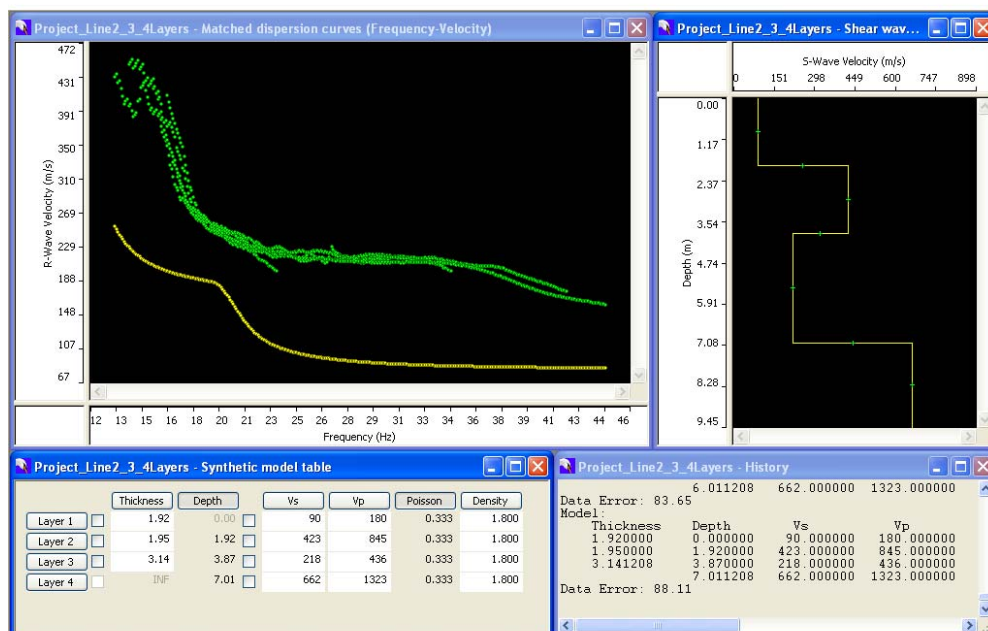


Figure 14-G Dispersion curve and soil profile Line 2-3 (thickness first layer increased in 1 m)

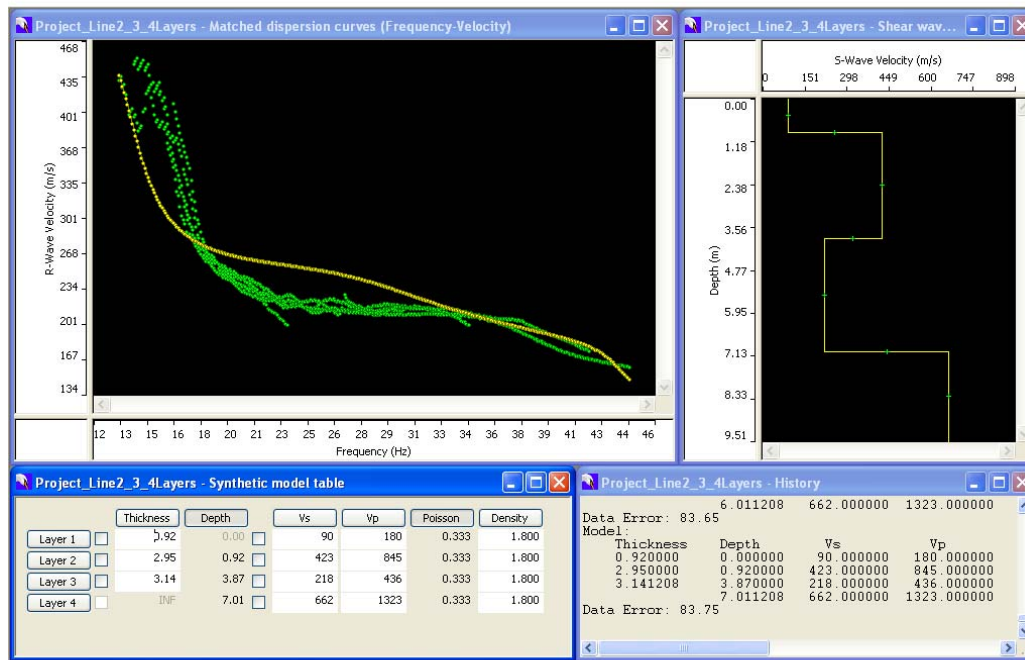


Figure 15-G Dispersion curve and soil profile Line 2-3 (thickness second layer increased in 1 m)

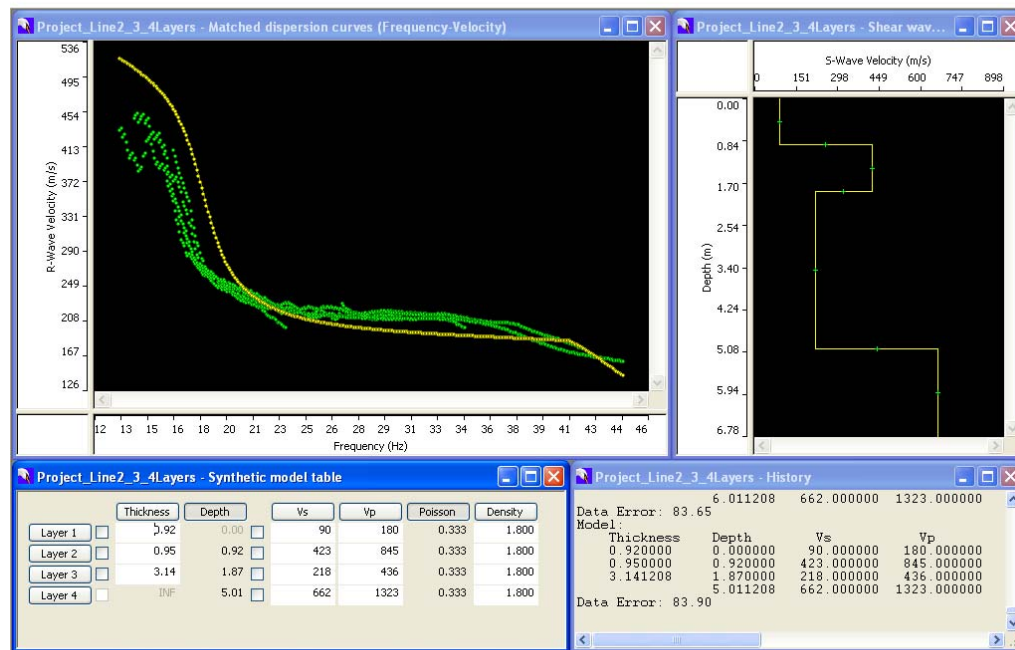


Figure 16-G Dispersion curve and soil profile Line 2-3 (thickness second layer decreased in 1 m)

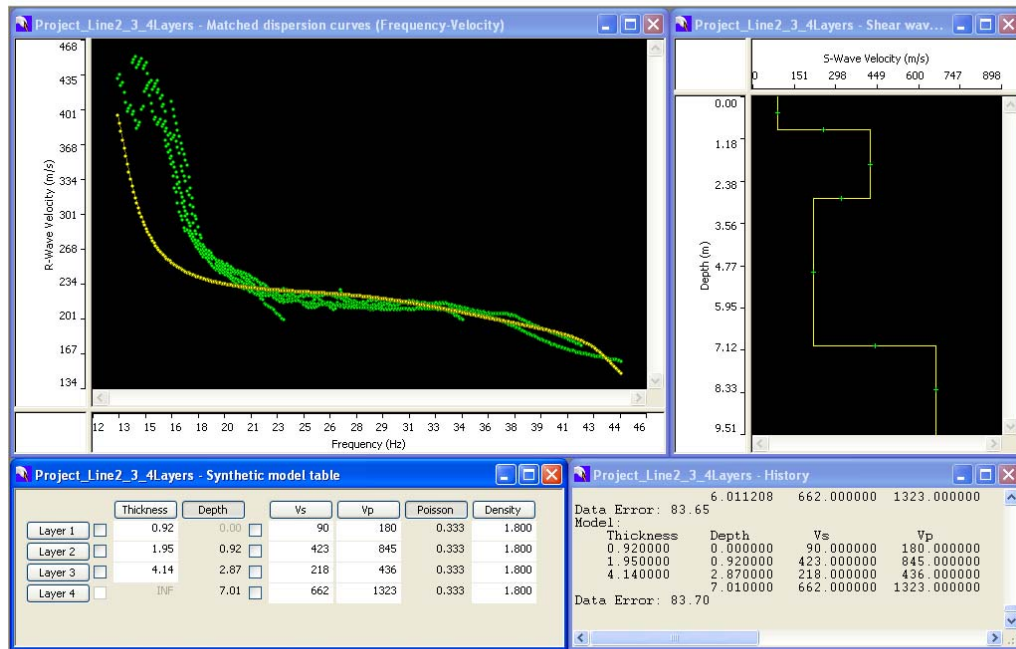


Figure 17-G Dispersion curve and soil profile Line 2-3 (thickness third layer increased in 1 m)

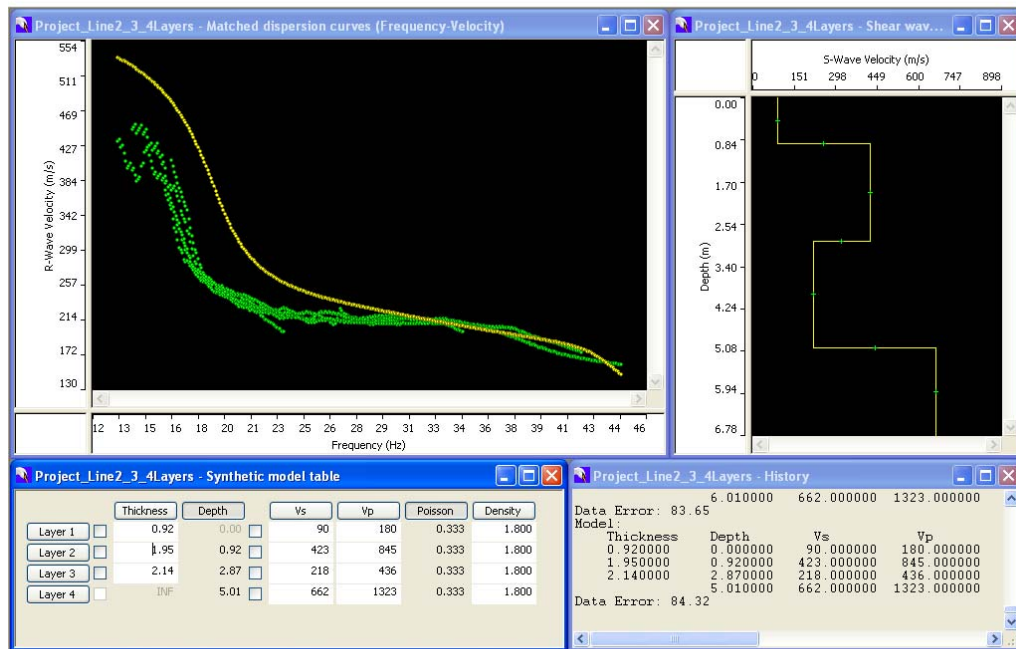


Figure 18-G Dispersion curve and soil profile Line 2-3 (thickness third layer decreased in 1 m)

Appendix H

Degradation curves from resonant column testing

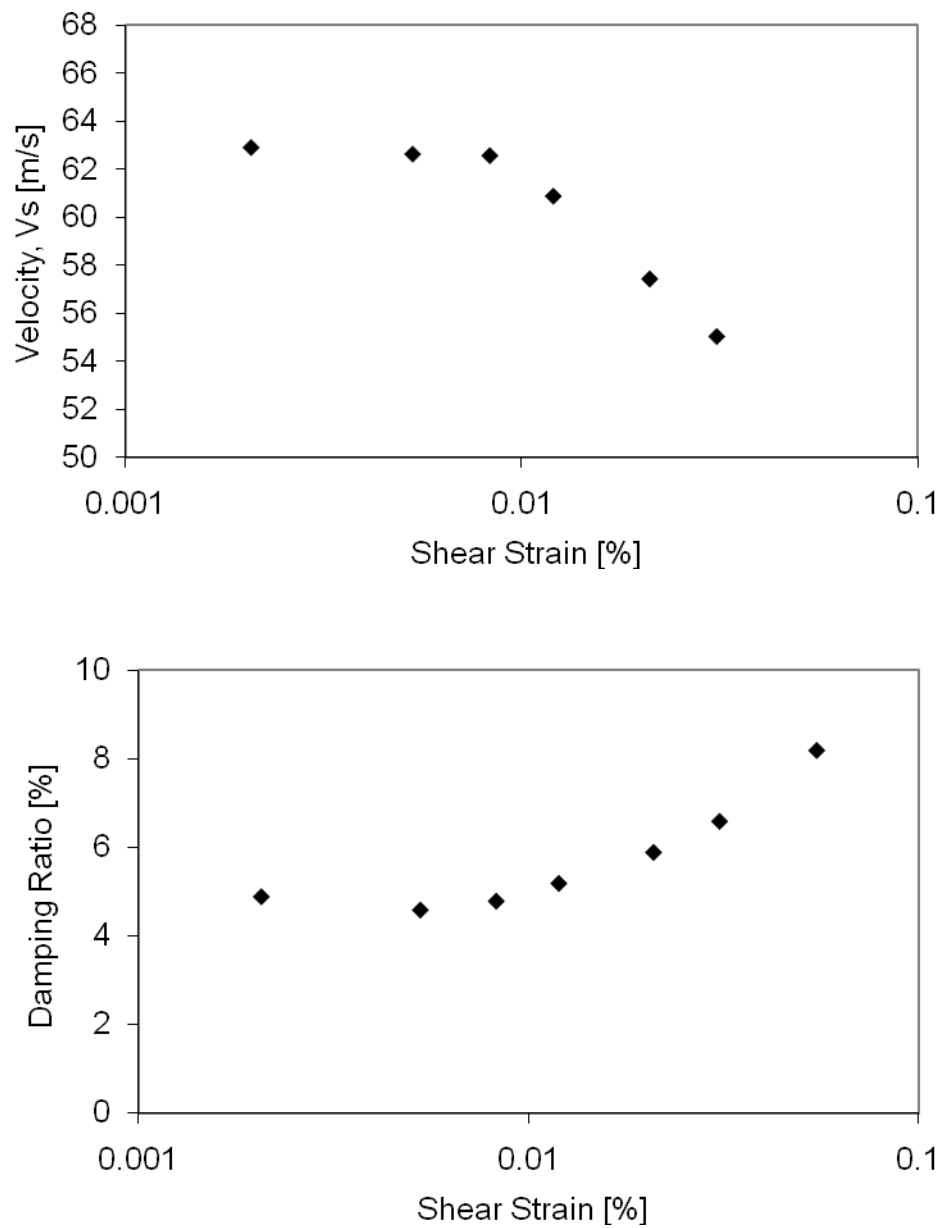


Figure 1-H. Wave velocity and damping degradation curves. Specimen 08-3 SH #1

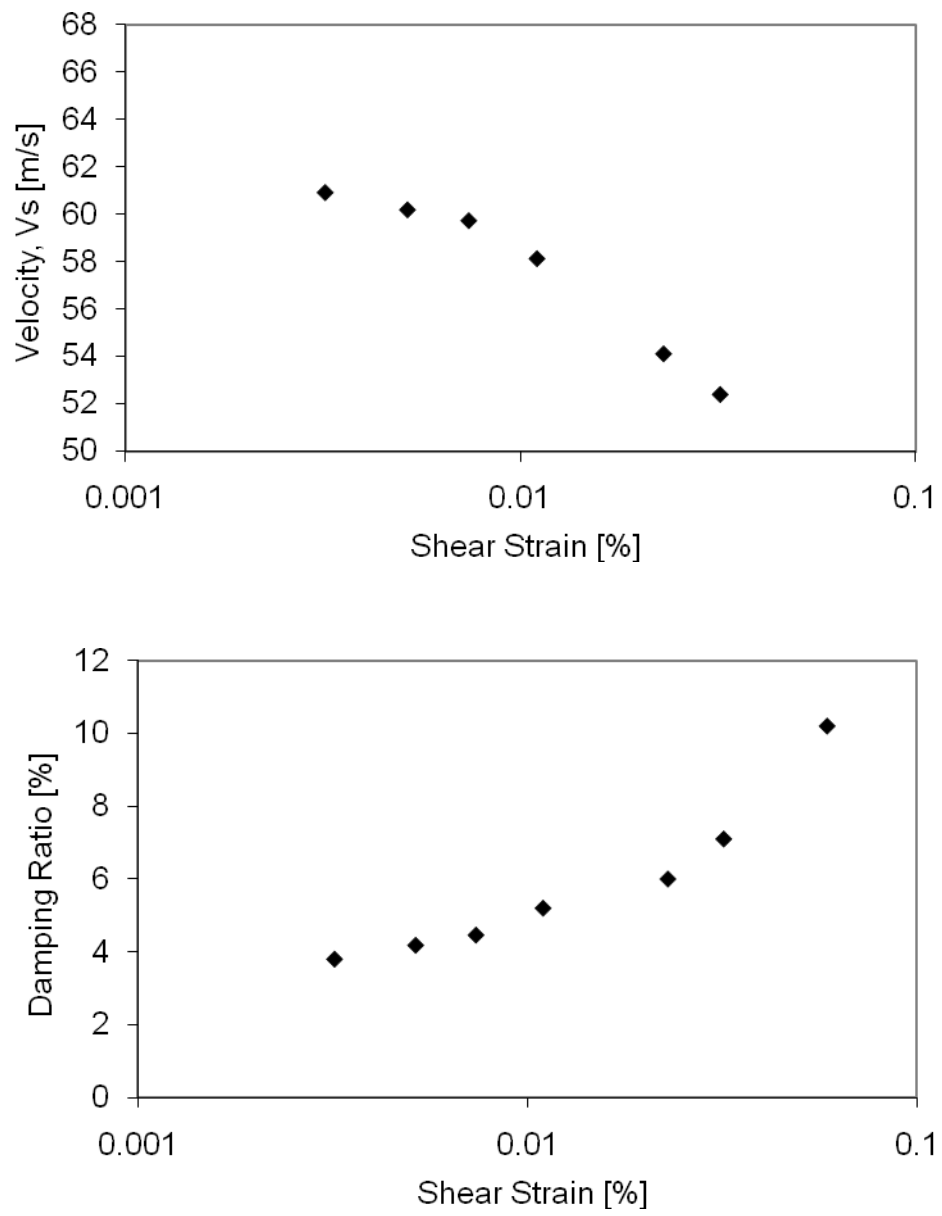


Figure 2-H. Wave velocity and damping degradation curves. Specimen 08-4 SH #1

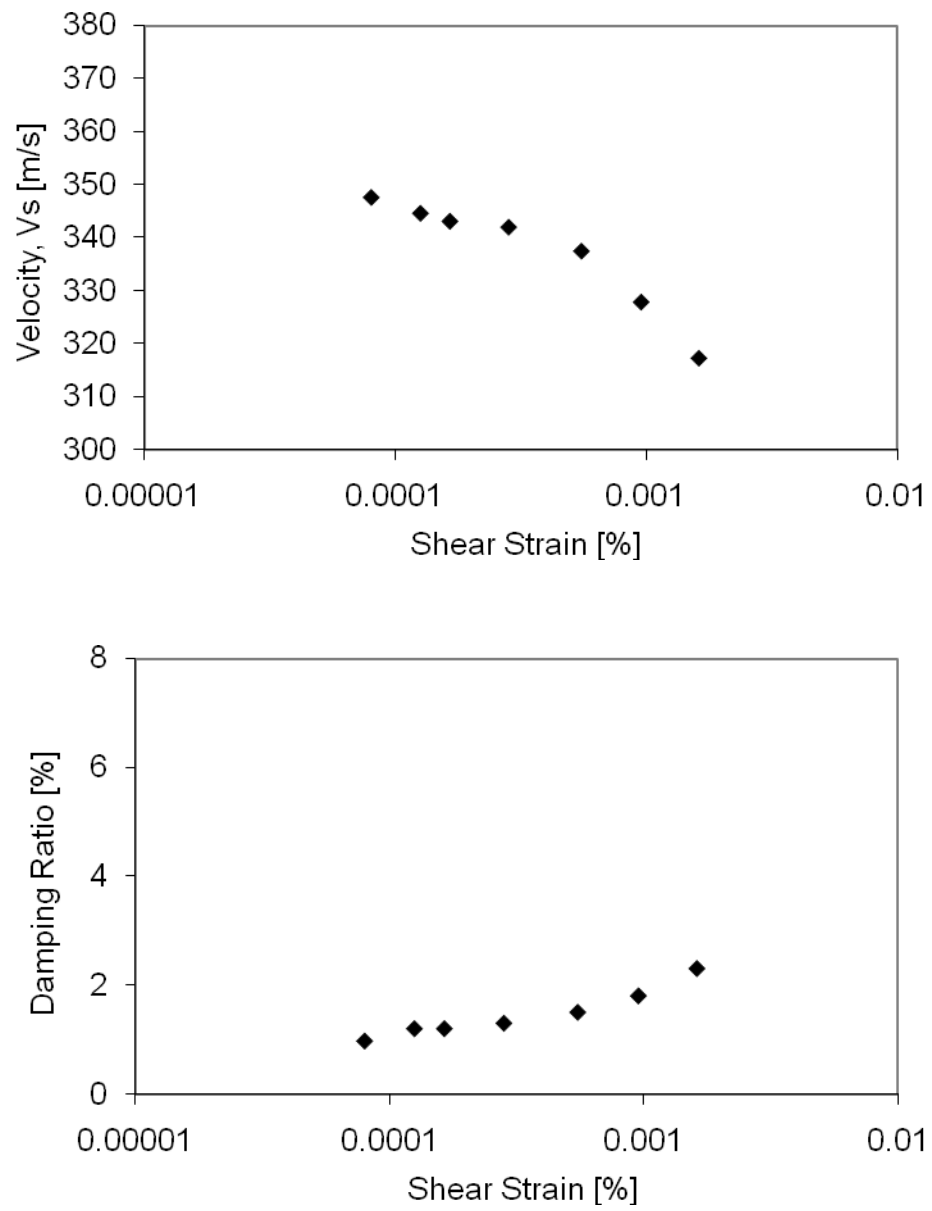


Figure 3-H. Wave velocity and damping degradation curves. Specimen 08-4 CS

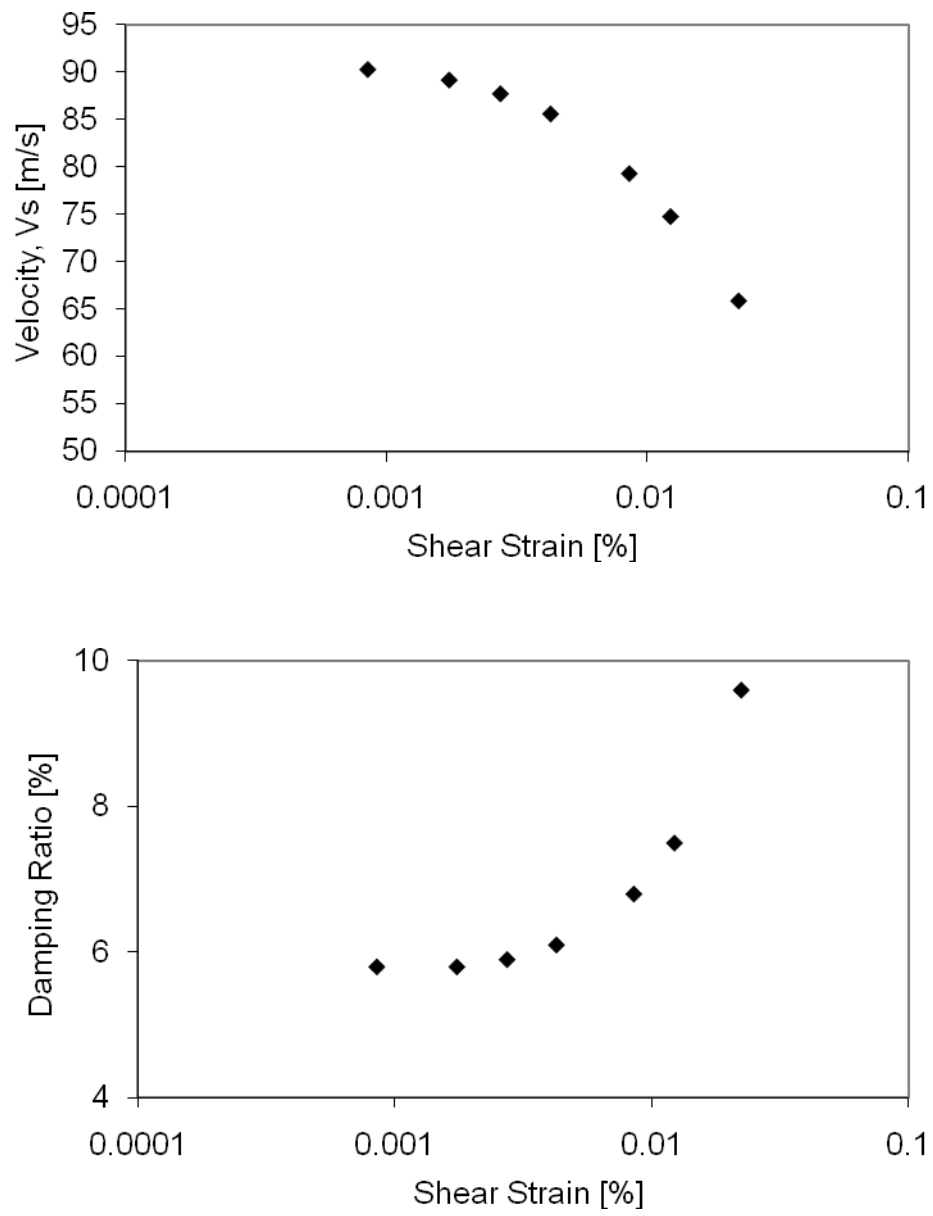


Figure 4-H. Wave velocity and damping degradation curves. Specimen 08-6 SH #2

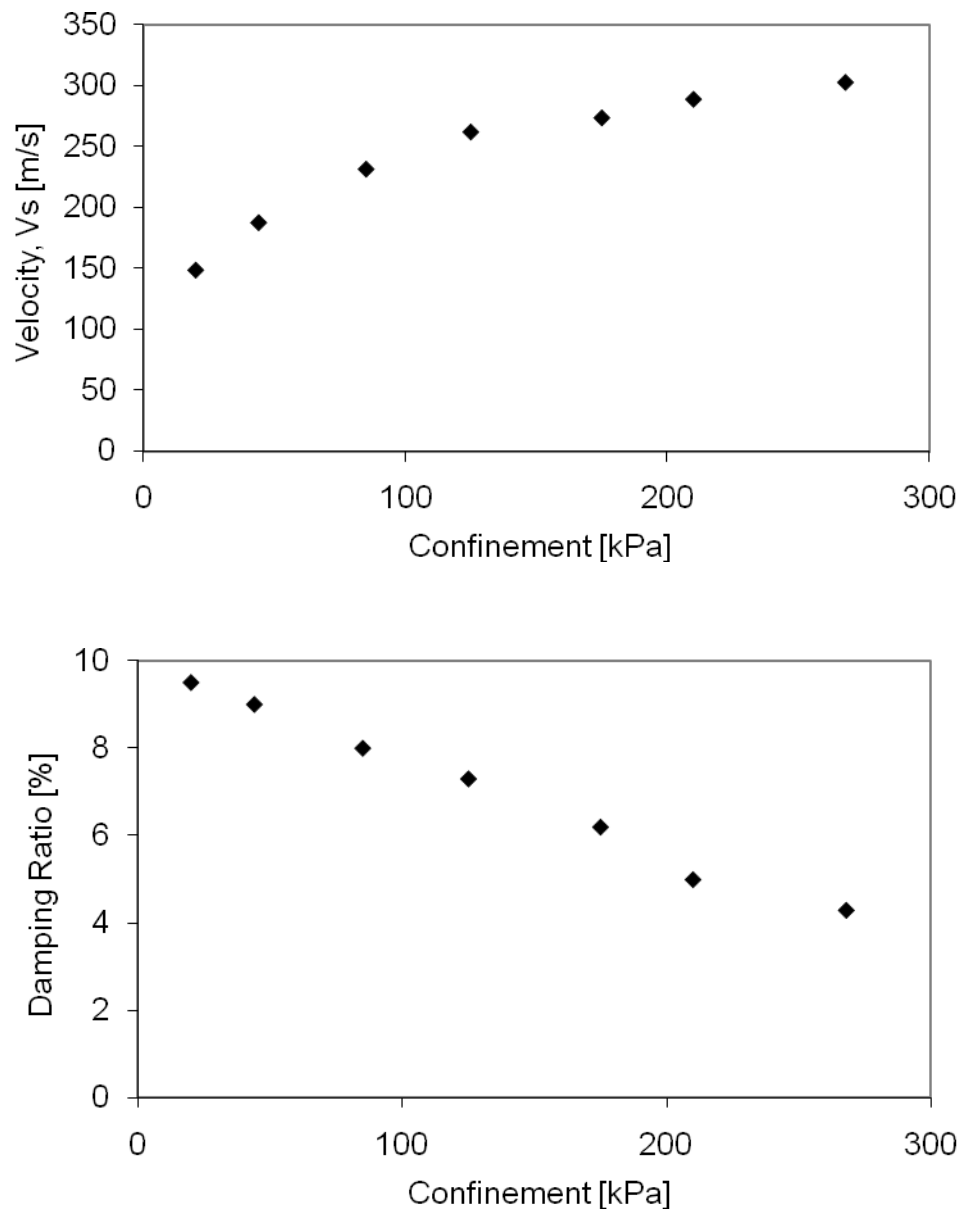


Figure 5-H. Wave velocity and damping against confinement. Specimen 08-7 SH #1

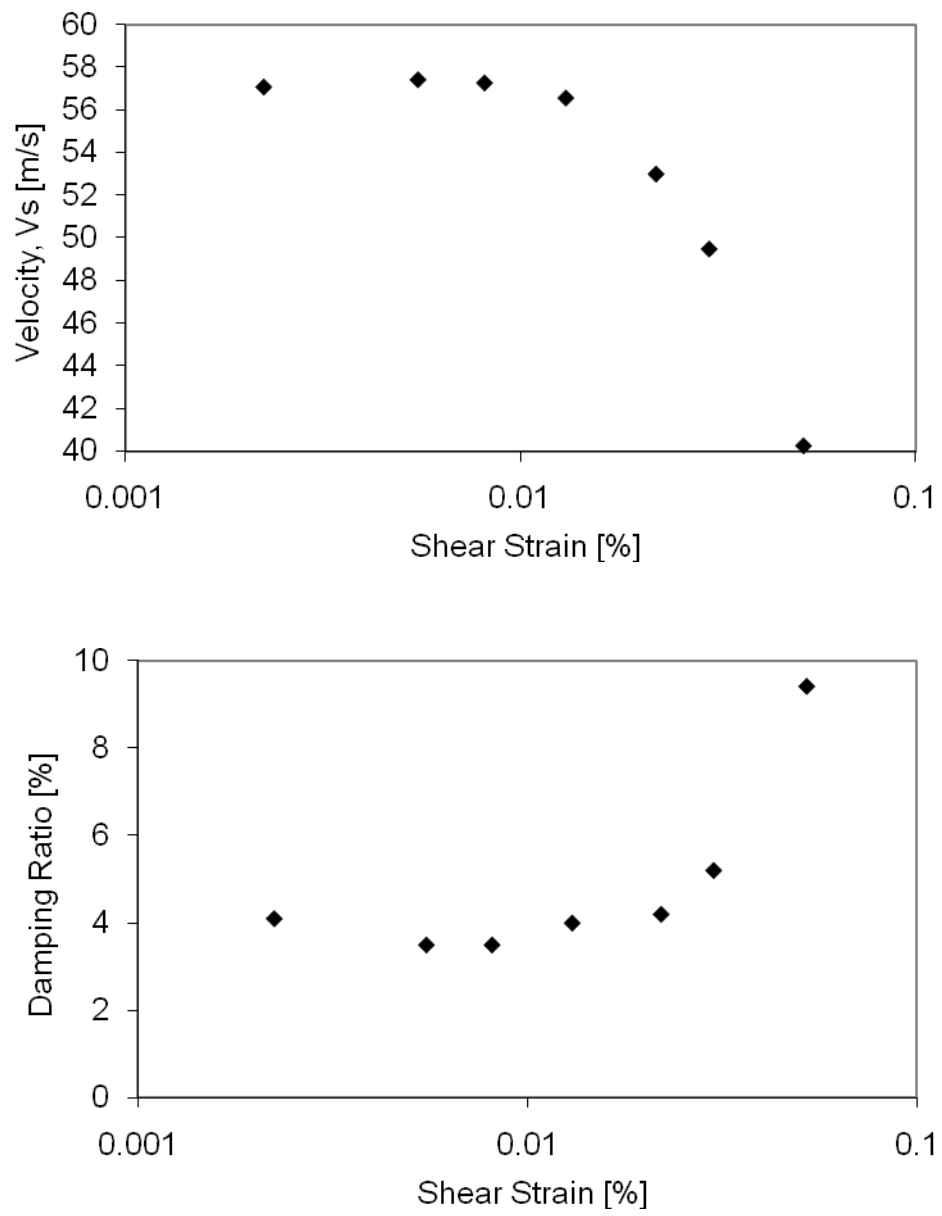


Figure 6-H. Wave velocity and damping degradation curves. Specimen 08-7 SH #5

Appendix I

Resonant column and electrical conductivity experimental setups



Figure 1-I. Resonant column experimental setup

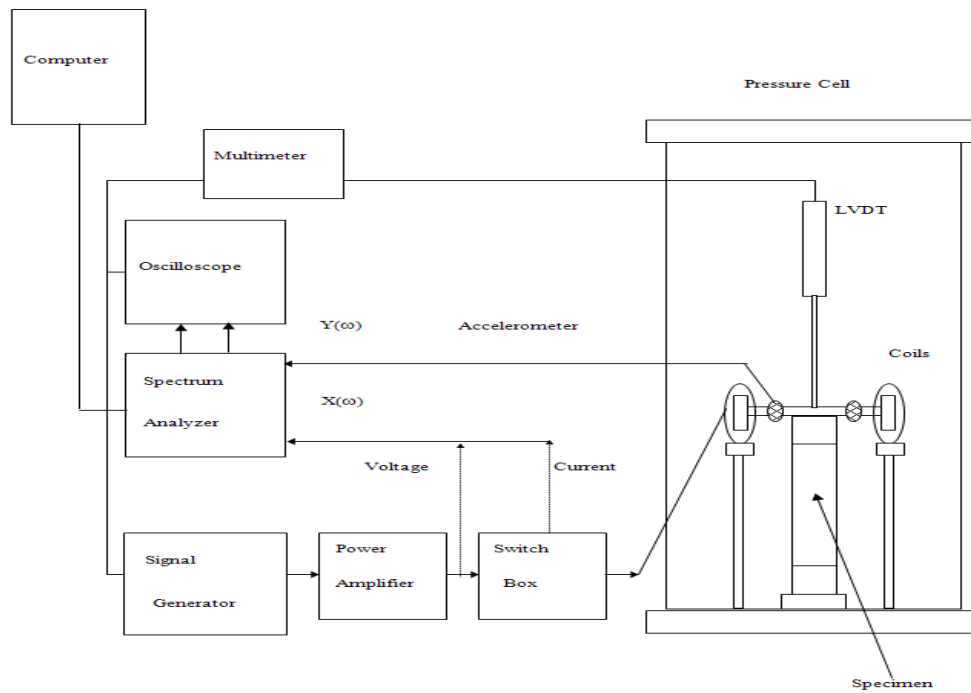


Figure 2-I. Resonant column – simplified interconnection diagram

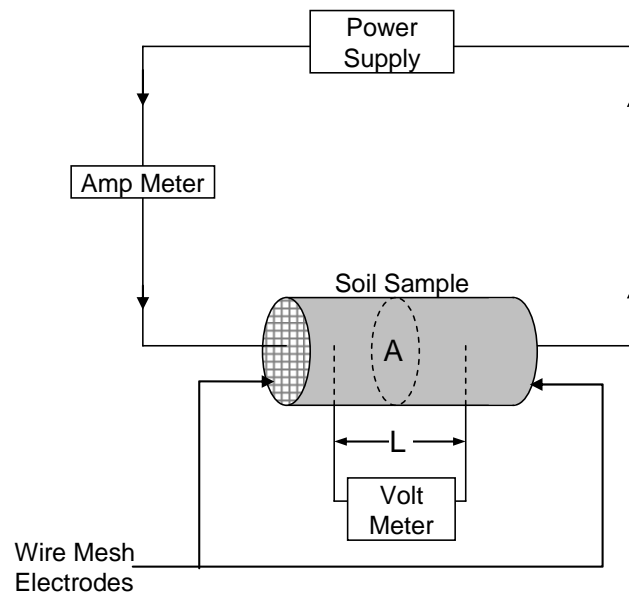


Figure 3-I. Soil conductivity experimental setup – simplified interconnection diagram

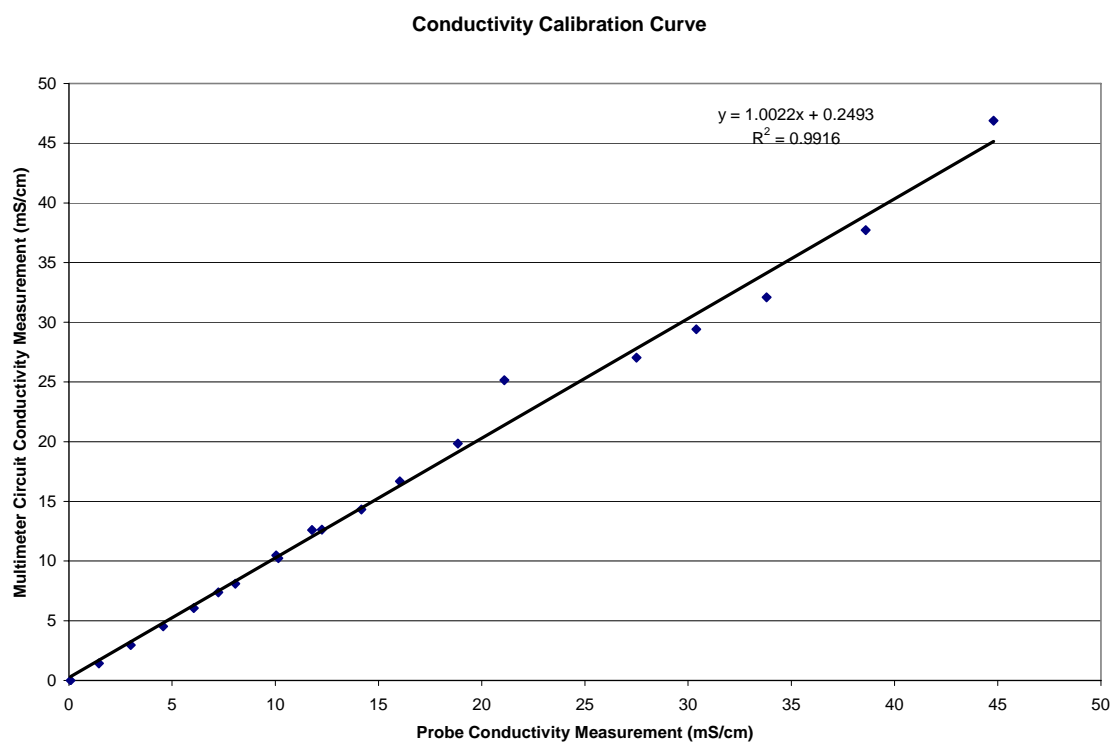


Figure 4-I. Calibration results for the soil conductivity measurements

Table 5-I. Field water sampling results. July 15, 2008, 2:30 p.m., sunny 25°C. Three well volumes to be purged (if possible) and tested

Borehole 08-4

Depth of well:	15.97 m below top of pipe (btop)		
Water level:	1.50 m btop		
Casing stickup:	0.80 m above ground surface (ags)		
Physical description:	cloudy, brownish grey, silty		
	V ₁	V ₂	V ₃
Volume purged (L):	29	5 (dry)	2 (dry)
Temperature (°C):	12.4	13.0	14.1
TDS (mg/L):	141	142	163
Conductivity (mS/m):	29.7	30.0	34.2

Borehole 08-3

Depth of well:	6.87 m btop		
Water level:	2.30 m btop		
Casing stickup:	0.82 m ags		
Physical description:	cloudy, brown, silty		
	V ₁	V ₂	V ₃
Volume purged (L):	6 (dry)	1 (dry)	1 (dry)
Temperature (°C):	15.0	15.2	15.4
TDS (mg/L):	275	249	258
Conductivity (mS/m):	57.1	51.8	53.8

Borehole 08-5

Depth of well:	13.60 m btop		
Water level:	1.96 m btop		
Casing stickup:	0.78 m ags		
Physical description:	cloudy, brownish grey, silty		
	V ₁	V ₂	V ₃
Volume purged (L):	23	1 (dry)	1 (dry)
Temperature (°C):	12.2	13.9	13.1
TDS (mg/L):	214	207	237
Conductivity (mS/m):	45.0	43.4	49.6

Appendix J

Frequency content of CPT signals

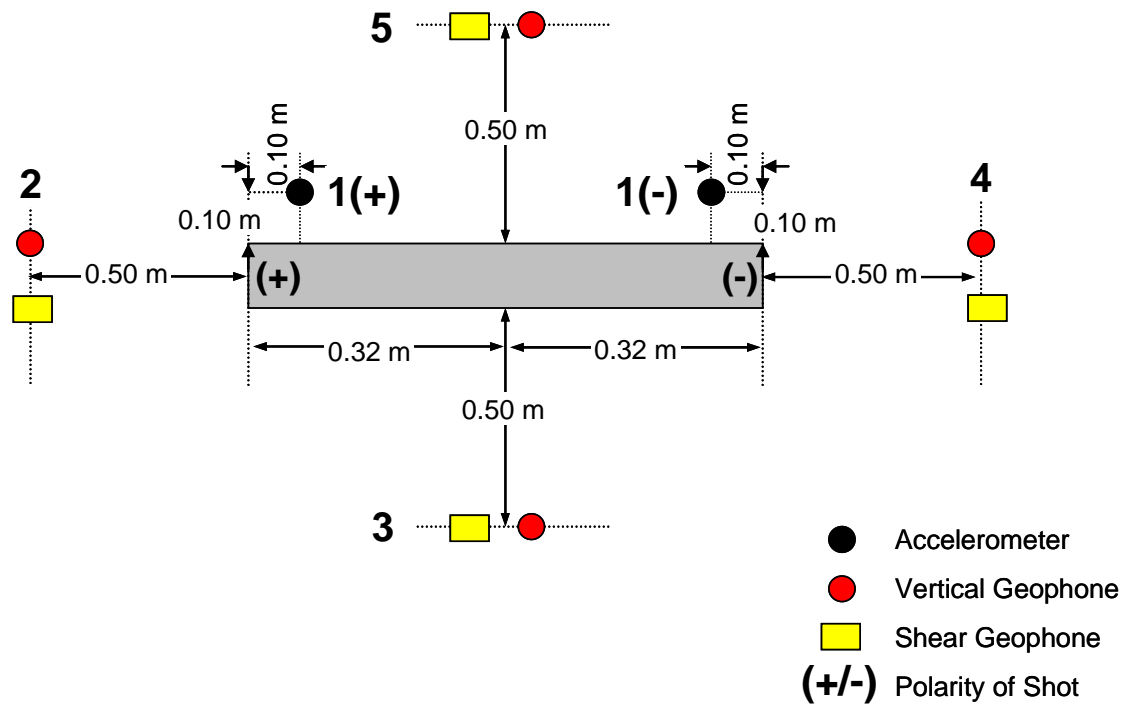


Figure 1-J. Surface geophone locations for CPT.

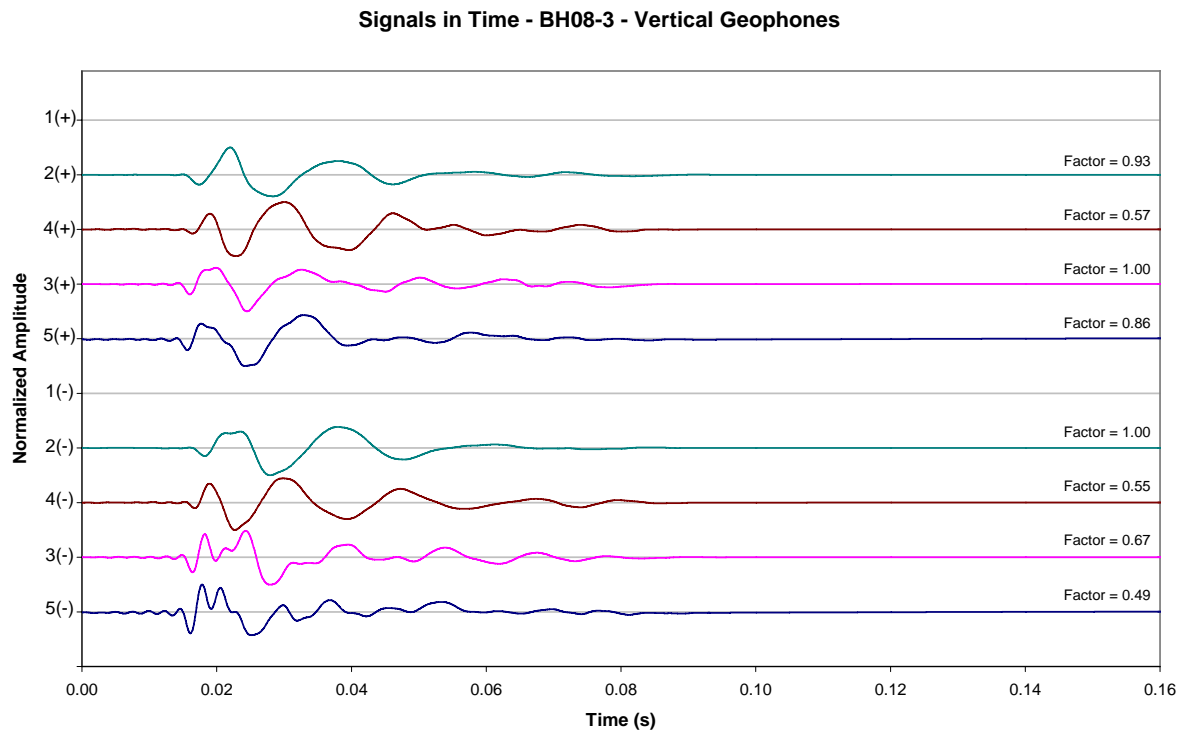


Figure 2-J. Time signals BH 8-03. Vertical geophones (surface)

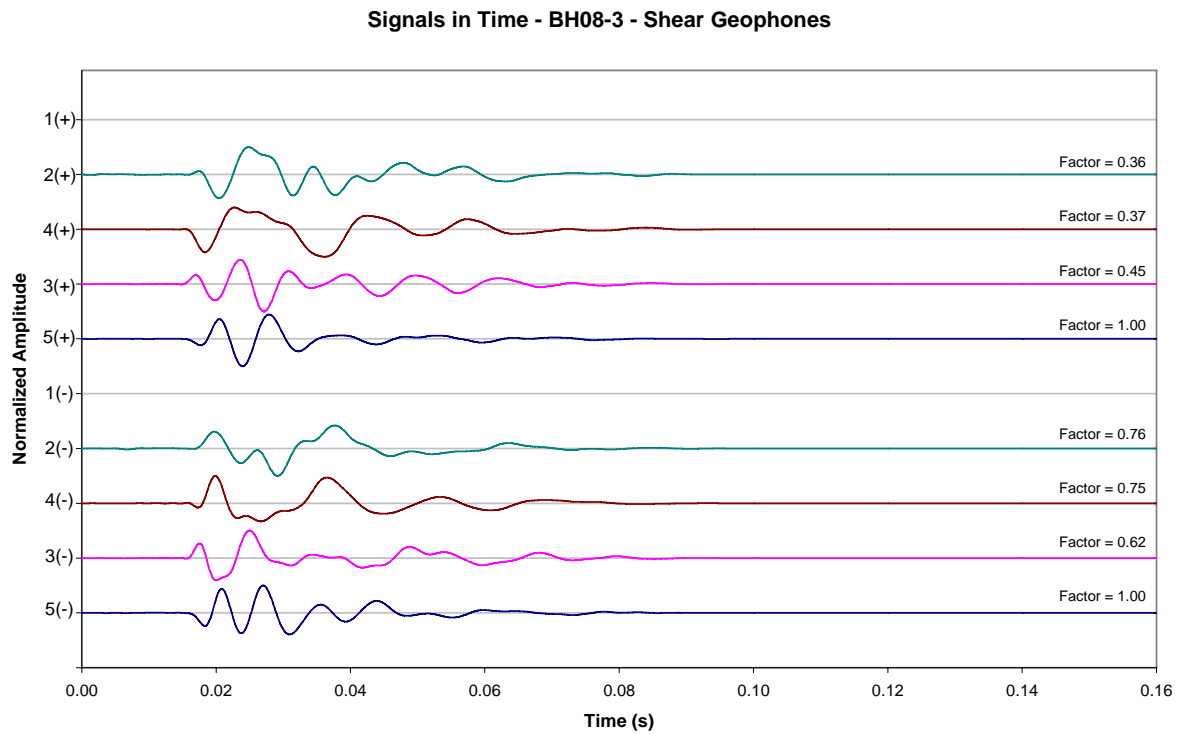


Figure 3-J. Time signals BH 8-03. Horizontal geophones (surface)

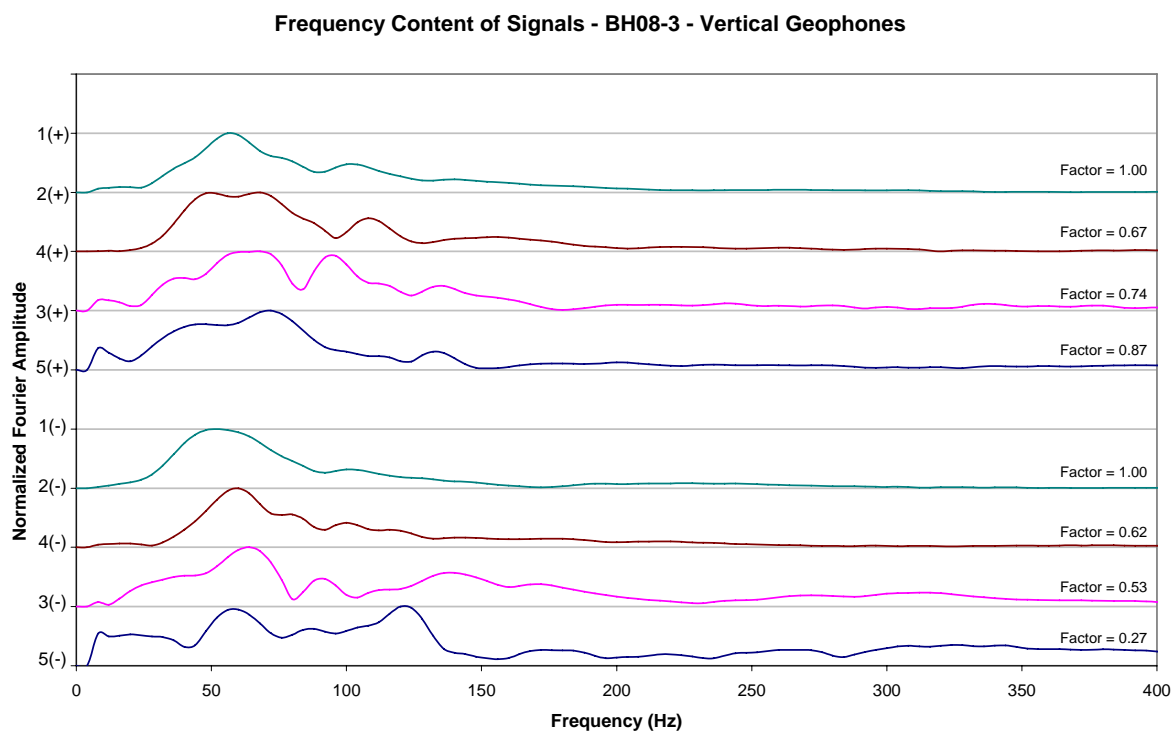


Figure 4-J. Fourier spectra BH 8-03. Vertical geophones (surface)

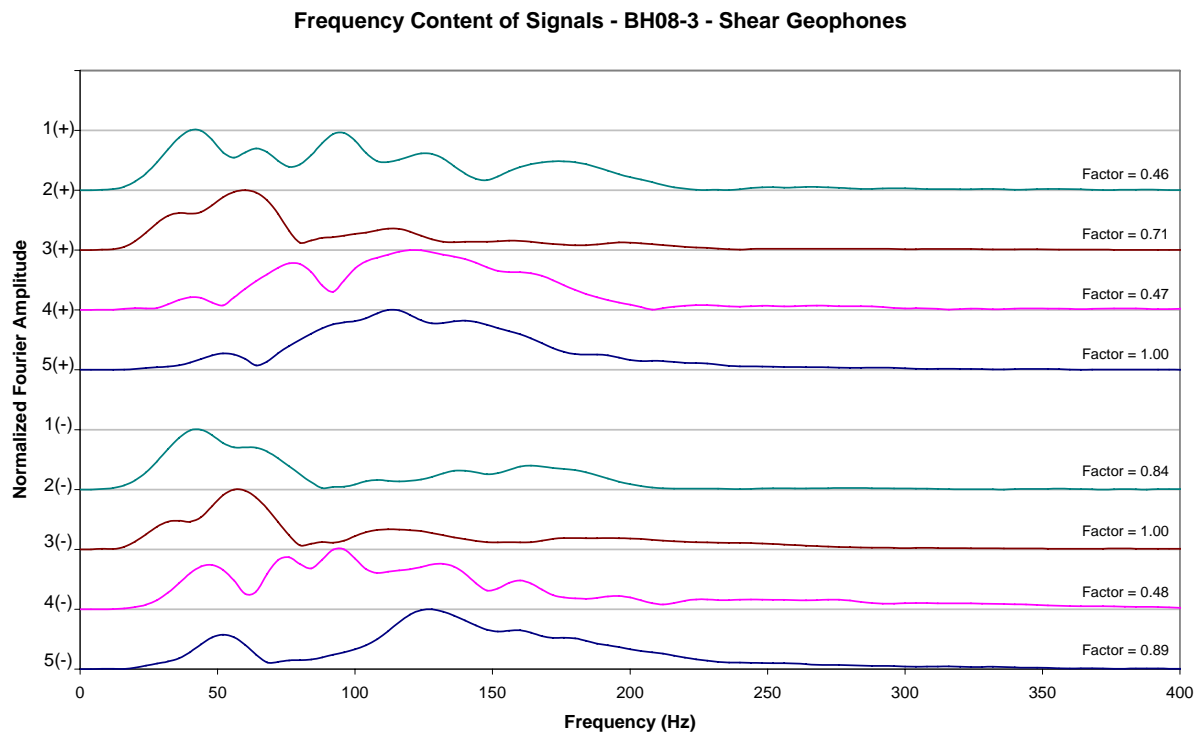


Figure 5-J. Fourier spectra BH 8-03. Horizontal geophones (surface)

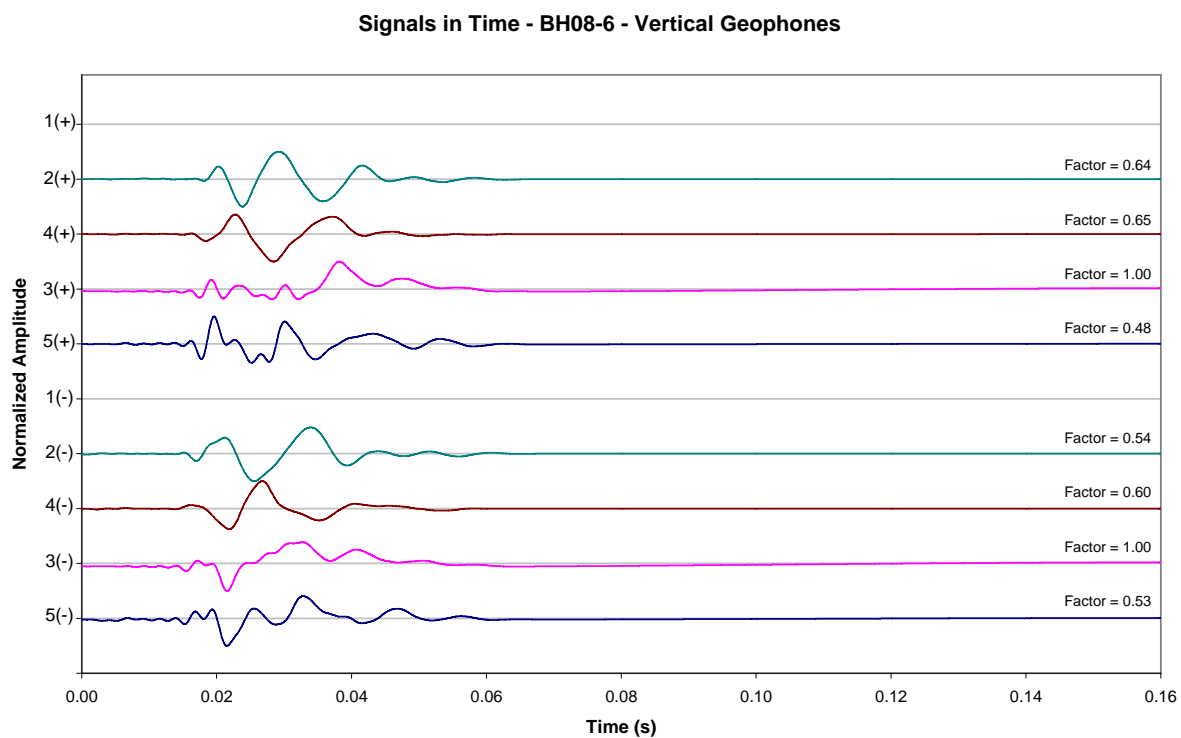


Figure 6-J. Time signals BH 8-06. Vertical geophones (surface)

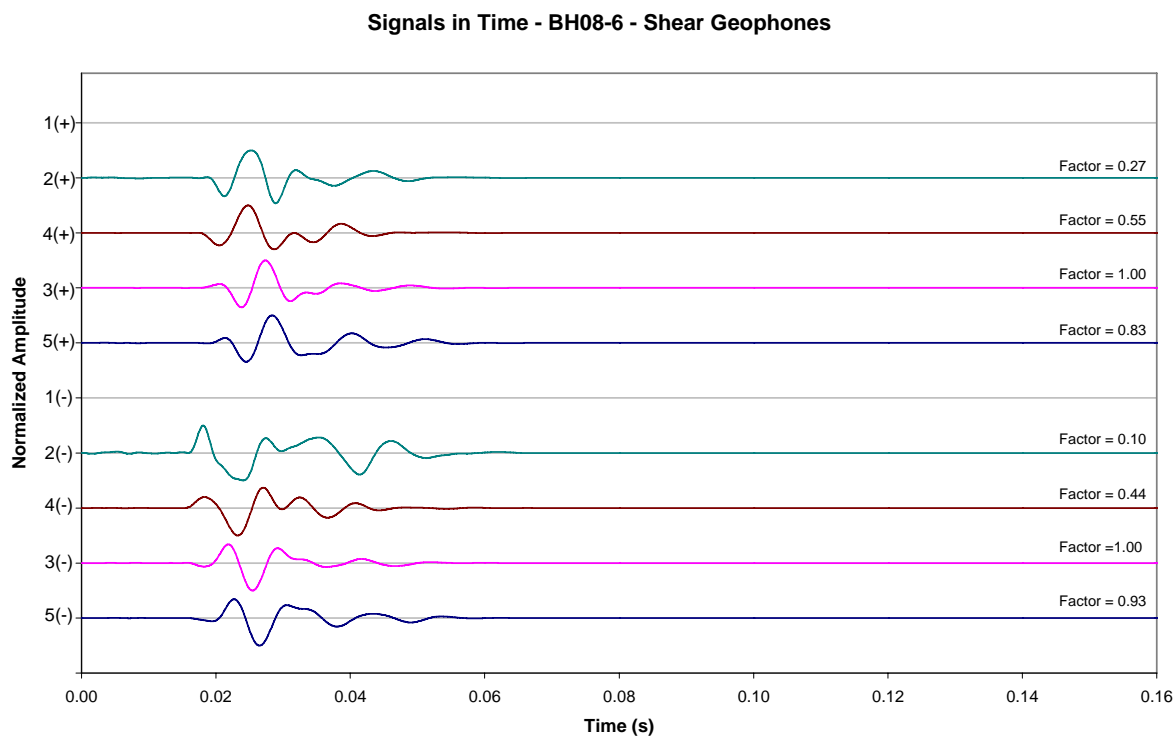


Figure 7-J. Time signals BH 8-06. Horizontal geophones (surface)

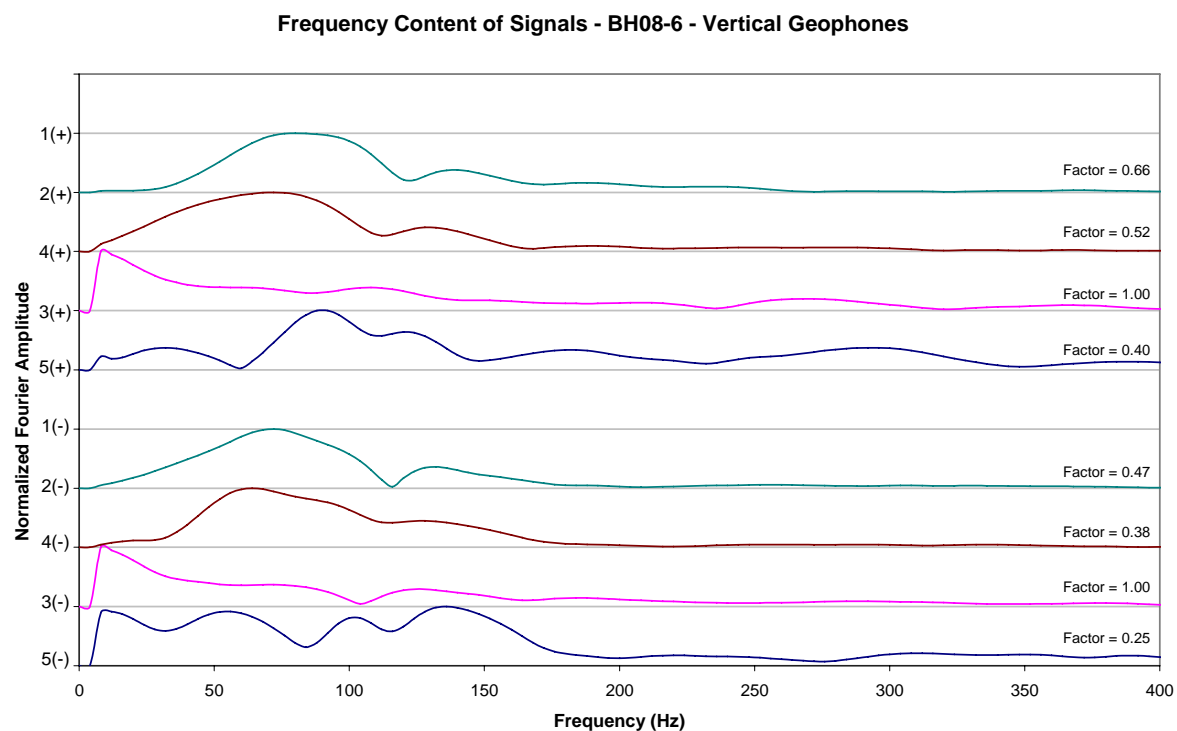


Figure 8-J. Fourier spectra BH 8-06. Vertical geophones (surface)

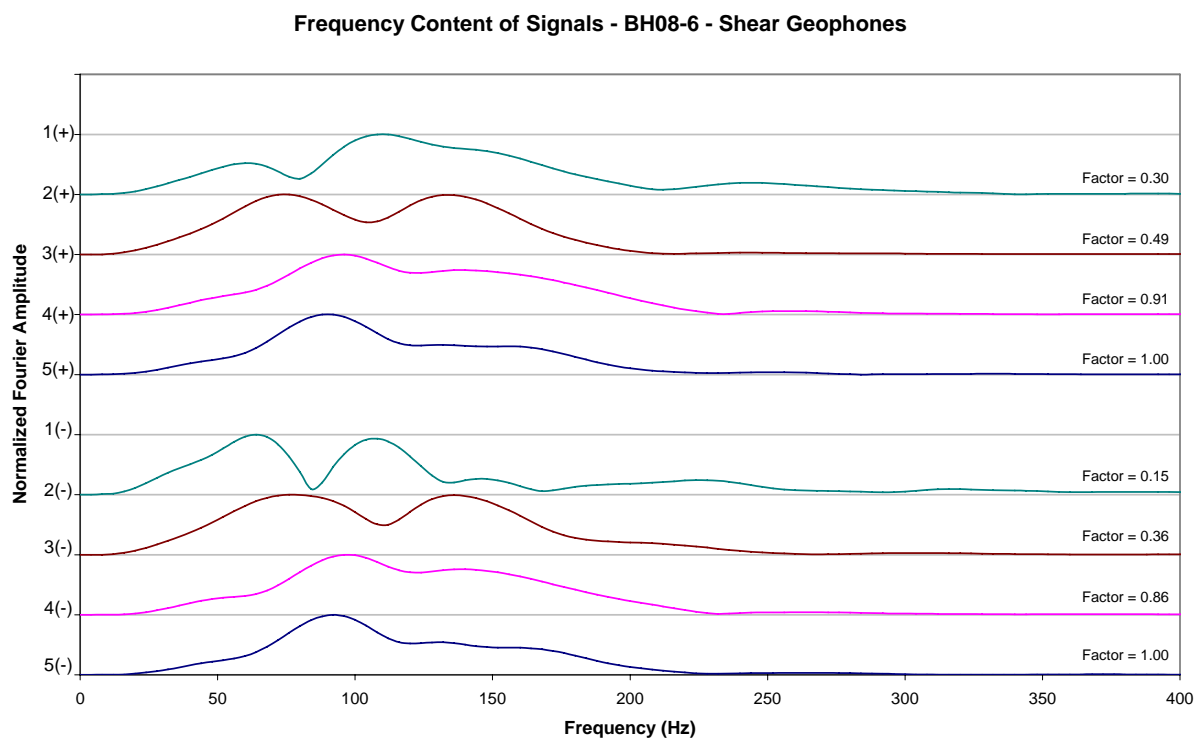


Figure 9-J. Fourier spectra BH 8-06. Horizontal geophones (surface)

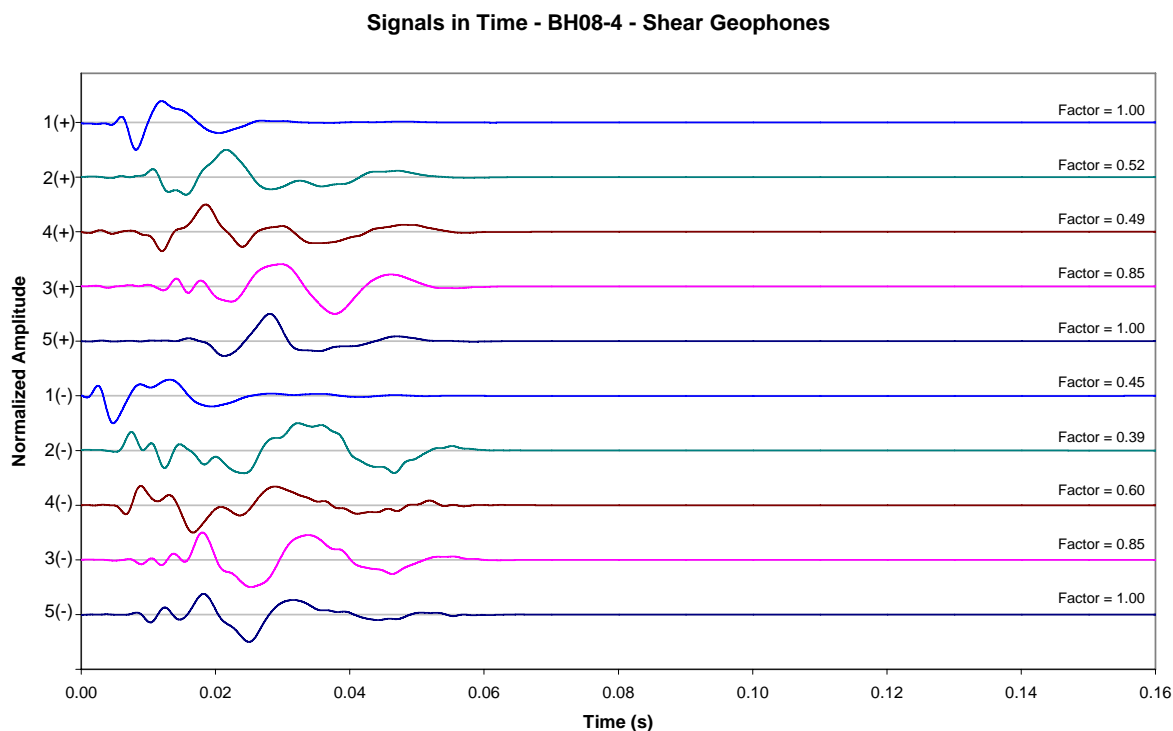


Figure 10-J. Time signals BH 8-04. Vertical geophones (surface)

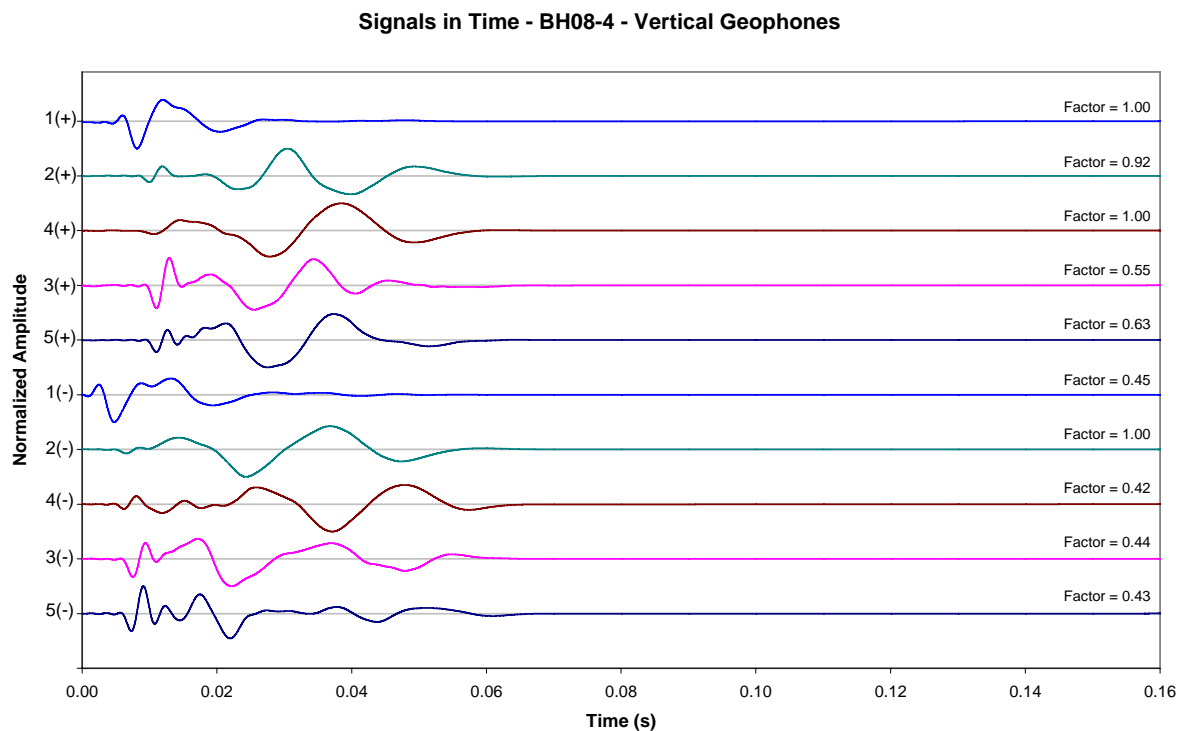


Figure 11-J. Time signals BH 8-04. Horizontal geophones (surface)

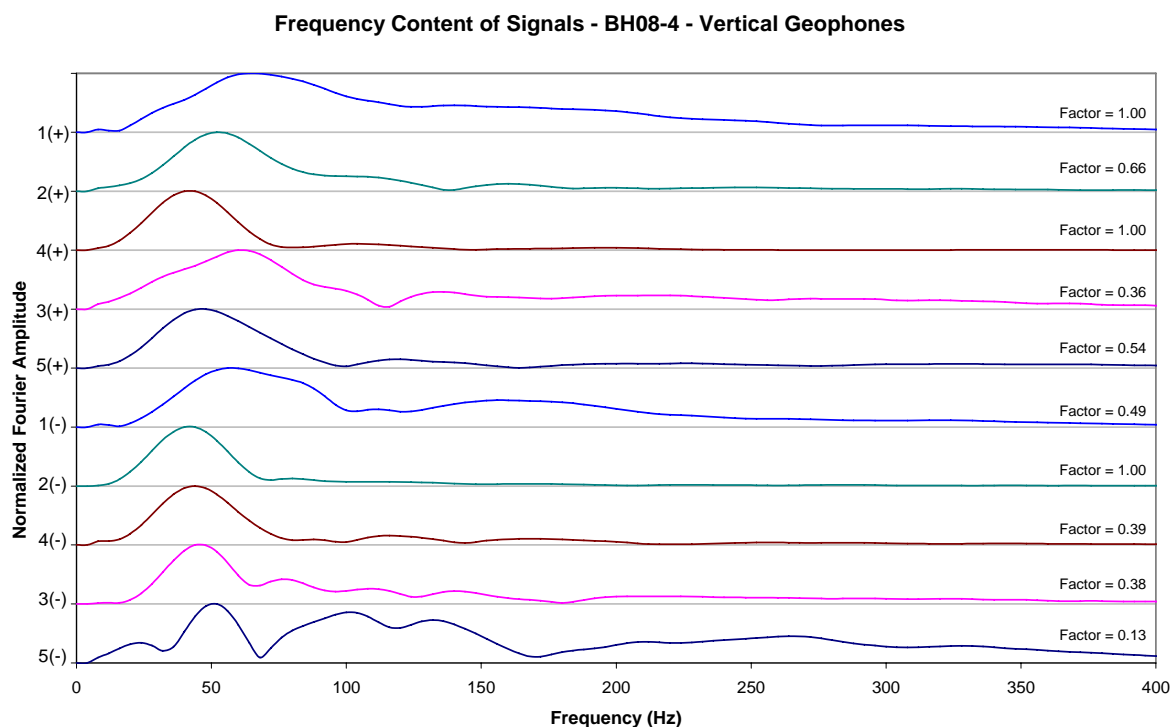


Figure 12-J. Fourier spectra BH 8-04. Vertical geophones (surface)

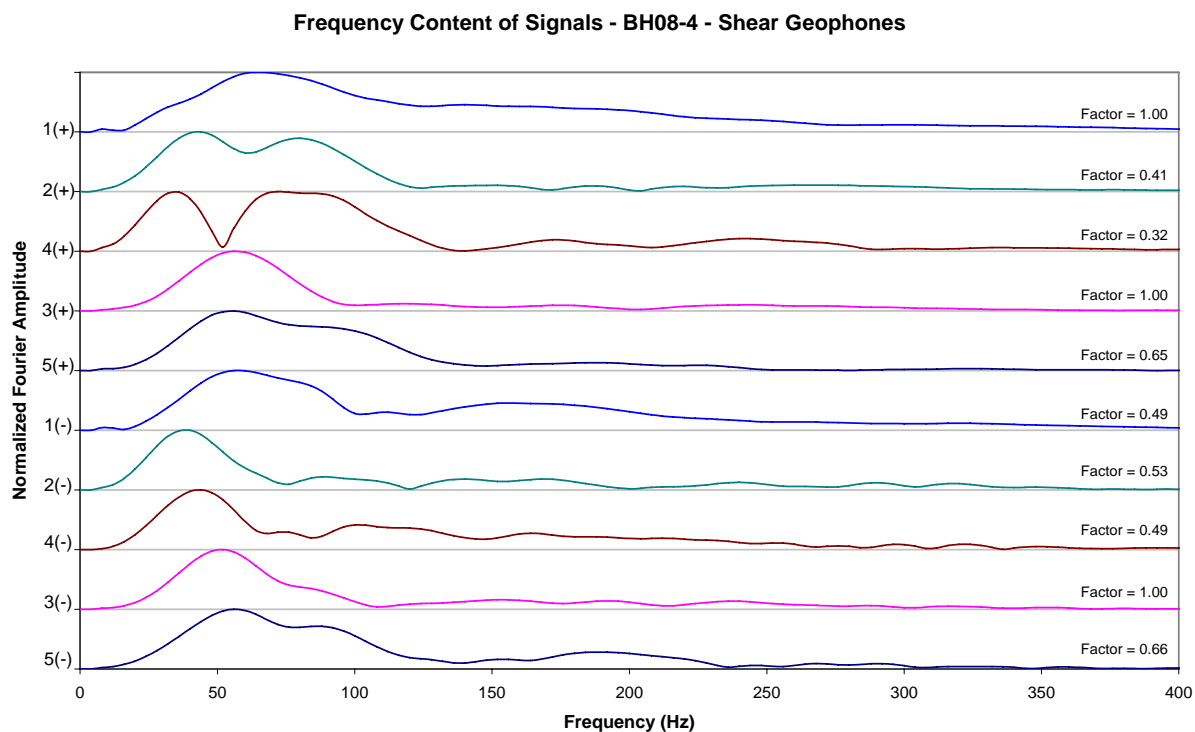


Figure 13-J. Fourier spectra BH 8-04. Horizontal geophones (surface)

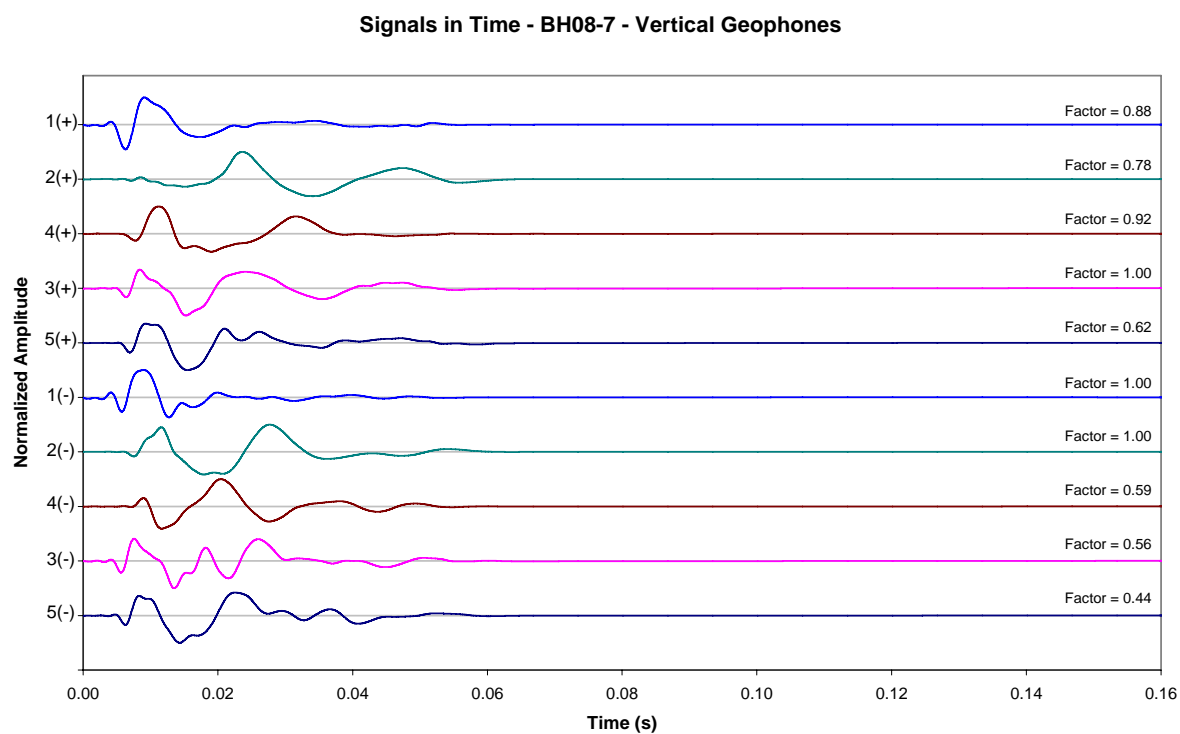


Figure 14-J. Time signals BH 8-07. Vertical geophones (surface)

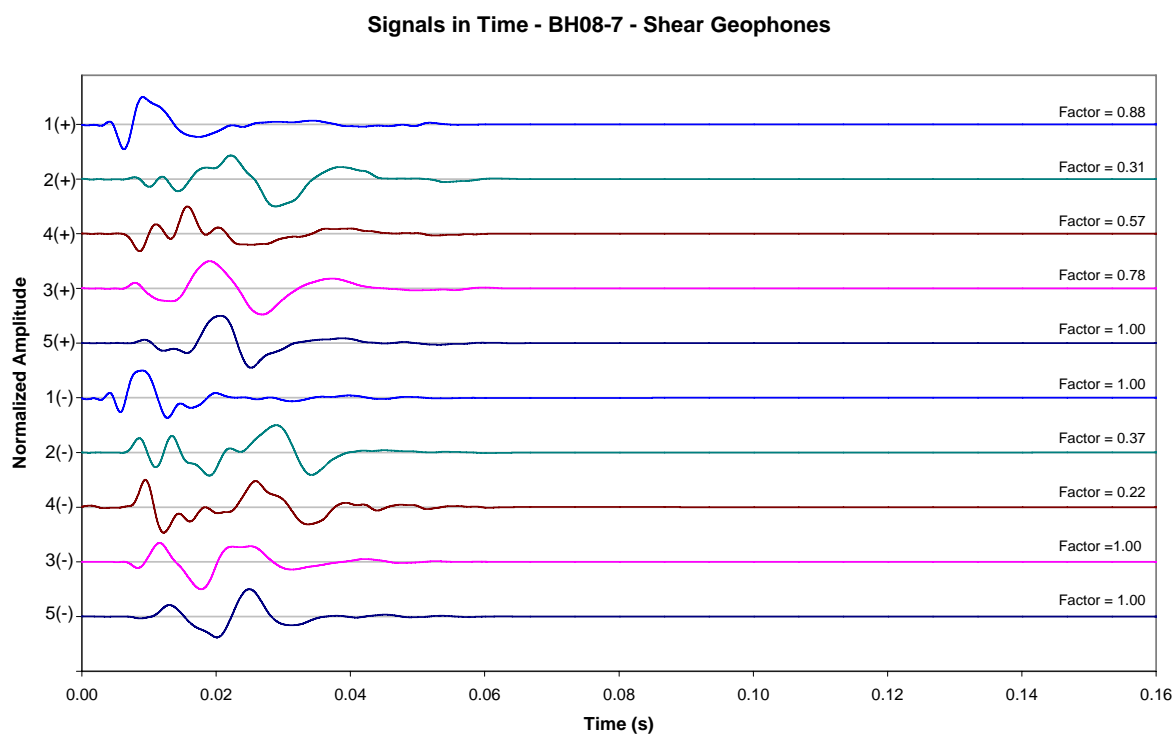


Figure 15-J. Time signals BH 8-07. Horizontal geophones (surface)

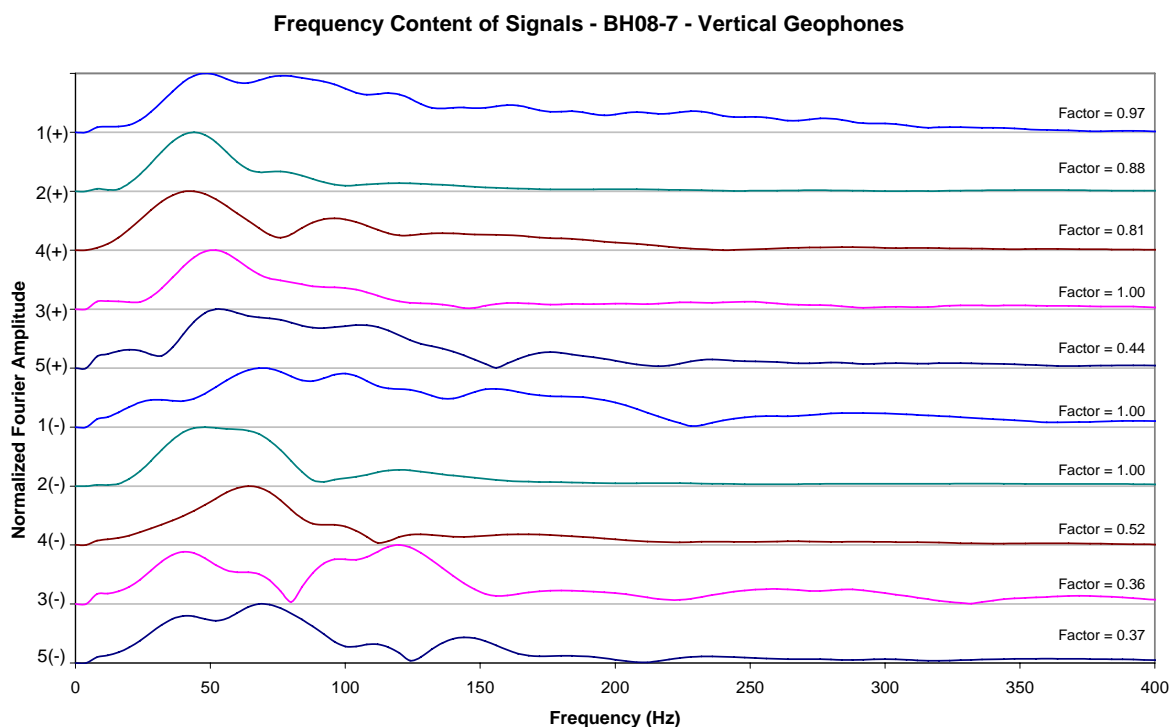


Figure 16-J. Fourier spectra BH 8-07. Vertical geophones (surface)

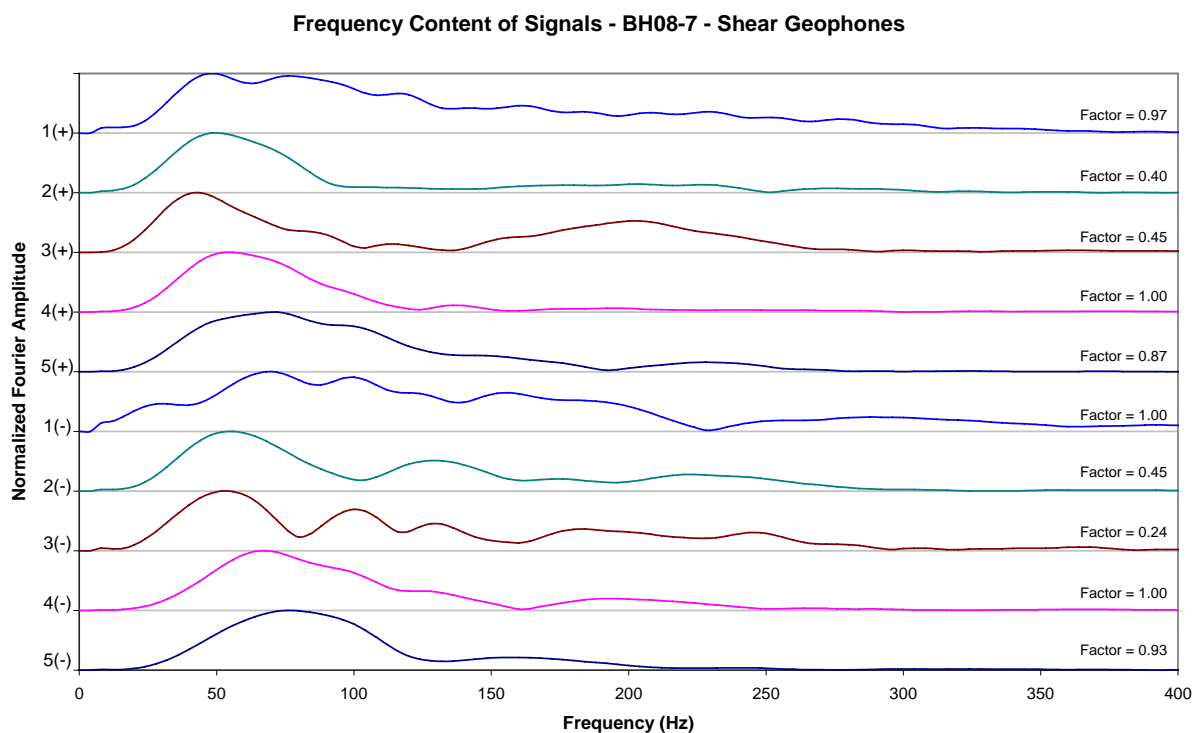


Figure 17-J. Fourier spectra BH 8-07. Horizontal geophones (surface)

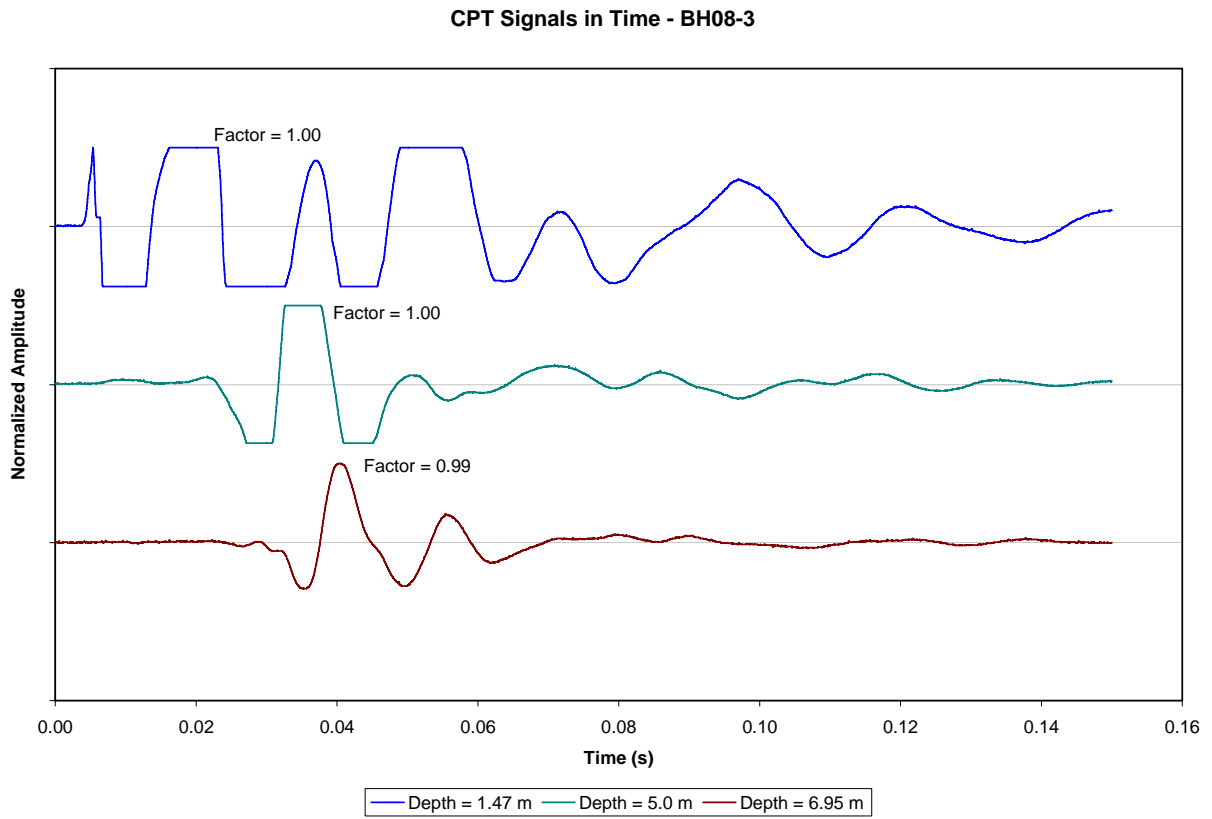


Figure 18-J. Time signals BH 8-03. Vertical geophones (borehole)

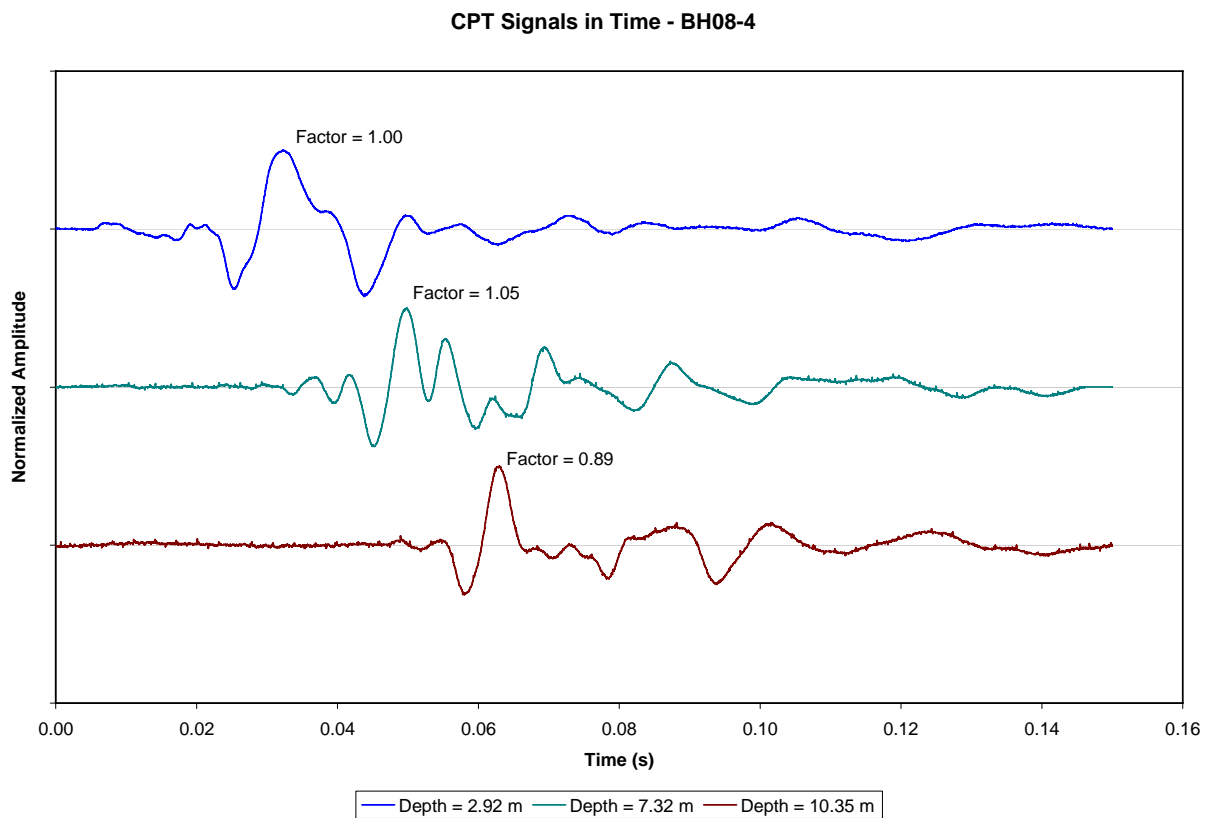


Figure 19-J. Time signals BH 8-04. Vertical geophones (borehole)

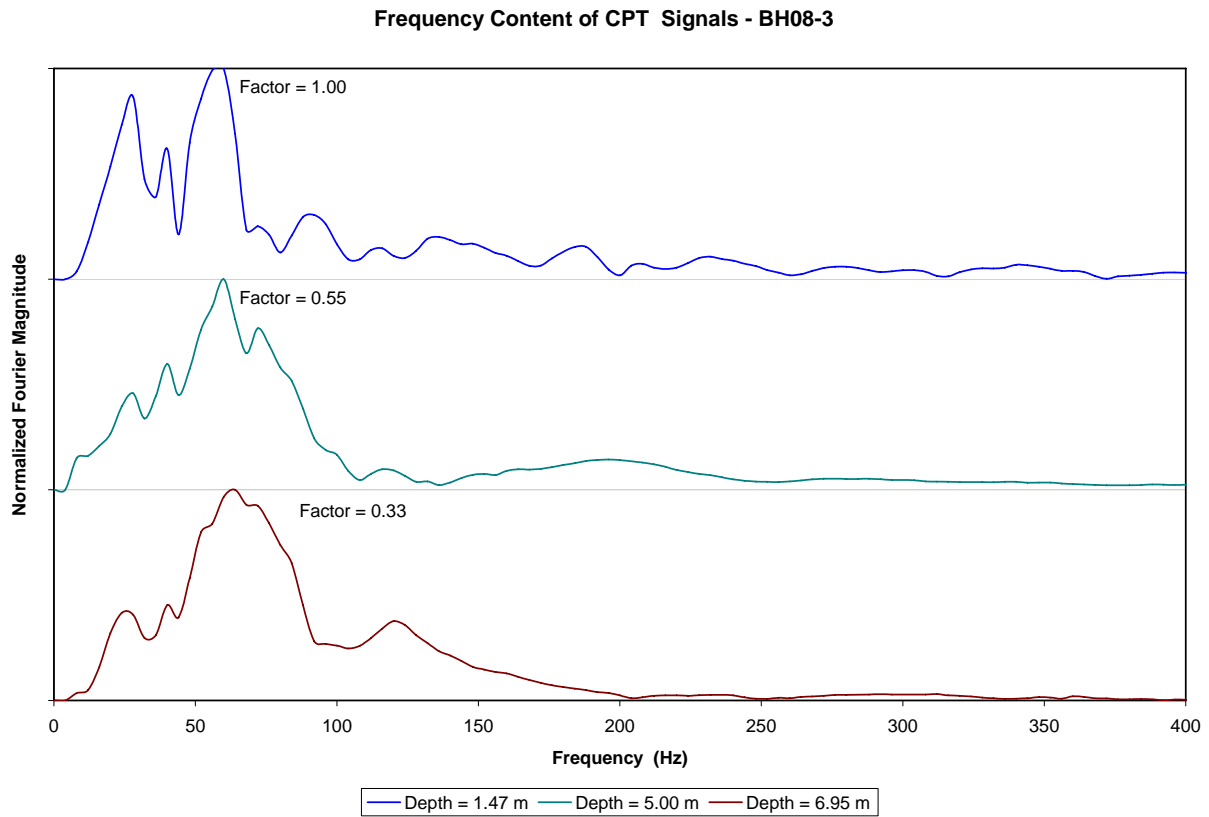


Figure 20-J. Fourier spectra BH 8-03. Vertical geophones (borehole)

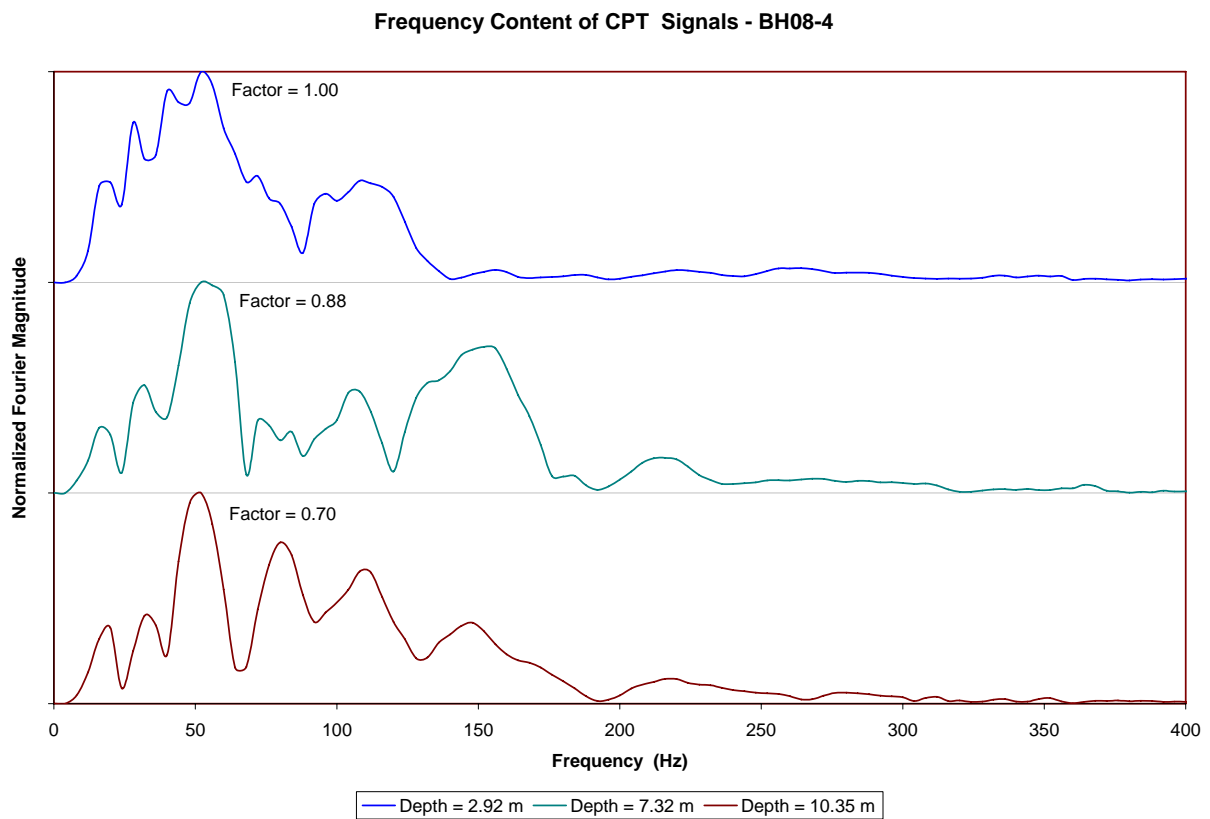


Figure 21-J. Fourier spectra BH 8-04. Vertical geophones (borehole)

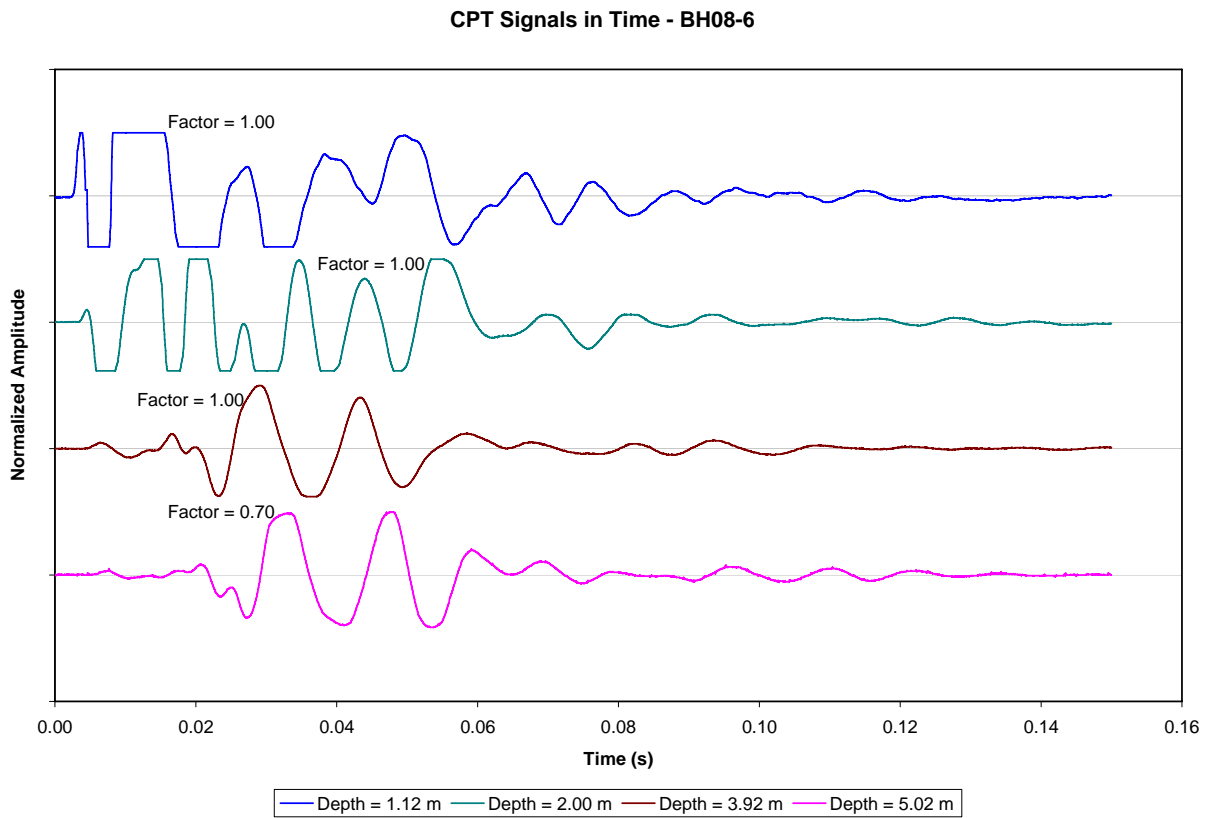


Figure 22-J. Time signals BH 8-06. Vertical geophones (borehole)

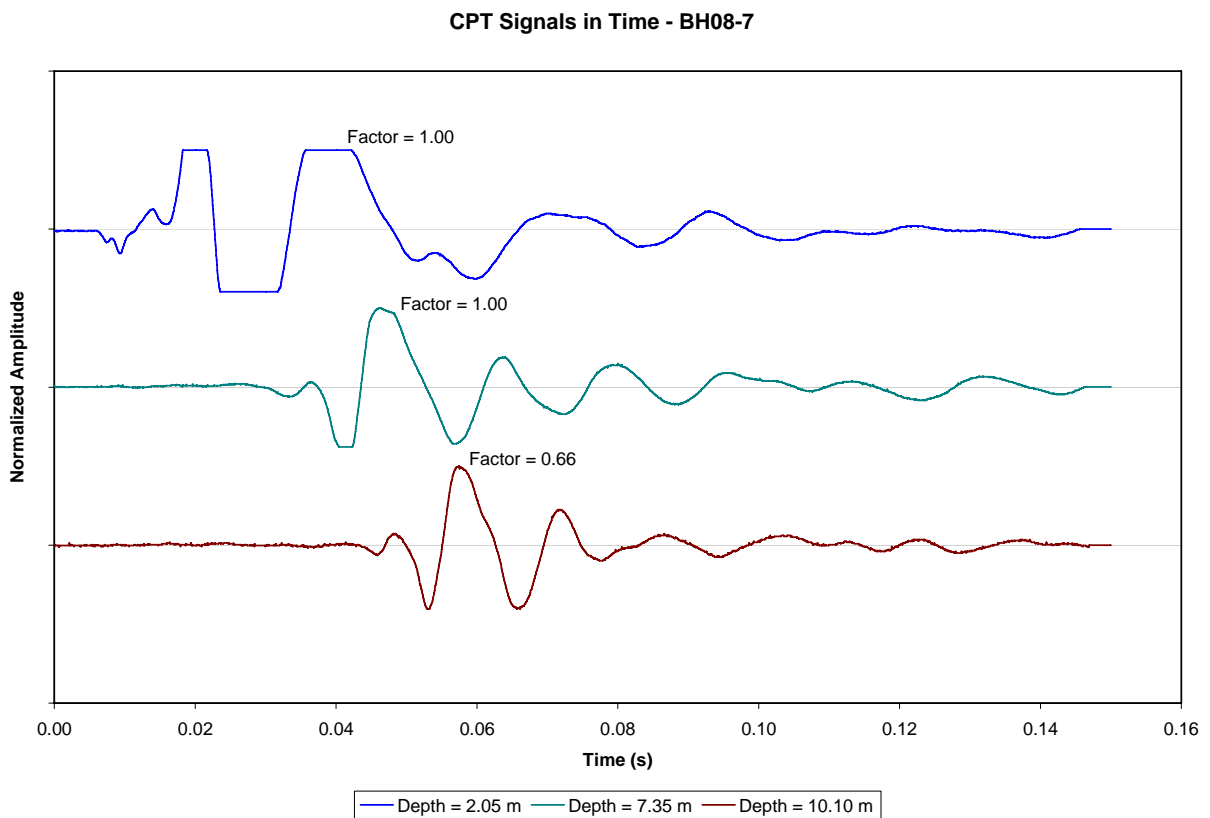


Figure 23-J. Time signals BH 8-07. Vertical geophones (borehole)

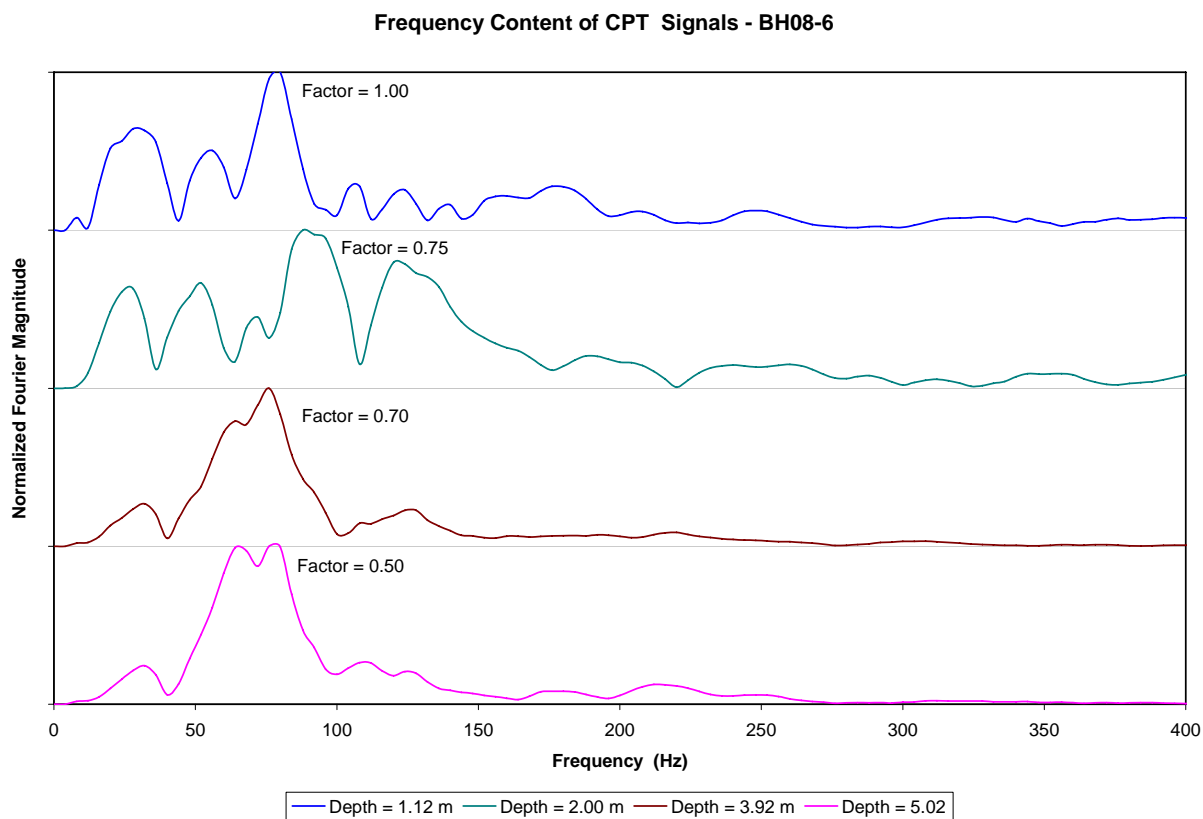


Figure 24-J. Fourier spectra BH 8-06. Vertical geophones (borehole)

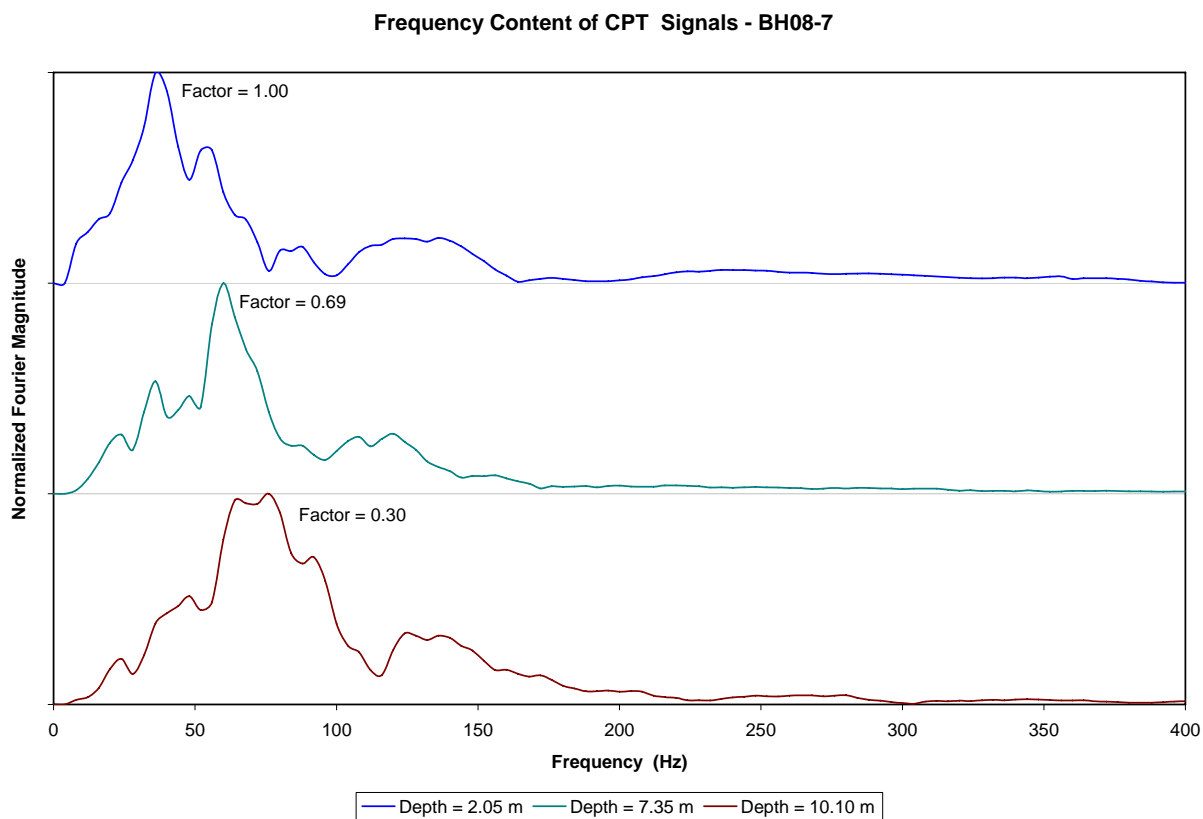


Figure 25-J. Fourier spectra BH 8-07. Vertical geophones (borehole)

Appendix 2

Geophysical Tests for Subsurface Investigations Highway 407 East Extension

Part 2: Field and Laboratory Tests

Geophysical Tests for Subsurface Investigations Highway 407 East Extension

Part II: Field and laboratory test results

Prepared for

Thurber Engineering Ltd.

December 23, 2008

Prepared by:

Giovanni Cascante Ph.D., P.Eng.
Paul Groves,
Fernando Tallavo, M.Sc.,
Yanjun Yang, M.Sc.,
Scott Piggott, M.Sc., and
Claudio Strobbia, Ph.D.

Department of Civil and Environmental Engineering
University of Waterloo Canada, N2L 3G1
E-mail: gcascant@uwaterloo.ca
Tel: (519) 888-4567 ext. 32098
Fax: (519) 888-4349

December 23, 2008

P.K. Chatterji, P.Eng., Ph.D.
President, Chairman of the Board
Thurber Engineering Ltd.
Suite 103, 2010 Winston Park Drive
Oakville, ON L6H 5R7

**Subject: Measurement of Dynamic Properties and Electrical Conductivity of Soil Samples -
Subsurface Investigations in Highway 407.**

Dear Dr. Chatterji,

Thank you for considering our expertise at the University of Waterloo for this project. Please find enclosed the report for the soil tests performed on the Shelby-tube samples from the site located at 1881 Nash Road, Oshawa, Ontario. Resonant column tests were performed on six samples from boreholes; conductivity and total dissolved solids measurements were taken in water samples from three boreholes; and cone penetration tests were performed at four locations on the week of August 4, 2008.

I trust that this report fulfills your requirements. Please contact me if you have any questions regarding the results presented in this report.

Respectfully submitted,



Giovanni Cascante, Ph.D., P.Eng.
Associate Professor, University of Waterloo
(Phone: (519) 888-4567 ext.32098)
(email: gcascant@civmail.uwaterloo.ca)

Attachments: Technical Report and Appendices A to C

1- Introduction

This report summarizes the results of soil testing performed on samples from the site at the 1881 Nash Road in Oshawa that is located along the East link row of proposed Highway 407 East Extension. The soil conditions in these areas present a number of highway design and costing issues; which include the depth of organic soils, the depth of compressible soils, the engineering properties of the soils, and the variation of stratigraphy along the alignment.

2- Scope of investigation

The scope of this investigation consisted of the following:

- Conduct resonant column tests and electrical conductivity measurements on six undisturbed soil samples from various soil layers. The soil samples are provided in Shelby-tubes extracted from boreholes advanced across the site.
- Analyze seismic data from CPT tests and compare them with laboratory measurements.

3- Laboratory testing and CPT tests

Shear wave velocity and electrical conductivity tests were performed in the laboratory and in the field on selected soil specimens to compare laboratory and field results. The testing program included resonant column tests, pore-water conductivity measurements, soil conductivity measurements, and cone penetration tests. Cone penetration tests were performed in-situ to estimate shear wave velocities and electrical conductivities in-situ using a different method. Resonant column tests and electrical conductivity measurements were performed on soil samples extracted from the boreholes: BH08-03, BH08-04, BH08-06, and BH08-07.

3.1- Resonant column tests

The results of resonant column tests tested using Stokoe type resonant column (RC) apparatus according to the standard ASTM D4015-92 are presented next. This device permits testing a specimen under axisymmetric loading in steady state vibration. This device operates at small shear strains between 10^{-6} and 10^{-3} . Two parameters are obtained from resonant column measurements: resonant frequency and damping coefficient. Wave velocity and attenuation are computed from these measurements. The computation of the damping coefficient assumes an equivalent, uniform, linear viscoelastic specimen.

The shear strain varies radially throughout the specimen; the representative value most often selected is the volumetric average shear strain.

Specimen preparation and testing methodology. The specimens were extracted from the Shelby tube using a hydraulic sample extractor. After removing the coverings, the weights and dimensions of the specimens were recorded. The specimens were then placed into a rubber membrane using a membrane holder and then placed in resonant column apparatus. The isotropic confinement was increased to achieve effective confinement equal to the effective vertical stress on the specimen.

At the specified effective confinement, each specimen was allowed to consolidate for 2 hours; then, the RC test was performed. Dynamic properties were evaluated using drained conditions. RC tests were performed first at low shear strain levels ($\gamma < 10^{-5}$); then the dynamic properties were evaluated at larger shear strain levels (maximum capacity of the RC device). A summary of the resonant column results and specimen properties is given in Table 1. The degradation curves for the specimens tested are presented in Appendix A. The experimental setup used for resonant column testing is presented in Appendix B. Sand specimens were not tested because the samples were completely disturbed (Appendix B).

Table 1: Summary of resonant column results and specimen characteristics.

Specimen	Confinement [kPa]	Depth [m]	Initial unit weight [kN/m ³]	Water content w [%]	Shear velocity [m/s]	Damping ratio [%]	Resonant frequency [Hz]
08-3 SH #1	76.7	4.88	19.5	19.5	53.5	3.90	17.2
08-4 SH #1	94.6	6.40	20.0	25.1	50.0	3.40	18.0
08-4 CS	215.9	14.33	22.8	20.1	381.2**	0.93	126.0
08-6 SH #2	25.8	1.22	21.2	12.3	84.5	5.28	29.3
08-7 SH #1	19.6	0.91	21.5	11.0	148.7*	9.50	50.1*
08-7 SH #5	109.2	7.93	19.9	26.3	58.9	3.32	19.1

Notes: * Extrapolated value, ** Velocity corrected for the stiffness of the device

The measurement of shear wave velocities and material damping ratios using the resonant column device were performed also using the non-resonant method (Khan et al. 2007), which allows the evaluation of wave velocity and damping as function of frequency. The summary results from the non-resonant, CPT, and geophysical tests is presented in Table 2.

The frequency content of the measured signals in CPT tests is critical for the correct interpretation of results. During CPT tests, the frequency content of the source was measured by placing four vertical and four horizontal geophones around the seismic source. The location of geophones, time traces, and Fourier spectra of the signals recorded at the ground surface are presented in Appendix C. The frequency ranges used in resonant column, CPT, and MASW tests are also summarized in Table 2.

The wave velocities computed from CPTs for deeper layers (depth > 4 m, silty clay) are generally in very good agreement with the values obtained from the MASW tests and the stratigraphy obtained from boreholes. The wave velocities for the shallower layers (depth < 4m, sand and silt) are significantly underestimated or overestimated (-150% to +50%) because the main wavelengths generated in these tests are between 2 m to 3.5 m (main frequencies between 60 Hz and 80 Hz). Thus, the computed wave velocities for shallow layers are affected by near-field effects and the relatively high velocity of the sand layer close to the ground surface.

The resonant column results are in good agreement with MASW test results and the stratigraphy indicated by borehole data only for superficial layers (depth < 1 m). The wave velocities for the silty clay and the till are significantly underestimated up to -250% and -63%, respectively, by the resonant column data measurements. The higher the clay content in the soil the larger is the underestimation of wave velocity in resonant column results. This underestimation is likely due to two main factors: sample disturbance and the generation of excess pore pressure during the extraction of the specimens from the Shelby tube. To evaluate the effect of the later factor, a clay specimen will be tested in the resonant column after allowing the sample to consolidate for a full week.

3.2- Measurements of soil and pore-water electrical conductivity

The results of laboratory measurements of electrical conductivity of five cylindrical soil specimens and of in-situ measurements of pore-water electrical conductivity are presented next. The experimental setup used for these measurements is given in Appendix B. The summary of conductivity tests on water samples from BH 8-03, BH 8-04, and BH 8-05 is also given in Appendix B.

Specimen preparation and testing methodology. The cylindrical soil specimens have an average diameter and length of 6.3 cm and 16.0 cm, respectively. Each measurement was completed by connecting the soil specimen in series with an amp meter and a power supply. An alternating voltage of 10 V peak-to-peak with a frequency of 500 Hz was used. The experimental setup was calibrated against conductivity measurements in de-ionized water with various salt concentrations using a conductivity meter (HACH CO150). The calibration showed good agreement between the two measuring techniques (Appendix I). Stainless steel wire mesh electrodes were used at the two opposing circular faces of the specimens. The ends of the sample were wetted with de-ionized water before applying the electrodes and the electrodes were held in place using elastic bands to improve the contact. The potential drops across various intervals along the length of the sample were also measured using two 1.6 mm diameter stainless steel electrodes. These electrodes were pushed up to the centre of the specimen in four different arrangements. Five-centimetre spacing measurements were taken along the length of the specimen (centre, centre left, and centre right); and, a ten-centimetre spacing measurement was taken at the centre of the specimen. The conductivity of the specimen is computed as the average of these four measurements.

The comparison of electrical conductivity measurements in the field and in the laboratory is given in Table 3. Field and laboratory measurements are in good agreement. The conductivity of the pore-water is larger than the conductivity of the soil as expected (Archie's Law).

Table 2: Comparison of results from resonant column, CPT, and geophysical tests.

	Resonant Column				MASW			Refraction		CPT Test			
	Depth m	Vs m/s	f-range Hz	D-ratio %	Depth m	Vs m/s	f-range Hz	Depth m	Vs m/s	Depth m	Vs m/s	f-range surf. Hz	f-range Hz
BH 08-3					0.46	90	13 - 44	0.75	130				
					1.90	423							
	4.88	62	22 - 50	4.6	4.44	218		3.55	380	3.04	191	25-200	12-200
					6.01	662		5.60	810	5.77	320	25-200	12-200
BH 08-4					0.30	62	9 - 26	0.93	125				
					1.28	320							
	6.40	61	22 - 50	3.8	4.68	188		5.58	430	4.92	242	10-140	10-200
	14.33	348	125 - 137	1.2	7.40	569		9.30	900	8.64	228	10-140	10-200
BH 08-6					0.71	119	16 - 37	0.75	115				
	1.22	90	25 - 45	5.8	1.99	433				2.76	118	25-200	10-150
					3.36	295		3.45	440	4.27	272	25-200	10-150
					4.17	1266		5.70	760				
BH 07-7					0.33	71	10 - 30	0.96	125				
	0.92	149	45 – 55	9.5	1.63	364							
					5.01	200		5.51	420	4.50	307	20-150	10-175
	7.93	57	22 - 50	3.5	7.40	653		9.10	858	8.52	225	20-150	10-175

Notes: Vs: shear wave velocity; f-range: frequency range of the measurement; f-range surf.: frequency range of the signals measured at the surface; D-ratio: material damping ratio.

Table 3: Comparison of electrical conductivity measurements.

	Field Measurements				Lab Measurements		
	Depth m	σ_{soil} mS/m	Dtw m	σ_{water} mS/m	Depth m	σ_{soil} mS/m	w %
BH 08-3	1.2	7.6 - 9.7	1.48				
	4.2	10.4 - 13.2					
	6.1	2.0 - 4.0		53.8	15.6	1.4	9
BH 08-4	1.1	7.6 - 9.7	0.70				
	6.4	10.4 - 13.2					
	10.7	2.0 - 4.0		34.2	7.6	2.6	26
BH 08-5	3.1	12.5 - 13.2	1.18				
	6.1	2.0 - 4.0		49.6			
BH 08-6	2.3	12.5 - 13.2			3.1	18.8	18
	4.6	2.0 - 4.0					
BH 07-7	1.9	7.6 - 9.7			3.8	9.1	19
	6.9	10.4 - 13.2			6.1	31.6	21
	10.1	2.0 - 4.0					

Notes: dtw: depth to water; σ : electrical conductivity.

4- Summary and Conclusions

- A geotechnical investigation consisting of six boreholes was conducted in the site to be used as ground truthing. The results from each geophysical test were analyzed and compared with the data from the boreholes. The electrical resistivity method gave the best indication of the depth of the till layer (less than 19% error).
- Laboratory and field measurements of wave velocity and electrical conductivity in general showed good agreement. CPT requires a higher frequency seismic source to improve the accuracy for shallow layers. Resonant column tests on clays are significantly affected by the excess pore pressure produced during sample extraction and sample disturbance.

5- References

- Annual book of ASTM standards, 2002. Standard Guide for Using the Seismic Refraction Method for Subsurface Investigations, ASTM D 5777-00, 04(02), pp. 309-312.
- ASTM D4015-92, 2000, "Standard Test Methods for Modulus and Damping of Soils by the Resonant-Column Method," American Society for Testing and Materials, Annual Book of Standards.
- Cerveny, V., Langer, J. and Psencik, I. (1974): Computation of geometrical spreading of seismic body waves in laterally inhomogeneous media with curved interfaces. *Geophys. J. R. astr. Soc.*, 38, 9-19.
- Graff, K. (1991). Wave motion in elastic solids. New York: Dover publications Inc.
- Gucunski, N., Ganji, V., and Maher, M.H., 1996. Effects of obstacles on Rayleigh wave dispersion obtained from the SASW test. *Soil Dynamics and Earthquake Engineering*, Volume 15: 223-231.
- Gucunski, N., Krstic, V., and Maher, M.H., 1998. Experimental procedures for detection of underground objects by the SASW test. In *Geotechnical Site Characterization*. Edited by Robertson and Mayne, Balkeme, Rotterdam: 469-472.
- Hagedoorn J.G. 1959, The Plus-Minus Method of Interpreting Seismic Refraction Sections, *Geophysical Prospecting* 7, 158–182
- Khan, Z., Cascante, G., and El-Naggar, H., Lai, C.G., 2008. Measurement of Frequency Dependent Dynamic Properties of Soils Using the Resonant Column Device. *Journal of Geotechnical and Geoenvironmental Engineering*, ASCE. In print.
- Kong, F.N., H. Westerdahl, and By, T.L., 1994. Borehole Radar Tunnel Detection at Gjovik, Norway. Norwegian Geotechnical Institute, Publication 194, pp. 1-10.
- McNeill, J. D., 1980. Electrical conductivity of soils and rocks, Geonics Technical Note TN-5, Geonics Limited, Mississauga.
- Menke W., 1989, *Geophysical Data Analysis: Discrete Inverse theory*, International Geophysics Series. San Diego: Academic Press. 289 pp.

- Nasseri, A., Phillips, Cascante, G., C. and Hutchinson, J., 2007. Effects of Underground Cavities on Rayleigh Waves – Numerical and Experimental Study. *Soil Dynamics and Earthquake Engineering*. 27(4): 300-313.
- NBCC 2005. National Building Code of Canada (NBCC) Volumes 1 and 2. 12th edition, National Research Council, Ottawa, Canada.
- Palmer, D., 1980, The Generalized Reciprocal Method of Seismic Refraction Interpretation, in Burke, K.B.S. (Ed.), *Society of Exploration Geophysicists*.
- Park C.B., Miller R.D., Xia J., 1999, Multichannel analysis of surface waves, *Geophysics*, 64(3), 800-808.
- Phillips, C., Cascante, G., and Hutchinson, D.J. 2000. Seismic surface waves to detect underground voids. *Proceedings of the Symposium on the Application of Geophysics to Engineering and Environmental Problems*, Arlington, Virginia: 29-37.
- Richart Jr., F.E.; Hall, J.R. and Woods, R.D., 1970. *Vibration of Soils and Foundations*. Prentice Hall, Inc., Englewood Cliffs, New Jersey.
- Strobbia C., Foti S., 2006, Multi Offset Phase Analysis (MOPA), *Journal of Applied Geophysics*, 56:300-313.
- Strobbia, C., 2002. Surface wave methods: acquisition, processing and inversion. PhD Diss. Politecnico di Torino. Italy.
- Zonge, K., Wynn, J., and Urquhart, S. 2006. Resistivity, Induced Polarization, and Complex Resistivity. In *Near-Surface Geophysics*, Ed. D. Buttler, SEG. Tulsa, OK. pp. 357-438

Appendix A

Degradation curves from resonant column testing

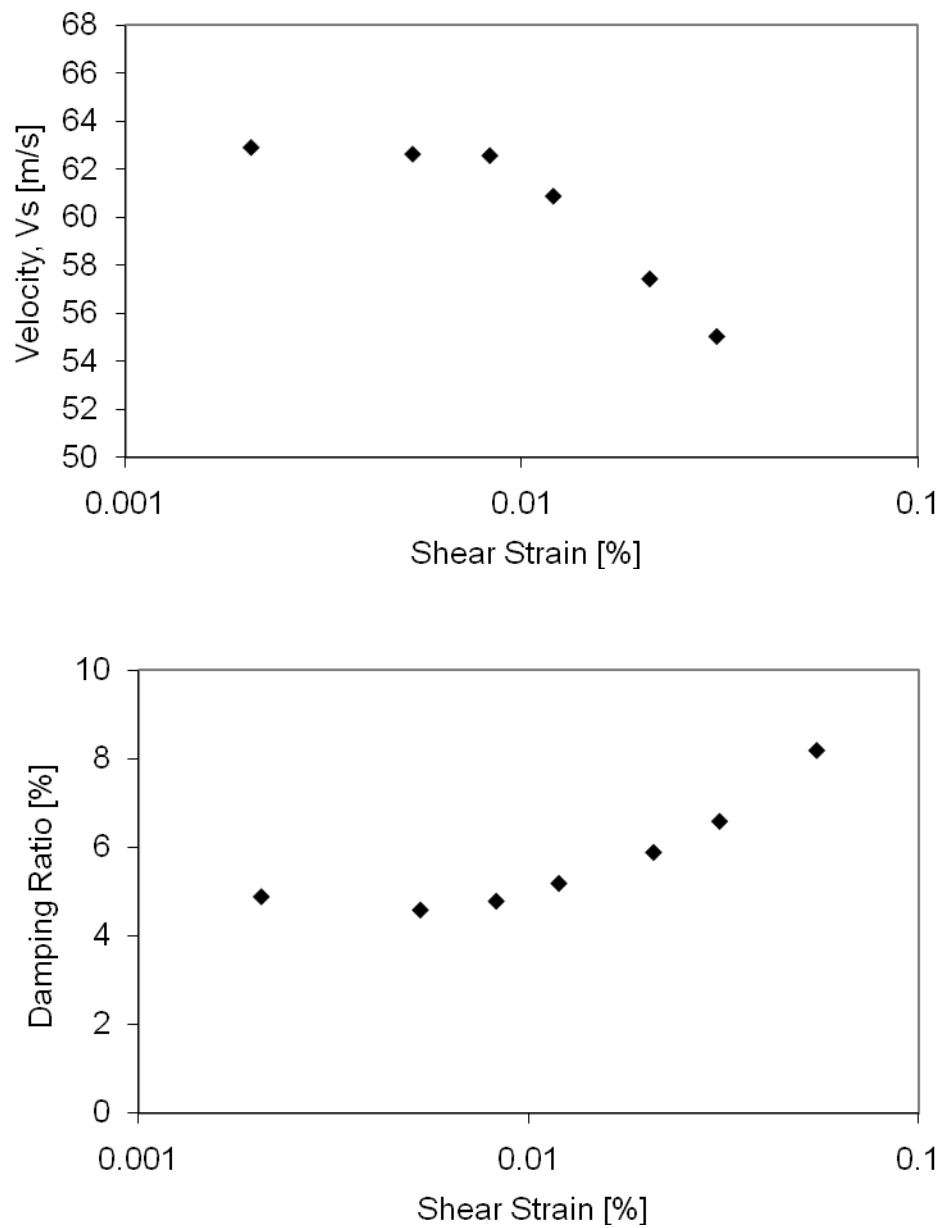


Figure 1-A. Wave velocity and damping degradation curves. Specimen 08-3 SH #1

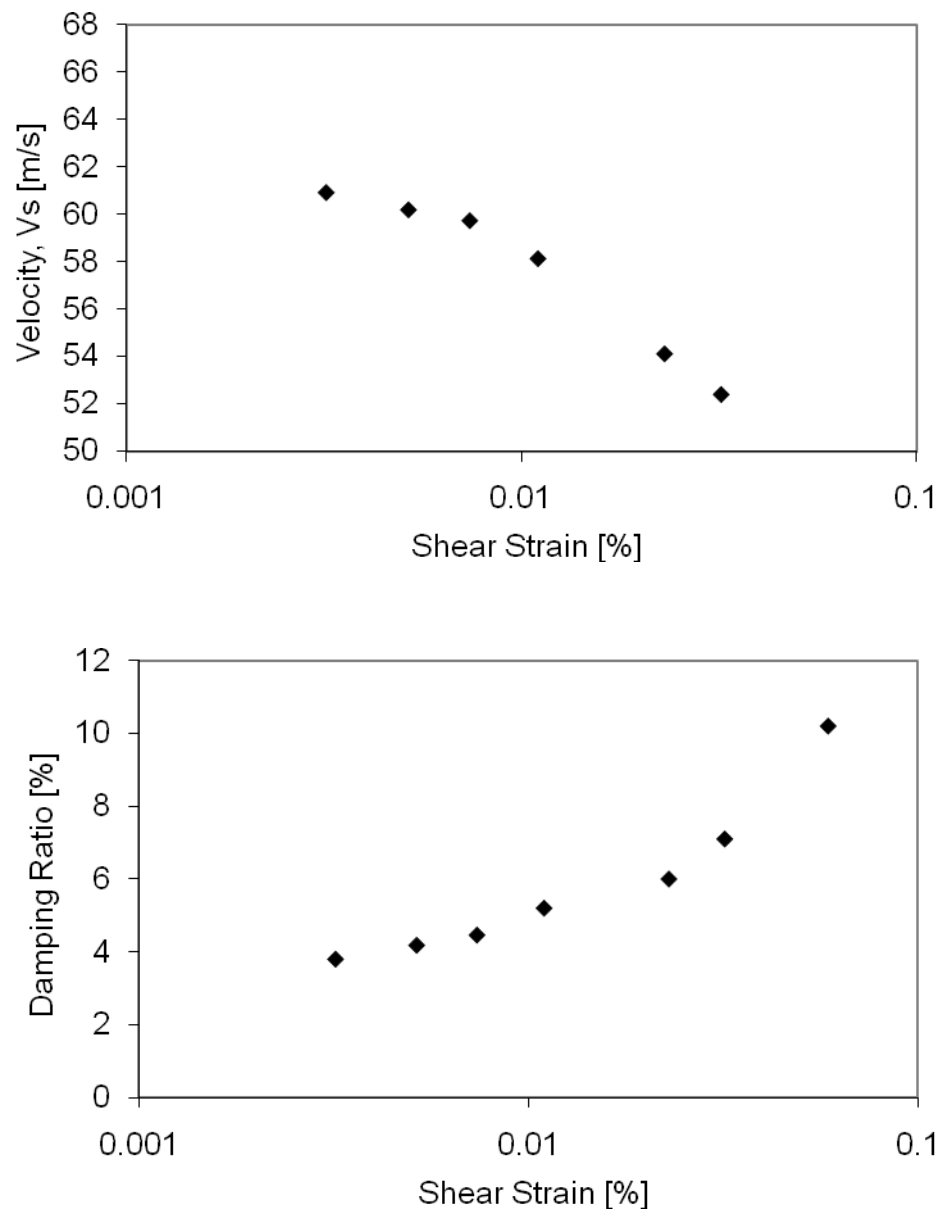


Figure 2-A. Wave velocity and damping degradation curves. Specimen 08-4 SH #1

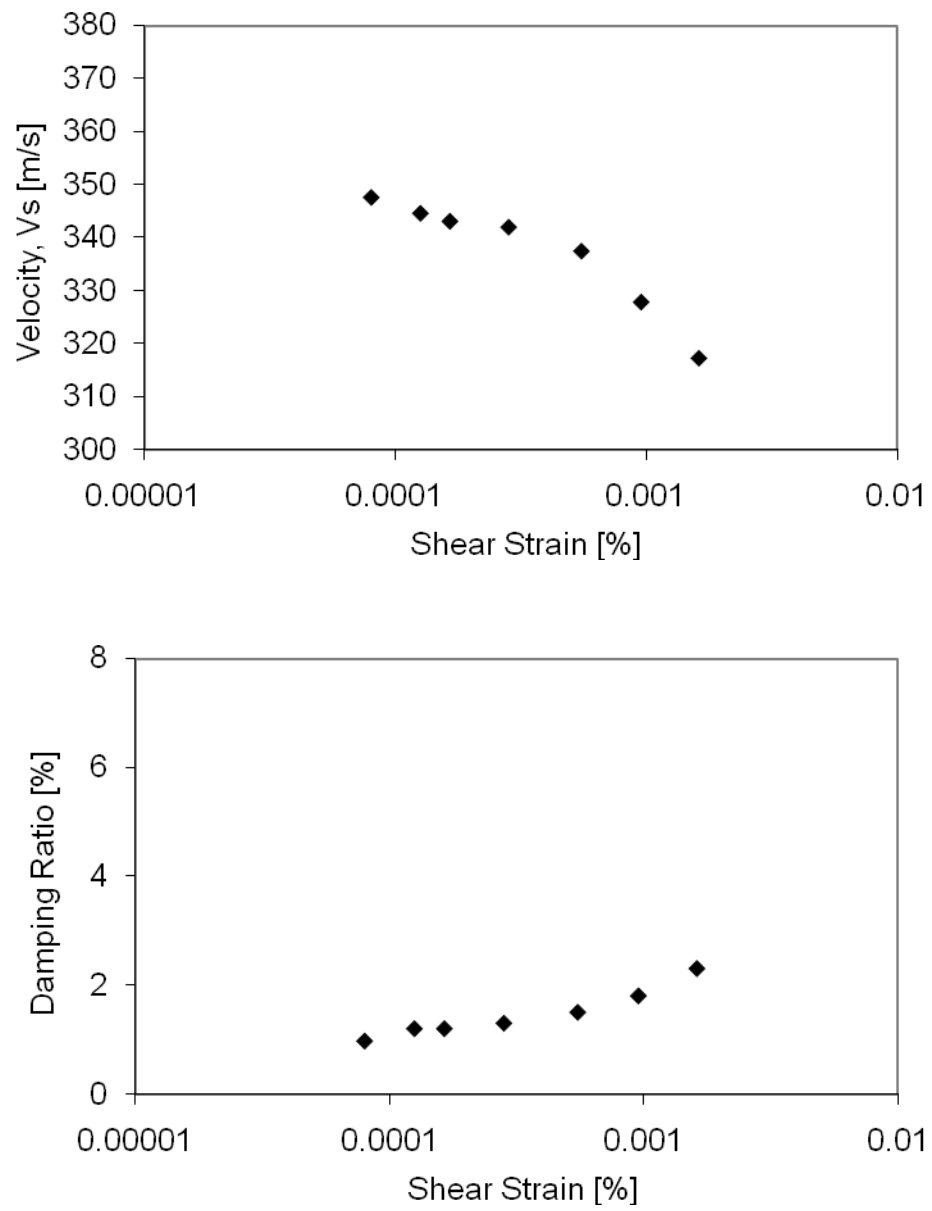


Figure 3-A. Wave velocity and damping degradation curves. Specimen 08-4 CS

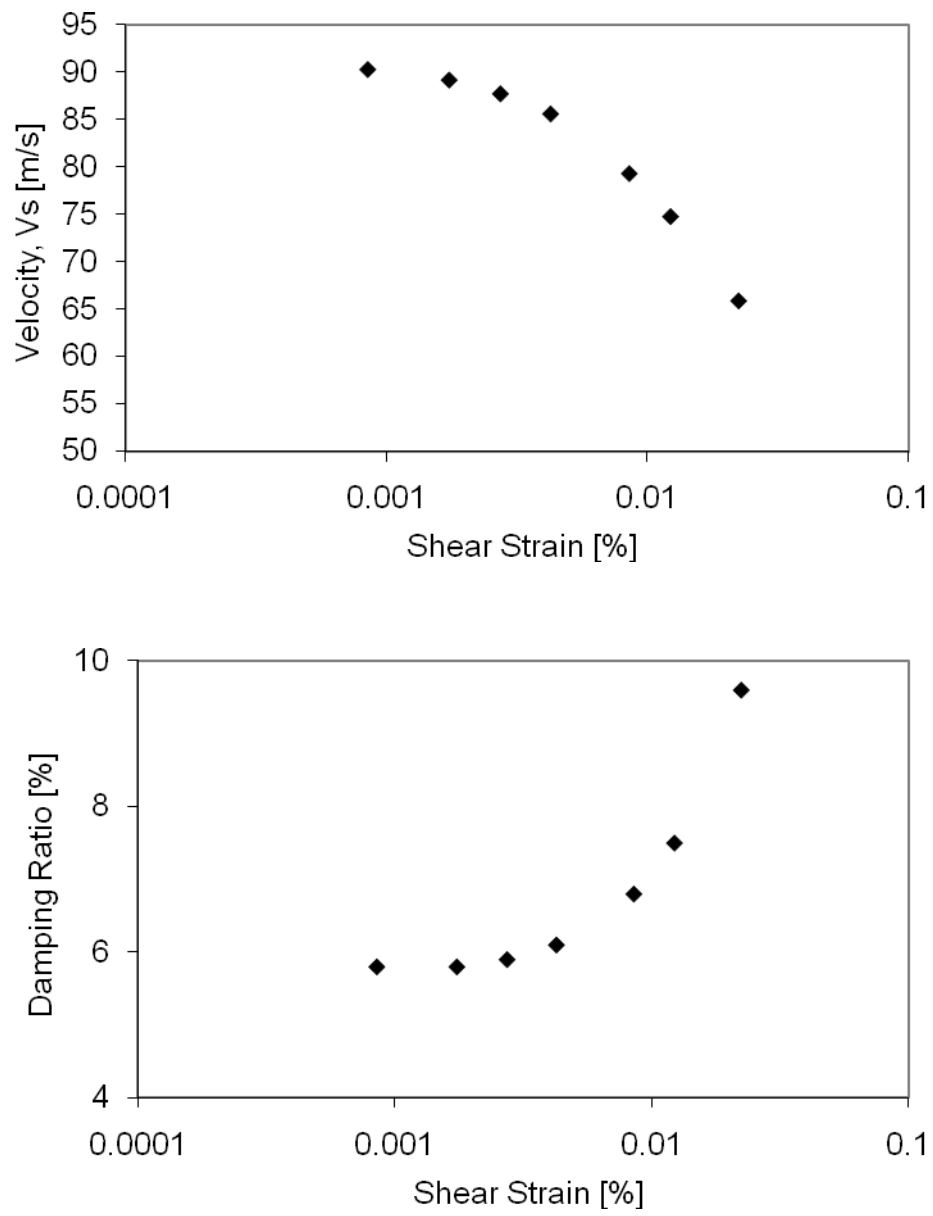


Figure 4-A. Wave velocity and damping degradation curves. Specimen 08-6 SH #2

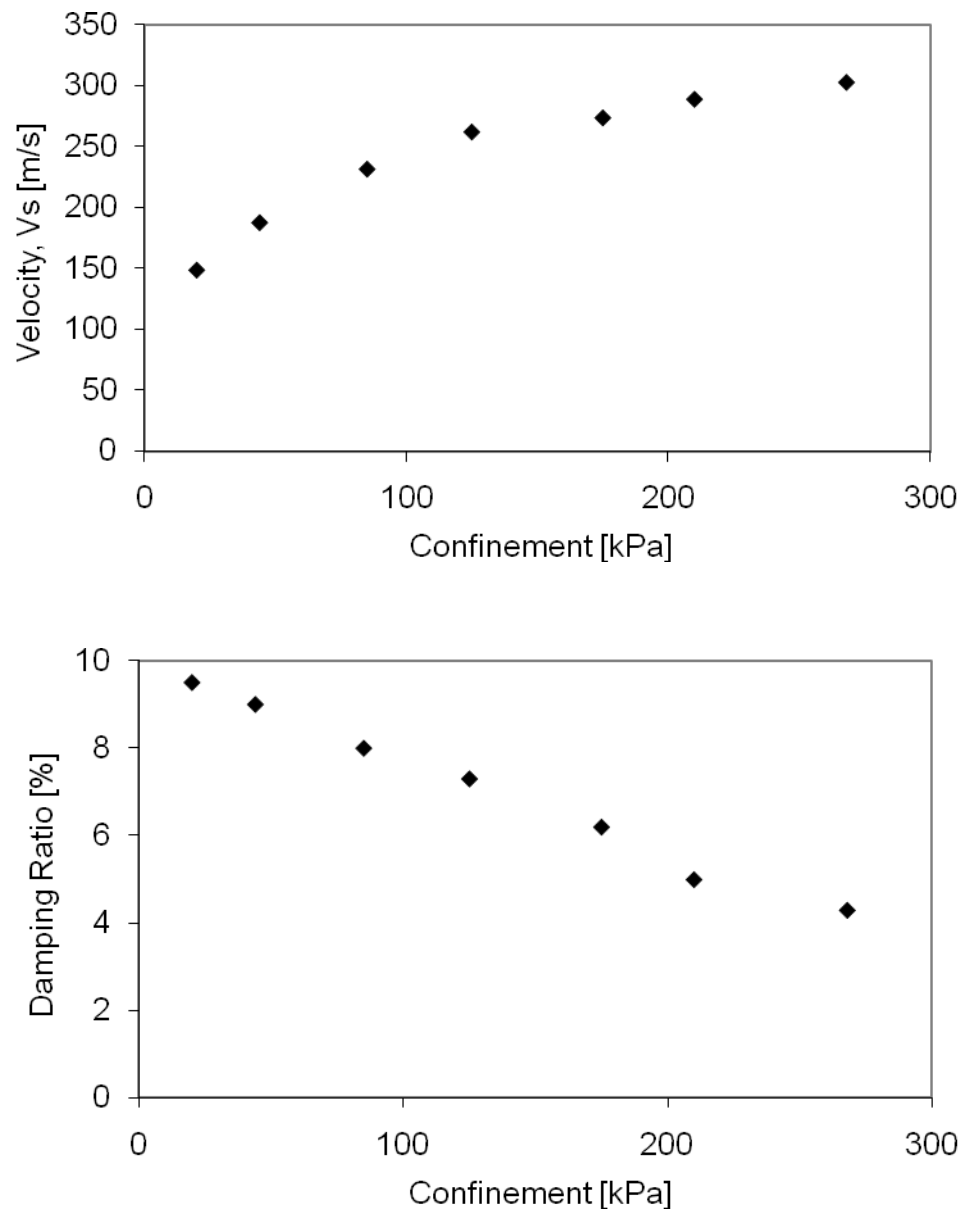


Figure 5-A. Wave velocity and damping against confinement. Specimen 08-7 SH #1

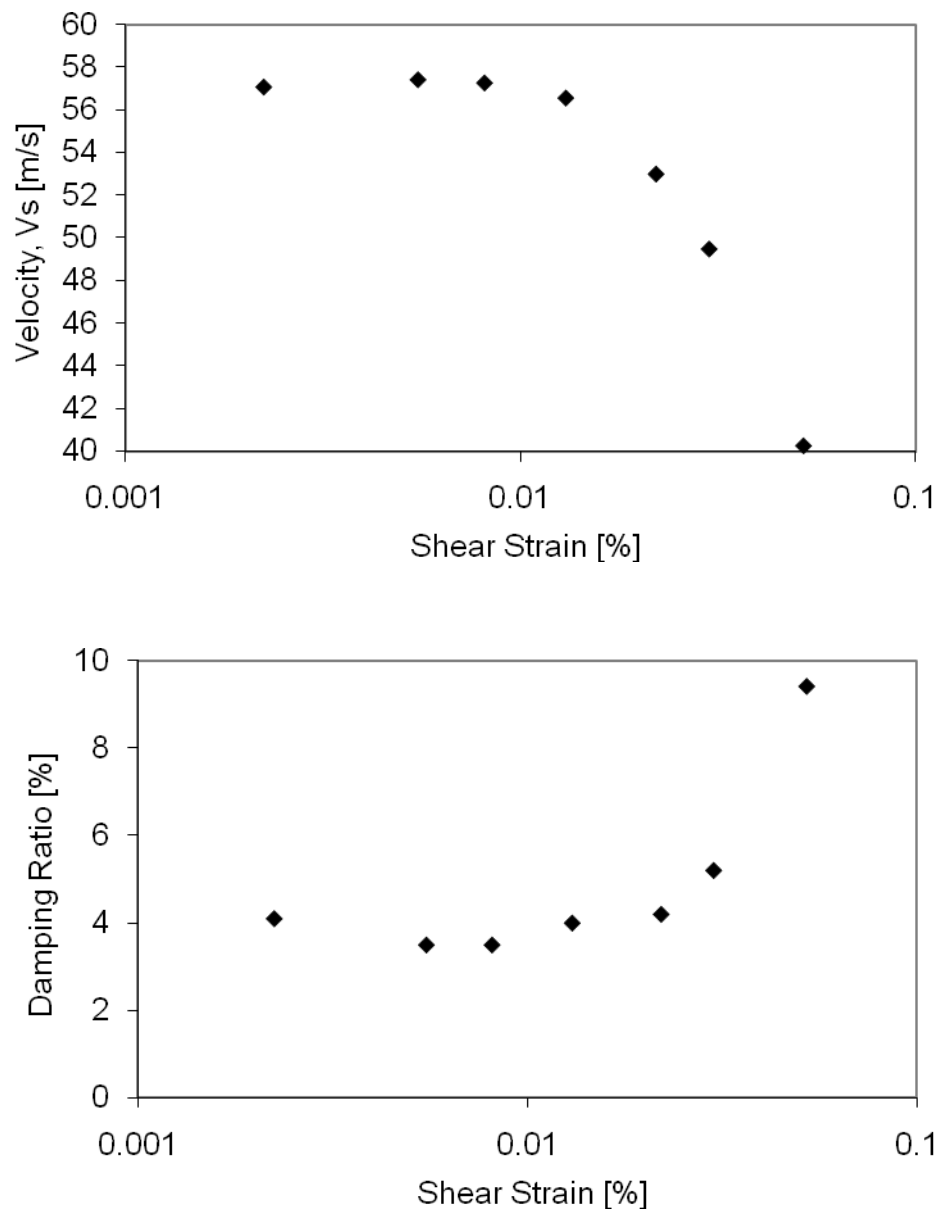


Figure 6-A. Wave velocity and damping degradation curves. Specimen 08-7 SH #5

Appendix B

Resonant column and electrical conductivity experimental setups



Figure 1-B. Resonant column experimental setup

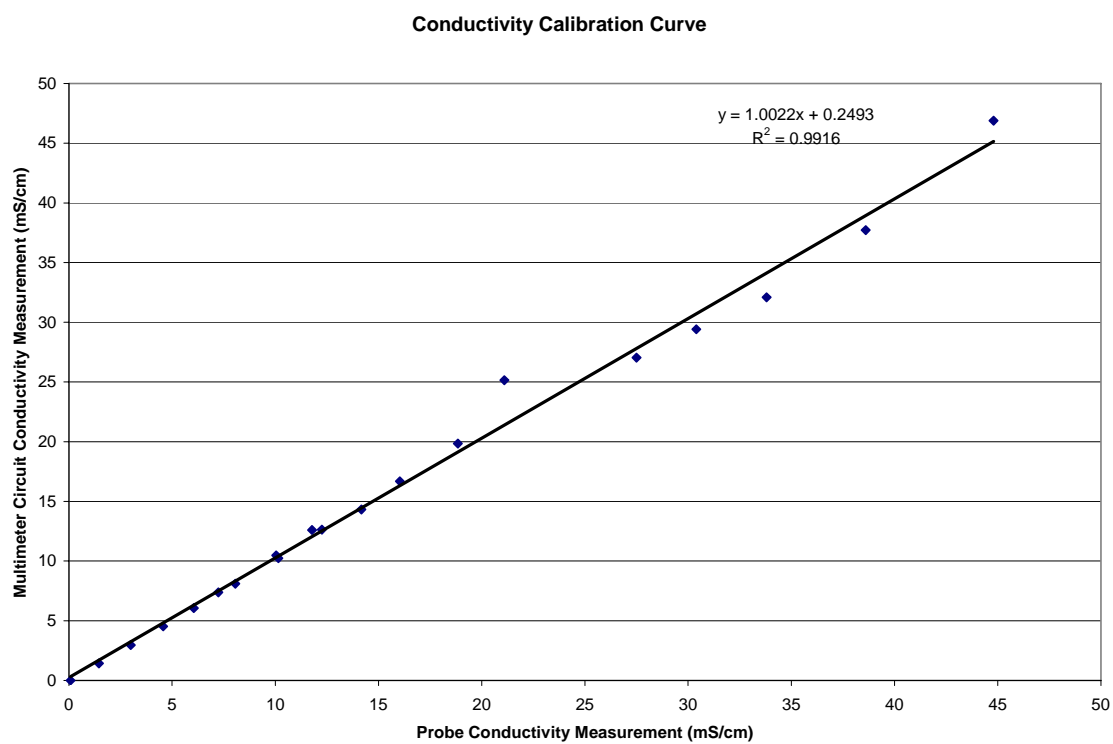


Figure 4-B. Calibration results for the soil conductivity measurements

Table 5-B. Field water sampling results. July 15, 2008, 2:30 p.m., sunny 25°C. Three well volumes to be purged (if possible) and tested

Borehole 08-4

Depth of well:	15.97 m below top of pipe (btop)		
Water level:	1.50 m btop		
Casing stickup:	0.80 m above ground surface (ags)		
Physical description:	cloudy, brownish grey, silty		
	V ₁	V ₂	V ₃
Volume purged (L):	29	5 (dry)	2 (dry)
Temperature (°C):	12.4	13.0	14.1
TDS (mg/L):	141	142	163
Conductivity (mS/m):	29.7	30.0	34.2

Borehole 08-3

Depth of well:	6.87 m btop		
Water level:	2.30 m btop		
Casing stickup:	0.82 m ags		
Physical description:	cloudy, brown, silty		
	V ₁	V ₂	V ₃
Volume purged (L):	6 (dry)	1 (dry)	1 (dry)
Temperature (°C):	15.0	15.2	15.4
TDS (mg/L):	275	249	258
Conductivity (mS/m):	57.1	51.8	53.8

Borehole 08-5

Depth of well:	13.60 m btop		
Water level:	1.96 m btop		
Casing stickup:	0.78 m ags		
Physical description:	cloudy, brownish grey, silty		
	V ₁	V ₂	V ₃
Volume purged (L):	23	1 (dry)	1 (dry)
Temperature (°C):	12.2	13.9	13.1
TDS (mg/L):	214	207	237
Conductivity (mS/m):	45.0	43.4	49.6

Appendix C

Frequency content of CPT signals

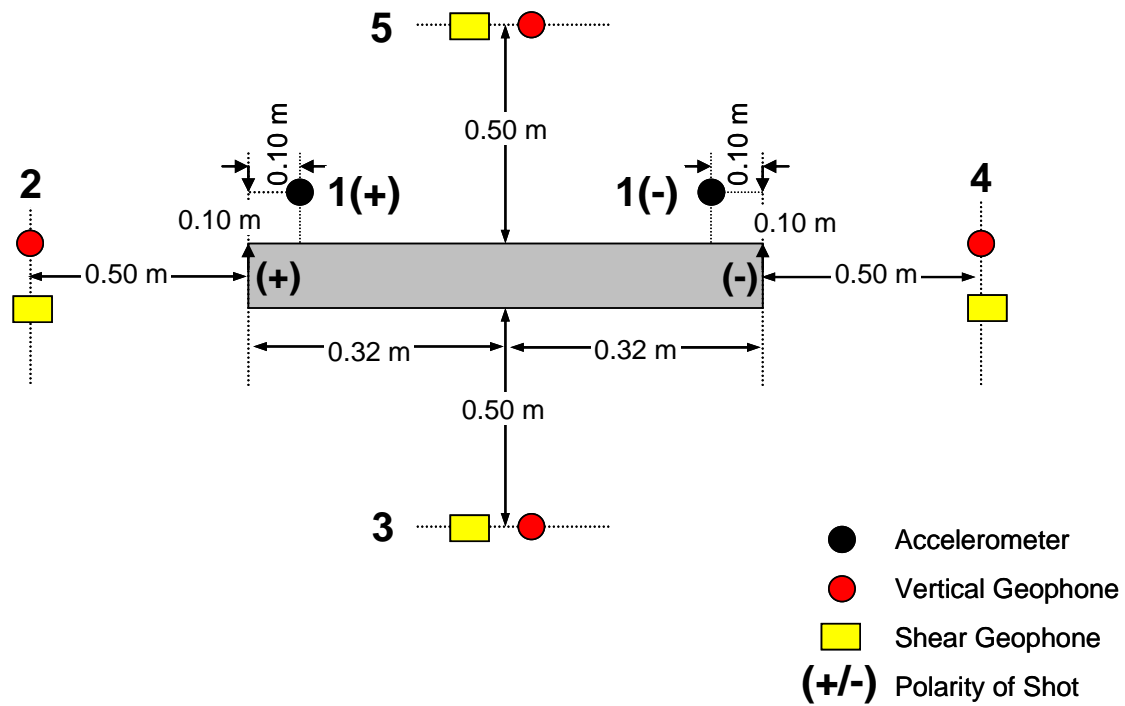


Figure 1-C. Surface geophone locations for CPT.

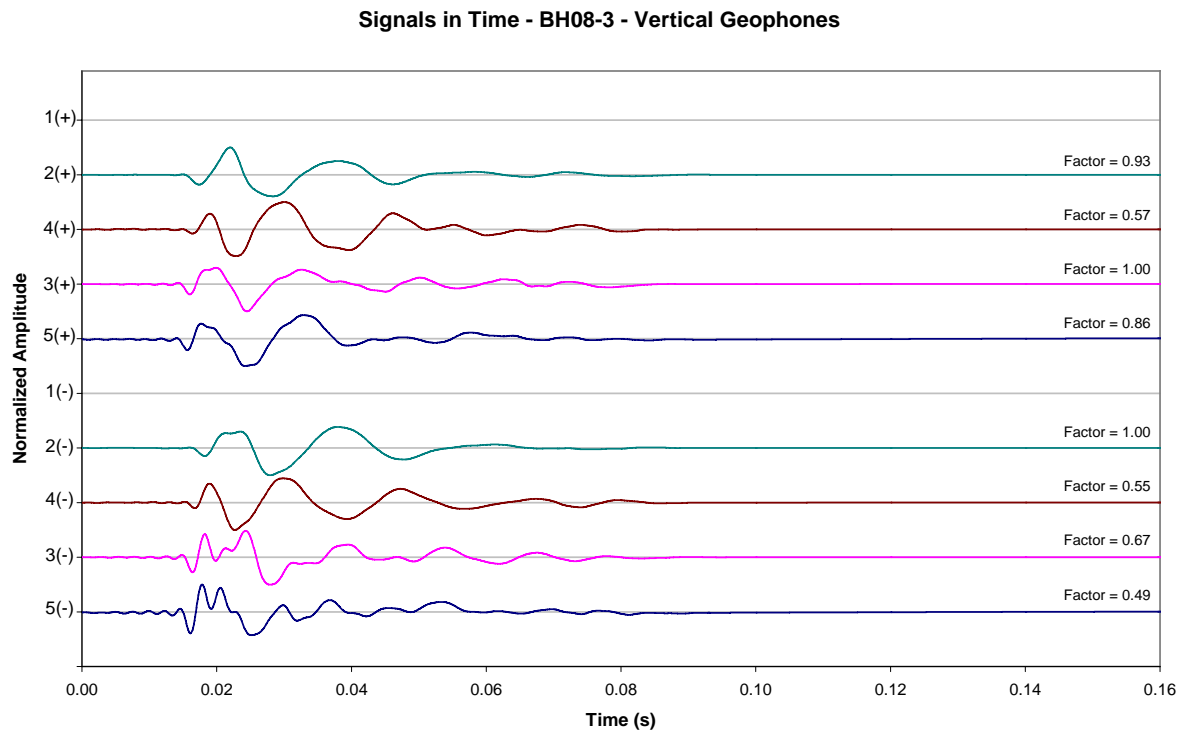


Figure 2-CC. Time signals BH 8-03. Vertical geophones (surface)

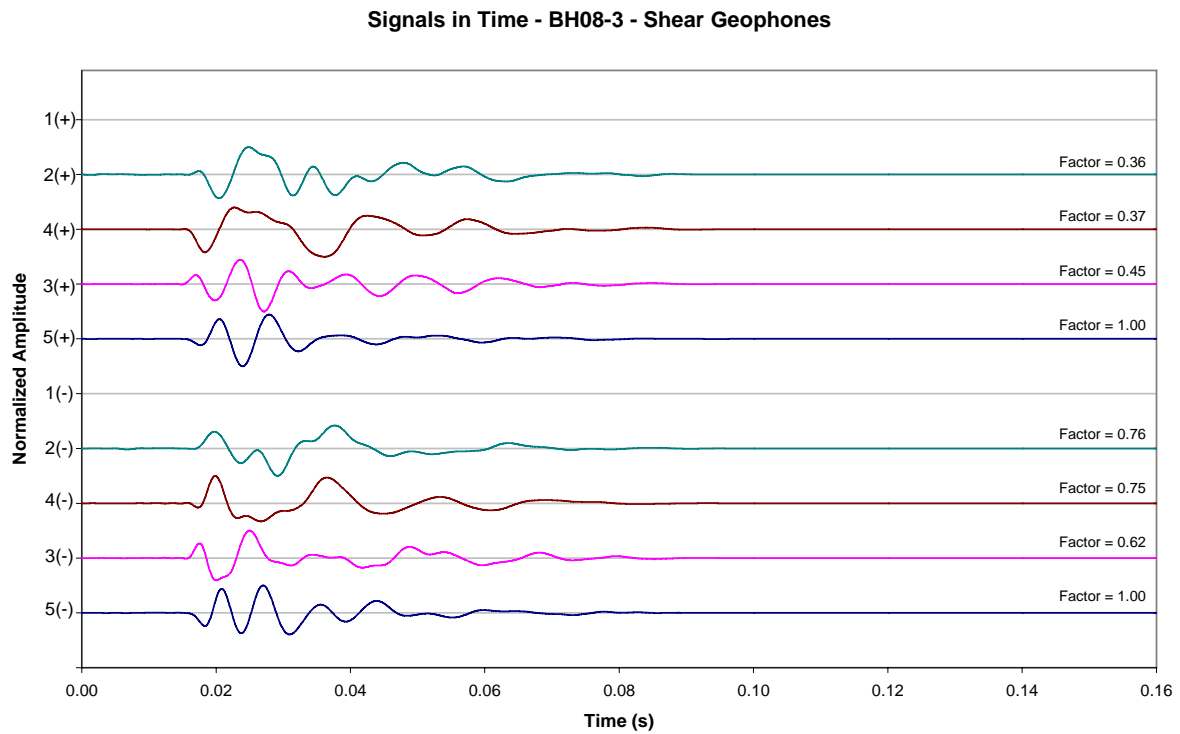


Figure 3-C. Time signals BH 8-03. Horizontal geophones (surface)

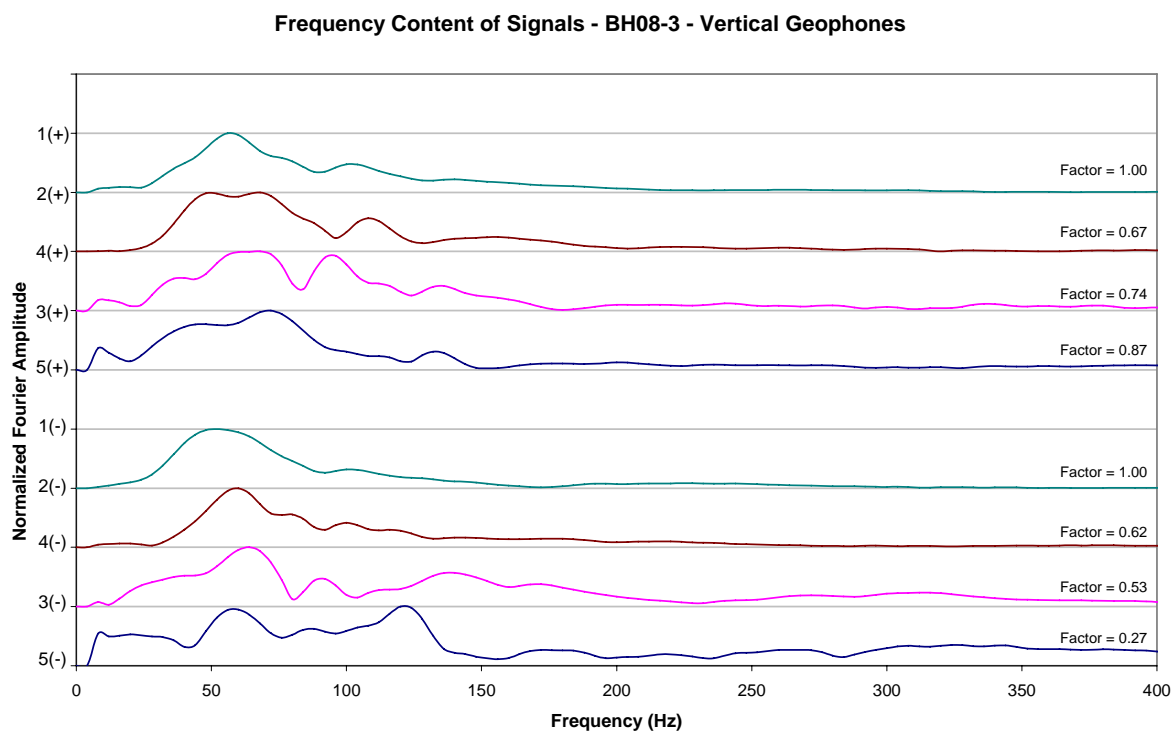


Figure 4-C. Fourier spectra BH 8-03. Vertical geophones (surface)

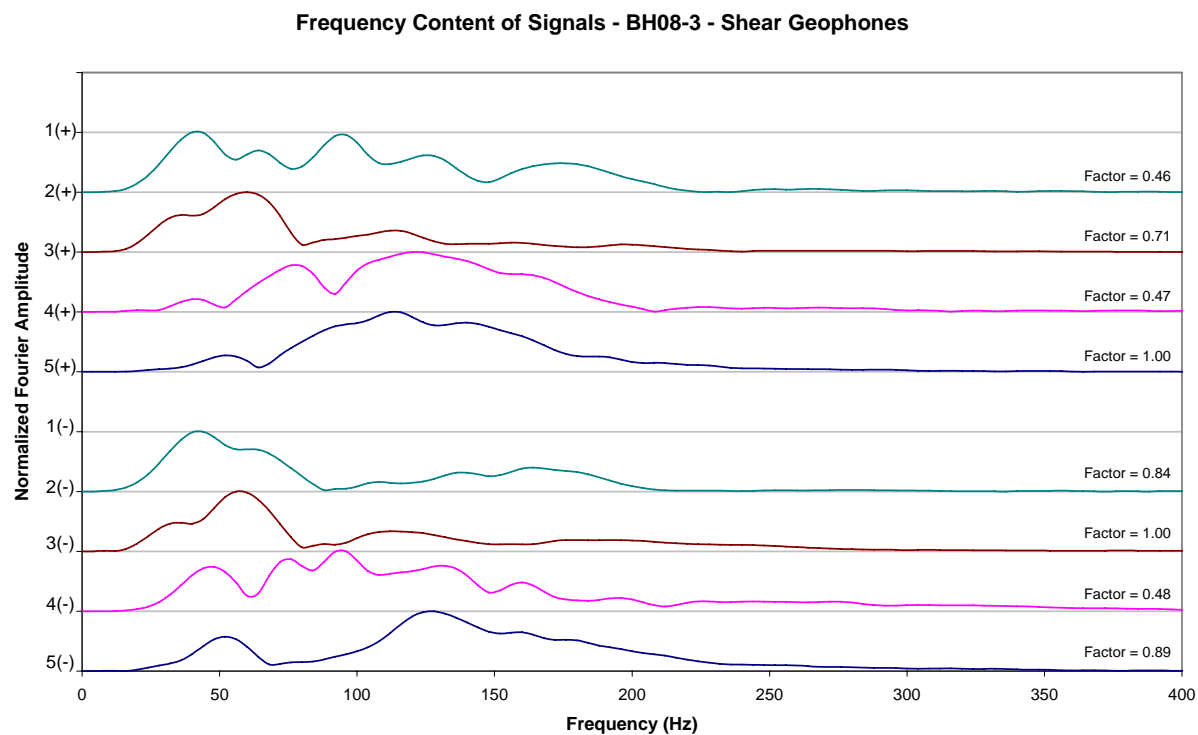


Figure 5-C. Fourier spectra BH 8-03. Horizontal geophones (surface)

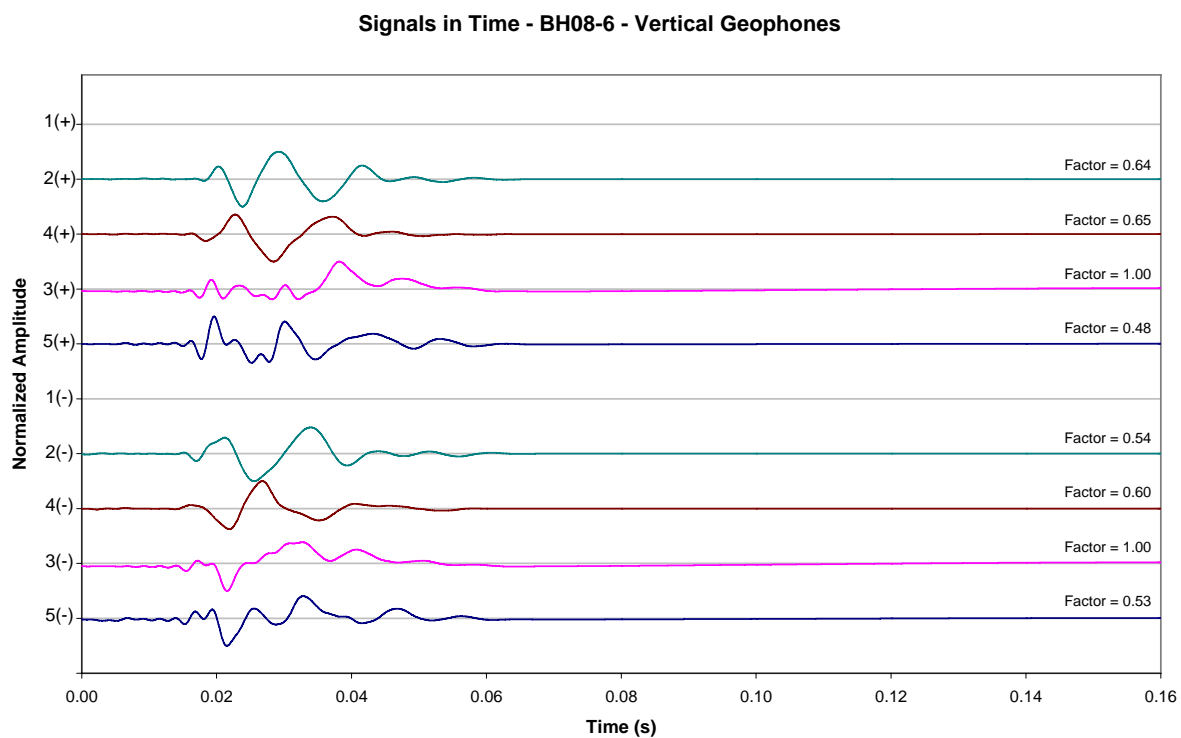


Figure 6-C. Time signals BH 8-06. Vertical geophones (surface)

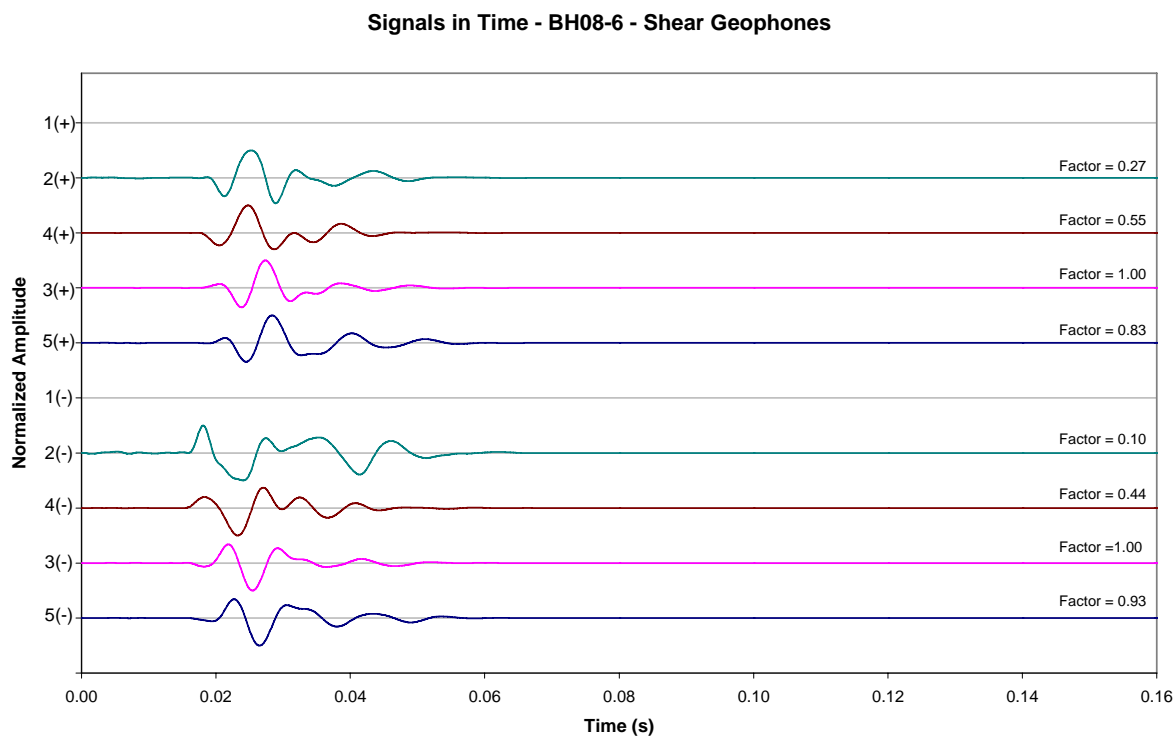


Figure 7-C. Time signals BH 8-06. Horizontal geophones (surface)

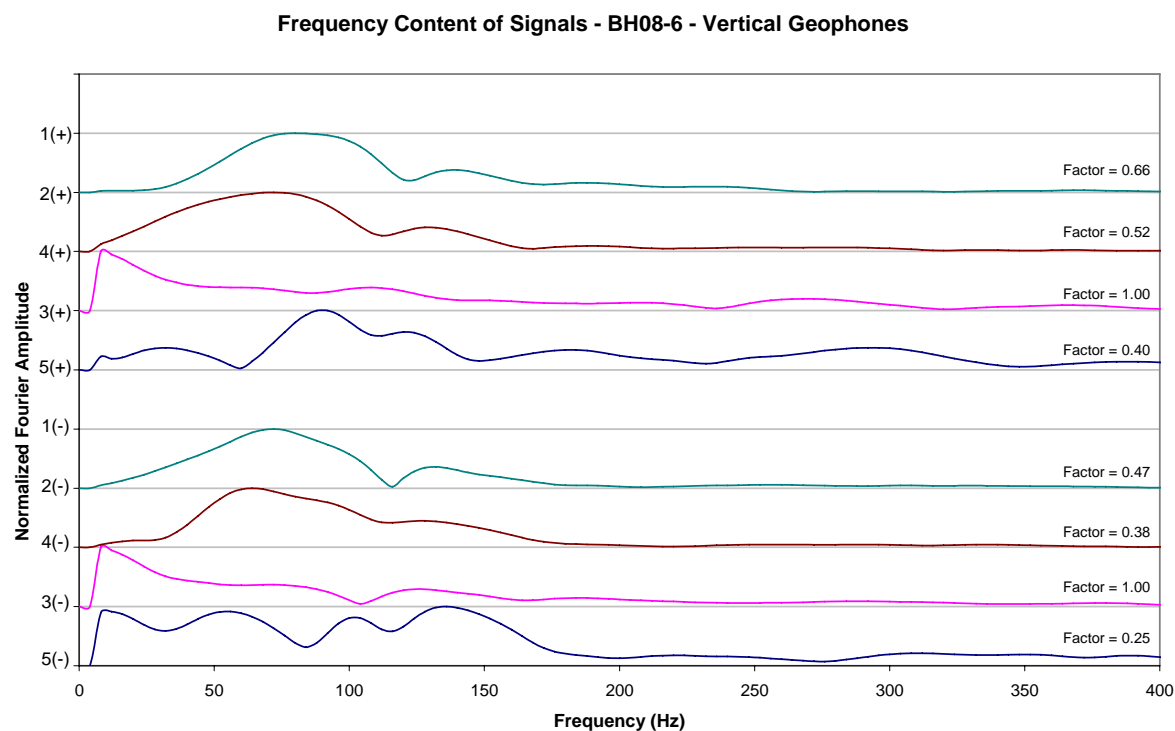


Figure 8-C. Fourier spectra BH 8-06. Vertical geophones (surface)

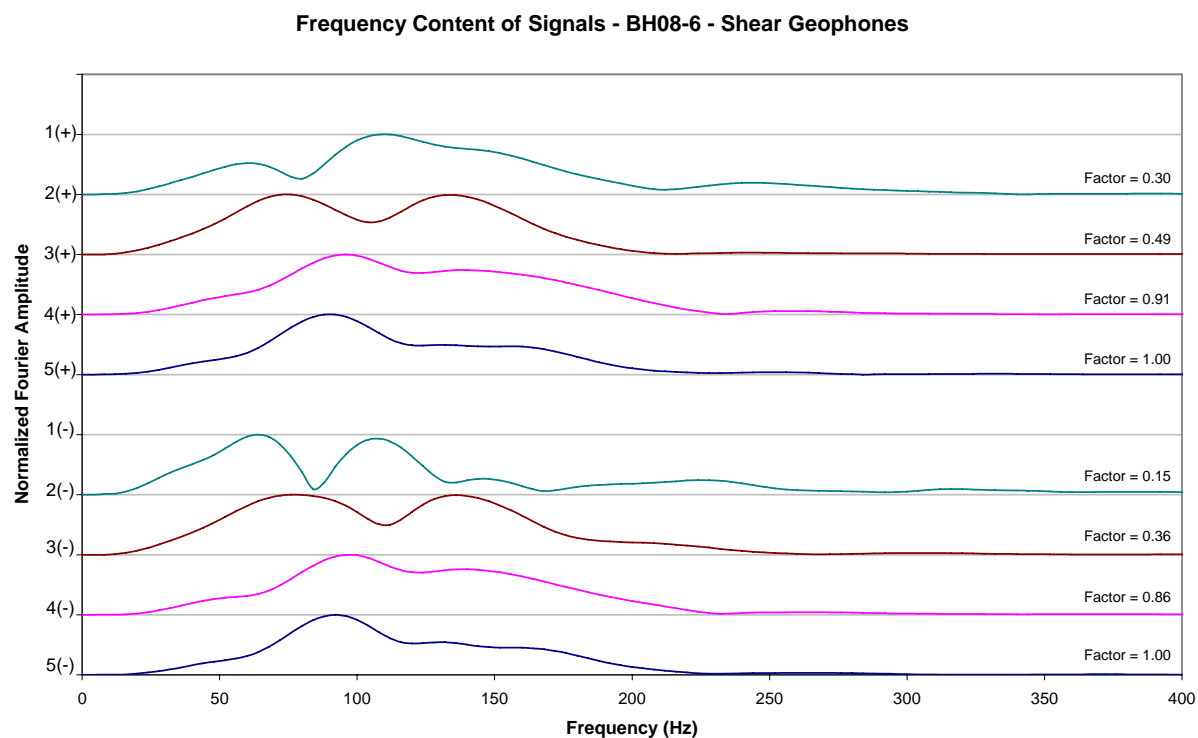


Figure 9-C. Fourier spectra BH 8-06. Horizontal geophones (surface)

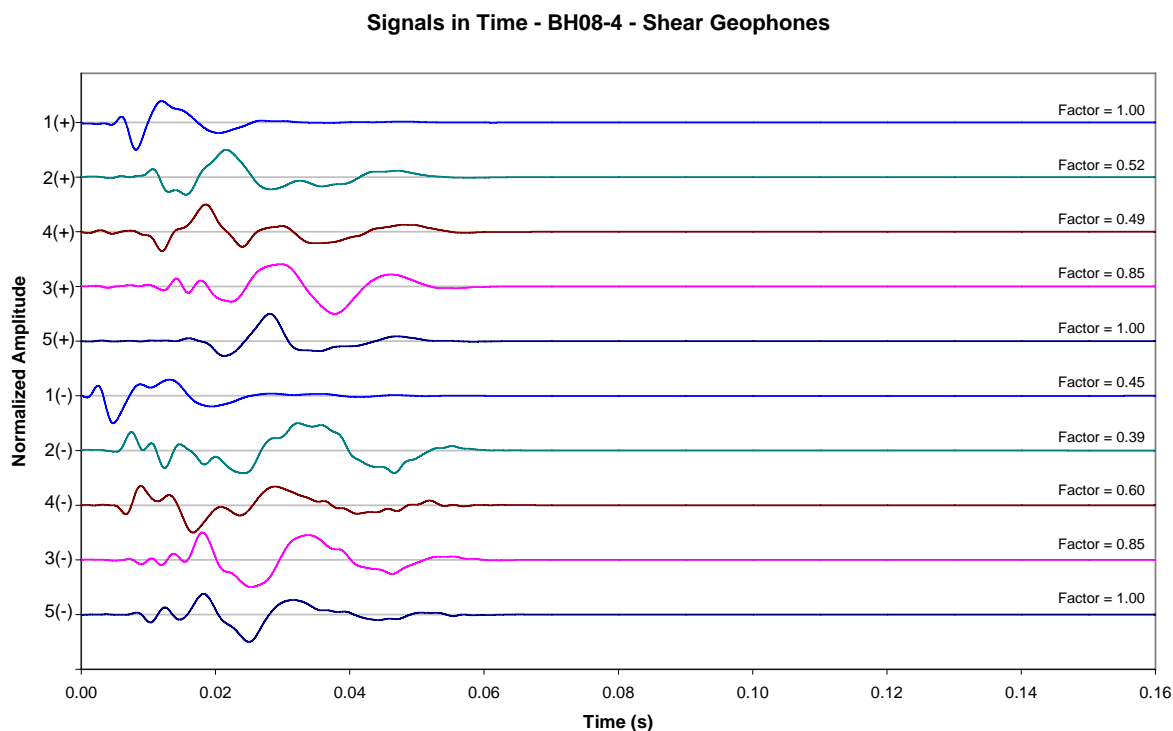


Figure 10-C. Time signals BH 8-04. Vertical geophones (surface)

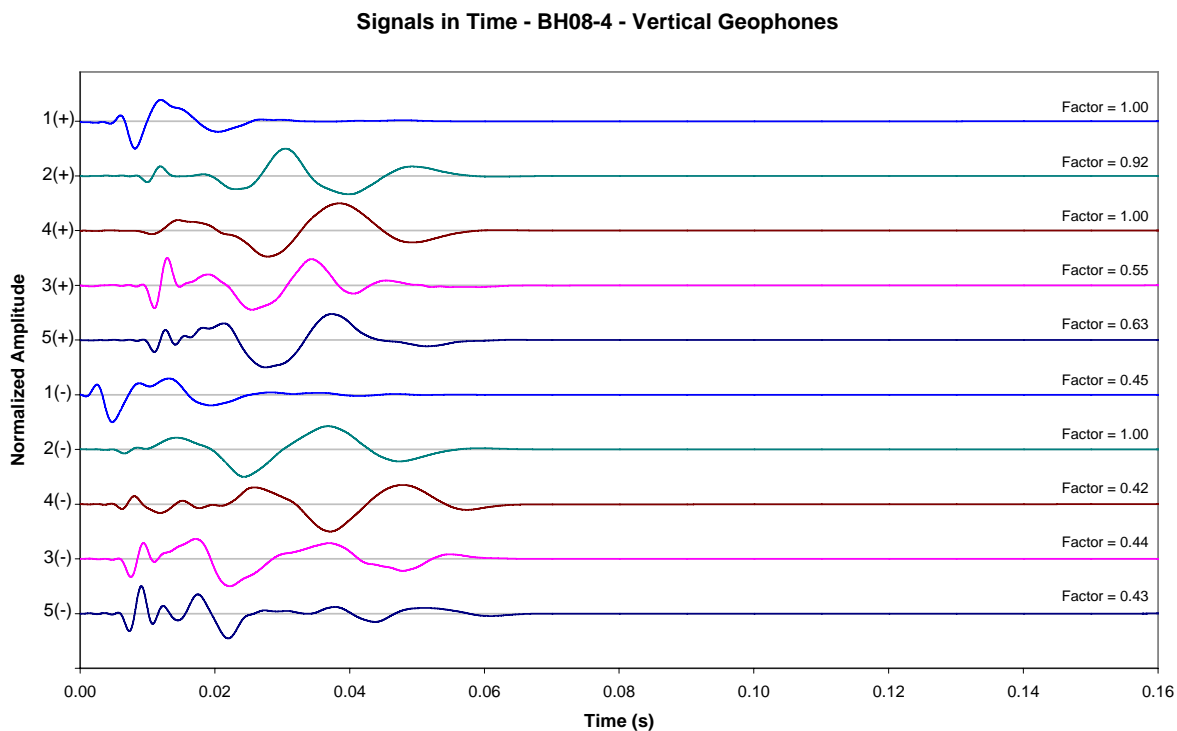


Figure 11-CC. Time signals BH 8-04. Horizontal geophones (surface)

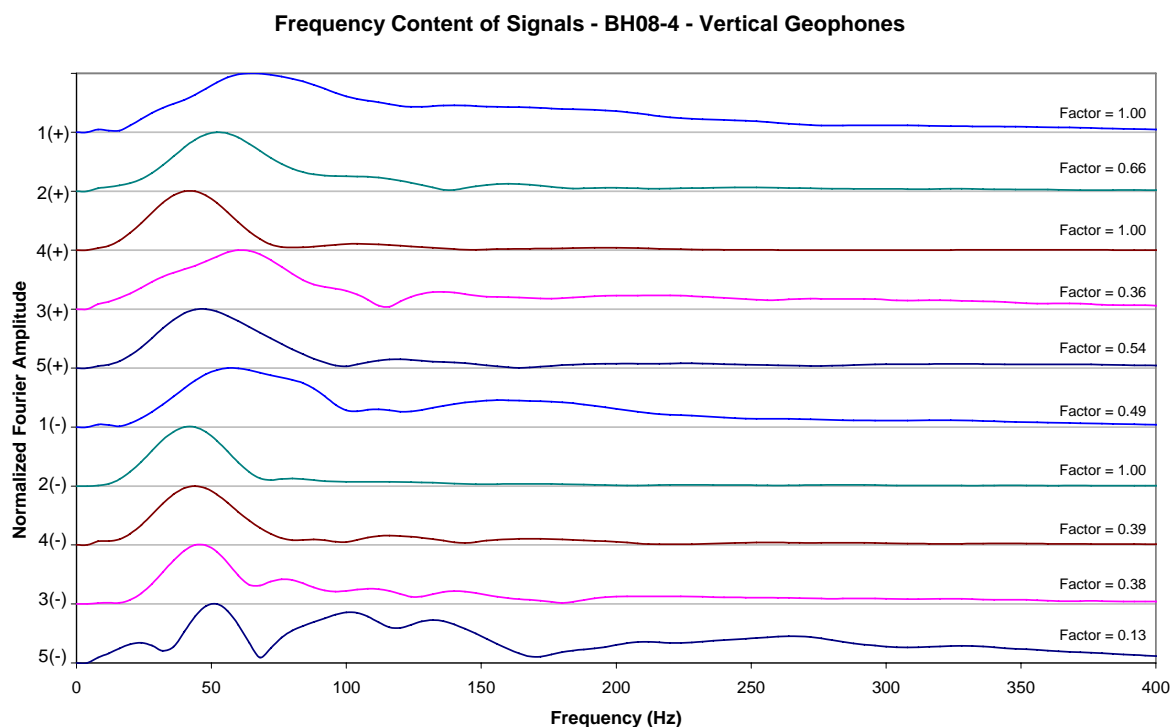


Figure 12-C. Fourier spectra BH 8-04. Vertical geophones (surface)

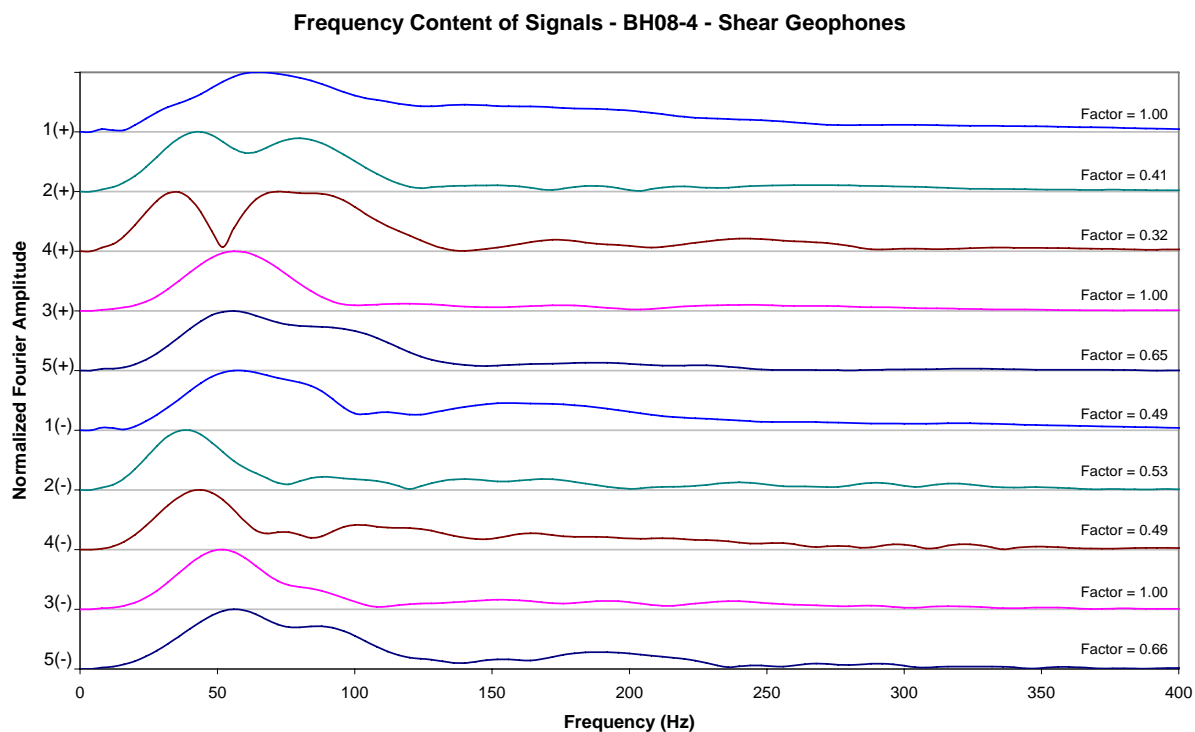


Figure 13-C. Fourier spectra BH 8-04. Horizontal geophones (surface)

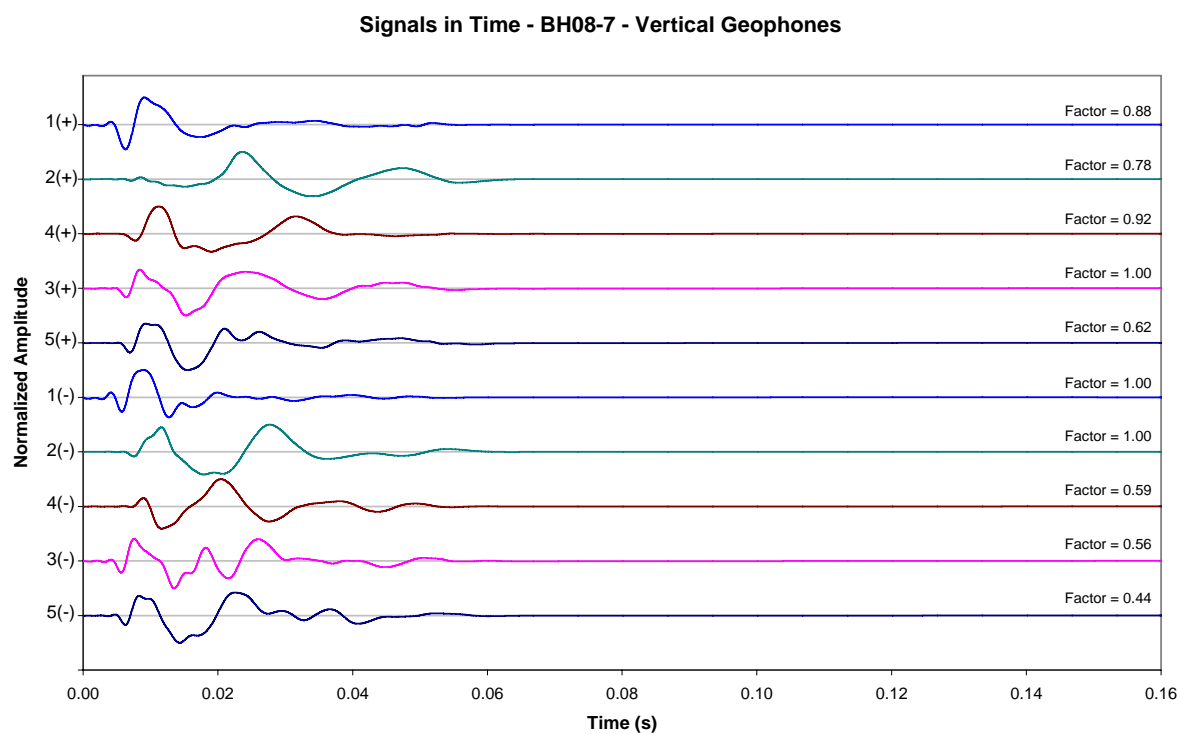


Figure 14-CC. Time signals BH 8-07. Vertical geophones (surface)

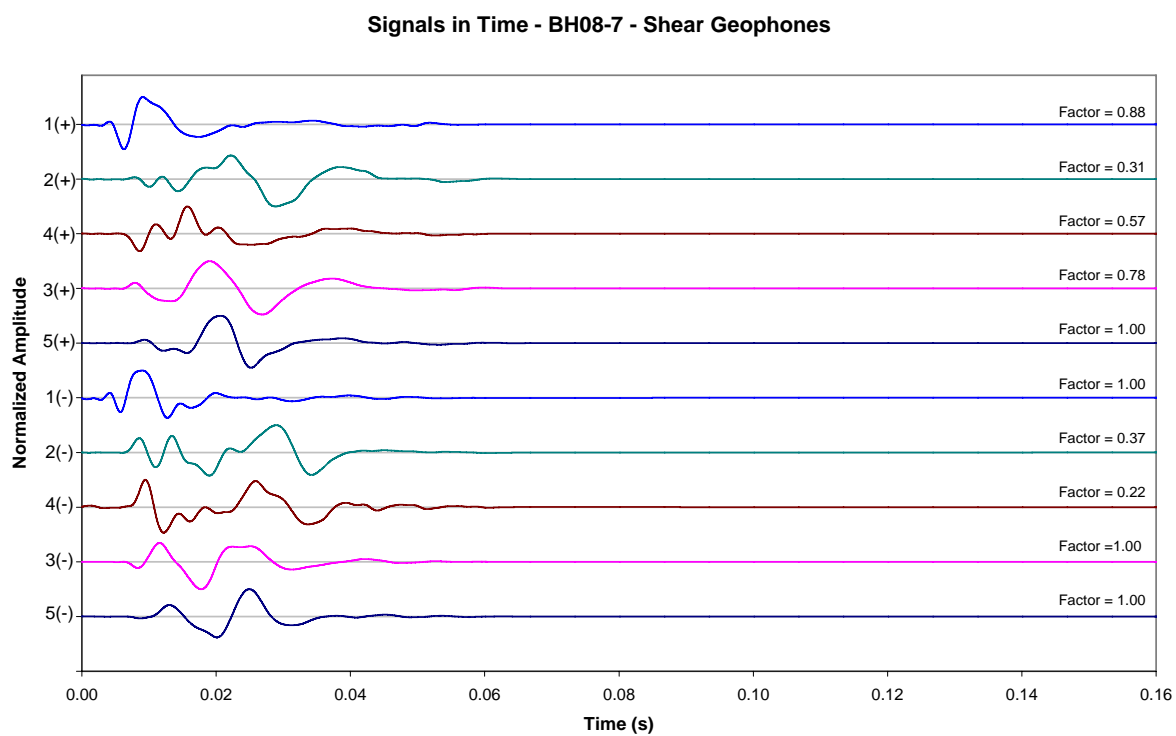


Figure 15-CC. Time signals BH 8-07. Horizontal geophones (surface)

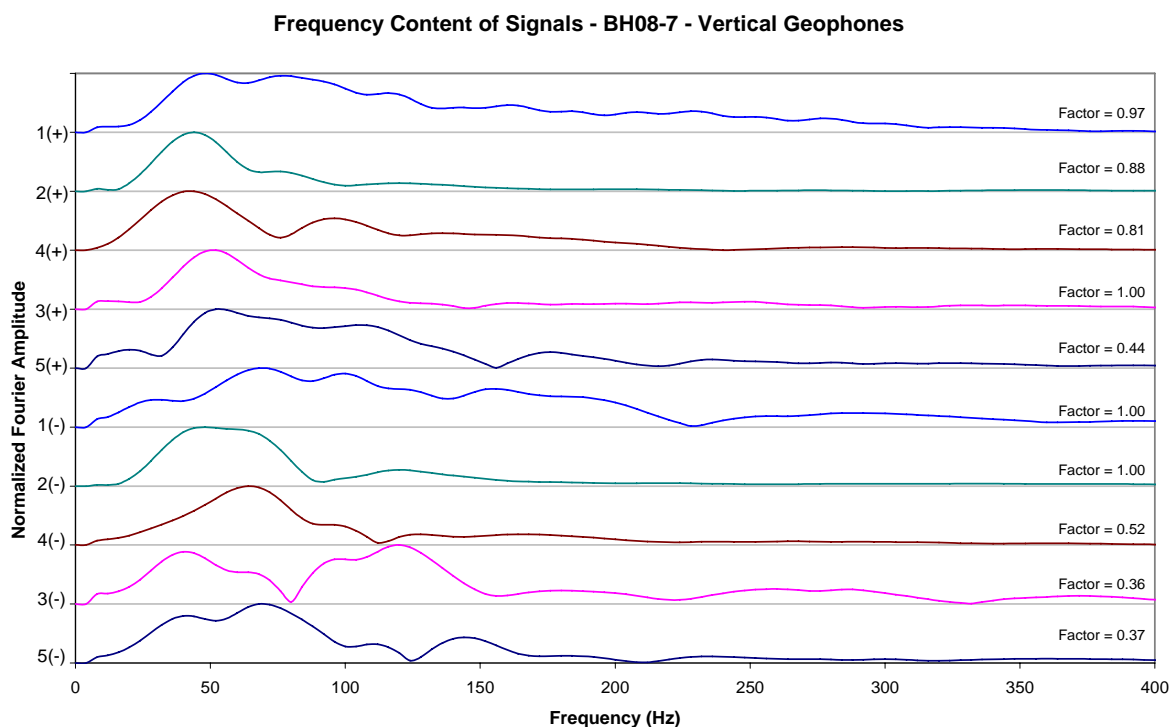


Figure 16-C. Fourier spectra BH 8-07. Vertical geophones (surface)

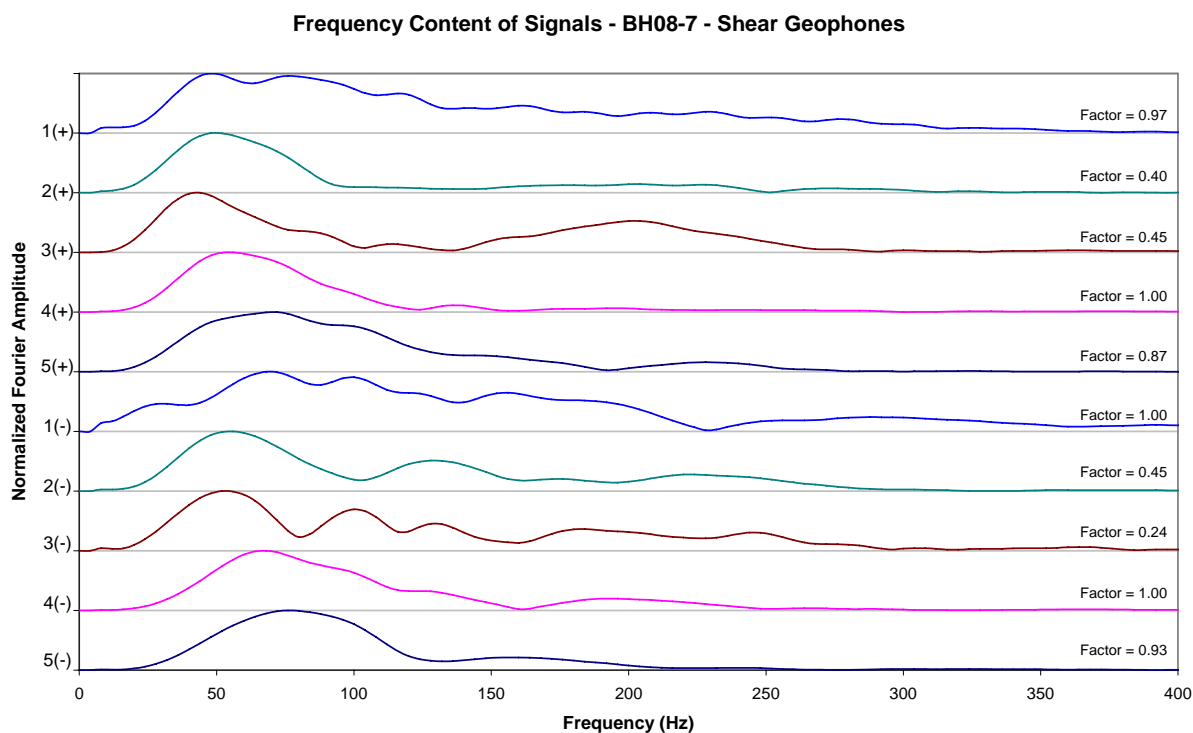


Figure 17-C. Fourier spectra BH 8-07. Horizontal geophones (surface)

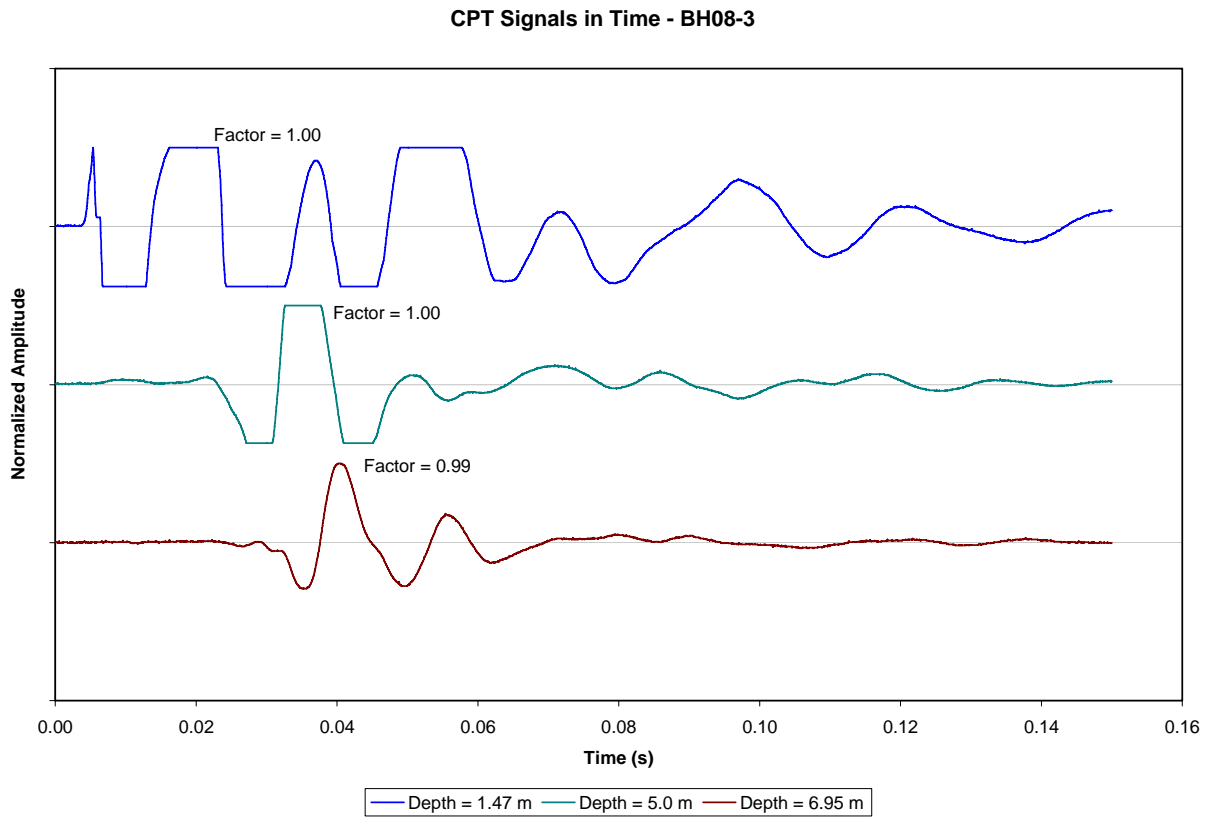


Figure 18-C. Time signals BH 8-03. Vertical geophones (borehole)

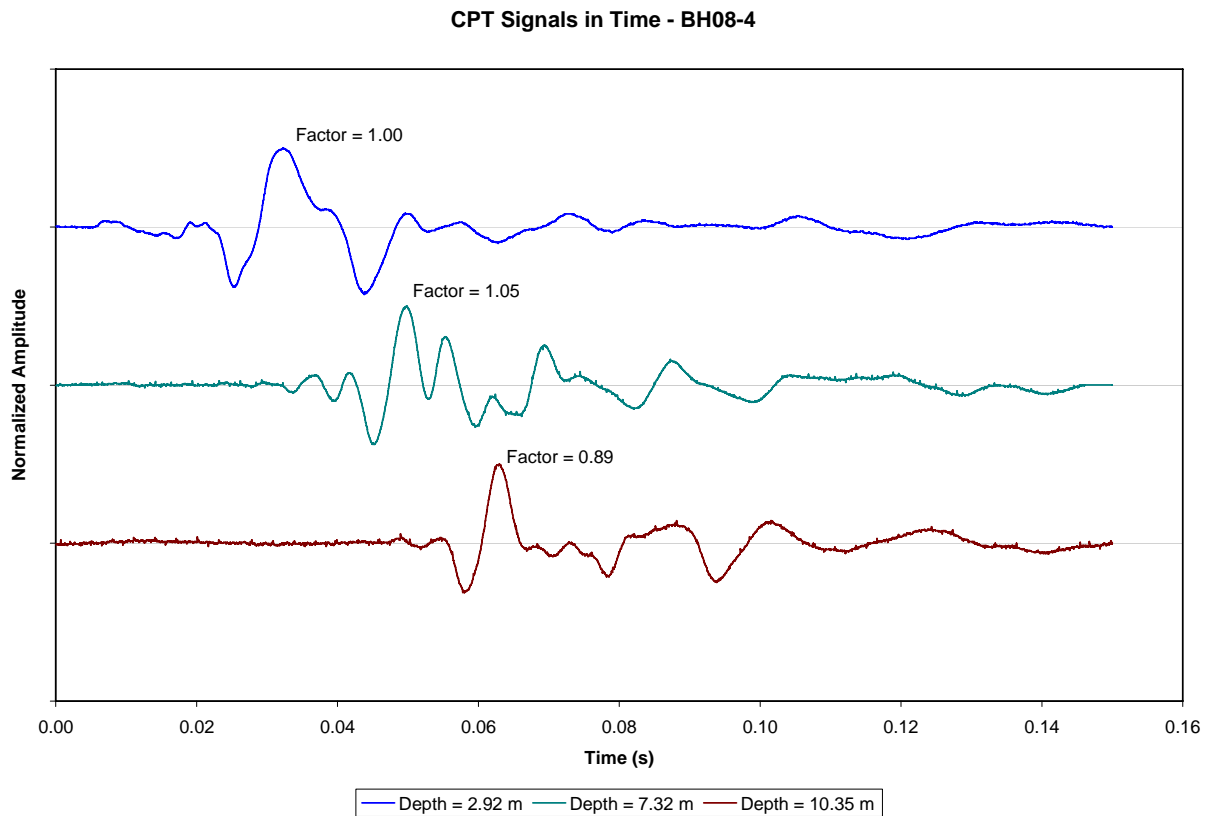


Figure 19-C. Time signals BH 8-04. Vertical geophones (borehole)

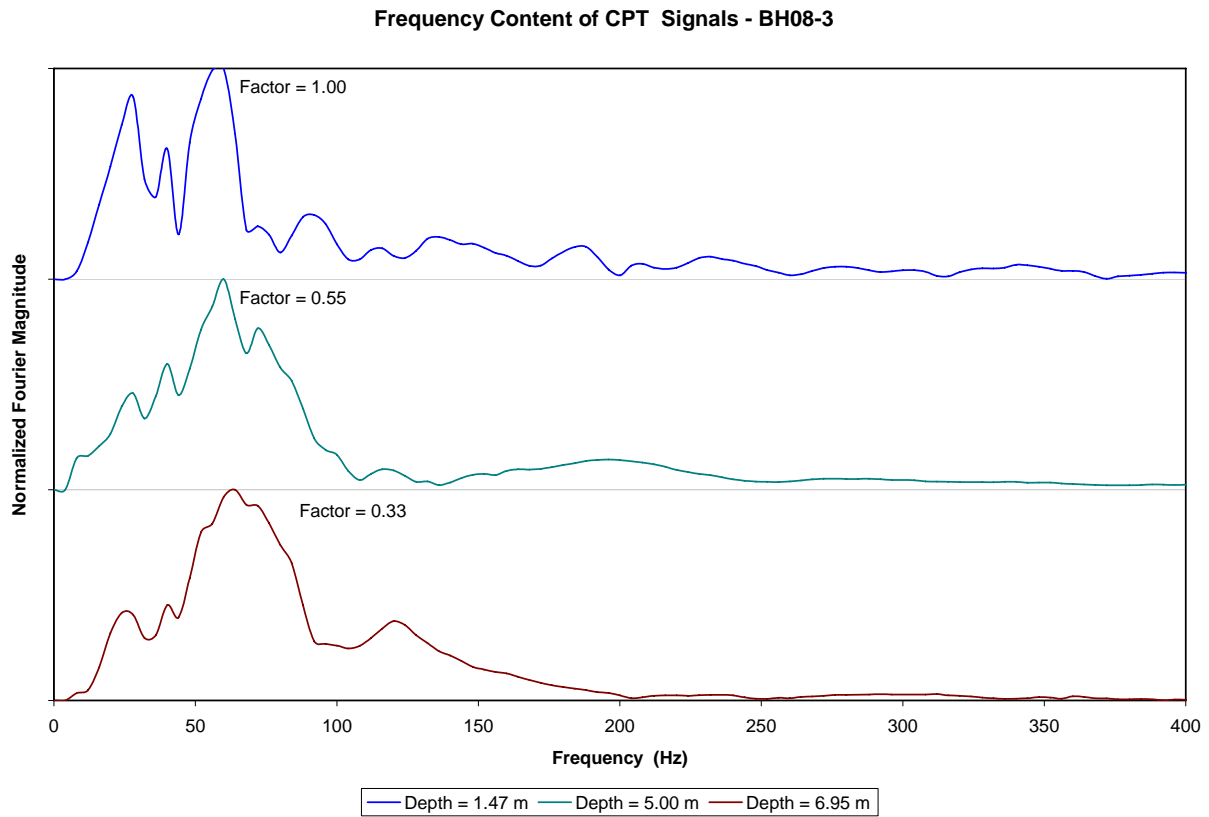


Figure 20-C. Fourier spectra BH 8-03. Vertical geophones (borehole)

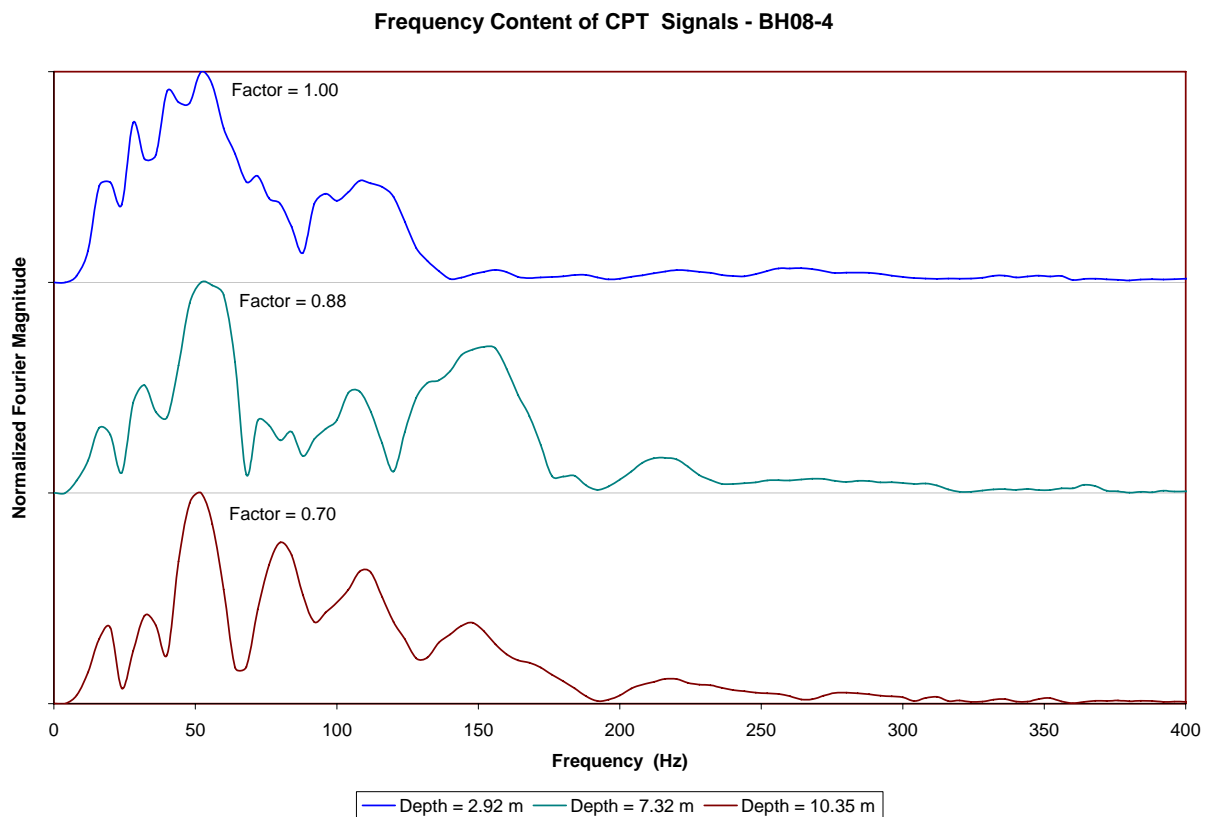


Figure 21-C. Fourier spectra BH 8-04. Vertical geophones (borehole)

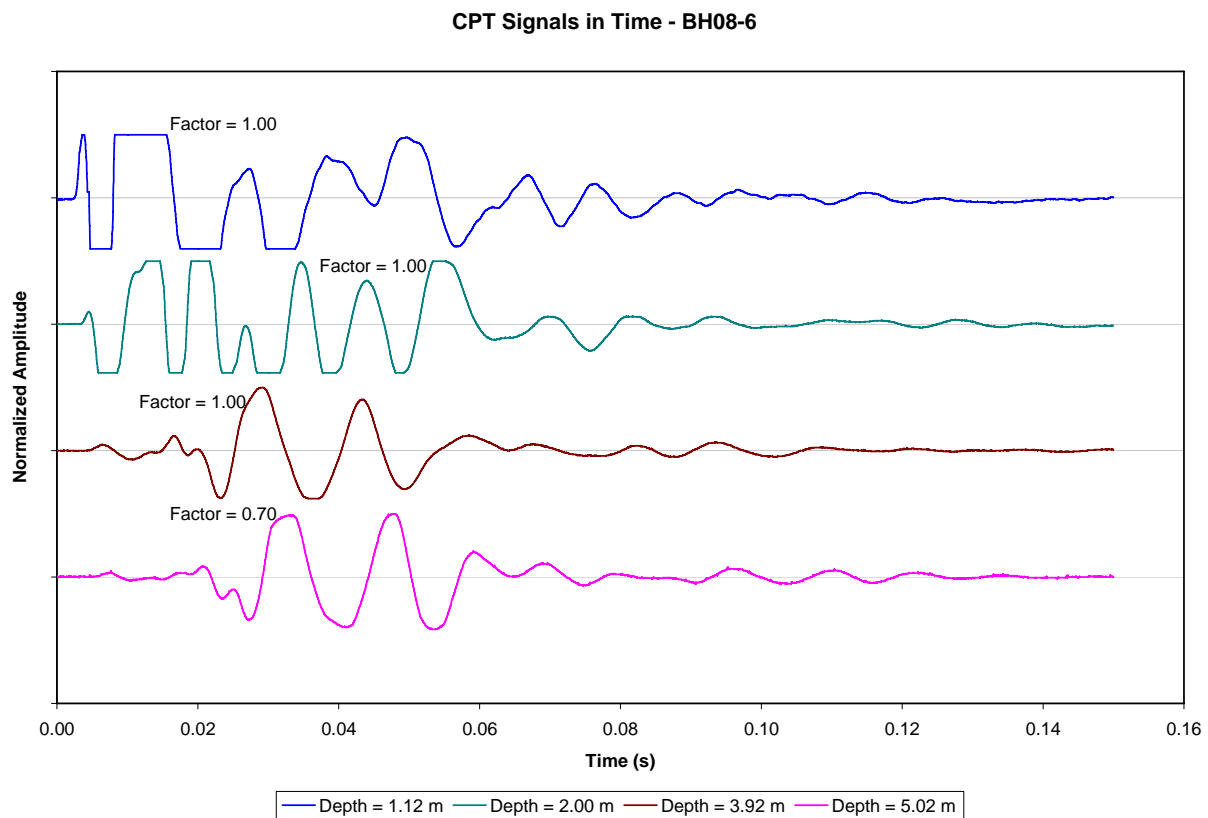


Figure 22-C. Time signals BH 8-06. Vertical geophones (borehole)

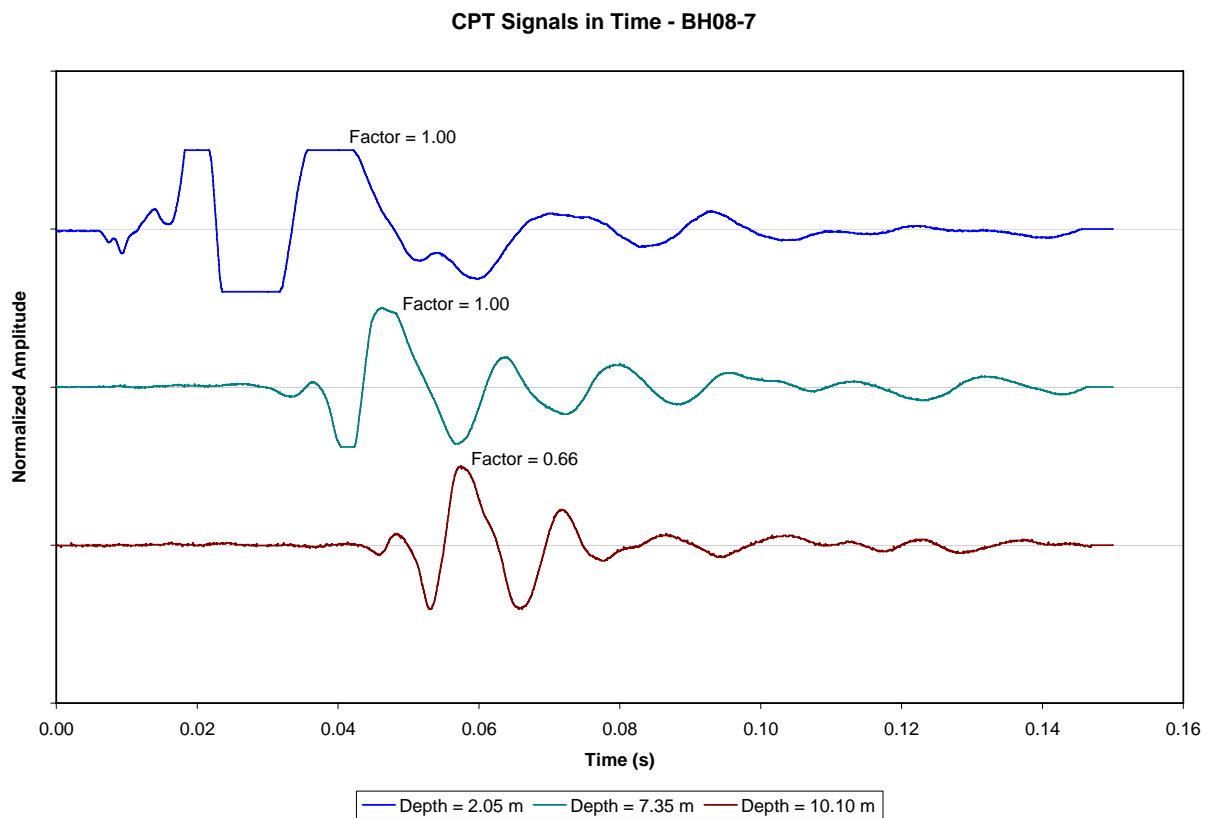


Figure 23-C. Time signals BH 8-07. Vertical geophones (borehole)

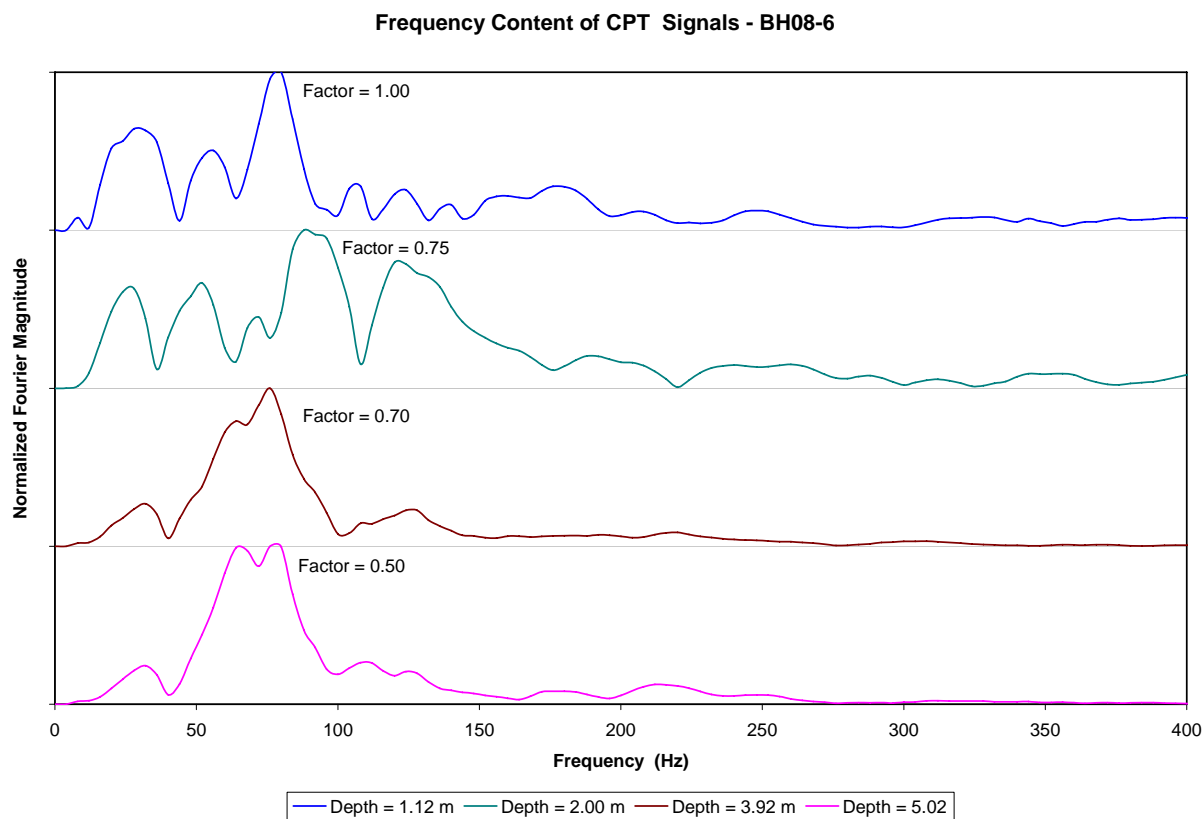


Figure 24-C. Fourier spectra BH 8-06. Vertical geophones (borehole)

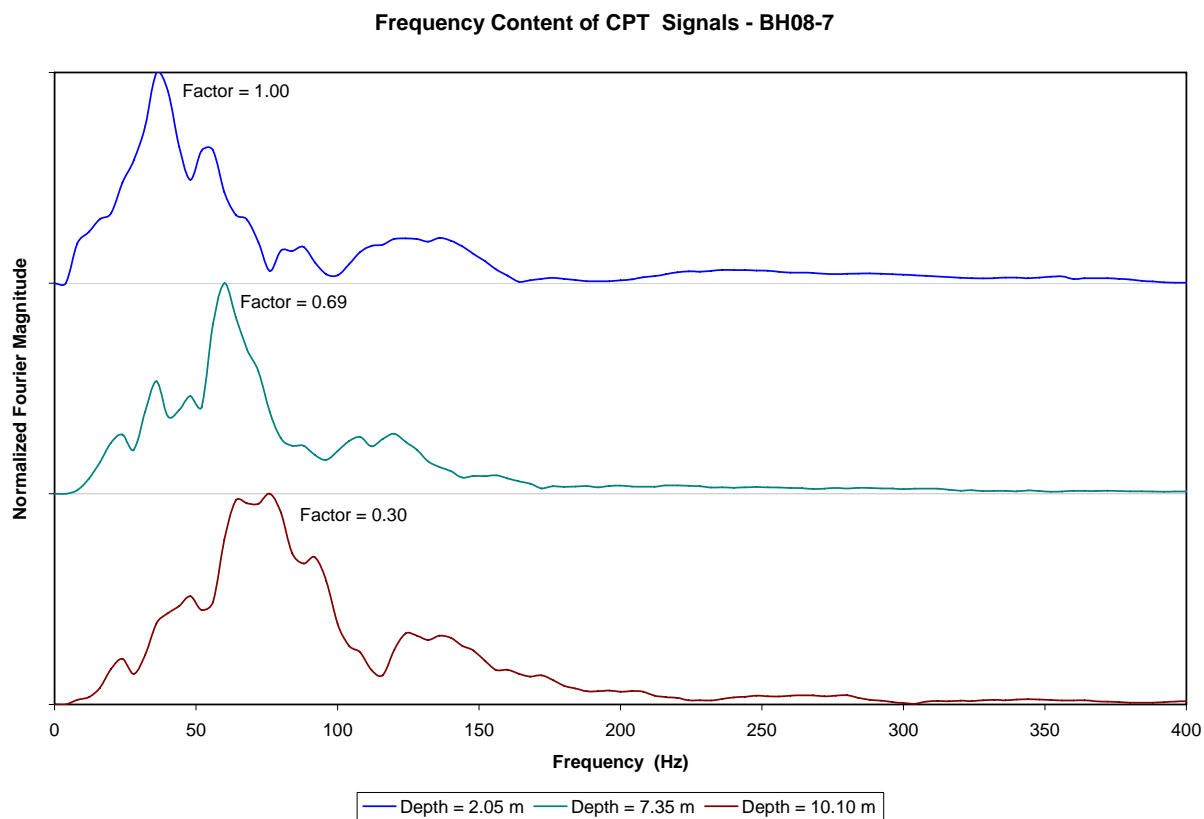


Figure 25-C. Fourier spectra BH 8-07. Vertical geophones (borehole)

Appendix 3

Borehole Logs

SYMBOLS, ABBREVIATIONS AND TERMS USED ON RECORDS OF BOREHOLES

1. TEXTURAL CLASSIFICATION OF SOILS

CLASSIFICATION	PARTICLE SIZE	VISUAL IDENTIFICATION
Boulders	Greater than 200mm	same
Cobbles	75 to 200mm	same
Gravel	4.75 to 75mm	5 to 75mm
Sand	0.075 to 4.75mm	Not visible particles to 5mm
Silt	0.002 to 0.075mm	Non-plastic particles, not visible to the naked eye
Clay	Less than 0.002mm	Plastic particles, not visible to the naked eye

2. COARSE GRAIN SOIL DESCRIPTION (50% greater than 0.075mm)

TERMINOLOGY	PROPORTION
Trace or Occasional	Less than 10%
Some	10 to 20%
Adjective (e.g. silty or sandy)	20 to 35%
And (e.g. sand and gravel)	35 to 50%

3. TERMS DESCRIBING CONSISTENCY (COHESIVE SOILS ONLY)

DESCRIPTIVE TERM	UNDRAINED SHEAR STRENGTH (kPa)	APPROXIMATE SPT ⁽¹⁾ 'N' VALUE
Very Soft	12 or less	Less than 2
Soft	12 to 25	2 to 4
Firm	25 to 50	4 to 8
Stiff	50 to 100	8 to 15
Very Stiff	100 to 200	15 to 30
Hard	Greater than 200	Greater than 30

NOTE: Hierarchy of Soil Strength Prediction

- 1) Laboratory Triaxial Testing
- 2) Field Insitu Vane Testing
- 3) Laboratory Vane Testing
- 4) SPT value
- 5) Pocket Penetrometer



4. TERMS DESCRIBING DENSITY (COHESIONLESS SOILS ONLY)

DESCRIPTIVE TERM	SPT "N" VALUE
Very Loose	Less than 4
Loose	4 to 10
Compact	10 to 30
Dense	30 to 50
Very Dense	Greater than 50

5. LEGEND FOR RECORDS OF BOREHOLES

SYMBOLS AND ABBREVIATIONS FOR SAMPLE TYPE	SS Split Spoon Sample	WS Wash Sample	AS Auger (Grab) Sample
	TW Thin Wall Shelby Tube Sample	TP Thin Wall Piston Sample	
	PH Sampler Advanced by Hydraulic Pressure	PM Sampler Advanced by Manual Pressure	
	WH Sampler Advanced by Self Static Weight	RC Rock Core	SC Soil Core

$$\text{Sensitivity} = \frac{\text{Undisturbed Shear Strength}}{\text{Remoulded Shear Strength}}$$

 Water Level
 Shear Strength Determination by Pocket Penetrometer

- (1) SPT 'N' Value Standard Penetration Test 'N' Value – refers to the number of blows from a 63.5kg hammer free falling a height of 0.76m to advance a standard 50 mm outside diameter split spoon sampler for 0.3 m depth into undisturbed ground.
- (2) DCPT Dynamic Cone Penetration Test – Continuous penetration of a 50 mm outside diameter, 60° conical steel point attached to "A" size rods driven by a 63.5 kg hammer free falling a height of 0.76 m. The resistance to cone penetration is the number of hammer blows required for each 0.3 m advance of the conical point into undisturbed ground.

UNIFIED SOILS CLASSIFICATION

MAJOR DIVISIONS		GROUP SYMBOL	TYPICAL DESCRIPTION
COARSE GRAINED SOILS	GRAVEL AND GRAVELLY SOILS	GW	Well-graded gravels or gravel-sand mixtures, little or no fines.
		GP	Poorly-graded gravels or gravel-sand mixtures, little or no fines.
		GM	Silty gravels, gravel-sand-silt mixtures.
		GC	Clayey gravels, gravel-sand-clay mixtures.
	SAND AND SANDY SOILS	SW	Well-graded sands or gravelly sands, little or no fines.
		SP	Poorly-graded sands or gravelly sands, little or no fines.
		SM	Silty sands, sand-silt mixtures.
		SC	Clayey sands, sand-clay mixtures.
FINE GRAINED SOILS	SILTS AND CLAYS $W_L < 50\%$	ML	Inorganic silts and very fine sands, rock flour, silty or clayey fine sands or clayey silts with slight plasticity.
		CL	Inorganic clays of low to medium plasticity, gravelly clays, sandy clays, silty clays, lean clays. ($W_L < 30\%$).
		CI	Inorganic clays of medium plasticity, silty clays. ($30\% < W_L < 50\%$).
		OL	Organic silts and organic silty-clays of low plasticity.
	SILTS AND CLAYS $W_L > 50\%$	MH	Inorganic silts, micaceous or diatomaceous fine sandy or silty soils, elastic silts.
		CH	Inorganic clays of high plasticity, fat clays.
		OH	Organic clays of medium to high plasticity, organic silts.
HIGHLY ORGANIC SOILS		Pt	Peat and other highly organic soils.
CLAY SHALE			
SANDSTONE			
SILTSTONE			
CLAYSTONE			
COAL			

METRIC

[illegible]

+³, ×³: Numbers refer to Sensitivity

ONTMT4S 0511.GPJ 2012TEMPLATE(MTO).GDT 9/3/13

RECORD OF BOREHOLE No BH-01

2 OF 2

METRIC

W.P. W.O. 07-20017 LOCATION Nash Road & Black Creek N 4 864 439.6 E 363 735.0 ORIGINATED BY SLL
 HWY 407 BOREHOLE TYPE Solid Stem Augers COMPILED BY WM
 DATUM Geodetic DATE 2008.02.15 - 2008.02.15 CHECKED BY SKP

SOIL PROFILE			SAMPLES			GROUND WATER CONDITIONS	ELEVATION SCALE	DYNAMIC CONE PENETRATION RESISTANCE PLOT					PLASTIC LIMIT W _p	NATURAL MOISTURE CONTENT W	LIQUID LIMIT W _L	UNIT WEIGHT γ kN/m ³	REMARKS & GRAIN SIZE DISTRIBUTION (%) GR SA SI CL
ELEV DEPTH	DESCRIPTION	STRAT PLOT	NUMBER	TYPE	"N" VALUES			20	40	60	80	100					
	Continued From Previous Page																
129.2	SAND and SILT, trace clay, trace gravel Dense to Very Dense Grey Moist (TILL)		9	SS	69		130										
11.2	END OF BOREHOLE AT 11.20 m. BOREHOLE OPEN TO 3.81m AND WATER LEVEL AT 3.2m UPON COMPLETION OF DRILLING. BOREHOLE BACKFILLED WITH BENTONITE TO SURFACE.																

RECORD OF BOREHOLE No 08-3

1 OF 2

METRIC

W.P. W.O. 07-20017 LOCATION Nash Road & Black Creek N 4 864 420.6 E 363 711.0 ORIGINATED BY GA
 HWY 407 BOREHOLE TYPE Hollow Stem Augers COMPILED BY WM
 DATUM Geodetic DATE 2008.07.08 - 2008.07.08 CHECKED BY SKP

SOIL PROFILE			SAMPLES			GROUND WATER CONDITIONS	ELEVATION SCALE	DYNAMIC CONE PENETRATION RESISTANCE PLOT				PLASTIC LIMIT W _P	NATURAL MOISTURE CONTENT W	LIQUID LIMIT W _L	UNIT WEIGHT γ kN/m ³	REMARKS & GRAIN SIZE DISTRIBUTION (%)	
ELEV DEPTH	DESCRIPTION	STRAT PLOT	NUMBER	TYPE	"N" VALUES			SHEAR STRENGTH kPa									WATER CONTENT (%)
139.8								20	40	60	80	100					
0.0	TOPSOIL: (75 mm)							20	40	60	80	100					
0.1	Silty CLAY , trace sand, occasional rootlets		1	SS	18												
139.2	Very Stiff																
0.6	Brown																
	Silty SAND , fine grained, occasional rootlets, occasional iron oxide staining		2	SS	23												
	Compact																
	Brown																
	Moist		3	SS	28												
137.6																	
2.3	Silty CLAY , trace sand		4	SS	50/ .150												0 61 39 (SI+CL)
	Hard																
	Grey		5	SS	33												
	Moist (CL)																
	becoming Firm to Soft																0 4 71 25
			1	TW	PH												

Continued Next Page

+³, ×³: Numbers refer to Sensitivity
 20
 15 10 5 10
 (%) STRAIN AT FAILURE

RECORD OF BOREHOLE No 08-3

2 OF 2

METRIC

W.P. W.O. 07-20017 LOCATION Nash Road & Black Creek N 4 864 420.6 E 363 711.0 ORIGINATED BY GA
 HWY 407 BOREHOLE TYPE Hollow Stem Augers COMPILED BY WM
 DATUM Geodetic DATE 2008.07.08 - 2008.07.08 CHECKED BY SKP

SOIL PROFILE			SAMPLES			GROUND WATER CONDITIONS	ELEVATION SCALE	DYNAMIC CONE PENETRATION RESISTANCE PLOT					PLASTIC LIMIT W _p	NATURAL MOISTURE CONTENT W	LIQUID LIMIT W _L	UNIT WEIGHT γ kN/m ³	REMARKS & GRAIN SIZE DISTRIBUTION (%) GR SA SI CL
ELEV DEPTH	DESCRIPTION	STRAT PLOT	NUMBER	TYPE	"N" VALUES			SHEAR STRENGTH kPa ○ UNCONFINED + FIELD VANE ● QUICK TRIAXIAL × LAB VANE									
	Continued From Previous Page																
	SAND and SILT some clay, trace gravel Very Dense Grey Wet (TILL)		9	SS	124		129										
			10	SS	111		128										
							127										
							126										
							125										
124.4			11	SS	50/												
15.4	END OF BOREHOLE AT 15.39 m. BOREHOLE OPEN TO 15.39 m AND WATER LEVEL AT 2.74 m. Well installation consists of 50mm diameter Schedule 40 PVC pipe with a 1.52 m slotted screen. WATER LEVEL READINGS: DATE DEPTH (m) ELEV. (m) 2008.07.15 1.5 138.3				.150												

Spoon sampler
sank 1.5m, no
sample recovered

RECORD OF BOREHOLE No 08-4

1 OF 2

METRIC

W.P. W.O. 07-20017 LOCATION Nash Road & Black Creek N 4 864 552.9 E 363 779.6 ORIGINATED BY GA
 HWY 407 BOREHOLE TYPE Hollow Stem Augers COMPILED BY WM
 DATUM Geodetic DATE 2008.07.07 - 2008.07.07 CHECKED BY SKP

SOIL PROFILE			SAMPLES			GROUND WATER CONDITIONS	ELEVATION SCALE	DYNAMIC CONE PENETRATION RESISTANCE PLOT					UNIT WEIGHT γ kN/m ³	REMARKS & GRAIN SIZE DISTRIBUTION (%)
ELEV DEPTH	DESCRIPTION	STRAT PLOT	NUMBER	TYPE	"N" VALUES			20	40	60	80	100		
139.5														
0.0	TOPSOIL: (75 mm)													
0.1	Silty CLAY, trace sand Very Stiff to Hard Mottled Brown to Grey (CL-ML)		1	SS	16		139							
			2	SS	20									
			3	SS	55		138							0 6 72 22
	(CL)		4	SS	27		137							
			5	SS	34		136							0 2 61 37
135.1														
4.4	Silty CLAY, occasional silt seams Very Soft to Firm Grey (CL-CI)		6	SS	1		135							
							134	2.3						
			1	TW	PH		133							
							132	1.8						
	occasional sand seams		2	TW	PH									
							131	3.4						
	trace sand, trace gravel		7	SS	2		130							1 9 37 53

Continued Next Page

+³, ×³: Numbers refer to
Sensitivity

20
15
10

(%) STRAIN AT FAILURE

RECORD OF BOREHOLE No 08-4

2 OF 2

METRIC

W.P. W.O. 07-20017 LOCATION Nash Road & Black Creek N 4 864 552.9 E 363 779.6 ORIGINATED BY GA
 HWY 407 BOREHOLE TYPE Hollow Stem Augers COMPILED BY WM
 DATUM Geodetic DATE 2008.07.07 - 2008.07.07 CHECKED BY SKP

SOIL PROFILE			SAMPLES			GROUND WATER CONDITIONS	ELEVATION SCALE	DYNAMIC CONE PENETRATION RESISTANCE PLOT					PLASTIC LIMIT	NATURAL MOISTURE CONTENT	LIQUID LIMIT	UNIT WEIGHT γ kN/m ³	REMARKS & GRAIN SIZE DISTRIBUTION (%)
ELEV DEPTH	DESCRIPTION	STRAT PLOT	NUMBER	TYPE	"N" VALUES			SHEAR STRENGTH kPa					W _p	W	W _L		
	Continued From Previous Page							20	40	60	80	100					

RECORD OF BOREHOLE No 08-5

1 OF 2

METRIC

W.P. W.O. 07-20017 LOCATION Nash Road & Black Creek N 4 864 488.0 E 363 664.3 ORIGINATED BY GA
 HWY 407 BOREHOLE TYPE Hollow Stem Augers COMPILED BY WM
 DATUM Geodetic DATE 2008.07.09 - 2008.07.09 CHECKED BY SKP

SOIL PROFILE			SAMPLES			GROUND WATER CONDITIONS	ELEVATION SCALE	DYNAMIC CONE PENETRATION RESISTANCE PLOT				PLASTIC LIMIT NATURAL MOISTURE CONTENT LIQUID LIMIT			UNIT WEIGHT γ kN/m ³	REMARKS & GRAIN SIZE DISTRIBUTION (%)			
ELEV DEPTH	DESCRIPTION	STRAT PLOT	NUMBER	TYPE	"N" VALUES			SHEAR STRENGTH kPa ○ UNCONFINED + FIELD VANE ● QUICK TRIAXIAL × LAB VANE				WATER CONTENT (%) w _P w w _L				GR	SA	SI	CL
139.2								20	40	60	80	100							
0.0	Clayey SILT , trace sand, trace gravel, some rootlets Very Stiff to Hard Brown		1	SS	30		139							○					
138.6	(FILL)																		
0.6	Sandy SILT , trace gravel, trace clay Dense Grey (FILL)		2	SS	42		138							○					
137.9	SAND , trace silt, trace rootlets, occasional wood fibres and organics Compact Dark Brown Moist (FILL)														○				
1.3			3	SS	18		137												
136.9																			
2.3	Silty CLAY , trace sand, trace gravel Very Stiff to Hard Brown to Grey (Cl)		4	SS	19		136								○				
			5	SS	18		135												
	with sand (CL)		6	SS	50		134									○			
133.1																			
6.1	Sandy SILT , some clay, trace gravel Very Dense Grey Wet (TILL)		7	SS	96		133							○					
							132												
131.6																			
7.6	SAND , trace silt, trace gravel Very Dense Grey Wet		8	SS	85		131							○					
130.6																			
8.6	Sandy SILT , trace gravel, occasional cobbles Very Dense Grey Wet																		
			9	SS	105/ .150		130							○					

Continued Next Page

+³, ×³: Numbers refer to
Sensitivity

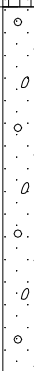
20
15
10
(%) STRAIN AT FAILURE

RECORD OF BOREHOLE No 08-5

2 OF 2

METRIC

W.P. W.O. 07-20017 LOCATION Nash Road & Black Creek N 4 864 488.0 E 363 664.3 ORIGINATED BY GA
 HWY 407 BOREHOLE TYPE Hollow Stem Augers COMPILED BY WM
 DATUM Geodetic DATE 2008.07.09 - 2008.07.09 CHECKED BY SKP

SOIL PROFILE			SAMPLES			GROUND WATER CONDITIONS	ELEVATION SCALE	DYNAMIC CONE PENETRATION RESISTANCE PLOT					PLASTIC LIMIT W _p	NATURAL MOISTURE CONTENT W	LIQUID LIMIT W _L	UNIT WEIGHT γ kN/m ³	REMARKS & GRAIN SIZE DISTRIBUTION (%) GR SA SI CL
ELEV DEPTH	DESCRIPTION	STRAT PLOT	NUMBER	TYPE	"N" VALUES			SHEAR STRENGTH kPa									
	Continued From Previous Page							20	40	60	80	100					
128.5							129										
10.7	SAND, trace silt, trace gravel Very Dense Grey Wet (TILL)		10	SS	100/ .150		128										
							127										
126.1			11	SS	104/ .150												
13.1	END OF BOREHOLE AT 13.11 m. BOREHOLE OPEN TO 13.11 m AND WATER LEVEL AT 1.83 m ON COMPLETION OF DRILLING. Well installation consist of 50 mm diameter Schedule 40 PVC pipe with a 1.52m slotted screen. WATER LEVEL READINGS: DATE DEPTH (m) ELEV. (m) 2008.07.15 1.2 138.0																

RECORD OF BOREHOLE No 08-6

1 OF 1

METRIC

W.P. W.O. 07-20017 LOCATION Nash Road & Black Creek N 4 864 442.2 E 363 682.5 ORIGINATED BY GA
 HWY 407 BOREHOLE TYPE Hollow Stem Augers COMPILED BY WM
 DATUM Geodetic DATE 2008.07.10 - 2008.07.10 CHECKED BY SKP

SOIL PROFILE			SAMPLES			GROUND WATER CONDITIONS	ELEVATION SCALE	DYNAMIC CONE PENETRATION RESISTANCE PLOT					PLASTIC LIMIT w _P	NATURAL MOISTURE CONTENT w	LIQUID LIMIT w _L	UNIT WEIGHT γ kN/m ³	REMARKS & GRAIN SIZE DISTRIBUTION (%) GR SA SI CL
ELEV DEPTH	DESCRIPTION	STRAT PLOT	NUMBER	TYPE	*"N" VALUES			SHEAR STRENGTH kPa ○ UNCONFINED + FIELD VANE ● QUICK TRIAXIAL × LAB VANE									
139.6								20	40	60	80	100					
0.0	TOPSOIL: (90 mm)																
0.1	Clayey SILT , trace sand, occasional gravel Brown (FILL)		1	TW	PH		139										
138.2			2	TW	PH												
1.4	PEAT , sandy, trace rootlets						138										
138.0	Dark Brown																
1.6	Sandy SILT , trace gravel Brown to Grey																
136.9							137										
2.7	Silty CLAY , trace sand Firm to Stiff Grey		3	TW	PH		136										
135.0							135										
4.6	Silty SAND , trace gravel Compact Grey		4	TW	PH												
			1	SS	20	▽	134								○		
133.8																	
5.8	END OF BOREHOLE AT 5.79 m. BOREHOLE OPEN TO 5.79 m AND WATER LEVEL AT 5.49 m ON COMPLETION OF DRILLING. BOREHOLE BACKFILLED WITH BENTONITE HOLE PLUG.																

+³, ×³: Numbers refer to Sensitivity 20 15 10 5 0 (%) STRAIN AT FAILURE

RECORD OF BOREHOLE No 08-7

1 OF 2

METRIC

W.P. W.O. 07-20017 LOCATION Nash Road & Black Creek N 4 864 488.0 E 363 755.6 ORIGINATED BY GA
 HWY 407 BOREHOLE TYPE Hollow Stem Augers COMPILED BY WM
 DATUM Geodetic DATE 2008.07.11 - 2008.07.11 CHECKED BY SKP

SOIL PROFILE			SAMPLES			GROUND WATER CONDITIONS	ELEVATION SCALE	DYNAMIC CONE PENETRATION RESISTANCE PLOT		PLASTIC LIMIT W _p	NATURAL MOISTURE CONTENT W	LIQUID LIMIT W _L	UNIT WEIGHT γ kN/m ³	REMARKS & GRAIN SIZE DISTRIBUTION (%) GR SA SI CL
ELEV DEPTH	DESCRIPTION	STRAT PLOT	NUMBER	TYPE	"N" VALUES			SHEAR STRENGTH kPa						
140.7								20 40 60 80 100						
0.0	TOPSOIL: (75 mm)							20 40 60 80 100						
0.1	Silty CLAY , trace sand Brown							20 40 60 80 100						
140.2								20 40 60 80 100						
0.5	SAND , trace silt, trace gravel, occasional cobbles Brown Wet		1	TW	PH		140							
							139							
							138							
							137							
137.0							137							
3.7	Silty CLAY , occasional sand or silt seams Grey		2	TW	PH		136							
							135							
							134							
							133							
			5	TW	PH		132							
							131							

Continued Next Page

+³, ×³: Numbers refer to
Sensitivity

20
15
10
(%) STRAIN AT FAILURE

RECORD OF BOREHOLE No 08-7

2 OF 2

METRIC

W.P. W.O. 07-20017 LOCATION Nash Road & Black Creek N 4 864 488.0 E 363 755.6 ORIGINATED BY GA
 HWY 407 BOREHOLE TYPE Hollow Stem Augers COMPILED BY WM
 DATUM Geodetic DATE 2008.07.11 - 2008.07.11 CHECKED BY SKP

SOIL PROFILE			SAMPLES			GROUND WATER CONDITIONS	ELEVATION SCALE	DYNAMIC CONE PENETRATION RESISTANCE PLOT					PLASTIC LIMIT W _p	NATURAL MOISTURE CONTENT W	LIQUID LIMIT W _L	UNIT WEIGHT γ kN/m ³	REMARKS & GRAIN SIZE DISTRIBUTION (%) GR SA SI CL
ELEV DEPTH	DESCRIPTION	STRAT PLOT	NUMBER	TYPE	"N" VALUES			SHEAR STRENGTH kPa									
	Continued From Previous Page																
130.6			1	SS	50/												
10.1	Sandy SILT , trace gravel																
130.5	Very Dense																
10.2	Grey (TILL)				.150												
END OF BOREHOLE AT 10.21 m. BOREHOLE OPEN TO 10.06 m AND WATER LEVEL AT 1.83 m ON COMPLETION OF DRILLING. BOREHOLE BACKFILLED WITH BENTONITE HOLEPLUG.																	

RECORD OF BOREHOLE No EL17-3

1 OF 2

METRIC

W.P. W.O. 07-20017 LOCATION N 4 864 616.2 E 363 677.5 Nash Road & Black Creek ORIGINATED BY WB
 HWY 407 BOREHOLE TYPE Solid Stem Augers COMPILED BY ES
 DATUM Geodetic DATE 2008.06.10 - 2008.06.10 CHECKED BY SKP

SOIL PROFILE			SAMPLES			GROUND WATER CONDITIONS	ELEVATION SCALE	DYNAMIC CONE PENETRATION RESISTANCE PLOT				PLASTIC LIMIT NATURAL MOISTURE CONTENT LIQUID LIMIT			UNIT WEIGHT γ kN/m ³	REMARKS & GRAIN SIZE DISTRIBUTION (%)					
ELEV DEPTH	DESCRIPTION	STRAT PLOT	NUMBER	TYPE	"N" VALUES			SHEAR STRENGTH kPa ○ UNCONFINED + FIELD VANE ● QUICK TRIAXIAL × LAB VANE				WATER CONTENT (%) w _p w w _L				GR	SA	SI	CL		
139.6						▽		20	40	60	80	100									
0.0	ASPHALT:(50mm)		1	AS																	
0.1	SAND, some gravel Loose Brown Moist (FILL)		1	SS	5																
138.3																					
1.4	Silty CLAY, trace sand, occasional oxide staining Stiff to Hard Grey-brown (CL)		2	SS	12													0	3	68	29
			3	SS	38																
			4	SS	32																
	some sand, trace gravel		5	SS	WH													1	19	40	40
134.2																					
5.5	SAND and SILT, trace gravel, trace clay Dense to Very Dense Grey Moist (TILL)		6	SS	36															Vane test attempted, would not turn	
			7	SS	51												2	44	45	9	
			8	SS	78												3	50	38	9	

Continued Next Page

+³, ×³: Numbers refer to
Sensitivity

20
15
10
(%) STRAIN AT FAILURE

METRIC

[illegible]

+³, ×³: Numbers refer to Sensitivity